Adsorption and Oxidation of Formaldehyde on Transition Metals Catalysts from Alkaline Aqueous Solutions

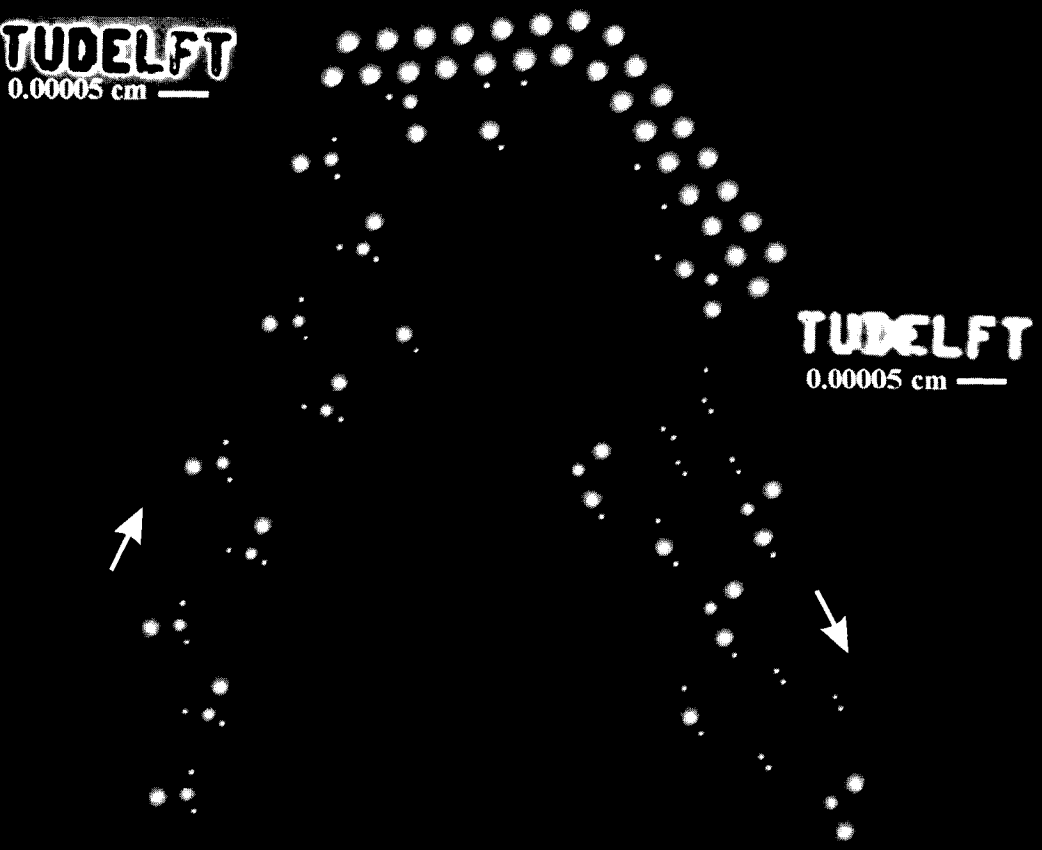

Marnix ten Kortenaar

nterfaculty Reactor Institute

Adsorption and Oxidation of Formaldehyde on Transition Metal Catalysts from Alkaline Aqueous Solutions

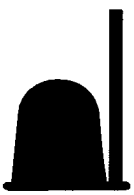

The research described in this thesis was conducted at the Department of Radiochemistry of the Interfaculty Reactor Institute, Delft University of Technology, Mekelweg 15, 2629 JB Delft, The Netherlands. It was carried out in collaboration with the Laboratory for Physical Chemistry, Faculty of Applied Sciences, Delft University of Technology, Julianalaan 136, 2628 BL Delft, The Netherlands.

Adsorption and Oxidation of Formaldehyde on Transition Metal Catalysts from Alkaline Aqueous Solutions

Proefschrift

ter verkrijging van de graad doctor
aan de Technische Universiteit Delft,
op gezag van de Rector Magnificus prof. dr. J.T. Fokkema,
voorzitter van het College voor Promoties,
in het openbaar te verdedigen op
maandag 1 december 2003 om 15:30 uur

Door

Marnix Victor ten Kortenaar

doctorandus in de Scheikunde
geboren te Voorburg

Dit proefschrift is goedgekeurd door de promotoren
Prof. dr. ir. J.J.M. de Goeij
Prof. dr. J. A. R. van Veen

Samenstelling promotiecommissie:

Rector Magnificus, Technische Universiteit Delft
Prof.dr.ir. J.J.M. de Goeij, Technische Universiteit Delft, promotor
Prof.dr. J. A. R. van Veen Technische Universiteit Eindhoven, promotor
Prof.dr. J. J. Kelly, Rijksuniversiteit Utrecht
Prof.dr. J. A. Moulijn, Technische Universiteit Delft
Prof.dr. J. Schoonman, Technische Universiteit Delft
Dr.ing. G. J. M. Koper, Technische Universiteit Delft
Ir. Z. I. Kolar, Technische Universiteit Delft

Published and distributed by:DUP Science

DUP Science is an imprint of
Delft University Press
P.O. Box 98
2600 MG Delft
The Netherlands
Telephone: +31 15 27 85 678
Telefax: + 31 15 27 85 706
E-mail: info@library.tudelft.nl

ISBN 90-407-2445-8

Keywords: Electrocatalysis, Formaldehyde, Metal Deposition

De Wetenschepper

Dromend staar ik in de ondergaande zon
Denkend hoe mijn weten ooit begon
Was het de Schepper die mijn weten schiep naar Zijn beeld?
Of was het mijn mensengeest die het weten had gewild?

Een vogel stijgt op in het licht van de zon
Daar waar het weten ooit begon
Ik voel zijn vleugels van warm licht
Mij wijs omarmen in het zicht

Het wijze licht en mijn weten smelten saam
Daar waar het weten ooit begon in Zijn naam
Ik schreeuw't eureka, ben slechts bij geloven gebaat
Om te kunnen scheppen, mijn weten van de dageraad

Marnix ten Kortenaar

Contents

List of Abbreviations and Symbols

Abbreviations

DEMS	Differential Electrochemical Mass Spectrometry
EIS	Electrochemical Impedance Spectroscopy
OCP	Open Circuit Potential
RDS	Rate-determining Step
SCE	Saturated Calomel Electrode
CPE	Constant Phase Element
PMT	Photon Multiplier Tube
IHP	Inner Helmholtz plane
OHP	Outer Helmholtz Plane
KIE	Kinetic Isotope Effect

Constants and Variables

K*	Calibration constant of the mass spectrometer [-]
n	Number of transferred electrons [-]
Γ	Concentration of adsorbed ions at the surface [mol cm^{-2}].
C	Concentration of adsorbate in the bulk solution [mol dm^{-3}]
μ_s	Linear absorption coefficient of ß-radiation in water [cm^{-1}]
R	The roughness factor of the electrode surface [-]
x	Gap thickness between electrode and the foil on the glass scintillator [cm]
F_b	Backscattering factor [-]
Z	Atomic number [-]
λ	Linear absorption coefficient [cm^{-1}]
E_{act}	Apparent activation energy [kJ mol^{-1}]
A	Real surface area [cm^2]
δ	Thickness diffusion layer [cm]
D	Diffusion constant [cm^2 s^{-1}]
C	Bulk concentration [mol dm^{-3}]
C_s	Surface concentration [mol cm^{-2}]
R_N	Natural gas constant [J mol K^{-1}]
F	Faraday constant [C mol^{-1}]
α	Electrochemical transfer coefficient [-]
I_f	Faraday current [mA]
I_{ion}	Current due to deionisation in DEMS measurements [mA]
N_s^{up}	Count rate of solution and adsorbate with electrode in 'up' position. [cps]
N_s^{d}	The net counting rate with the electrode in the down position [cps]
$\Delta V(\omega)$	Sinusoidal voltage perturbation [V]
$\Delta I(\omega)$	Sinusoidal current response to voltage perturbation [mA]

N_{ads}	Net counting rate of adsorbate with electrode in the 'down' position [cps]
KIE	Kinetic isotope effect [-]
E_{act}	Apparent activation energy [kJ mol^{-1}]
τ	General residence time [s]
τ_c	Residence time of species in the chemisorbed state [s]
τ_p	Residence time of species in the physisorbed state [s]
τ_s	Residence time of species in the solution [s]
τ_i	Residence time of species in the irreversible sink state [s]
Q	Quantity of species in a specific state [nmol]
Q_c	Quantity of species in the chemisorbed state [nmol]
Q_p	Quantity of species in the physisorbed state [nmol]
Q_s	Quantity of species in the solution [nmol]
Q_i	Quantity of species in the irreversible sink state [nmol]
q	General quantity of radio-labelled species in a specific state [nmol]
R	Resistance [Ω]
C	Capacitor [F]
Y_o	Time-independent diffusion element [s]
B	Time-dependent diffusion element [s Ω^{-1}]
$Z_O(\omega)$	Finite diffusion layer impedance [Ω]
$Z_w(\omega)$	Warburg impedance [Ω]
$\Delta V(\omega)$	The voltage perturbation [V]
$\Delta I(\omega)$	The current response to the voltage perturbation [mA]
ε_o	Dielectric constant in vacuum [-]
ε_r	Dielectric constant of the specific medium [-]
Q_{dl}	Charge at the double layer [C]
ΔG_{ad}	Gibbs free adsorption energy [kJ mol]
ΔH_{ad}	Adsorption enthalpy [kJ mol]
ΔS_{ad}	Adsorption entropy [kJ mol]
$\Delta H_{M(HCOO)n}$	Metal-formate formation enthalpy [kJ mol]
θ	Normalized surface coverage [-]
$Z_{IHP}(\omega)$	Impedance associated with the IHP [Ω]
$Z_{OHP}(\omega)$	Impedance associated with the OHP [Ω]
M	Atomic mass [-]
L	Average inter-atomic bond length [nm]
q	Radiolabeled quantity of species in a specific state [nmol]
Z_{re}	Real impedance [Ω]
Z_{im}	Imaginary impedance [Ω]
x	

Chapter 1

General Introduction

The electrocatalytic oxidation of formaldehyde on transition metals has been studied extensively over the past decades in view of its application in electroless metal deposition. Most studies have focussed on the elucidation of reaction mechanisms although little effort has been made to describe the reaction kinetically. The kinetics of the catalytic reaction may depend on the metal-reactant adsorption enthalpies in a volcano-type fashion, a dependence that is generally assumed to validate the so-called Sabatier principle. This principle states that optimum catalytic properties arise at optimum surface coverage of reactants at the catalyst and at optimum metal-reactant bond strengths. The verification of the volcano-type dependence and the related validation of Sabatier's principle for the metal-formaldehyde system was the scientific motivation to conduct the research described in this thesis. To arrive at this stage, the kinetics of the oxidation of formaldehyde was studied first on gold by voltammetry, electrochemical impedance spectroscopy and differential electrochemical mass spectrometry (Chapter 3 and 4). Then, the adsorption characteristics of the formaldehyde-gold system were examined by the radiotracer thin-gap technique (Chapter 5). The models that resulted from these studies have served as springboard for the comparison of reaction rates on other metals than gold (Chapter 6 and 7). Experimental methods are given in Chapter 2, while a summary of related work that was considered to be beyond the scope of this thesis is described in Chapter 8. Final discussions and recommendations are drawn up in Chapter 9.

1.1 Introduction

Catalysis refers to the area of science and technology that uses substances, called catalysts, which change the mechanism and kinetics of a reaction without changing the thermodynamics of that reaction.[1] The first reports on catalysis go back to 1796 when von Marum described the dehydrogenation of alcohols using metals but it was not until 1836 before Berzelius defined this area of science as catalysis.[2] Today, an estimated one-sixth of all manufactured goods in industrialized countries are made using catalysts with thirteen of the top twenty synthetic chemicals being produced directly or indirectly by catalytic processes.[1] Generally, catalysis is thereby classified as homogeneous catalysis if the catalyst is present in the same phase as the reagents, as heterogeneous catalysis if it is in a different phase, and as electrocatalysis when an electrical potential difference exists across the catalyst-reactant interface.[1-4]

The virtue of catalysts to promote reaction rates results from their role as substrate in the adsorption of reactants and products, a view that was set out by Sabatier in 1912.[1,2,4] A volcano-type relationship was reported for the dependence of the metal-dependent rates of ethene hydrogenation on the metal-reactant adsorption enthalpies, which led to Sabatier's principle, implying that optimum catalytic reaction rates arise at optimum surface coverage of reactants and at optimum metal-reactant bond strengths.[1,2,4-6] The principle is widespread in heterogeneous catalysis today, although the derivation of the principle from volcano-type relationships in electrocatalyis may be disputed, as it goes along with some poorly verified implicit assumptions:

- The contribution of the entropy to the Gibbs free adsorption energy is neglected, as the principle is settled on volcano-plots that use adsorption enthalpies rather than Gibbs free adsorption energies.
- The optimum adsorption heat in the volcano-type relationship is assumed to reflect an optimum surface coverage, an optimum bond strength and (often) an optimum residence time of reactants at the surface as well.[2,4]
- The contribution of solution effects in the thermodynamics and kinetics of the adsorption process is neglected, as volcano plots generally employ adsorption enthalpies obtained from the gas-phase or thermodynamic heats of formation.[3,6,7,9,10]

One of the main reasons for the absence of a profound empirical base for Sabatier's principle in electrocatalysis seems associated with the difficulties to determine the *in-situ* values of the adsorption enthalpy, the surface coverage and the residence time of species at the catalytic surface.[11] These values cannot be determined by conventional electrochemical techniques but an attempt has been made in this thesis by using the radiotracer thin-gap technique in combination with electrochemical impedance spectroscopy (EIS), voltammetry and differential electrochemical mass spectrometry (DEMS).[12,13] The oxidation of formaldehyde on transition metals has been chosen as

model reaction for three reasons: First, the mechanism is relatively simple and well understood, enabling a better focus on the kinetic and thermodynamic aspects of the reaction.[14] Second, the reaction has great practical relevance in the area of electroless metal deposition. Enhanced insight into the metal-dependent kinetics of the reaction seems for instance particularly interesting in the improved control of small-dimensional, selective plate processes.[14,15] Third, the required isotopic-labelled forms of formaldehyde ($^{14}CH_2O$ and CD_2O) are easily available and suitable to the radiotracer thin-gap technique.[14-16]

As most knowledge on the formaldehyde-metal system comes from studies related to electroless metal deposition, this Chapter will commence by addressing the role of formaldehyde in these processes. Then, the mechanism of the oxidation of formaldehyde is discussed, followed by a brief overview of techniques and methods used to describe the kinetics and thermodynamics of the reaction. The discussion is followed by a summary of literature on volcano-type relationships and an analysis of empirical conditions that would allow the validation of Sabatier's principle for the transition metal-formaldehyde system. Finally, the work preceding this thesis is chronologically overviewed and the scope of this thesis is given.

1.2 Electroless Plating

Background - Electroless metal deposition (or plating) is an autocatalytic process by which metals can be deposited from a solution without the use of an external electrical current.[14,15] The metal ions and the reducing agent are both supplied from the same solution, making the process applicable to conductive and non-conductive substrates. Well-known examples of industrial electroless plating processes refer to the nickel plating of car parts or the copper plating of printed circuit boards in microelectronics.[17,18] The relatively cheap and simple way of plating still makes it a growing process in industry although difficulties with the kinetic control of selective, small-scale plate processes have limited the application in ultra large-scale integration (microelectronics).[18-25]

The art of electroless plating is to run the reaction between the metal ions and the reducing agent at the substrate while suppressing it to occur in the solution. This may be achieved by choosing the right combination of the metal ion and the reducing agent as well as by using complexing agents like EDTA. The latter prevents the direct reaction between the reducing agents and the metal ions in solution. Initiation of the metal deposition process can be achieved by using a metallic substrate that induces the adsorption of the reducing agent and subsequent deposition of at least one monolayer of metal atoms. Propagation may then occur in an autocatalytic fashion, provided that the deposited metal layer catalyses the adsorption and oxidation of the reducing agent as well. Metals that can be plated by electroless plating (sometimes referred as electroless metals)

are: Cu, Ni, Au, Ag, Pt, Ir, Pd, Ru, Rh, Cd, Sn, Pb, Sb, Bi, In and Co. Most of these metals are transition metals and are known as good dehydrogenation catalysts.[8,26,27] Examples of well-known reducing agents are formaldehyde, sodium borohydride, dimethylamine borane, hydrazine and sodium hypophospite.[14,15,17]

Kinetics - The kinetics of electroless plating may be understood in terms of the mixed potential theory. In this theory, the plate potential or open circuit potential (OCP) is the potential where the oxidation reaction balances the reduction reaction (Figure 1):[15,28]

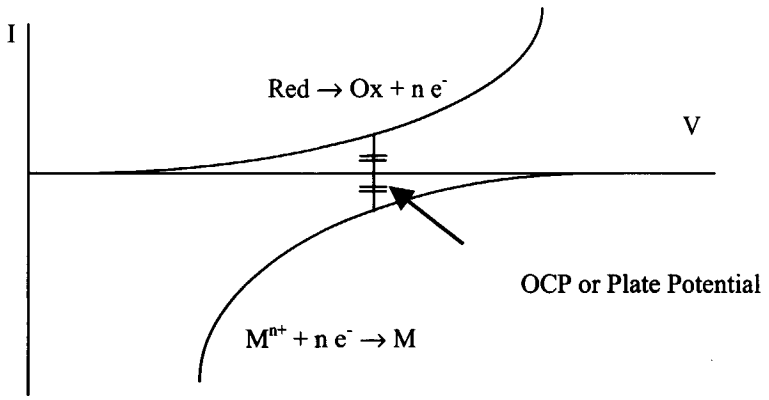

Figure 1. ***Electroless plating: A reducing agent is oxidized at a catalytic substrate. Released electrons are consumed by metal ions that are deposited.***

The rate of plating may be predicted from the theoretical values of the cathode and anode current at the OCP.[14,15] When the space between the anodic and cathode voltammograms at the OCP is large, the rate of plating is high; when it is small, the rate of plating is low. Hence, the shape of both voltammograms determines the deposition rate and the plate potential under plating conditions. This shape may be calculated using the classical Butler-Volmer equation (or Tafel equation) although this approach would be limited, as it assumes electron-transfer controlled reaction rates, an assumption that may still apply to the reduction of metal ions, but not to the catalytic oxidation of formaldehyde.[15,28-30] The rate of the latter is likely to have a catalytic, more chemical character, as witnessed by the relatively high values of the activation energies and the strong dependence of the rate on the chemical potential (catalyst, temperature, pH etc.).[8,31-36]

1.3 Reaction Mechanism

The oxidation of reducing agents applied in electroless metal deposition has been studied in view of its key role in the overall rate of plating.[14,15,17] A summary of these studies was made by van den Meerakker *et al.* in 1980, concluding that only one mechanism may describe the oxidation of any reducing agent on any metal applied in

electroless metal deposition.[26,27] As this mechanism is the most cited one in literature, and as it was confirmed for the electro-oxidation of formaldehyde in a range of more recent studies, the basic equations of the mechanism are summed up.

In aqueous solution formaldehyde exists as the gem-diol, which may ionise in alkaline to form the electro-active enolate anion:[37,38]

$CH_2(OH)_2 + OH^- \leftrightarrow CH_2OHO^- + H_2O$ [1] (Ionisation)

The presence of CH_2OHO^- was confirmed by UV spectroscopy with an absorption band at 215 nm.[38] The pK_a of the gem-diol is high under the conditions examined in this thesis (pK_a ~13) and the pH of the solution may be assumed to have a constant value, as the weakly acidic gem-diol is ionised by the strongly alkaline NaOH.[34,35,37,39] The oxidation of the enolate anion may proceed in various steps: First, the ion diffuses to the electrocatalytic surface, followed by the successive physisorption and chemisorption. The chemisorbed intermediate is oxidized to formate, yielding an electron and atomic hydrogen. Adsorbed hydrogen may react to molecular hydrogen, or react with hydroxyl ions to water and a second electron. Released electrons may be consumed by metal ions (electroless plating) or transferred to the electrode surface (electrocatalysis):[8,26,27,31-35,40-44]

$CH_2OHO^- \leftrightarrow CH_2OHO^-_{surface}$ [2] *(Diffusion)*

$CH_2OHO^-_{surface} \leftrightarrow CH_2OHO^-_{phys}$ [3] *(Physisorption)*

$CH_2OHO^-_{phys} \leftrightarrow \bullet CHOHO^-_{ad} + \bullet H_{ad}$ [4] *(Chemisorption))*

$\bullet CHOHO^-_{chem} + OH^- \rightarrow HCOO^- + H_2O + e^-$ [5] *(Oxidation, Desorption)*

$\bullet H_{ad} + \bullet H_{ad} \rightarrow H_2\uparrow$ [6] *(Hydrogen Evolution)*

$\bullet H_{ad} + OH^- \rightarrow H_2O + e^-$ [7] *(Oxidation, Desorption)*

Clearly, an intricate mechanism is under study, and some aspects of it are still under discussion. However, for the moment it is assumed to be correct and it will serve as base for the discussion of data in this thesis. This assumption will turn out to be reasonable, as shown later in this thesis.

1.4 Radiotracer Thin-Gap Technique

Methodology - As mentioned, the absence of an extensive study on the basis of Sabatier's principle in electrocatalysis seems associated with the limitations of conventional electrochemical and spectroscopic techniques to determine the values of the adsorption enthalpies and the times of residence of species at the catalytic surface. A solution may nevertheless come from the use of the radiotracer thin-gap technique.[12,45] This technique is based on a press-down and pull-up procedure of a flat electrode to and from a flat glass scintillator. It enables the *in-situ* registration of the quantity of radioactive species adsorbed on the electrode under equilibrium and non-equilibrium conditions (steady state and dynamic state) as well as the simultaneous measurement of the oxidation rate and surface coverage.[10,46,47] Another beneficial feature refers to the ability to verify the

presence of a clean metal surface by comparing the voltammograms recorded in conventional electrolytes with those reported in literature. Although any flat surface can be used as substrate, adsorption studies are restricted by the availability of soft-β emitting and α-emitting radionuclides.[48]

Compartimental Analysis - The adsorbed quantities obtained from the radiotracer measurements may be fitted by compartimental analysis to obtain values for the residence times of species at the catalytic surface.[49,50] Compartimental analysis conceives the adsorption process by pseudo-stable states, called compartments, which are interconnected by mass flows. Derivation of the best fitting compartmental model is performed in two steps: First, the number of compartments required to describe the data properly is derived from the number of exponents used to fit the adsorption kinetic curves.[49-51] Then, the sets of first order linear differential equations for each model with the determined number of compartments are derived and fitted to the data. Rate constants, intercompartment flows and times of residence are obtained from the best fitting set of equations.

Thermodynamic Energies - Assuming Langmuir-conditions at low adsorbate concentrations, the values for the respective Gibbs adsorption energies, the adsorption enthalpies, and the adsorption entropies can be derived from the initial slopes of the adsorption isotherms at different temperatures by linear least square fitting.[51]

Complementary Insight - A shortcoming of the radiotracer thin-gap technique is that determination of values kinetic parameters occurs in a non-direct fashion from modelling of the adsorption and exchange data. The first order set of mathematical differential equations is thus assumed to describe the real transport processes well.[49,50] To meet this limitation, and to gain an unprejudiced, kinetic view of the formaldehyde oxidation reaction, complementary techniques like DEMS, EIS and Voltammetry have been used in this thesis.[52-55] The use of equivalent circuit fitting procedures for the description of electro-organic oxidation EIS data had not been reported before at the time this thesis was written. A similar comment applies to the use of compartimental analysis for the description of kinetic adsorption data in electrocatalysis.

1.5 Volcano-type Relationships

Heterogeneous Catalysis - A practical example of a well-known volcano-type relationship in heterogeneous catalysis refers to the dependence of the transition metal-variable rate of decomposition of formic acid (with a structure closely related to that of formaldehyde) on the metal-reactant adsorption heats.[56] The volcano plot shows a maximum for platinum, iridium and palladium, a left-wing tail for silver and gold, and a right-wing tail for nickel and copper. The location of metals in the volcano plot cannot be correlated with valence states or atomic numbers given in the periodic Table, as tails and

peaks of the volcano do not coincide with the groups or periods of the periodic Table. Other entities like atomic orbitals or work functions may therefore be taken into consideration to understand the location of the metals in the volcano plot.

Electrocatalysis - A well-known volcano-type relationship in electrocalysis refers to the dependence of the potential of hydrogen evolution in acid solution on the metal-hydrogen adsorption enthalpies at a current density of 1 $mAcm^{-2}$.[45,57] This dependence shows a maximum for palladium and platinum, a right-wing tail for silver, nickel, gold and palladium, and a left-wing tail for metals like gallium and mercury. The data points for the metals applied in electroless plating are nevertheless roughly located in a straight-line fashion. This observation is roughly in concordance with the curved dependence of the exchange current density of hydrogen evolution in acid solution on the metal-hydrogen adsorption enthalpies (Figure 2).

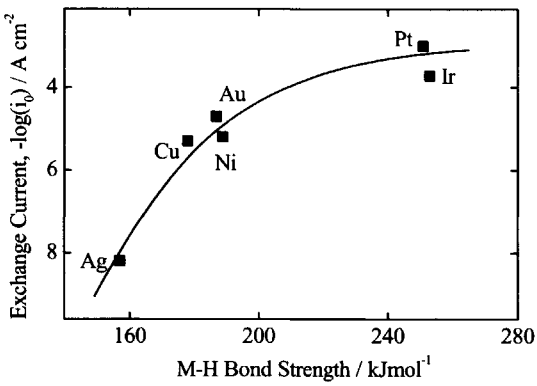

Figure 2. *Exchange currents for electrolytic hydrogen evolution versus strength of intermediate metal-hydrogen bond formed during the electrochemical reaction.*

The relation in Figure 2 nevertheless contradicts observations made in alkaline solutions by Bindra *et al.*[8] The latter group made a categorisation of metals from group VIII and IB according to hydrogen adsorption energies and compared these with the formaldehyde oxidation rates in alkaline solutions. Three types of metals were proposed, with the metals relevant for this thesis set in brackets:[8]

- Metals from group IB with positive free energies of hydrogen adsorption, characterised by the evolution of hydrogen during the oxidation of formaldehyde (Cu, Au, Ag).

- Metals from group VIII with free energies of hydrogen adsorption close to zero, characterised by the absence of hydrogen evolution during the oxidation of formaldehyde (Pd, Pt, Ir).
- Metals from group VIII with negative free energies of hydrogen adsorption characterised by a low catalytic activity for the oxidation of formaldehyde (Ni).

Metal-Formaldehyde System - Only one report has addressed the presence of a volcano-type relationship for the dependence of the formaldehyde electro-oxidation rates on the metal-formate formation enthalpies.[8] Platinum and palladium were found as peak of a rough volcano with gold and silver tailing left wing, and copper and nickel tailing right wing (Figure 3).

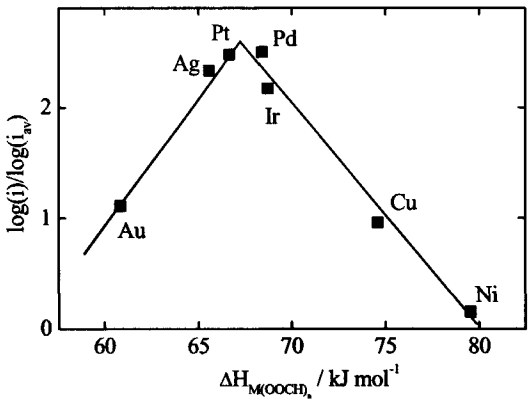

Figure 3. *Volcano plot for the dependence of the relative rate of oxidation of formaldehyde (0.1 M) in NaOH (1.0 M) on the metal-formate formation enthalpies.*

The scientific relevance of this volcano for the data presented in this thesis may nevertheless be disputed, as rates relative to the average rates were presented that were obtained at pH-values different to those employed in this thesis. Besides, data were obtained under non-steady state conditions, at undefined potentials and metal-formate formation enthalpies were taken rather than adsorption enthalpies.[8] However, the results do roughly correlate with those discussed above for the heterogeneous catalytic rate of decomposition of formic acid on transition metals. Namely, three similar groups may be recognized in both volcano's: Ag and Au as left-wing tail, Pt, Ir and Pd as top, and the less noble Cu and Ni as right-wing tail.

1.6 Sabatier's Principle

As mentioned, Sabatier's principle states that optimum catalytic reaction rates arise at an optimum surface coverage of reactants and at an optimum metal-reactant bond strength.[58] The principle is based on a relationship between a kinetic observable (reaction rate) measured under non-equilibrium conditions and a thermodynamic property that applies under equilibrium conditions (adsorption enthalpy). Contemplating the criteria for the validation of the principle in the electrocatalytic oxidation of formaldehyde on transition metals, brings up the following four empirical conditions:

1) The metal-dependent formaldehyde oxidation rate (i) should depend on ΔH_{ad} or (ΔG_{ad}) in a volcano-type fashion.
2) Values of ΔH_{ad} approach those of ΔG_{ad} in order to allow the derivation of Sabatier's principle from a volcano that uses adsorption enthalpies (ΔH_{ad}).
3) Values of ΔG_{ad} or ΔH_{ad} in the gas-phase should approach those in the liquid phase in order to allow the use of adsorption energies obtained in the gas-phase.
4) Values of ΔG_{ad} have to correlate with the residence times of species at the surface (τ) and with the surface quantities (Q).[58]

The latter condition in turn assumes the absence of multilayer adsorption and the validity of Eyring's generally accepted picture of fixed and time-invariant potential fields with transition states being in equilibrium with thermodynamic minima.[7]

1.7 Chronological Overview of Work preceding this Thesis

Original Approach - In the original approach to meet the objective for this thesis, it was planned to study adsorption and exchange rates on transition metal colloids (rather than on electrodes) by using radiotracer-experiments and compartmental analysis. The colloids were chosen as substrates, as previous similar studies were successfully made using cadmium-sulphide colloids, and as electroless plating occurs at surfaces that are not polarized externally as well.[59] Attempts were therefore made to prepare pure, monodisperse and small transition-metal colloids, as these would offer high, relatively well-specified, surface areas and a minimised interference between the adsorption of chemical agents and reducing agents. The electric dispersion of silver wires, as described for the first time by Ritter for tellurium already in 1808, was applied first to meet these goals.[60] Surprisingly, the resulting dispersions contained sub-nanometre sized clusters that remained stable for weeks. An extensive study was made next of the dispersion mechanism, the formation of the particles and the stability of the sub-nanometre sized silver clusters. Related to these studies, a new method was further developed that enabled selective silver-plating of silicon structures in the lowest dimensions reported ever for the deposition of metal from aqueous solutions. The pictures on the cover of this thesis is an example of this process, showing the selective silver deposition of 100 nm wide lines

(written as 'TUDelft') at an aspect ratio of 4.25. Three publications resulted from these studies, which are summed up in more detail in Chapter 8.

To still verify Sabatier's principle for the metal-formaldehyde system, attempts were made to study the adsorption of [^{14}C]-labelled formaldehyde on silver colloids that had been prepared by anodic dispersion. Various quantities of [^{14}C]-labelled formaldehyde were added to different colloidal dispersions, each settled for different periods of time. Particles were then separated from the solution by ultra-centrifugation and/or ultra-filtration, followed by measuring the particle-free solutions on radioactivity by liquid scintillation counting. However, no reproducible decreases in radioactivity with increasing amounts of formaldehyde were obtained. Similar unsatisfactory results were obtained later for silver and gold sols prepared by chemical reduction. Most likely, the coalescence of colloids upon the addition of formaldehyde accounted for the fruitless attempts, as the colour of the sols changed with increasing amounts of formaldehyde.

Modified Approach – During the colloidal studies the radiotracer thin-gap technique described by Wieckowski *et al.* was considered as a better alternative, as it measured adsorption on defined surfaces in a straightforward *in-situ* fashion. However, as some concerns also existed on the possible low signal for the formaldehyde-transition metal system related to the relatively small electrode surface areas employed for this technique, it was decided to run some test experiments at the facilities of Wieckowski (University of Illinois). Successful adsorption measurements were obtained within a month in the USA. A dedicated set-up was built in Delft, which took approximately one year. It went along with some other experimental studies described in this thesis. Studies on silver particles and plating were finished off after the radiotracer thin-gap technique had been constructed.

1.8 Scope and Survey of this Thesis

The following issues have been defined as the final scope of this thesis:

- Elucidation of adsorption kinetics, reaction kinetics and thermodynamics of the formaldehyde-electro-oxidation reaction on different transition metals under different conditions.
- Demonstration of the added value of EIS using equivalent circuit fitting procedures and the radiotracer thin-gap technique in the study of an electrocatalytic oxidation reaction.
- Verification of the presence of a volcano-type relationship for the metal-formaldehyde system and verification of the validity to derive Sabatier's principle from this relationship.

To meet these goals, the mechanism, kinetics and thermodynamics of adsorption and oxidation have been elucidated on gold at different pH-values, concentrations and

temperatures first (Chapter 3-5). Then, the influence of the metals and their physical properties on the kinetics of the reaction has been discussed (Chapter 6). The view acquired from these studies has been used to discuss the outcome of the radiotracer adsorption studies on transition metals other than gold (Chapter 7). Experimental details have been given in Chapter 2, while a summary of work that was considered to be beyond the scope of this thesis is presented in Chapter 8. Final discussions and recommendations are drawn up in Chapter 9.

1.9 References

(1) Shriver, D. F.; Atkins P. W.; Langford, C. H.; in *Inorganic Chemistry*, Oxford University Press, 1st edition, Oxford, UK, 1990, p 542.

(2) Stoltze. P.; in *Introduction to heterogeneous catalysis*, Technical University of Denmark, Denmark, 2002, p 2.

(3) Bockris, J. O. M.; Khan, S. U. M.; In *Surface Electrochemistry*, Plenum Press, New York and London, (1993), p 290.

(4) Peereboom, M.; Frens, G.; In *Reactiekinetiek*, Delftse Uitgevers Maatschappij, Delft, The Netherlands, 1992, p 37.

(5) Norskov, J. K.; Bligaard, T.; Logadottir, A.; Bahn, S.; Hansen, L. B.; Bollinger, M.; Bengaard, H.; Hammer, B.; Sljivancanin, Z.; Mavrikakis, M.; Xu, Y.Dahl, S.; Jacobsen, C. J. H.; *J. of Catalysis,* **2002**, 209, 275-278.

(6) Knor, Z.; *Applied Catalysis A: General*, **2003**, 245, 185-189.

(7) Laidler, K. J.; Meiser, J. H.; in *Physical Chemistry,* Houghton Mifflin Company, 1995, p 382.

(8) Bindra, P.; Roldan, J.; *J. Electrochem. Soc.*, **1985**, 132, 2582.

(9) See ref. (3), p 247.

(10) Christensen, P. A.; Hamnett, A.; In *Techniques and Mechanisms in Electrochemistry*, Chapman & Hall, 1994, p 6.

(11) See ref. (3), p 2.

(12) Krauskopf, E. K.; Chan, K.; Wieckowski, A.; *J. Phys Chem.*, **1987**, 91, 2327.

(13) MacDonald, J. R.; In *Impedance Spectroscopy*, Chapter 4, John Wiley & Sons, New York, 1987, p 41.

(14) Paunovic, M.; In *Electrochemistry in Transition*; Murphy, O. J., Srinivasan, S., Conway, B. E., Eds.; Chapter 30, Plenum Press, New York, 1992, p 479.

(15) Okinaka, Y.; Osaka T.; In *Advances in Electrochemical Science and Engineering*; Gerischer, H., Tobias, C. W., Eds.; Vol. 3, VCH Publishers Inc., New York, 1994, p 55.

(16) Jusys, Z.; *J. Electroanal. Chem.*,**1994**, 375, 257.

(17) Kuzmik, J. J.; In *Electroless Plating*; Hajdu, J. B., Mallory, G. O., Eds.; Chapter 14, American Electroplaters and Surface Finishers Scoiety, Orlando, 1990, p 377.

(18) Shacham-Diamand, Y.; Sun, B.; Yip, V.; Bielski, R.; In *The Electrochemical Society Proceedings*; Vol. 94-31, 1994, p 136.

(19) Kortenaar, M. V. ten; Goeij, J. J. M.; Kolar, Z. I.; Frens, G.; Lusse, P. J.; Zuiddam, M. R.; Drift, E. van der.; *J. Electrochem. Soc.*, **2001**, 148, C28.

(20) Shacham-Diamand, Y.; *J. Micromech. Microeng.*, **1991**, 1, 66.

(21) Cho, J. S. H.; Kang, H. K.; Wong, S. S.; Shacham-Diamand, Y.; *MRS Bulletin*; June **1993**, 31.

(22) Putten, A. M. T. van der; Bakker, J. W. G. de; *J. Electrochem. Soc.*, **1993**, 140, 2221.
(23) Ting, C. H.; Paunovic, M.; *J. Electrochem. Soc.*, **1989**, 136, 456.
(24) Ting, C. H.; Paunovic, M.; Pai, P. L.; Chiu, G.; *J. Electrochem. Soc.*, **1989**, 136, 462.
(25) Brandow, S. L.; Dressick, W. J.; Marrian, C. R. K.; Chow, G. M.; Calvert, J. M.; *J. Electrochem. Soc.*, **1995**, 142, 2233.
(26) Meerakker, J. E. A. M. van den; *J. Appl. Electrochem.*, **1981**, 11, 387.
(27) Meerakker, J. E. A. M. van den; *J. Appl. Electrochem.*, **1981**, 11, 395.
(28) Ohno, I.; In *Electroless Deposition of Metals and Alloys*, M. Paunovic, I. Ohno, Editors, Proceedings Vol. 88-12, The Electrochemical Society, Pennington, New Jersey, 1988, p 129.
(29) Gileadi, G.; in *Electrode Kinetics*, VCH Publishers, New York, 1993, p 8.
(30) See ref. (3), p 8.
(31) Ohno, I.; Wakabayashi, O.; Haruyama, S.; *J. Electrochem. Soc.*, **1985**, 132, 2323.
(32) Beltowska-Brzezinska, M.; *Electrochim. Acta*, **1985**, 30, 1193.
(33) Enyo, M; *J. Appl. Electrochem.*, **1985**, 15, 907.
(34) Kortenaar, M. V. ten; Kolar, Z. I.; Goeij, J. J. M. de.; Frens, G.; *J. Electrochem. Soc.*, **2001**, 148, 1.
(35) Kortenaar, M. V. ten; Tessont C.; Kolar, Z. I.; Weijde, H. van der.; *J. Electrochem. Soc.*, **1999**, 14, 2146.
(36) See ref. (3), p 577.
(37) Walker, J. F.; In *Formaldehyde*, Reinhold Publ. Corp., New York, 3rd edition, 1964, p 214.
(38) Avramov-Ivic, M. L.; Adzic, R. R.; Bewick, A.; Razaq, M.; *J. Electroanal. Chem*, **1988**, 35, 725.
(39) Meerakker, J. E. M van den, Scholten, E.; *Ber. Bunsenges. Phys. Chem.*, **1989**, 93, 786.
(40) Beltowska-Brzezinska, M.; *J. Electroanal. Chem.*, **1985**, 187, 167.
(41) Enyo, M; *J. Appl. Electrochem.*, **1985**, 15, 907.
(42) Burke, L. D.; O'Dwyer, K. J.; *Electrochim. Acta*, **1990**, 11, 1829.
(43) Burke, L. D.; O'Dwyer, K. J.; *Electrochim. Acta,* **1990**, 11, 1821.
(44) Avramov-Ivic, M. L.; Anastasijevic, N. A.; Adzic, R. R.; *Electrochim. Acta*, **1990**, 35, 725.
(45) Appleby, A. J.; In *Comprehensive Treatise of Electrochemistry*, Conway, B. E., Yeager, E., Khan, S. U. M., White, R. E., Eds.; Plenum Press, New York, 1983, p 230.

(46) Shi, Z.; Lipkowski, J.; Gamboa, M.; Zelenay, P.; Wieckowski, A.; *J. Electroanal. Chem.*, **1994**, 366, 317.

(47) Horanyi, G.; *Electrochim. Acta.*, **1980**, 25, 43.

(48) Wieckowski, A.; In *Modern Aspects of Electrochemistry no 21*; White, R. E.; Bockris, J. O. M.; Conway, B. E.; Plenum Press, New York, 1990, p 65.

(49) Godfrey, K.; In *Compartmental Models and Their Application*, Academic Press, New York, 1983, p 58.

(50) Shipley, R. A.; Clark, R. E; In *Tracer Methods for In Vivo Kinetics*, Academic Press, New York, 1972, p 45.

(51) Kortenaar, M. V. ten; Kolar, Z. I.; Goeij, J. J. M. de.; Frens, G.; *Langmuir*, **2002**, 18, 10279.

(52) Epelboin, I.; Wiart, R.; *J. Electrochem. Soc.*, **1971**, 118, 1577.

(53) Boukamp B. A.; Equivalent Circuit (Users manual), University of Twente, The Netherlands, 1989.

(54) Keddam, M.; Mattos, O. R.; Takenouti, H.; *J. Electrochem. Soc.*, **1981**, 128, 266.

(55) Epelboin, I.; Gabrielli, C.; Keddam, M.; Takenouti, H.; *Electrochim. Acta*, **1975**, 20, 913.

(56) See ref. (1), p 563.

(57) Gates, B. C.; Katzer, J. R.; Schuit, G. C. A.; In *Chemistry of Catalytic Processes*, McGraw-Hill, New York, 1979, p 112.

(58) Moulijn, J. A.; Leeuwen, P. W. N. M.; Santen, R. A.; in *Catalysis, An Integrated Approach to Homogeneous, Heterogeneous and Industrial Catalysis*, Elsevier Science Publishers B. V., Amsterdam The Netherlands, 1993, p 83.

(59) Hövell van Wezeveld en Westerflier, S. W. F. M.; Interfacial Cadmium Exchange in Equilibrated Aqueous Suspensions of Cadmium Sulphide: *A Compartimental Analysis Assisted Radiotracer Study*, PhD Thesis, TU Delft, The Netherlands, 1990.

(60) Ritter, J. W.; *J. Chem. Phys.*, **1808**, 5, 439.

Chapter 2

Techniques, Methods, Experiments

The techniques, methods and experiments used to collect the data for this thesis are discussed. Electrochemical impedance spectroscopy (EIS) was applied to obtain a qualitative view of the rate of oxidation of formaldehyde on gold in alkaline solutions. Fitting of the data was performed by so-called equivalent-circuit procedures. Voltammetry and chronoamperometry were applied to derive the apparent activation energies (E_{act}) and kinetic isotope effects (KIE) of the reaction. The gas evolution properties of the system were addressed by differential electrochemical spectroscopy (DEMS), while the adsorption kinetics and thermodynamics were addressed by the radiotracer thin-gap technique. The kinetic and thermodynamic aspects were examined first on gold at different pH-values, concentrations and potentials. Then, the composition of the solution was held constant and the reaction was studied on transition metals other than gold.

2.1 General Approach

To extend the qualitative mechanistic description given in Chapter 1 to a quantitative kinetic model, the effect of the partial reaction steps in the overall rate of oxidation of formaldehyde on transition metals were studied. Different techniques and methods were used to meet this goal.[1,2] The identification of the rate-determining step (RDS) and its dependence on both the metals and the composition of the solution was of special relevance, as it was considered to rule the overall rate of plating.[3-7] The choice of techniques, methods and conditions was based on the mechanism presented in Chapter 1 and the most important underlying consideration are summed up below:

Techniques - To confirm the occurrence of (Step [1]) of the mechanism, some redox titration's were carried out using KI as oxidising agent.[8] The influence of diffusion (Step [2]) was studied using a rotating disc electrode by voltammetry and EIS. Physisorption and chemisorption (Step [3] and Step [4]) were examined by the radiotracer thin-gap technique and compartimental analysis. The formation of formate and water (Step [5] and Step [7]) was studied using voltammetry and EIS. Moreover, differential electrochemical mass spectrometry (DEMS) was applied to study the hydrogen-evolution characteristics and to confirm the view that no CO_2 forms at lower overpotentials.[9,10]

Conditions - Rates were determined at different pH-values in order to gain insight into the importance of Step [5] and Step [7] in the overall rate of the reaction, as these steps depend on the pH by stochiometry. Besides, the concentrations of the reactants and the temperatures were varied in order to determine the respective adsorption isotherms, the reaction orders and the activation energies (E_{act}) of the system. Moreover, rates were studied at different potentials and at different scan rates in order to see if rates had a faradic, diffusive or capacitive character.

Kinetic Isotope Effects - Insight into the relative importance of Step [4] through Step [7] in the overall reaction kinetics was obtained by determining the kinetic isotope effects (KIE) under conditions where Step [1] through Step [3] were known to play a minor role in the overall rate of the reaction. A value of the KIE of ~7 was reasonably assumed to reflect a rate-limiting role of the C-H bond rupture in the overall reaction kinetics (Step [4]).[5,11] A value of 1 indicates a major role of formate (Step [5]), as no rupture of hydrogen bonds are involved in this step. A value lower than one was assumed to reflect a major role of the desorption of molecular hydrogen or water (Step [6]) and/or Step [7]), as further discussed in Chapter 4.[5,11]

Activation Energies - Quantitative insight into the catalytic impact of the metal surface and surrounding molecules on the rate of the reaction was obtained by bearing in mind that the value of E_{act} for a non-catalytic, rate-limiting C-H bond rupture step is metal invariable and equal to the dissociation energies of C-H and C-D (338.1 kJ mol^{-1} and 341.4 kJ mol^{-1} respectively).[12] Moreover, an electrochemical reaction with a rate-limiting

electron transfer step may be characterized by a value of the KIE of 1 and a value of the E_{act} that depends on the potential applied in a linear fashion.[13] In addition, the value of the E_{act} is positive when the rate of the reaction increases at increasing temperatures and negative when the rate of the reaction decreases at increasing temperatures. Note, that a negative activation energy calculated from the Arrhenius equation implies the presence of a so-called pre-equilibrium in the reaction (rather than a large influence of the entropy in E_{act}), as the Arrhenius slope depends only on the enthalpy of activation.

Influence of the Metal Catalyst - The influence of the metal catalyst on the rate of the reaction has been studied by measuring the current response for the oxidation of formaldehyde on various metals by voltammetry. Two different reaction pathways may lead to desorption of adsorbed hydrogen: adsorbed hydrogen may react to molecular hydrogen on copper (by Step [6]), and to water on platinum, iridium, palladium and nickel (by Step [7]). On gold and silver, both reactions may proceed simultaneously. Besides, palladium is not only known as a good adsorbent for hydrogen, but as a good absorbent for hydrogen as well.[3,4,6,14,15,16]

2.2 Electrochemical Impedance Spectroscopy

2.2.1 Background

Electrochemical impedance spectroscopy (EIS) is based on the sinusoidal voltage perturbation of an electrochemical steady-state process with the simultaneous registration of the sinusoidal current response.[17-19] The phase difference and amplitude of the current signal are measured at different input frequencies and contain kinetic and mechanistic information on processes in and at the electrode as well as on reactions proceeding in the solution.[17-21] Data are often plotted in the complex plane (Nyquist diagram) with each data point constructed at the end of a tensor that has a length equal to the current amplitude and an angle relative to the real axis that is equal to the specific phase difference. The sinusoidal voltage perturbation is small and imposed upon the steady-state voltage of the cell, allowing the assumption that the steady-state current depends on the voltage applied in a linear fashion within the voltage range of perturbation.[1,2] Hence, the information extracted from the non-linear current response is assumed to reflect the kinetics of the steady-state process.[17,18,20]

The art of the technique is to extract the right kinetic information from the vast amount of data and the complex Nyquist diagrams. This may be achieved by fitting the data using a transfer function or a so-called electrical equivalent circuit.[17,19,21] In the transfer function approach, the correlation of the reaction mechanism and the kinetic model is made prior to the fitting procedure, whereas in the equivalent-circuit approach this is mainly done after the assessment of the most appropriate circuit.[17,18,22] A disadvantage of the electrical equivalent-circuit approach may be nevertheless that often no straightforward relation

applies between the physical elements of the fitted equivalent circuit and the chemical steps of the reaction.[17-21] The features of the circuit, the relative and absolute value of the elements and their dependencies on relevant system parameters may nevertheless provide insight into the double layer structure and kinetics of the reaction.[22] A circuit that mimics data well may therefore still set a proper base for further elucidation of the reaction by complementary techniques like DEMS, voltammetry and the radiotracer thin-gap technique.[6,7]

As the mechanism for the oxidation of formaldehyde (CH_2O) consists of seven steps, the transfer function approach goes along with a complex derivation of formulas with an associated low reliability and causality of the fits.[19,21] As a consequence, the equivalent circuit approach was chosen. This approach offered the possibility to gain a qualitative unprejudiced view of the reaction kinetics, as over 50 physical models were fitted without assuming one mechanism to be valid a priori.

2.2.2 Qualitative Approach

Realizing that the overall kinetics of the electro-oxidation reaction is ruled by the kinetics of the rate-determining step (RDS), it is important to find out whether this RDS manifests itself as a capacitance, as a resistor or as a diffusive loop. Diffusive behaviour at very low frequencies for instance, is interpreted as a diffusive rate-limiting step under steady-state conditions, and may therefore link up with either Step [1] or a product-related diffusion step.[18] The transport number of OH^- is approximately four times higher than the transport number of formaldehyde and formate. Diffusion steps associated with OH^- may therefore be ruled out, an assumption frequently made.[24,25] A capacitance at low frequencies may correlate with adsorption or desorption steps although still some dispute exists about the origin of negative capacitances (also referred as inductive behaviour).[26-28] Resistive behaviour at low frequencies is usually encountered when faradic behaviour (transfer of an electron in the RDS) applies to the overall kinetics of the reaction. In this case, Tafel behaviour will apply characterized by a linear log i - V relationship.[20]

2.2.3 Materials

The EIS experiments were carried out in a conventional three-electrode glass cell. The working electrode was a gold wire, partly wrapped by teflon tape in order to keep the constant surface area of ~3.1 cm^2 (diameter wire 2 mm, purity 99.99%, Goodfellow, England). The Teflon-taped part of the wire was just held above the meniscus of the solution. A platinum foil counter electrode and a double junction saturated calomel electrode (SCE) were used as counter electrode and reference electrode respectively. The cell and counter electrode were rinsed with perchloric acid (1 M) followed by rinsing with millipore water (Milli-Q system, 18.2 $M\Omega cm^{-1}$) prior to the experiments. The working

electrode was cleaned by rinsing with perchloric acid (1M) and water, followed by polarizing at a potential of -2.0 V *vs.* SCE for 60 s to strip surface impurities.

Solutions were prepared from chemicals of analytical grade (Sigma, Belgium). Both CH_2O and deuterated paraformaldehyde (CD_2O, D quantity >99.0% in formaldehyde, Thamer Diagnostica, The Netherlands) were dissolved by ultrasonic vibration. The exact concentration of CH_2O of three solutions containing 0.1 M NaOH and 0.1 M CH_2O was determined iodometrically as a function of time.[29] Assuming that all paraformaldehyde had dissolved as CH_2O after ultrasonic vibration, the solutions contained 99.6% to 99.8% CH_2O eight minutes after ultrasonic vibration and did not decrease by more than 1.6 % over the period of an impedance measurement (~24 hours). As the impure character of the formaldehyde solutions is generally encountered in practical plating processes as well, no attempts were made to further purify the solutions and concentrations were assumed constant over the period of a measurement.[29-31]

2.2.4 Methods

The steady-state V-i curves were recorded using a scanning potentiostat (EG&G, PAR, type 363). Potentials were stepped at 25 mV and currents were measured when the current remained approximately constant (remaining within 5 μA for at least 30 s). No gas was bubbled through the cell to minimize evaporation of the volatile formaldehyde. Impedance spectra were recorded using a Solartron 1255 HF frequency response analyzer connected to a Solartron electrochemical interface (type 1286). Data acquisition and control of the set potentials was performed using the ISIS computer program.[32] Potentials were chosen slightly positive of the open circuit potential (OCP), as these conditions approached those in practical electroless solutions most satisfactorily, and as side-reactions do virtually not occur under these conditions.[18-20]

Spectra recorded at an AC voltage of 5 mV showed strong noise at low frequencies and the AC perturbation was therefore set at 15 mV. Measurements were performed in triplicate at each potential in the frequency range between 1 mHz and 60 kHz, after conditioning the current at each potential step for 300 s. The spectra presented in this thesis are the third spectrum measured each time, although no significant differences were seen between the triplicate spectra. The OCP conditioned within seconds, but the conditioning time was set at 300 s as well. The cell was stored in a Faraday cage during the measurements. Fitting of the data and assessment of the data on causality, linearity and stability of the system by Kramers-Kronig transformation was performed using the "Equivalent Circuit" software package.[19]

2.2.5 Data Evaluation

Fitting was usually attended by the fact that a particular spectrum could be fitted well by

more than one circuit. This problem, *i.e.* of identifying the most likely circuit as well as of distinguishing partial processes involved, was alleviated by fitting a range of spectra measured at different, but closely related, potentials and concentrations. Besides, data were measured for CD_2O. The information obtained from the literature and from the data obtained by the radiotracer thin-gap method, DEMS and voltammetry further facilitated to choose the most plausible circuit. Moreover, one circuit was sought that described the formaldehyde oxidation satisfactorily under all conditions examined.

The fitted circuits were composed of defined elements, *i.e.* the use of constant phase elements (CPE) was circumvented deliberately.[18] Correlation of the circuit to practical systems is helped by including elements with practical significance. The CPE is usually encountered in 'black box' approaches but contains various (electro)chemical obscurities. Contrary to R, C and W, no straightforward physical interpretation has been given yet.[2,3,21]

2.3 Voltammetry and Chronoamperometry

2.3.1 Introduction

Voltammetry is based on the perturbation of an electrochemical system by a potential that changes constantly with time. The simultaneously recorded current contains information on processes proceeding in the solution, at and in the working electrode. Voltammetry is referred to as linear sweep voltammetry when the potential ramp concerns a single sweep and as cyclic voltammetry when the potential is cycled between two extremes.[33-36] Chronoamperometry is based on imposing a sinusoidal potential on an electrochemical system with the simultaneous recording of the current response as a function of time.[37]

2.3.2 Materials

Solutions were prepared from chemicals of analytical grade (Sigma, Belgium, and Milli-Q water ~18.2 MΩ cm^{-1}). Both CH_2O and CD_2O (D quantity in formaldehyde 99%, Thamer Diagnostica, The Netherlands) were dissolved by ultrasonic vibration. Nitrogen was bubbled through the solutions at ~five bubbles per second.

Disk-shaped polycrystalline metal electrodes (99.99%, Goodfellow, England) with a diameter of 5 mm were attached to a copper electrode holder that had been embedded in polytetrafluoroethylene (PTFE). The holder and electrode were connected to a rotator that in turn was linked with the potentiostat. Voltammograms were recorded at 16 rps, unless stated otherwise. Electrodes were polished manually using 3, 1, and 0.25 μm diamond paste followed by a thorough rinsing with water. A platinum electrode and a Hg/Hg_2SO_4 (sat. K_2SO_4) electrode was used as counter electrode and reference electrode, respectively.

2.3.3 Methods

Cyclic voltammograms and current transients (chronoamperometry) were recorded using a 362 EG&G PAR potentiostat and a double wall, single-compartment glass cell. Prior to each measurement, a cyclic voltammogram was recorded in 0.1 M NaOH to confirm the presence of the clean metal surface from the characteristic voltammogram (Figure1).[38-43]

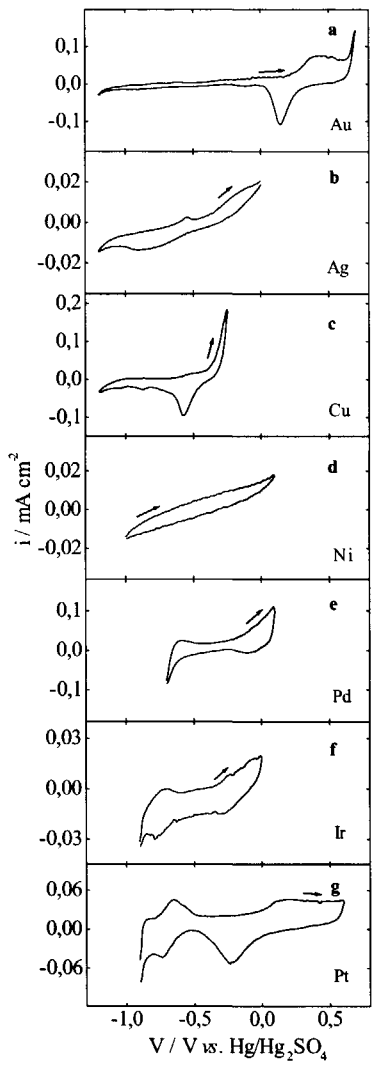

Figure 1. *Cyclic voltammograms recorded at a scan rate of 50 mV s^{-1} in solutions containing 0.1 M $KClO_4$.*

Then, voltages were cycled at 50 mV s^{-1} in the formaldehyde solutions of interest until signals were reproducible. Voltages were cycled between -1.5 V *vs.* Hg/Hg_2SO_4 and 0.2 V *vs.* the potential where a sudden drop in the formaldehyde electro-oxidation current occurred due to the oxidation of the metal surface.[44] Definite cyclic voltammograms were then recorded in the solutions of interest at a sweep rate of 10 mV s^{-1}.

An attempt was made to derive the roughness factors of the electrodes by comparing double layer capacitances (C) of the electrodes with the minimum value of 22 μFcm^{-2} reported for single crystalline gold (111) surfaces.[45] The capacitances were calculated from i = Cv (where: C is the capacitance [F cm^{-2}], i the current density [mA cm^{-2}] and v the scan rate [V s^{-1}]) at voltages where current densities were reversible, approximately independent of the potential, and zero at very slow scan rates.[46] This method may contain a significant error, but as it is impossible to derive all surface areas by one method with high accuracy, and as relative comparisons between metals and solutions were considered more important than absolute determinations, the values of the roughness factors were assumed as practicable (Table 1).[45-47]. Current densities in this thesis are expressed in real surface areas, unless stated otherwise.

Metal	Capacitance / μF	Surface Area / cm^2	Roughness Factor / -	V / V *vs.* Hg/Hg_2SO_4
Ag	37.0	1.68	3.36	-0.47
Cu	70.1	3.19	6.38	-0.81
Pd	21.7	0.99	1.98	-0.34
Ni	11.6	0.53	1.06	-0.51
Au	36.0	1.64	3.28	-0.85
Ir	57.3	2.60	5.20	-0.58
Pt	17.9	0.81	1.62	-0.49

Table 1. *Surface data obtained for the metals studied by voltammetry.*

The dependence of the reaction rate on temperature was studied by slowly heating the solutions and recording voltammograms simultaneously. In this way, the heating time was kept to a minimum and results were seen to be most reproducible. The temperatures given in the text are averages of the initial and final temperatures of each positive scan. Moreover, no data could be obtained for the oxidation of CD_2O on nickel at higher temperatures, as current densities fluctuated around zero. The values of the KIE for nickel

were therefore obtained by recording one voltammogram at room temperature for the solution containing CH_2O, followed by the immediate exchange with the solution containing CD_2O (leaving one drop of the solution containing CH_2O on the electrode) and the recording of the voltammogram.

Current transients were recorded at different potentials by first polarizing the electrode for 1 min at 0.3 V *vs.* the potential where the drop in current associated with the oxidation of the gold surface was seen. Then, the electrode was held at the OCP for 1 minute, and stepped to the potential of interest, while recording the current as a function of time.

2.3.4 Data Evaluation

To investigate the diffusive or kinetic character of the reaction, the current transients were fitted by (square)root-functions and exponential functions using Microsoft Origin software. The derivation of the values of E_{act} was performed at each potential from the slopes of the Arrhenius plots by linear least-squares fitting using Microsoft Mathematica software. Confidence intervals of 95% of these fits were included in the data. Note, that E_{act} represent apparent activation energies, as it assumed the validity of the Arrhenius equation and as the pH of the solution and the potential of the reference electrode were assumed constant at all temperatures during a measurement.

2.4 Differential Electrochemical Mass Spectrometry

2.4.1 Introduction

Differential Electrochemical Mass Spectrometry (DEMS) is based on the simultaneous measurement of volatile products and the current at various potentials.[9,10] A porous working electrode is used that is attached to a solution-impermeable Teflon membrane, which is connected to the cell and the gas chamber of the mass spectrometer.[9,10]

2.4.2 Materials and Methods

The DEMS measurements were conducted using a Leybold Quadruvac PGA 100 mass spectrometer.[5,9,10] A Hg/HgO electrode was used as the reference electrode in all measurements. The products were examined for CO_2, H_2, HD and D_2 using a gold electrode of which the cyclic voltammogram attested to clean gold (Figure 2a).[48] The calibration constant, K*, of the mass spectrometer was obtained by recording the faradaic current and hydrogen current in 0.1 M NaOH (Figure 2b), and using Equation 1:[33]

$$K^* = \frac{I_{ion}(H_2)}{n I_f(H_2)} \qquad (1)$$

Where: $I_f(H_2)$ refers to the faradaic current for hydrogen evolution, n to the number of electrons (being 2 under the assumption that gas evolution can be described by the

standard hydrogen evolution reaction in alkaline, aqueous solution: 2 H_2O + 2 e^- → 2 H_2 + 2 OH^-), and I_{ion} the ion current for m/ z = 2.[12]

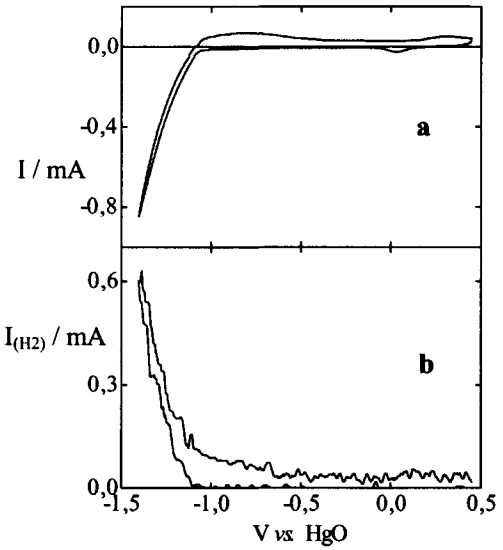

Figure 2. *(a) Cyclic voltammgram for gold in 0.1 M NaOH at a scan rate of 10 mV s^{-1}. (b) Corresponding mass signal for H_2.*

2.5. Radiotracer Thin-Gap Technique

2.5.1 Introduction

This technique is based on the measurement of radiolabelled molecules or ions adsorbed at a flat electrode by pressing down and pulling up the working electrode to and from a flat glass scintillator (Figure 3).[49-52] The glass scintillator converts ionising radiation into light pulses that are next converted to electric signals by a photon multiplier tube (PMT), amplified and stored in a multi-channel analyser. The overall signal (from a window between two selected channel settings) results from species adsorbed both at the electrode and trapped in the gap between the electrode and the scintillator.[49] For this reason, the signal originating from radiolabelled species, trapped in the gap between the electrode and the scintillator, is determined under conditions when no adsorption occurs.[52,53]

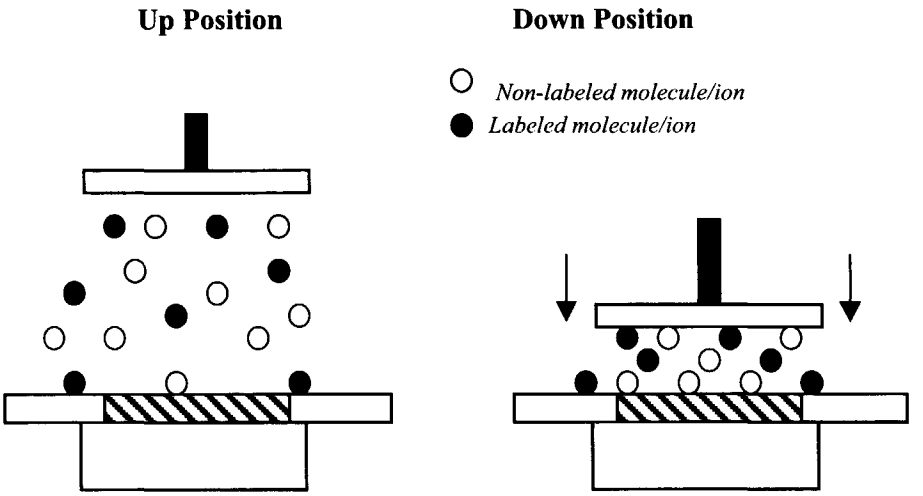

Figure 3. *Schematic representation of the radiotracer thin-gap technique: Labelled species in the gap between the electrode and the scintillator, are detected when the electrode is in the up position. Labelled species adsorbed at the electrode and trapped in the smaller gap between the electrode and the scintillator are detected when the electrode is in the down position.*

2.5.2 Materials and Equipment

Solutions were prepared from chemicals of analytical grade (Sigma, Belgium) and milli-Q water (Millipore, 18.2 $M\Omega cm^{-1}$). Both formaldehyde and deuterated formaldehyde (D quantity in CD_2O > 99%, Thamer diagnostica, The Netherlands) were dissolved in water by ultrasonic vibration. The [^{14}C]-labeled CH_2O (ICN, the Netherlands) used for the radiotracer adsorption studies had a specific activity of 1.99 GBq $mmol^{-1}$ and a radioactive concentration of 0.7 GBq ml^{-1}. The [^{35}S]-labeled Na_2SO_4 (ICN, the Netherlands) used for the determination of the gap thickness had a radioactivity of 104 MBq (carrier free).

Disk-shaped polycrystalline metal electrodes (thickness 5 mm, diameter 11.5 mm, 99.99%, Goodfellow, England) were optically cut and polished using 1.0 μm and 0.25 μm diamond paste. A platinum electrode and a Hg/Hg_2SO_4 (sat. K_2SO_4) electrode were used as counter electrode and reference electrode, respectively. The metal electrodes were pre-treated by rinsing with 0.1 M $HClO_4$, followed by potentiodynamic cycling between –1.3 V and 0.4 V *vs.* Hg/Hg_2SO_4 in 0.1 M NaOH. Cycling was continued until signals were reproducible and indicative for clean metals (Figure 4).[38-43]

The potential-dependent radiotracer studies were carried out using a scanning potentiostate (EG&G, type 362) and a double-wall glass cell which was connected to a thermostate.[53,54] The bottom of the cell consisted of a glass scintillator embedded in a ceramic disc covered by a protecting, transparent polyethylene film. Light signals were detected, amplified and collected using a photomultiplier tube (PMT, Thorn EMI, type: B2F/RFI) a power supply (EG&G Ortec, type 478), an amplifier (Canberra, type: TSCA, 2015A) and a multi-channel analyser as the data collector (Tracor Northern, type: 7200). The high voltage supply to the PMT operated at 1500 V during all measurements. Nitrogen was bubbled through the cell in each experiment at ~3 bubbles per second, as counted by the eye.

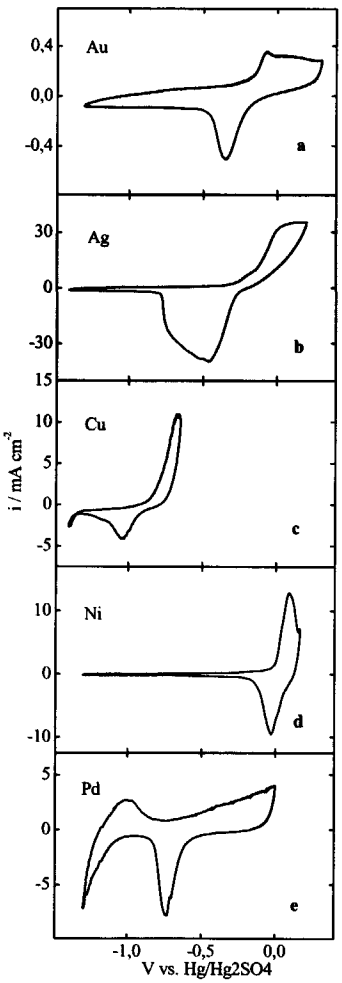

Figure 4. *Cyclic voltammograms obtained in 0.1 M NaOH at a scan rate of 50 mV s^{-1} for the metals used in the radiotracer studies.*

2.5.3 Methods

The theory behind the thin-gap method has been described in detail elsewhere[49], but as slightly different procedures were followed, the modified procedure is briefly summed up: A flat electrode is pressed against the polyethylene foil (thickness 0.1 mm) and the glass scintillator in the bottom of the cell. The amount of species adsorbed at the electrode can be obtained from Equation 2:[49,53,54]

$$\Gamma = \frac{N_{ads} C 10^{-3}}{N_s^{up} \mu_s R F_b \exp(-\mu_s x)} \tag{2}$$

Where: Γ (mol cm^{-2}) is the concentration of adsorbed ions at the surface. N_{ads} (cps) is the net count rate from the adsorbate on the electrode surface counted when the electrode is in the 'down' position. N_s^{up} (cps) is the counting rate from the solution and the adsorbate at the polyethylene foil counted when the electrode is in the 'up' position. C (mol dm^{-3}) is the concentration of adsorbate in the bulk solution. μ_s is the linear absorption coefficient of ß-radiation in water (300 cm^{-1} for [^{14}C], 256 cm^{-1} for [^{35}S] at 295 K). R (-) is the roughness factor of the electrode surface, x (cm) is the gap thickness between the electrode and the foil on the glass scintillator, F_b (-) is the backscattering factor which can be obtained from:

$$F_b = 2 - \exp\left[\frac{-Z}{40}\right] \tag{3}$$

Where: Z is the atomic number ($Z \geq 4$). F_b amounts to 1.86 for gold.[52,55]

The gap thickness, x, must be calibrated under conditions when no adsorption occurs.[52,53] As these conditions did not apply to the formaldehyde-gold system (see below), the gap thickness was obtained by measuring the up and down signals for the gold sodium-sulphate system (^{35}S has a ß-energy spectrum comparable to that of ^{14}C).[54] Increasing amounts of a radioactive [^{35}S]-labelled Na_2SO_4 solution (radioactive concentration 104 MBq ml^{-1}) were injected into 10 ml 0.1 M $HClO_4$ at –0.6 V *vs.* Hg-Hg_2SO_4. Signals were recorded in the up and down position (Figure 5).

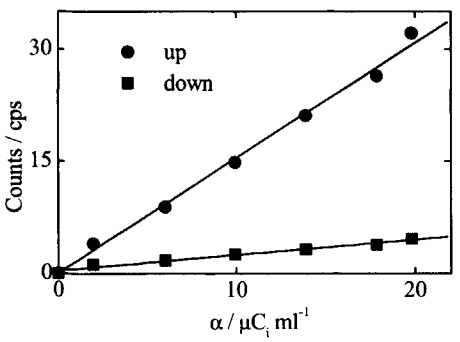

Figure 5. *System responses at different concentrations of [^{35}S]Na_2SO_4 in 0.1 M $HClO_4$. Electrode potential: –0.6 V vs. Hg/Hg_2SO_4.*

The gap thickness was calculated from Equation 4:[52,54]

$$\frac{N_s^d}{N_s^{up}} = [1 - \exp(-\mu_s x)][1 + (F_b - 1)\exp(-\lambda x)] \quad (4)$$

Where: N_s^d is the counting rate (cps) in the down position. The ratio N_s^d / N_s^{up} is called the squeeze efficiency. λ is the linear absorption coefficient (cm^{-1}) in water for the backscattered ß-radiation, which can be obtained from Equation 5:[52]

$$\lambda = \frac{225\mu_s}{(106 + Z)} \quad (5)$$

As adsorption of formaldehyde on the polyethylene foil could eclipse the signal originating from the electrode surface, it was examined by liquid scintillation counting: Five pieces of polyethylene film were dipped for different periods of time into 100 ml of a [^{14}C]-labeled formaldehyde solution containing 0.1 M NaOH and 10^{-2} M CH_2O (radioactive concentration: 0.04 MBq ml^{-1}). Then, pieces were thoroughly rinsed with 0.1 M NaOH, dipped into 10 ml Ultima Gold XR scintillation cocktail (Packard), and counted using a liquid scintillation counter (Packard, type: Tricarb 2750/LL). As signals obtained did not increase at longer times, and as they did not differ from pieces that were not exposed to the radioactive solution, it was assumed that no significant irreversible adsorption of formaldehyde on the film had occurred.

As repeated polishing of the optically cut electrodes induced a roughening of the metal surface, the gap thickness was determined for gold as a function of the number of polishing treatments (Figure 6).

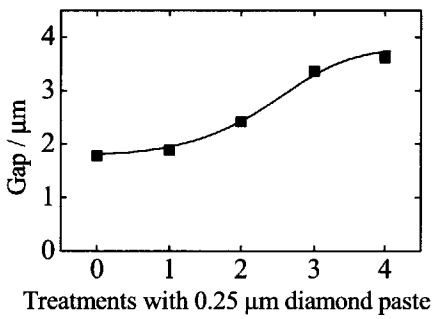

Figure 6. *Gap thickness as a function of the number of scouring treatments.*

As the electrodes treated twice with 0.25 µm diamond paste yielded most reproducible voltammograms, it was decided to conduct all measurements with these electrodes (Figure 7a).[55] The roughness factor of the electrode was derived from the cyclic voltammograms recorded in 0.1 M $NaClO_4$ by the procedure discussed in Section 2.2.2 (Figure 7b).[45]

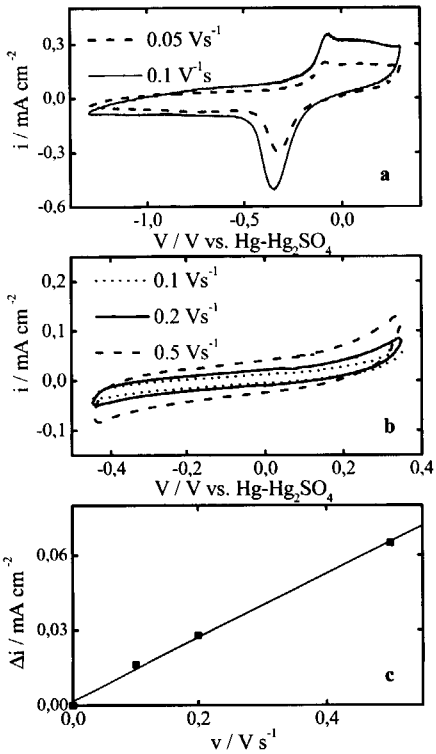

Figure 7. *(a) Cyclic voltammograms obtained in 0.1 M NaOH for the gold electrode used in the radiotracer experiments. (b) Cyclic voltammograms for the same electrode in 0.1 M $NaClO_4$. (c) Dependence of the capacitive current on the scan rate.*

The linear dependence of the current with increasing scan rates at –0.48 V *vs.* Hg/Hg_2SO_4 for gold confirmed the capacitive character of the current (Figure 7c). The current densities were not entirely independent of the potential for any metal but still the double layer capacitances were derived. The impact of the erroneous determination seemed acceptable, as values were in rough agreement with the values of the metal electrode used in voltammetry. Moreover, as the main focus of the adsorption study was laid on the differences in response to the various solutions rather than on the detailed elucidation of absolute numbers, each value was assumed as practicable (Table 2).

After determining the various constants of Equation 2, the net counting rates originating from the adsorbate on the electrode, N_{ads}, were obtained by first collecting counts when the electrode was in the down position. Then, both the background signal, measured prior

to the injection of the radiolabelled species into the cell, and the signal originating from the radioactive solution in the thin layer was subtracted. The latter was calculated from the squeeze efficiency obtained for the gold-sodiumsulphate system (Figure 5).[54] Each value in the plots discussed in this thesis are an average result of six times counting for 20 s.

Metal	Capacitance / $\mu F\ cm^{-2}$	Roughness Factor / -	V / V *vs.* Hg/Hg_2SO_4
Au	65.9	3.00	-0.89
Ag	105.8	4.81	-0.52
Cu	74.9	3.40	-0.82
Ni	53.0	2.41	-0.62
Pd	32.2	1.46	-0.93

Table 2. *Surface data for the metal electrodes used in the radiotracer experiments*

2.5.4 Measurement Procedures

Adsorption Kinetics - The adsorption kinetics of formaldehyde on the metal electrodes was studied by first injecting 9 ml 0.1 M NaOH into the glass cell with the gold electrode held in the up position. The electrode was then pressed down and 1.1 ml of [^{14}C]-labelled formaldehyde solution containing 0.1 M NaOH and 10^{-2} M CH_2O (radioactive concentration: 3.4 MBq ml^{-1}) was injected into the cell and homogenized by air bubbling. When neither adsorption nor diffusion of the labelled formaldehyde into the trapped solution layer had occurred, as revealed by the constant, low response of the system, the electrode was lifted. The electrode was then held in the up position until complete homogenisation of the labelled formaldehyde in the thin gap and adsorption of formaldehyde onto the electrode had occurred. Complete homogenisation was deduced from the unchanged up and down signal under conditions where no adsorption occurred (*i.e.* the gold-sulphate system).[54] Adsorption was seen from the increased signal when the electrode had been pressed down. The procedure of holding up the electrode for a fixed period of time, pressing it down, and measuring was repeated for the gold-formaldehyde system until the down signal remained constant.

Exchange Kinetics - When adsorption of molecules at the gold surface had completed, the electrode was pressed down and the solution was pumped out. The trapped solution had thereby remained in the gap, as revealed by the unchanged response of the system. Then,

10 ml of a non-labeled formaldehyde solution containing CH_2O and NaOH at the same concentration as used for the adsorption experiment (described above), was injected into the cell. The electrode was repeatedly held in the up position for different periods of time and pressed down until the down signal remained constant. The adsorption and exchange kinetics were studied at the open circuit potential (OCP) in solutions, as listed in Table 3.

Procedure	T / °C	$[CH_2O]$ / 10^{-3} mol dm^{-3}	[NaOH] / mol dm^{-3}	$[CD_2O]$ / 10^{-3} mol dm^{-3}	OCP / V *vs.* Hg/Hg_2SO_4
1	23	10	0.1	-	-1.04
2	23	-	0.1	10	-1.01
3	38	10	0.1	-	-1.07
4	53	10	0.1	-	-1.10
5	23	10	0.005	-	-0.46
6	23	10	1.0	-	-1.07
7	23	0.17	0.1	-	-0.97

Table 3. *Solutions and conditions used for the adsorption and exchange experiments.*

Potential Dependence - The dependence of the adsorption of formaldehyde on the potential applied was studied by first injecting 100 µl of a [^{14}C]-radiolabeled formaldehyde solution (radioactive concentration: 37 MBq ml^{-1}) into 10 ml 0.1 M NaOH. Then, the up and down signals were measured, first at the OCP, then at the most negative potential of interest and then at higher potentials. Data were collected at each potential when counting rates remained constant. After stepping to the highest potential, the electrode was held at the OCP for 20 minutes. Then, the concentration was raised by injecting known quantities of unlabeled formaldehyde into the cell. Again, the quantity of the electrode was measured at different potentials.

Temperature Dependence - The adsorption at different temperatures was studied by raising the temperature stepwise from room temperature to ~55 °C, while measuring the counting rates. After completing the measurements at the OCP, the potential was stepped to 300 mV *vs.* OCP (see Table 1). The count rates were then measured again, first at higher temperatures, then at lower temperatures.

2.5.5 Reproducibility and Reliability of Data

Reproducibility - In addition to the extensive testing of the system on signal responses upon the adsorption of formaldehyde on gold, the reproducibility of the measurements was verified more specifically by duplicate measurements of the adsorption and exchange kinetics on gold from a solution that contained 10 mM formaldehyde and 0.1 M NaOH. The first measurement is further referred as the test measurement. The whole cell was cleaned after this test measurement, deconstructed and rebuilt to carry out the definite measurements for gold. As half the quantity of tracer was used in the test measurement relative to the definite one, fewer pulses were obtained in the test measurement. The number of counts in the test measurements was therefore normalized to the number of counts in the definite measurement. This normalization was not requested for the exchange measurements, as both measurements were normalized to one. Without discussing the information on the adsorption kinetics yet, a good resemblance between both data was seen, attesting to the reproducibility of the system (Figure 8).

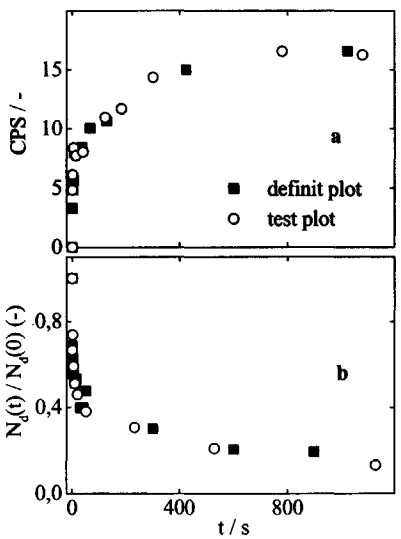

Figure 8. *Results obtained for two independent adsorption (a) and exchange (b) kinetic measurements.*

Evaluation of Systematic Errors – The accuracy of the calculated surface concentration (Γ) depends on the accuracy of the measurements of μ, f_b, R and C (equation 2). The parameters μ, C and F_b can be treated as accurate parameters while the systematic error in the roughness factor for gold generally ranges in the order of 15%.[56] For other metals only rough estimates are available. Hence, an error will be likely present in the absolute values

of the roughness factors. However, as the surfaces were all determined by the same method, and as the differences in responses upon the adsorption of formaldehyde on various metals from various solutions were large, these errors seemed acceptable. Besides, the rate constants determined for the exchange kinetic measurements were determined from the relative decays in data points rather than from calculated surface concentrations, implying that an erroneous roughness factor would not affect these rate constants at all.

Evaluation of Statistical Errors – In addition to the systematic errors hidden in the constants of Equation 2, some errors may arise from the counting statistics.[56] These errors are generally assumed to follow Poisson statistics and lie in the range of $\sqrt{(Nt)}$, with N being the count rate. As an order of magnitude, ~6000 counts were obtained per six times counting for 20 s at the end of adsorption kinetic measurement, while ~2000 counts were obtained at the end of an exchange experiment. As these counting rates go along with an error in the order of magnitude of 2-3% of the total signal, the error was considered as acceptable. Finally, the relative error in the surface concentration measurements also depends on the bulk concentration of the adsorbate in the solution, on the specific activity of the adsorbate and on the time of counting. For typical activities in the experiments of ~3.7 10^8 Bq and bulk adsorbate concentrations up to 10^{-2} M, the absolute errors will lay below 15% for each data point.[56] More than one data point was measured in all curves, reducing the overall error substantially.

2.5.5 Compartmental Analysis.

Fitting Procedure - To describe the overall adsorption and exchange process at the OCP in a quantitative fashion, a compartmental analysis was carried out:[57,58] The overall adsorption process was conceived by various (pseudo)stable states, called compartments, which were interconnected by mass flows of formaldehyde. The rates of the formaldehyde mass flows were assumed to obey first order kinetics with rate constants being independent of both formaldehyde concentration in the solution and surface coverage. Moreover, the concentration of formaldehyde (exchange experiments) and its specific radioactivity (adsorption experiments) were assumed constant in the compartments during each measurement.[57,58] Derivation of the most appropriate compartmental model was performed by first determining the minimum amount of compartments required to describe the data properly. Then, the sets of differential equations associated with each possible model for the determined number of compartments were derived and fitted to the data, first to the adsorption kinetic curves and then to the exchange kinetic curves. The equations were solved simultaneously for the various rate constants using MicroMath Scientist software. In addition to the compartmental analysis, various root functions were fitted to the data in order to see if diffusion had played an important role in the kinetics of the adsorption process.[59]

Derivation of the Model - It was frequently seen that a particular adsorption or exchange curve could be fitted well by more than one set of equations. Seeking one model that described all curves satisfactorily alleviated this problem, and enabled a better comparison of different results. Besides, a model was sought which was plausible in terms of the respective mechanism outlined in Chapter 1, the fitted equivalent circuit and the double-layer structure (Chapter 3). Moreover, it was sometimes seen that, even although fits turned out reasonable, plausible and unique, errors in the fitted rate constants were still in the range of tens of percents. As it was unclear to which extent these errors arose from the inadequacy of the model, from the limited number of data or from statistical scattering of data, no detailed evaluation of errors in the fitted constants could be made. However, as different initial values of the rate constants (input values) yielded roughly similar relative differences between rate constants, the values of the respective rate constants, the residence times and the inter-compartment flows were further evaluated. The absolute values of the adsorption kinetic rate constants should nevertheless be interpreted as an order of magnitude for reasons outlined above.

2.6 References

(1) Gileadi, G.; in *Electrode Kinetics*, VCH Publishers, New York, 1993, p 405.

(2) Christensen, P. A.; Hamnett, A.; In *Techniques and Mechanisms in Electrochemistry*, Chapman & Hall, 1994, p 36.

(3) Paunovic, M.; In *Electrochemistry in Transition*; Murphy, O. J., Srinivasan, S., Conway, B. E., Eds.; Chapter 30, Plenum Press, New York, 1992, p 479.

(4) Okinaka, Y.; Osaka T.; In *Advances in Electrochemical Science and Engineering*; Gerischer, H., Tobias, C. W., Eds.; Vol. 3, VCH Publishers Inc., New York, 1994, p 55.

(5) Jusys, Z.; *J. Electroanal. Chem.*,**1994**, 375, 257.

(6) Kuzmik, J. J.; In *Electroless Plating*; Hajdu, J. B., Mallory, G. O., Eds.; Chapter 14, American Electroplaters and Surface Finishers Scoiety, Orlando, **1990**, p 377.

(7) Shacham-Diamand, Y.; Sun, B.; Yip, V.; Bielski, R.; In *The Electrochemical Society Proceedings*; Vol. 94-31, **1994**, p 136.

(8) Walker, J. F.; In *Formaldehyde*, Reinhold Publ. Corp., New York, 3rd edition, **1964**, p 214.

(9) Gootzen, J. F. E.; PhD Thesis, University of Technology Eindhoven, The Netherlands, 1997, p 7.

(10) Frelink, T.; PhD Thesis, University of Technology Eindhoven, The Netherlands, 1995, p 9.

(11) Isaacs, N. S.; In *Physical Organic Chemistry*, Longman Group UK Ltd. 1st edition, Harlow, UK, 1987, p. 261.

(12) Weast, R. C.; *CRC Handbook of Chemistry and Physics*, CRC Press Inc., 66th edition, Boca Raton, 1985, p. F-175.
(13) See ref. (1), p 108.
(14) Meerakker, J. E. A. M. van den; *J. Appl. Electrochem.*, **1981**, 11, 387.
(15) Meerakker, J. E. A. M. van den; *J. Appl. Electrochem.*, **1981**, 11, 395.
(16) Kortenaar, M. V.;Kolar, Z. I.; Goeij, J. J. M. de.; Frens, G.; *J. Electrochem. Soc.*, **2001**, 148, 1.
(17) Bard, A. J.; Faulkner L. R.; In *Electrochemical Methods*, Chapter 5 and 11, Wiley & Sons Inc., New York, 1980.
(18) MacDonald, J. R.; In *Impedance Spectroscopy*, Chapter 4, John Wiley & Sons, New York, 1987.
(19) Boukamp B. A.; Equivalent Circuit (Users manual), University of Twente, The Netherlands, 1989.
(20) Gileadi, G.; In *Electrode Kinetics*, VCH Publishers, New York, 1993, p 403.
(21) Gabrielli, C.; In *Identification of Electrochemical Processes by Frequency Response Analysis*, Manual Solartron Instrumentation Group, Chapter 1, Morris Bros Ltd., England, 1980.
(22) Kortenaar, M. V.; Tessont C.; Kolar, Z. I.; Weijde, H. van der.; *J. Electrochem. Soc.*, **1999**, 14, 2146.
(23) Kortenaar, M. V.;Kolar, Z. I.; Goeij, J. J. M. de.; Frens, G.; *Langmuir*, **2002**, 10, C43.
(24) Gimenez, I.; Diard, J. P.; Le Gorrec, B.; Maximovitch, S.; *Electrochim. Acta*, **1988**, 33, 137.
(25) See ref. (12), p F-87.
(26) Bai, L.; Conway, B. E.; *Electrochim. Acta*, **1993**, 38, 1803.
(27) Bai, L.; Conway, B. E.; *J. Electrochem. Soc.*, **1991**, 138, 2897.
(28) See ref. (1), p 10.
(29) Walker, J. F.; In *Formaldehyde*, Reinhold Publ. Corp., New York, 3rd edition, 1964, p 214.
(30) Meerakker, J. E. M van den, Scholten, E.; *Ber. Bunsenges. Phys. Chem.*, **1989**, 93, 786.
(31) Ohno, I.; Wakabayashi, O.; Haruyama, S.; *J. Electrochem. Soc.*, **1985**, 132, 2323.
(32) ISIS version 5.3, program (re)written by the University of Technology, Delft, 1996.
(33) Baltruschat, H.; Anastasijevic, N. A.; Beltowska-Brzezinska, M.; Hambitzer, G.; Heitbaum, J.; *Ber. Bunsen-Ges. Phys. Chem.*,**1990**, 94, 996.
(34) Beltowska-Brzezinska, M.; *Electrochim. Acta*, **1985**, 30, 1193.
(35) Boukamp, B.; *Solid State Ionics*, **1993**, 62, 131.

(36) See ref. (2), p 36.
(37) See ref. (17), p 10.
(38) Bindra, P.; Roldan, J.; *J. Electrochem. Soc.*, **1985**, 132, 2582.
(39) Enyo, M; *J. Appl. Electrochem.*, **1985**, 15, 907.
(40) Enyo, M.; *J. Electroanal. Chem.*, **1986**, 201, 47.
(41) Burke, L. D.; O'Dwyer, K. J.; *Electrochim. Acta*, **1990**, 11, 1829.
(42) Burke, L. D.; O'Dwyer, K. J.; *Electrochim. Acta*, **1990**, 11, 1821.
(43) Burke, L. D.; Nugent, P. F.; *Gold Bulletin*, **1997**, 30, 43.
(44) Radoslav R. Adzic and Milka L. Avramov-Ivic, *J. Electroanal. Chem.*, **1982**, 134, 177.
(45) Shi, Z.; Lipkowski, J.; Gamboa, M.; Zelenay, P.; Wieckowski, A.; *J. Electroanal. Chem.*, **1994**, 366, 317.
(46) See ref. (1), p 15.
(47) Bockris, J. O. M.; Khan, S. U. M.; In *Surface Electrochemistry*, Plenum Press, New York and London, (1993), p 97.
(48) Nishimura, K.; Machida, K.; Enyo, M.; *J. Electroanal. Chem.*, **1988**, 251, 103.
(49) Krauskopf, E. K.; Chan, K.; Wieckowski, A.; *J. Phys Chem.*, **1987**, 91, 2327.
(50) Avramov-Ivic, M. L.; Adzic, R. R.; Bewick, A.; Razaq, M.; *J. Electroanal. Chem*, **1988**, 35, 725.
(51) Zelanay, P. Wieckowski, A.; *J. Electrochem. Soc.*, **1992**, 139, 2555.
(52) Szklarczyk, M.; Smolinski, S.; Sobkowski, J.; *Electrochimica Acta*, **1994**, 39, 1903.
(53) Thomas, A. E.; Sung, Y. E.; Gamboa-Aldéco, M.; Franaszczuk, K.; Wieckowski, A.; *J. Electrochem. Soc.*, **1995**, 142, 476.
(54) Zelenay, P.; Rice-Jackson, L. M.; Wieckowski, A.; *J. Electroanal. Chem.*, **1990**, 283, 389.
(55) Kolics, A.; Thomas, A. E.; Wieckowski, A.; *J. Chem. Soc., Faraday Trans.*, **1996**, 92, 3727.
(56) Sung, Y. E.; Thomas, A.; Gamboa-Aldeco, M.; Franaszczuk, K.; Wieckowski, A.; *J. Electroanal. Chem.*, **1994**, 378, 131.
(57) Godfrey, K.; in *Compartmental Models and Their Application*, Academic Press, New York, 1983, p 58.
(58) Shipley, R. A.; Clark, R. E; in *Tracer Methods for In Vivo Kinetics*, Academic Press, New York, 1972, p 45.
(59) See ref. (4), p 10.

Chapter 3

Anodic Oxidation of Formaldehyde on Gold Studied by Electrochemical Impedance Spectroscopy*

The anodic oxidation of formaldehyde on gold in alkaline aqueous solutions was studied by electrochemical impedance spectroscopy (EIS). One equivalent circuit was found to mimic all impedance spectra measured for formaldehyde (CH_2O) and deuterated formaldehyde (CD_2O) in various solutions at different voltages. The circuit is in line with the reaction mechanism proposed in Chapter 1. The resistors and capacitors of the circuit depend on the voltage in a logarithmic fashion, implying that the overall kinetics of the overall reaction may be unravelled in different Butler-Volmer-type reaction steps. A double layer structure was constructed from the fitted capacitors, which described the double layer of the system by an inner Helmhotz plane (IHP) and an outer Helmholtz plane (OHP) mediating the solution and the electrode surface. A negative capacitance (inductive loop) and a negative resistance were further observed at low frequencies, which suggested the depletion of negative charge in the IHP upon charging the electrode surface positively. As the inductive loop became more apparent for solutions containing CD_2O than for those containing CH_2O, and as it depended on the pH to great extent, it was related to the desorption of formate rate and the adsorption of enolate anions. Data were Kramers Kronig transformable and a χ^2-value of ~10^{-4} or less was attained in all fits.

* *Journal of the Electrochemical Society 146 (1999) 2146.*

3.1 Introduction

This chapter addresses the kinetic and electrostatic features of the oxidation of formaldehyde reaction on gold under different conditions by EIS. First, an electrical equivalent circuit is derived that is expected to describe the current responses of the system to the sinusoidal voltage perturbations. Then, the fitted circuit is given and the values of the elements are discussed, followed by a search for correlations between elements and reaction steps. A double layer structure is derived from the fitted capacitors that will serve as springboard for the description of adsorption processes in the next chapters. Finally, the reliability, causality and linearity of the data and the fits are discussed.

3.2 Results and Discussion

3.2.1 Expected Circuit

Reaction Model - Recalling the reaction mechanism set out in Chapter 1, a corresponding equivalent circuit may be derived, assuming that each reaction step can be represented directly by an electrical sub-circuit (element or combination of elements). This assumption may not hold, as outlined in Section 2.2.1, but it may help to explain the peculiar shape of the spectra and the dependencies of the elements on the voltage applied. The reaction considered is shown schematically in Figure 1.

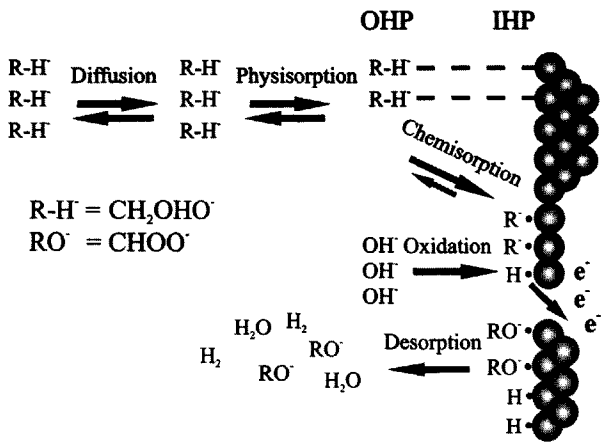

Figure 1. *Reaction model of the anodic oxidation of formaldehyde on gold in alkaline aqueous solutions as based on data presented in literature*

Diffusion of the enolate anion is followed by physisorption, chemisorption and a parallel set of reactions, *i.e.* the respective formation and desorption of hydrogen, water and formate. The corresponding double layer structure may be imagined by chemisorbed

species in the Inner Helmholtz Plane (IHP), physisorbed species in the Outer Helmholtz Plane (OHP) and species captured in the electrostatic field of the electrode (Figure 1b).[1-4]

Diffusion Elements - The absence of significant convection gives rise to a relatively large Nernst diffusion layer, in particular at higher overpotentials and at lower formaldehyde concentrations. This layer typically reaches a thickness between 1 and 10 mm under the 'stationary' conditions examined, assuming that the rate of the reaction is governed by diffusion and that migration does not play a significant role in the rate of the enolate anion transport (no rotating disc electrode was used).[4,5] Hence, diffusive or so-called Warburg behaviour may be observed, characterised by the 45° slope in the Nyquist diagram and a corresponding 'W' element (defined below) in the circuit. Deviations from this Warburg behaviour may result from strong hydrogen evolution (increased convection), or opposing reactant and product fluxes (non-linear concentration gradients).[1,5]

Faraday Impedance - As the faradic current is accompanied by the simultaneous charging of the double layer, the reaction may be represented by the parallel unit, (Z_f C_{dl}), where Z_f is the Faraday impedance and C_{dl} the overall double layer capacitance.[5] The Faraday impedance represents reaction steps that may occur under steady-state conditions, and usually, the so-called Randles circuit is considered to apply, implying that the Faraday impedance comprises the diffusion-related elements as well.[5,6] However, the nanometre-sized electrostatic field (typically $1/\kappa$, with κ being the Debye length) at the electrode is the driving force for reactions charging processes at the gold surface and induces the millimetre-sized concentration gradient in the solution in a second stage. Consequently, the Warburg impedance (W) may be chosen outside the (Z_f C_{dl}) unit.[1,4] This concept, *i.e.* of W in series with both C_{dl} as well as Z_f, will appear correct, as shown later, but is little envisaged in calculations of the total electrode impedance.[2] These do nevertheless usually deal with either smaller Nernst diffusion layers, or with a smaller contribution of specific adsorption to the overall impedance of the interfacial system.[1,3,5]

Other Elements - The reaction steps may be conceived by Arrhenius-like activation energies, each approximated by a resistance. The charging and discharging of the IHP and OHP upon physisorption, chemisorption, oxidation and desorption bring in capacitors parallel to these resistors.[3,5] These sub-circuits are embedded in the Faraday impedance and are introduced as: (R_{phys} C_{phys}), (R_{chem} C_{chem}), and (R_{des} C_{des}). The oxidation to formate and water as well as the recombination of H_{ad} to H_2 do likely occur parallel since both reactions proceed on bare gold-sites.[6-8] These reactions are accompanied by changes in the double layer structure of the IHP and may therefore be represented by (R_{ox} C_{ox}). The transfer of electrons to the gold electrode may be represented by a charge transfer

resistance R_{ct}, embedded in the Faraday impedance, as usual.[2,9,10] The solution resistance, R_{sol}, has been introduced as a distinct resistance in series with the remaining impedances.[2,5,6,9] Figure 2a sums up the various considerations.

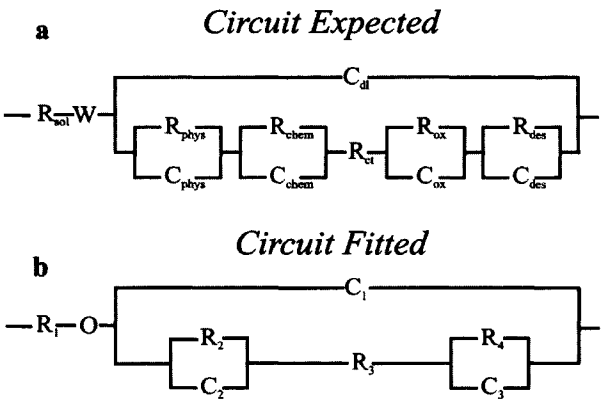

Figure 2. *(a) Circuit expected to describe the impedance data most satisfactory. (b) Circuit fitted to all impedance data.*

3.2.2 Fitted Circuit

Over 50 plausible circuits were endeavoured, of which only the circuit shown in Figure 2b was capable to mimic all spectra with a chi-square value (χ^2) around 10^{-4} or less. These values correspond to fitting errors of less than one percent of the overall impedance values. Generally, the χ^2-statistics should be less than 10^{-5} if the data are said to fit within the noise level of the measurement. The χ^2-values of 10^{-4} are higher, but as the circuit mimics all spectra reasonable, and as its features were considered to correlate with the mechanism in Section 1.3, the fitting results were further evaluated.

Comparison of Figure 2a with Figure 2b shows that various impedances have merged, or have vanished because of negligible values in the frequency range investigated. Replacement of the Warburg element, W, which assumes an infinite thickness of the diffusion layer, for the finite-diffusion layer based elements, O and B, was found to emend the quality of the fit.[2,3] The related dispersion relations can be obtained by solving Fick's second law under different boundary conditions:[1,2,11,12]

$$Z_W(\omega) = \frac{\Delta V_S(\omega)}{\Delta I_S(\omega)} = \frac{1}{Y_O(j\omega)^{0.5}} \tag{1}$$

$$Z_O(\omega) = \frac{\Delta V_S(\omega)}{\Delta I_S(\omega)} = \frac{\tanh\left[B(j\omega)^{0.5}\right]}{Y_O(j\omega)^{0.5}} \tag{2}$$

Where: $Z_O(\omega)$ and $Z_w(\omega)$ are the diffusion dispersion relations [Ω]; $\Delta V(\omega)$ the voltage perturbation [V], $\Delta I(\omega)$ the current response to the voltage perturbation [mA], ω the frequency [Hz] and j the imaginary number [-]. Y_o and B are the fitted parameters (Y_o is represented by W or O) and are defined as:

$$Y_O = \frac{n^2 F^2 A C D^{0.5}}{RT} \tag{3}$$

$$B = \frac{\delta}{D^{0.5}} \tag{4}$$

Where: δ is the thickness of the diffusion layer [cm]; A, the real surface area of the working electrode [cm^2]; D, the diffusion constant of the species concerned [$cm^2\ s^{-1}$]; n, the number of electrons transferred per ion oxidised [-]; F, the Faraday constant [$C\ mol^{-1}$]; C, de concentration in the bulk [$mol\ cm^{-3}$].

At first sight, the fitted elements may provide the diffusion coefficient and the thickness of the diffusion layer directly. However, the system seems more complicated, as it is likely that the diffusion elements fitted correlate with the net diffusion effects of the various species, rather than with that of one electroactive species. As mentioned, the transport of OH^- may be ruled out, but diffusion of, particularly, hydrogen, the enolate anion and formate remain to be taken along.[13] In addition, migration effects may not be rejected *a priori* with diffusion layer thickness encountered in the current study, as the concentration gradient was small (no rotating disc was used) relative to the potential gradient.[1]

3.2.3 Discussion of the Spectra

0.1 M NaOH and 0.01 M CH_2O - The steady state V-i curves and the impedance spectra measured for solutions containing 0.1 M NaOH and 0.01 M CH_2O are shown in Figure 3. Clearly, the impedance spectra reflect the change in kinetics of the various partial reactions relative to each other and to the dc potential. Examination of the impedance behaviour at low frequencies reveals resistive behaviour at about -1.1 V while diffusive behaviour prevails at 0.5 V. The negative slope of the steady-state current at ~0.4 V manifests accordingly in the impedance spectra with loops in the second quadrant. Moreover, spectra reveal simple behaviour, *i.e.* the seven time constants associated with the different steps of the mechanism given in Chapter 1 are not reflected accordingly by the spectra. Clearly, various steps have either similar time constants, or differ significantly, the latter resulting in the camouflage of the rapid partial reactions of the mechanism.

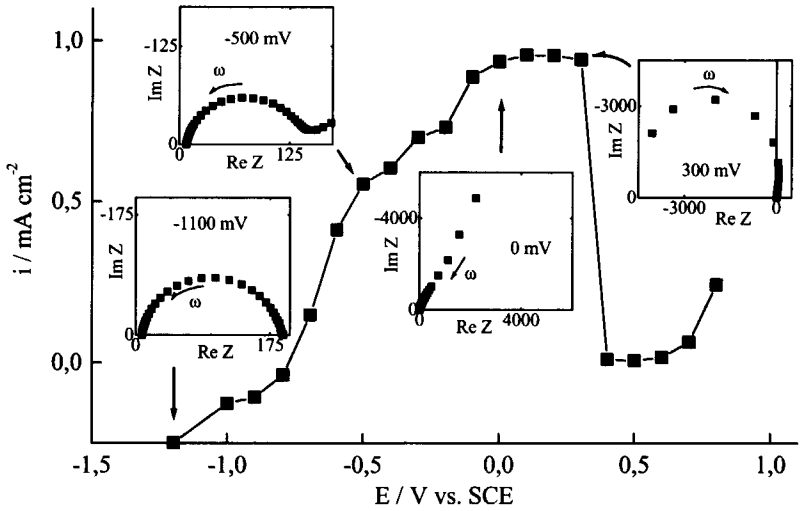

Figure 3. *Impedance spectra and steady-state voltage-current plots obtained for solutions containing 0.01 M CH_2O and 0.1 M NaOH.*

0.05 M NaOH and 0.1 M CH_2O - The measured and fitted impedance spectra in 0.05 M NaOH and 0.1 M CH_2O as well as the steady-state current density are shown in Figure 4:

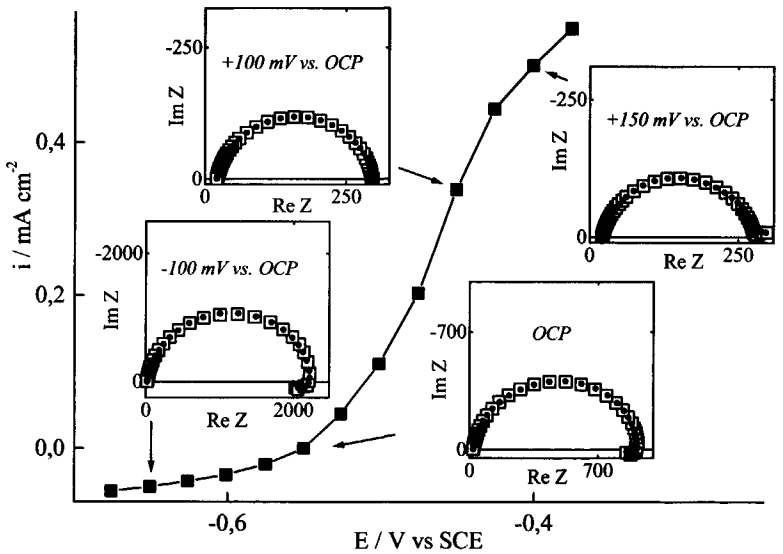

Figure 4. *Measured (□) and fitted (●) impedance spectra together with the steady state current density obtained in 0.1 M CH_2O and 0.05 M NaOH.*

Negative capacitive behaviour prevails at low potentials while positive capacitive behaviour rules at higher potentials, reflecting the change in the rate-determining step (RDS) at increasing potentials under pseudo steady-state conditions.

Although the fitted equivalents turned out to be very good in the Nyquist diagrams, some small deviations were encountered at high and low frequencies (Figure 5). The deviations are smaller than ~1% of the measured values and are explained by statistical scattering of data as well as by the incompleteness of the circuit. Simple parallel (RC) fits yielded poor χ^2-values of approximately 10^{-2}, and failed to explain both the flattened shape of the semicircle as well as the negative capacitance at low frequencies. The imperfect shape of the semicircle was therefore tackled by embedding an additional, positive and parallel (RC) unit in the Faraday impedance. The negative capacitance was met by introducing a negative parallel (RC) unit in the Faraday impedance.

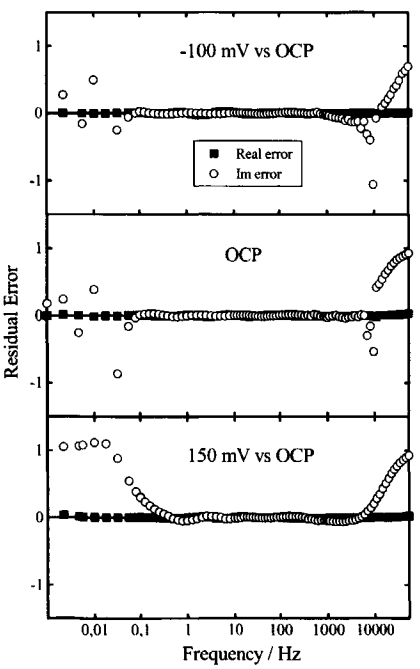

Figure 5. *Residual errors for spectra obtained in 0.1 M CH_2O and 0.05 M NaOH. (■ Real error, ○ Imaginary error)*

The values of fitted elements are listed in Table 1 and plotted at different potentials in Figure 6. The elements of the Faraday impedance (R_2, R_3, R_4, C_2 and C_3) depend on the potential in a logarithmic manner, with either positive slopes (R_2, R_3, C_2) or negative ones (R_4, C_3). No Tafel behaviour (linear log i-V plot) was observed in any of the steady-state V-i plots, which is explained by the complicated character of the reaction: First, relatively

small impedances associated with diffusion are seen (Table 1). Second, a negative impedance (negative R and C) is hidden in the system at low frequencies, implying that the local rate of the responsible charging processes are controversially in counter phase with the charging of the counter layer. The sudden change in value of the responsible elements (R_4 and C_3) from negative values to positive ones upon slightly changing the potential at higher potentials relative to the reference electrode suggests that the overall impedance has a different character than the interfacial impedance in a conventional electrochemical (Tafel-type) reaction. Note, that the negative capacitance in the spectra was always accompanied by the presence of both a negative R and a negative C in the representative (RC) unit. The negative impedance has been further reported for systems exhibiting galvanostatic potential oscillations.[14]

V / mV *vs.* OCP	O / 10^{-2} $s^{0.5}$ Ω^{-1}	B / 10^{-1} $s^{0.5}$	R_2 / 10^2 Ω	R_3 10^3 Ω	R_4 10^2 Ω	C_1 10^{-4} F	C_2 /10^{-3} F	C_3 / 10^{-1} F	χ^2 / 10^{-5}
-150	1.21	2.32	2.95	1.36	-	2.28	1.45	-	14.0
-125	1.18	2.35	3.01	1.48	-3.51	2.12	1.13	-0.77	14.5
-100	1.13	2.20	2.55	1.44	-2.01	1.96	1.07	-0.87	11.3
-75	1.09	1.97	3.45	1.42	-2.78	1.84	0.61	-0.80	15.3
-50	1.08	1.73	3.58	1.24	-1.81	1.79	0.63	-1.22	16.2
-25	1.08	1.54	4.06	1.09	-1.54	1.78	0.52	-0.88	22.0
OCP	1.05	1.46	3.08	0.88	-1.09	1.75	0.64	-2.49	11.1
25	1.03	1.35	2.01	0.68	-0.59	1.73	0.84	-4.06	10.3
50	1.15	1.05	1.19	0.41	-0.27	1.71	0.88	-8.39	8.9
75	1.14	1.00	0.73	0.30	-0.15	1.70	1.16	-13.66	7.0
100	1.25	0.83	0.53	0.20	-0.08	1.68	1.07	-18.32	5.4
125	1.08	0.94	0.45	0.19	0.11	1.74	1.42	113.1	6.8
150	1.01	0.94	0.42	0.16	0.15	1.76	1.54	51.05	8.6

Table 1. *Value of the fitted elements for solutions containing 0.1 M CH_2O and 0.05 NaOH. The OCP was –0.55 mV vs. SCE.*

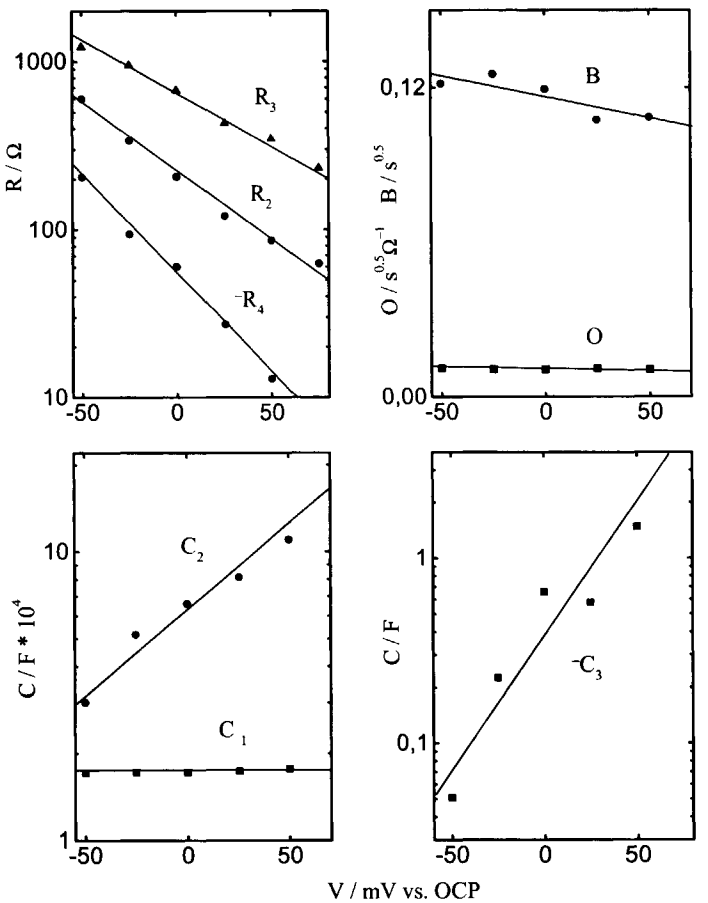

Figure. 6. *Dependence of the elements of the circuit fitted (Fig. 1c) on the potential applied for solutions containing 0.1 M CH_2O and 0.05 M NaOH. The OCP was -0.55 V vs. SCE.*

0.1 M CH_2O and 0.1 M NaOH - Impedance spectra and fitted equivalents for solutions containing 0.1 M formaldehyde and 0.1 M NaOH are shown in Figure 7. The values of the fitted elements are listed in Table 2 and plotted in Figure 8 (a line to guide the eye has been drawn through the fitted values).

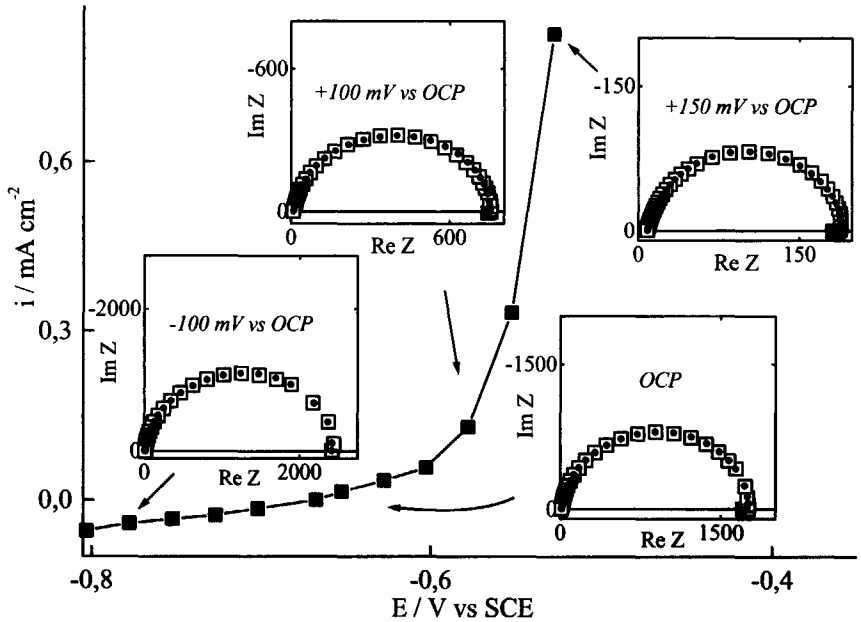

Figure 7. *Impedance spectra measured (□) and fitted (●) at various potentials together with the steady state current for solutions containing 0.1 M CH_2O and 0.1 M NaOH.*

Smaller negative capacitive loops are reflected by the spectra than for the less alkaline solutions (Figure 4). The higher rate of oxidation at the higher hydroxyl concentration is evident by comparing the steady state V-i plots of Figure 4 with that of Figure 7. Contrary to the less alkaline system discussed above, none of the elements fitted showed clear logarithmic dependencies on the dc potential. This observation is explained by the irregular hydrogen evolution of the system at different potentials: The relative amount of electrons tunnelling to the electrode for each formaldehyde molecule alters with each dc potential, as discussed in Chapter 4.[7] The variation in hydrogen evolution may be accompanied by an irregular convective contribution to the local transport properties of the various reactants and products at the interface.

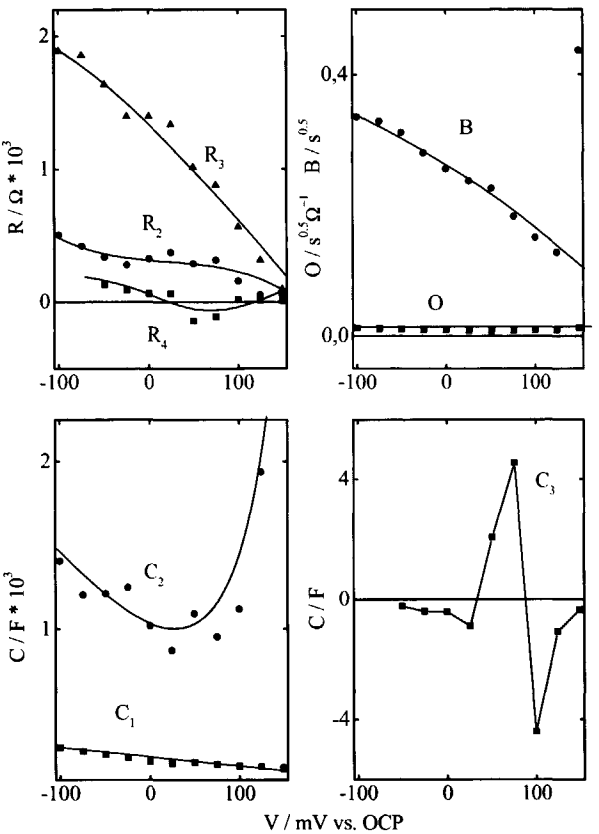

Figure 8. *Dependence of the elements of the fitted circuit on the dc potential for solutions containing 0.1 M CH_2O and 0.1 M NaOH. The OCP was -0.68 V vs. SCE*

V / mV vs. OCP	O / 10^{-2} $s^{0.5}$ Ω^{-1}	B / 10^{-1} $s^{0.5}$	R_2 / 10^2 Ω	R_3 / 10^3 Ω	R_4 / 10^2 Ω	C_1 / 10^{-4} F	C_2 / 10^{-3} F	C_3 / 10^{-1} F	χ^2 / 10^{-5}
-125	1.23	1.17	9.92	1.63	-4.47	1.81	0.19	-1.24	15.9
-100	1.23	1.16	7.33	1.48	-2.41	1.77	0.25	-1.87	11.1
-75	1.17	1.20	6.47	1.43	-2.79	1.72	0.28	-1.76	8.0
-50	1.12	1.22	6.01	1.23	-2.05	1.72	0.30	-0.51	7.9
-25	1.07	1.25	3.38	0.95	-0.94	1.72	0.52	-2.25	6.0
OCP	1.07	1.19	2.07	0.68	-0.60	1.72	0.66	-6.54	6.4
25	1.12	1.08	1.21	0.43	-0.27	1.74	0.81	-5.75	3.8
50	1.06	1.09	0.86	0.35	-0.13	1.77	1.10	-14.79	3.5
75	1.24	0.86	0.63	0.23	0.25	1.70	0.57	0.07	7.9
100	1.19	0.87	0.51	0.20	0.18	1.71	0.70	0.10	1.3
125	0.97	1.04	0.38	0.18	0.20	1.87	1.96	37.44	6.6
150	0.93	1.06	0.45	0.20	0.19	1.85	1.85	20.88	6.5

Table 2. *Values obtained for the elements fitted for solutions containing 0.1 M CH_2O and 0.1 M NaOH. The OCP was –0.68 V vs. SCE.*

0.1 M CD_2O and 0.1 M NaOH - The spectra and fitted equivalents for solutions containing 0.1 M CD_2O and 0.1 M NaOH are shown in Figure 9.

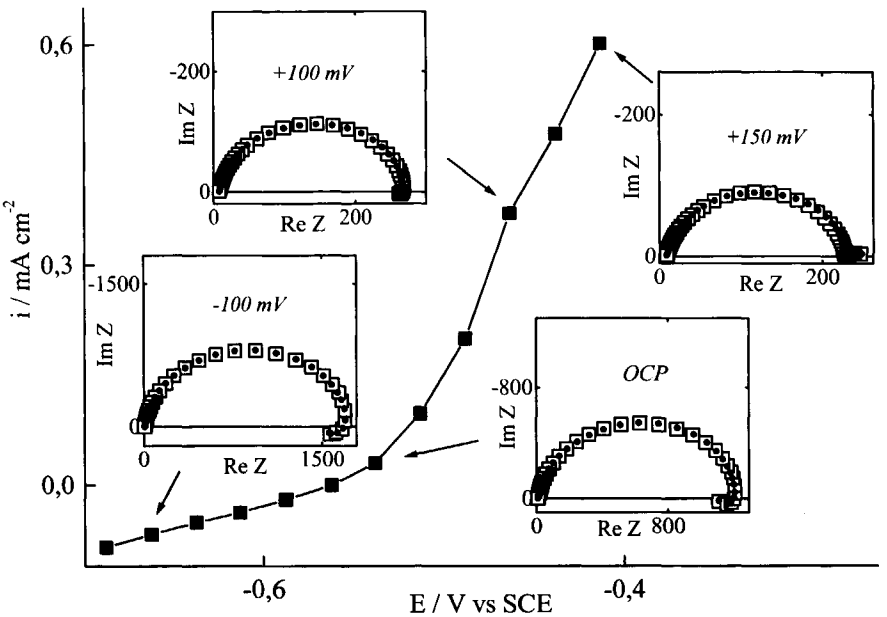

Figure. 9. *Impedance spectra measured (□) and fitted (●) at various potentials together with the steady state current for solutions containing 0.1 M CD_2O and 0.1 M NaOH..*

Pronounced negative capacitive behaviour can be seen at low frequencies, implying that other steps than diffusion or charge transfer steps are rate-limiting when the reaction runs in the steady state. Again, a flip of the small loop at low frequencies occurs from negative values of the imaginary impedance to positive ones at higher potentials.

The dependencies of the fitted elements on the dc potential are shown in Figure 10, with the values of the elements listed in Table 3. It is obvious from Figure 10 that values of the elements depend on the potential in a logarithmic fashion. Moreover, the steady-state current of Figure 4 relative to that of Figure 7 shows a substantial KIE, suggesting that the rate of the C-H bond rupture affects the rate of the reaction to great extent (*see* also Chapter 4).

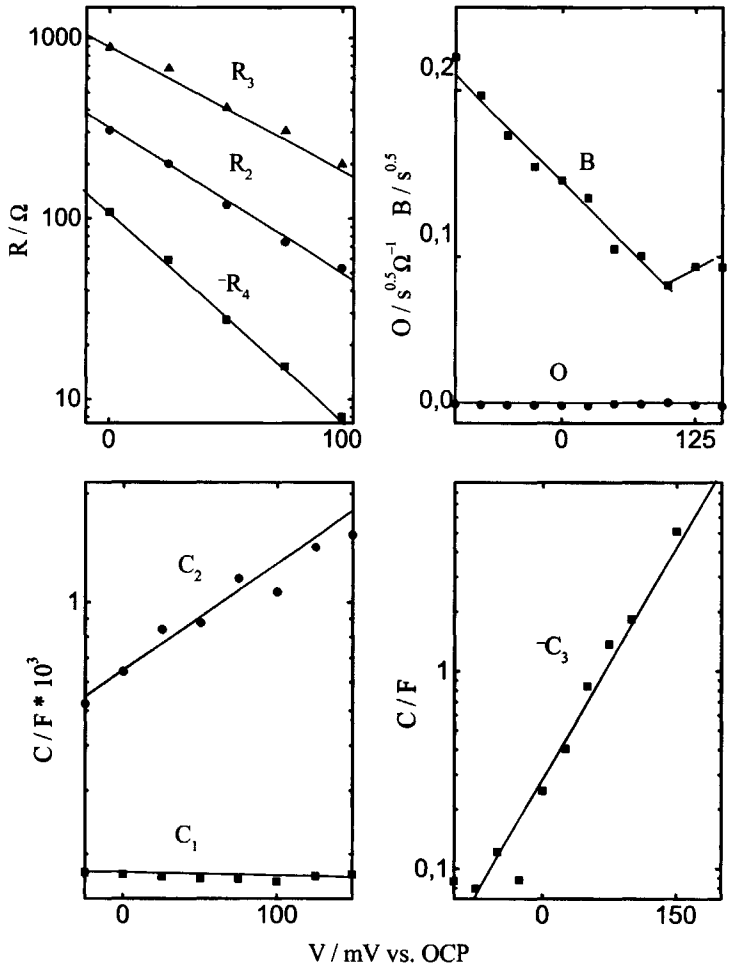

Figure 10. *Dependence of the elements of the circuit fitted (Fig. 1c) on the potential applied for solutions containing 0.1 M CD_2O and 0.1 M NaOH. The OCP was -0.56 V vs. SCE.*

V / mV vs OCP	O / 10^{-2} $s^{0.5}$ Ω^{-1}	B / 10^{-1} $s^{0.5}$	R_2 / 10^2 Ω	R_3 / 10^3 Ω	R_4 / 10^2 Ω	C_1 / 10^{-4} F	C_2 / 10^{-3} F	C_3 / F	χ^2 / 10^{-5}
-125	1.15	3.06	5.87	1.63	-	3.05	1.69	-	22.0
-100	1.12	3.35	5.05	1.89	-	2.92	1.41	-	8.0
-75	1.11	3.28	4.19	1.86	-	2.70	1.20	-	4.7
-50	1.02	3.11	3.37	1.63	-1.28	2.52	1.21	-0.23	3.6
-25	0.98	2.80	2.79	1.39	-0.87	2.33	1.25	-0.40	5.8
OCP	0.89	2.56	3.25	1.39	-0.64	2.10	1.02	-0.42	6.8
25	0.83	2.37	3.73	1.33	-0.61	1.98	0.87	-0.88	8.3
50	0.76	2.26	2.88	1.01	1.44	2.04	1.09	2.07	7.4
75	0.82	1.83	3.14	0.88	1.11	1.92	0.95	4.55	12.6
100	0.88	1.51	1.58	0.57	-0.16	1.80	1.12	-4.40	11.8
125	0.93	1.28	0.54	0.31	-0.12	1.78	1.94	-1.08	8.3
150	1.18	4.37	0.51	0.10	-0.09	1.64	0.18	-0.35	3.7

Table 3. *Values obtained from fitting of the spectra for the various elements (0.1 M CD_2O, 0.1 M NaOH, OCP: -0.56 V vs SCE)*

3.2.4 Discussion of Fitted Capacitors

General Remarks - Capacitive behaviour at frequencies as low as 1 mHz hides a few interesting concepts, as it suggests that strong capacitive effects are present when the reaction proceeds in the (pseudo) steady state. Namely, the value of the impedance of a capacitor is inversely proportional to the frequency:[2]

$$Z_C(\omega) = \frac{1}{j\omega C} \tag{5}$$

The capacitive effects are particularly reflected by C_3 as this capacitor has by far the highest absolute value under all conditions. The value of C_3 is negative when a negative

capacitive loop is present and vice versa (Table 1-3). The origin of the capacitive behaviour may be sought in the solution side of the double layer(s), as neither poisoning nor oxidation of the gold sites occurs under the conditions examined.[15-18]

Electrostatic Structure of the IHP - Some interesting conclusions may be drawn from the values of the fitted capacitors by taking into account that the capacitance of a capacitor is proportional to the respective charge, the surface area of the charged layer(s) and the dielectric constant. Besides, it is inversely proportional to the distance and potential difference between the charged layers:

$$C = \frac{Q_{dl}}{\Delta V} = \frac{\varepsilon_0 \varepsilon_r A}{d} = \frac{1}{j\omega C} \qquad (6)$$

First, it is clear that the Farad-sized capacitors fitted represent compact double layer structures with highly polarising media.[4] The large capacitance related to C_3 may represent processes in the IHP, as this layer may be expected to be the most compact layer due to specific adsorption.[4] The Farad-sized values of the capacitance go along with dielectrical constants of $\sim 10^4$, which is much higher than the dielectric constant of formaldehyde and water (between ~2 and ~80).[13] The highly polarising media are therefore explained by the presence of highly polarizing radicals between the layers, as a result of chemisorbed enolate anions and adsorbed hydrogen (according to the mechanism in Section 1.3). Additional support for this view is given in Chapter 5.

Second, as a capacitor is proportional to $Q_{dl}/\Delta V$, Farad-sized capacitors represent double layers with a relatively small potential gradient. This small gradient related to C_3 (and most likely to the IHP) has been proposed for double structures dealing with specific adsorption, but the empiric evidence for the actual presence in the reaction has never been reported.[6,19,20] Note, that contrary to an ordinary capacitor, C_3 depends on the dc potential. C_3 should therefore be regarded as an adsorption *pseudo* capacitor.[19]

Charging Times of the IHP – As the value of C_3 may be both positive and negative (Table 1-3), the potential gradient related to C_3 may be both positive and negative as well. The sudden change from positive to negative values upon slightly changing the potentials (Figure 4 and Figure 9) suggests that the time constants associated with the corresponding charging processes of C_3 have similar values. This observation seems further supported by the absence of hysteretic behaviour in the cyclic voltammograms under kinetic conditions and the values of the KIE around 1, as discussed in Chapter 4.[7,8]

As the characteristic charging time of ideal Farad-sized capacitors ($\tau = RC$) and Farad-sized adsorption pseudo capacitors ($\tau = R_{ad} C$, where R_{ad} is the total resistance associated with charging of the adsorption layer) lie in the time range of seconds or minutes, the rate-determining step in the overall kinetics of the reaction seems to manifests in C_3.[19] Namely, the time to charge this capacitor approaches, or even exceeds the mean time at

which species are oxidised under the pseudo steady-state conditions considered in the present studies. This view is illustrated by the following example: Assuming that two electrons are released for each formaldehyde molecule oxidised, a typical steady-state current density of 0.25 mA/ cm^2 and 5×10^{15} gold sites per real cm^2, the mean reaction time for each formaldehyde molecule to be oxidised would amount to approximately 6 seconds. Practically, the time to attain ideal steady-state conditions was nevertheless seen to take 20 minutes. The difference between 6 s and 20 minutes is explained by slow charging (adsorption) effects, a view which is supported practically by the radiotracer data (Chapter 5) and theoretically by the calculation of the charging (adsorption) time related to C_3: If I = 0.1 mA and ΔG_{ads} = 40 kJ mol^{-1}, then using $R_{ad} = \Delta G_{ads} / (n \cdot F \cdot I)$, R_{ad} = 290 Ω. For a typical value of C_3 of 5 F, the time to attain the steady state amounts to 1450 s (using $\tau = CR_{ad}$).[7,19]

Correlation of Capacitors with the Actual Reaction - The unit for an adsorption pseudo capacitance is often considered as R(RC), *i.e.* a resistor in series with capacitor that is parallel to a resistor.[19,20] Given the circuit fitted, the adsorption pseudo capacitance may be hidden in $R_3(R_4C_3)$. C_2 is much smaller than C_3 and is always characterised by positive values. Its value does not depend significantly on the NaOH concentration or on H/D substitution effects (*see* below), but dependence is seen on the potential. C_2 may therefore be regarded as an adsorption pseudo capacitor reflecting changes in the OHP (Figure 1). Taking into account these considerations, and taking into account the order of magnitude of values of the fitted capacitors, the electrostatic picture of the interfacial system may be represented schematically by Figure 11.

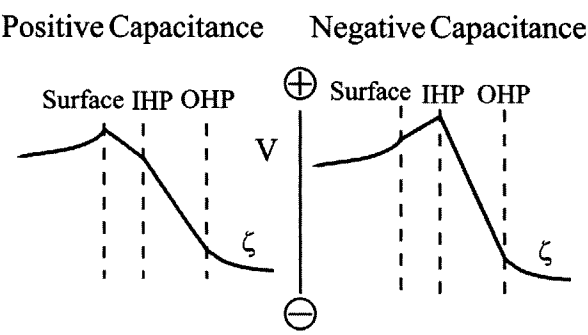

Figure 11. *Schematic representation of the (time-variant) electrostatic structure of the double layer, as based on the values of the capacitors.*

Summary - It is suggested that C_3 correlates with the rate-determining step of the reaction and that the time to attain steady-state conditions is very large due to slow charging and

discharging rates. C_2 and C_3 are adsorption pseudo capacitors representing the OHP and IHP respectively. C_1 is a pure capacitor reflecting the charging of the Nernst diffusion layer. The high values of the capacitors may be correlated with highly polarizing radicals and the occurrence of chemisorption.

3.2.5 Discussion of Fitted Resistors

Tafel-type Dependencies - The linear 'log R-V' lines related to R_2, R_3 and R_4, as shown in Figure 6 and Figure 10, suggest that the dependence of the reaction on the dc potential (overpotential) cannot be split into Ohm-type relationships (although this relationship holds at each single dc potential). Instead, different Tafel-type (linear V-log I) relationships seem to be present in the overall reaction.[21] The detailed elucidation of the chemical origin of each process is difficult and subject to the next chapters, but something may be said at this stage about R_2. This resistance has slopes of ~118 mV dec^{-1} and may therefore reflect a conventional electrochemical (electron-transfer controlled) process.[20,21] The value of R_2 is always much lower than the other resistances of the circuit, explaining the absence of a Tafel slope of 118 mV dec^{-1} in the overall reaction.[2-4] The small negative resistance, R_4, has slopes of ~-80 to -90 mV dec^{-1} and its value is positive when C_4 is positive (and vice versa). Its presence is explained by accumulation of $HCOO^-$ and CH_2OHO^- species in the OHP and IHP (*see* below).

KIE and R_3 - A look at Table 1, 2 and 3 shows that R_3 always has the highest value and that it may therefore be referred as the rate-limiting resistance of the circuit under steady-state conditions (the capacitances approach zero then). Besides, as a KIE applies to the overall rate of the reaction under the conditions studied (shown quantitatively in Chapter 4 and qualitatively by comparing the steady-state current of Figure 7 with Figure 9), the rate of the C-H bond rupture plays a major role in the overall reaction rate.[6-8] Both observations suggest that R_3 correlates with the C-H bond rupture step (step [4] in the mechanism of Section 1.3). To verify this observation, the ratio between the values of R_3 ('rate-determining resistance') related to the CH_2O and CD_2O were calculated using Table 2 and 3 (Table 4):

V / V *vs.* OCP	*-0.1*	*-0.5*	*0.0*	*0.5*	*0.1*	*0.125*	*0.15*
$R_3(CD_2O)$ /$R_3(CH_2O)$	1.28	1.32	2.04	2.89	2.85	1.72	0.5

Table 4. *Calculated values of the KIE for the largest resistance R_3.*

Without discussing details, the values of the calculated ratios are in reasonable agreement with the values of the KIE presented in Chapter 4 (Figure 7): Both values ranged between ~1 and ~3 at low overpotentials and drop below 1 at higher potentials. The presence of

values higher than one and the correlation between the values of R_3 and the KIE-data (Chapter 4) thus indicate that R_3 correlates with the rate-limiting step of the reaction and that it may reflect transitions of species between the IHP and OHP.

Correlations of R_2, R_3 and R_4 with the reaction - As mentioned, the unit for an adsorption pseudo capacitance is often considered as R(RC), *i.e.* a resistor in series with capacitor that is parallel to a resistor.[19,20] Given the circuit fitted and the fact that R_3 may correlate with the transition between the IHP and OHP, as well as the fact that C_3 was considered to correlate with the charging of the IHP, the transitions to and from the IHP seem further reflected by $R_3(R_4C_3)$. The possible negative values of R_4 may be in line with the presence of negative activation energies in the reaction (due to slow desorption rates and an associated pre-equilibrium).

Summary - The relative values of the resistances may explain the absence of linear Tafel slopes under steady state conditions. Both R_3 and R_4 correlate with the (rate-limiting) transition of species between the IHP and OHP. R_3 correlates with the rate-limiting bond rupture step, while R_4 may be related to desorption rates (and to related negative activation energies). R_2 has slopes similar to an ideal electrochemical two-electron process.

3.2.6 Diffusive Behaviour

The diffusive properties of the system are reflected by the parameters Y_0 (or O) and B. Generally B was seen to decrease with increasing potentials implying the build up of a concentration gradient. The thickness of the diffusion layer amounted to ~3-10 μm, as calculated from the fitted B-values and a diffusion coefficient of 1×10^{-5} cm^2 s^{-1}.[15,22] Calculated values for the diffusion coefficient from the O-values nevertheless yielded much smaller diffusion coefficients. Apparently, the diffusive properties of the system are more complicated than described by Fick's second law. This conclusion is further supported by the absence of Levich behaviour at higher overpotentials (Chapter 4).[4] The contribution of diffusion to the overall kinetics of the reaction at low potentials is nevertheless small at potentials considered in the current studies.

3.2.7 Negative Capacitances

Origin - To further understand the origin of the negative capacitance in the spectra, the influence of the NaOH concentration on the capacitive behaviour was studied at different potentials (Figure 12).

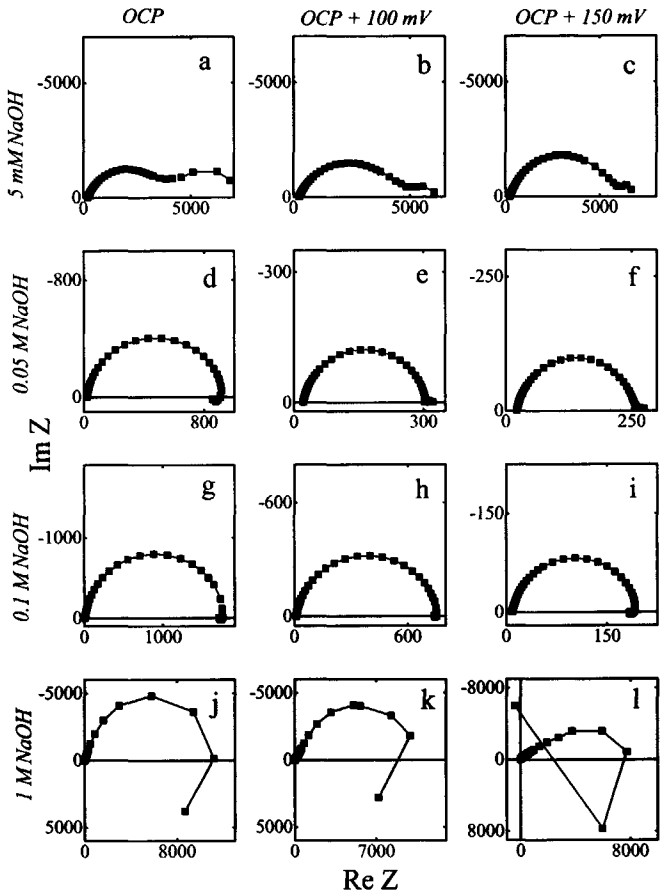

Figure 12. *Impedance spectra obtained at different potentials for solutions containing 0.1 M CH_2O and respectively: 5 mM NaOH (a-c), 0.05 M NaOH (d-f), 0.1 M NaOH (g-i) and 1 M NaOH (j-l).*

Clearly, the negative capacitive loop diminishes at lower NaOH concentrations. The increase in the rate of desorption (step 5 and 7 of the mechanism in Section 1.3) by increasing the NaOH concentration may therefore favour the size of the negative capacitive loop. As adsorbed hydrogen is unstable on gold, it is likely that the negative capacitive behaviour is related to the desorption of formate rather than to the desorption of molecular hydrogen or water.[23-26] Furthermore, the magnitude of the real Z values suggest that the negative capacitive behaviour does not depend substantially on the absolute rate of the overall reaction: the value of real Z may be both small and large to observe the negative capacitive loop.

The negative capacitive loop is slightly more apparent for CD_2O than for CH_2O, suggesting that the rate of chemisorption is involved in the negative loop rather than the rate of physisorption (Figure 13 and Tables 2 and 3).

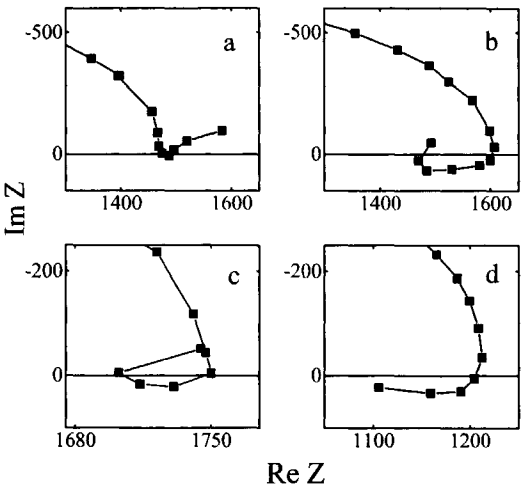

Figure 13. *Impedance spectra obtained at OCP (a, c) for solutions containing 0.1 M NaOH and respectively 0.01 M CH_2O (a), 0.01 M CD_2O (b), 0.1 M CH_2O (c) and 0.1 M CD_2O (d).*

In addition, it was frequently observed that the negative capacitive loop was more apparent at lower potentials although no clear trends were seen. The origin of the negative loops cannot be sought in the modifications of the gold surface, as neither oxidation nor poisoning of the electrode occurs. The reduction of oxygen is not involved either as loops are observed too at potentials where virtually no oxygen reduction occurs.

Ratio of chemisorption and desorption rates - Conway and Bai have studied the occurrence of negative capacitive behaviour for reactions with a single adsorbed intermediate.[27,28] Their observations suggested that negative capacitive loops are observed when the rate of adsorption meets the rate of desorption. To understand the negative capacitive behaviour in the current reaction, it may be appropriate to distinguish between adsorption ('charging') steps and desorption ('discharging') steps. The physisorption step and chemisorption step (Step [2] and step [3] in the mechanism of Section 1.3) oppose charging of the electrode: Positive charging of the electrode surface is attended by an *increase* of negatively charged species in the solution side layer of the IHP and OHP respectively. On the other hand, positive charging of the electrode favours desorption of

negatively charged dehydrogenated enolate anions at low overpotentials, as hydroxyl ions attack adsorbed species resulting in a *decrease* of negatively charged formate species in the solution side layer of the IHP. As mentioned, the rate of adsorption may be slowed down relative to the rate of desorption by using CD_2O or by increasing the NaOH concentration. In both cases, the negative loop increases and the appearance of the loop therefore seems to depend on the ratio of the rate of chemisorption relative to the rate of desorption (*i.e.* r_{ads}/r_{des}). If it is higher than one, negative loops may be observed, if it is smaller than one, positive loops may be observed. Figure 14 illustrates this view with the double layer structure taken from the values of the fitted capacitors.

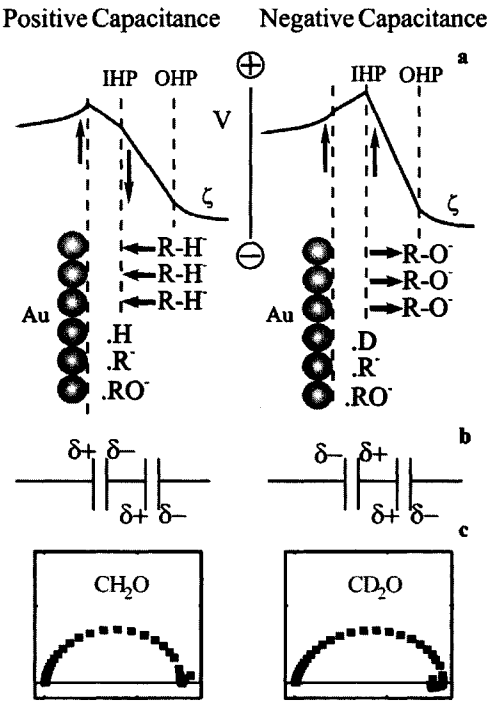

Figure. 14. *Model explaining negative capacitive behaviour. Positive or negative charging of the gold surface is accompanied by a decrease or increase of negatively charged species in the solution side layer of the IHP. The corresponding capacitors are shown (b). An example of the positive or negative loop is shown as well (c).*

A few specific notes can be made regarding the observation that the ratio r_{chem} / r_{des} likely governs the presence of negative or positive capacitive loop:

- The charge of the $\bullet CH_2OHO^-_{ad}$, $\bullet CHOHO^-_{ad}$ and $CHOO^-$ species are equal and, based on the reasoning that a rate-determining chemisorption step opposes negative capacitive behaviour as the capacitive behaviour is then ruled by the rate of desorption, it is more correct to explain the loop by the total charge adsorbed per unit time relative to the total charge desorbed per unit time in the IHP.
- The observation that a negative capacitive loop can turn into a positive one by slightly changing the conditions suggest that the rate of charging meets the rate of discharging, which is conform the observations of Bai and Conway[27,28].
- The negative value of R_4 may be further understood by realizing that R_4 is positive when C_3 is positive (and vice versa), as well as by taking into account that when the rate of charging is more rapid than the rate of discharging, accumulation of CH_2OHO^- and $HCOO^-$ in the OHP occurs. The accumulation will result in a decline of the current (and reflected by the negative resistance R_4). The inhibiting effect due to accumulation of species in the IHP may lead to poisoning in the most extreme case (Chapter 4).

3.2.8 Reliability of the Data and the Circuit

The reliability, linearity and causality of the impedance data measured in 0.05 M NaOH were examined by Kramers-Kronig transforms.[3,6,29] Clearly, both real values and imaginary values were transformable attesting to the reliability of the data (Figure 15). It may be pointed out that the capacitors and resistors simply arise from fitting and that their corresponding capacitive and resistive effects in the actual reaction is not ascertained. However, both negative and positive capacitances are practically present in the spectra at low frequencies, implying that the responsible processes are extremely slow. In addition, the unique character of the circuit with good fits and logarithmical dependencies of the comprising elements on the potential support the actual presence of according capacitive structures in the reaction, a view which is further confirmed in Chapter 4 and 5.

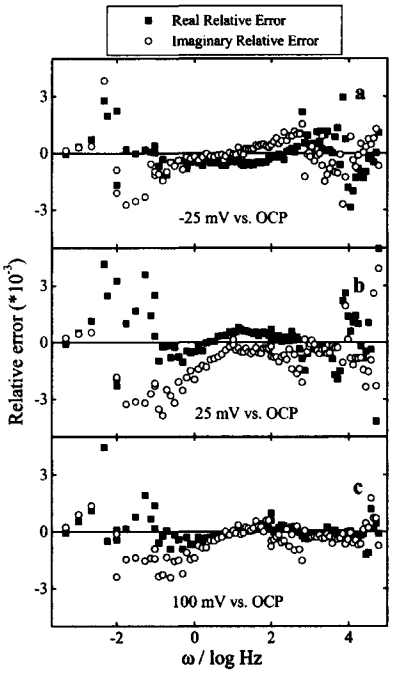

Figure. 15. *Kramers-Kronig transforms of spectra obtained for solutions containing 0.1 M CH_2O and 0.05 M NaOH at various potentials.*

3.3 Conclusions

- One equivalent circuit under all conditions studied can describe the anodic oxidation of formaldehyde on gold. The circuit fits data well and explains the absence of a Tafel slope under kinetic conditions.
- The resistors and capacitors of the circuit depend on the potential applied logarithmically under conditions were the amount of hydrogen evolution is potential-invariable.
- The circuit conceives the electrostatics of the system by an IHP and an OHP mediating the solution and the gold surface.
- Correlations were made between the elements of the circuit and the practical system (Figure 16): C_1 correlates with the charging of the Nernst diffusion layer (called C_{DL}). C_2 is an adsorption pseudo-capacitor representing charging processes of the OHP (C_{OHP}). C_3 is an adsorption pseudo capacitor too representing charging steps of the IHP (C_{IHP}). O and B represent the complicated, non rate-determining, diffusive properties of the system. R_1 is the solution resistance (R_{SOL}). R_2 represents charge transfer steps although other processes may be hidden in it as well (R_{CT}). R_3 may

correlates with the C-H bond rupture step (R_{BR}) and R_4 may reflect the inhibition of the reaction by an opposing flux of charged products (R_{DES}).

- The rate of the reaction is likely governed by the rate of chemisorption of CH_2OHO^- species and by the rate of desorption of $\bullet CHOHO^-_{ad}$ species. Depending on the ratio of their rates, negative or positive capacitive behaviour is observed reflected by positive or negative values of the corresponding resistors and capacitors.
- The high values of the C_{IHP} point towards the presence of free radicals between the IHP and the electrode surface. The slow charging of the IHP may support the occurrence of a slow chemisorption.

Circuit Fitted

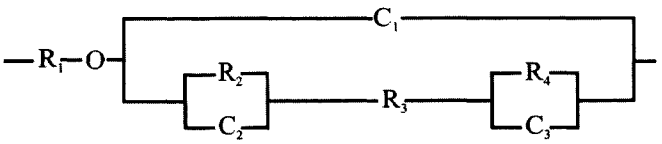

Circuit Interpreted

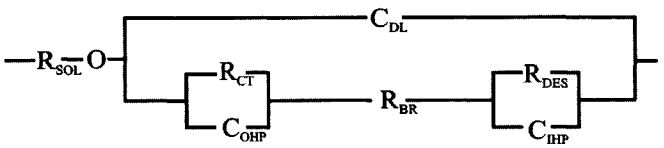

Figure. 16. *Correlation of reaction steps with the fitted elements (see text for explanation)*

3.4 References

(1) Faulkner L. R.; Bard, A. J.; In *'Electrochemical Methods'*, Chapter 5 and 11, Wiley & Sons Inc., New York, 1980.

(2) MacDonald, in *Impedance Spectroscopy*, Chapter 4, John Wiley & Sons, New York (1987).

(3) Boukamp, B. A.; Equivalent circuit (Users manual), University of Twente (1989).

(4) Gileadi, E.; *Electrode Kinetics*, Chapter. 2.2, VCH Publishers, New York (1993), p.10.

(5) Gabrielli, C.; In *Identification of Electrochemical Processes by Frequency Response Analysis*, Monograph by the Solartron Instrumentation Group, Chapter 1, Morris Bros Ltd., England (1980).

(6) Kortenaar, M. V.; Tessont C.; Kolar, Z. I.; Weijde, H. van der.; *J. Electrochem. Soc.*, **1999**, 14, 2146.

(7) Kortenaar, M. V.;Kolar, Z. I.; Goeij, J. J. M. de.; Frens, G.; *J. Electrochem. Soc.*, **2001**, 148, 1.

(8) Kortenaar, M. V.;Kolar, Z. I.; Goeij, J. J. M. de.; Frens, G.; *Langmuir*, **2002**, 18, 10279.

(9) Gimenez, I.; Diard, J. P.; Le Gorrec, B.; Maximovitch, S.; *Electrochim. Acta*, **1988**, 33, 137.

(10) Epelboin, I.; Gabrielli, C.; Keddam, M.; Takenouti, H. *Electrochim. Acta*, 1975, 20, 913.

(11) B. A. Boukamp, *Solid State Ionics*, **1993**, 62, 131.

(12) Keddam, M.; Mattos, O. R.; Takenouti, H.; *J. Electrochem. Soc.*, **1981**, 128, 266.

(13) Weast, R. C.; In *CRC Handbook of Chemistry and Physics*, p. F-87 , CRC Press Inc., 66th edition, Boca Raton (1985).

(14) Koper, M. T. M.; Hachkar, M.; Beden, B.; *J. Chem. Soc., Faraday Trans.*, **1996, 92,** 3975.

(15) Beltowska-Brzezinska, M.; *Electrochim. Acta*, **1985**, 30, 1193.

(16) Beltowska-Brzezinska, M.; *J. Electroanal. Chem.*, **1985**, 187, 167.

(17) Burke, L. D.; Nugent, P. F.; *Gold Bulletin*, **1997**, 30, 43.

(18) Enyo, M; *J. Appl. Electrochem.*, **1985**, 15, 907.

(19) Gileadi, E.; *Electrode Kinetics*, Chapter. 2.2, VCH Publishers, New York (1993), p. 167.

(20) Bockris, J. O. M.; Khan, S. U. M.; In *Surface Electrochemistry*, Plenum Press, New York and London, (1993), p 97.

(21) Christensen, P. A.; Hamnett, A.; In *Techniques and Mechanisms in Electrochemistry*, Chapman & Hall, (1994), p 36.

(22) See ref (13), p. F-131.

(23) Meerakker, J. E. A. M. van den; *J. Appl. Electrochem.*, **1981**, 11, 387.

(24) Meerakker, J. E. A. M. van den; *J. Appl. Electrochem.*, **1981**, 11, 395.

(25) Enyo, M.; *J. Electroanal. Chem.*, **1986**, 201, 47.

(26) Burke, L. D.; O'Dwyer, K. J.; *Electrochim. Acta*, **1990**, 11, 1829.

(27) Bai, L.; Conway, B. E.; *Electrochim. Acta*, **1993**, 38, 1803.

(28) Bai, L.; Conway, B. E.; *J. Electrochem. Soc.* **1991**, 138, 2897.

(29) ISIS version 5.3, program (re)written by the University of Technology, Delft, 1995.

Chapter 4

Oxidation of Formaldehyde on Gold Studied by DEMS and Voltammetry*

The electrocatalytic oxidation of formaldehyde (CH_2O) and deuterated formaldehyde (CD_2O) on gold in aqueous, alkaline solution has been studied at different pH-values, concentrations, potentials, and temperatures by voltammetry, chronoamperometry and differential electrochemical mass spectrometry. The H_2, D_2, and CO_2 gas evolution kinetics depend to great extent on the pH, potential, and temperature but likely play a minor role in the overall rate of the electro-oxidation reaction. The evolution of hydrogen at the open-circuit potential (OCP) and the current efficiencies larger than 100% pointed towards the occurrence of a non-electrochemical dehydrogenation reaction parallel to the electro-oxidation reaction. The values of the kinetic isotope effects (KIE) and the apparent activation energies (E_{act}) suggested that the overall rate of the electro-oxidation reaction is determined by the hydroxyl-catalysed chemisorption of the enolate anion at low potentials, by the desorption of the formate anion at higher potentials, and by diffusion at the highest potentials. The apparent activation energies ranged in value between -25 and 60 kJ mol^{-1}, confirming the highly catalytic properties of gold and the solution in the overall rate of the reaction and the possible presence of a pre-equilibrium in the overall reaction.

Journal of the Electrochemical Society E327, (2001) 148(8).

4.1 Introduction

This chapter aims to extend the qualitative view of the formaldehyde electro-oxidation reaction set in the previous chapters to a more quantitative one. First, the gas evolution properties of the reaction are addressed by DEMS with special focus on the hydrogen evolution characteristics. Next, rotating disc measurements and chronoamperometry are used to gain insight into the transport properties of the system. Then, voltammetry is applied to determine the apparent activation energies (E_{act}) and the kinetic isotope effects (KIE) of the reaction. Finally, a model is derived that describes the electro-oxidation reaction in a semi-quantitative fashion.

4.2 Results and Discussion

4.2.1 Gas Evolution

0.1 M NaOH and 0.1 M CH_2O - The electro-oxidation current and corresponding mass signals of H_2 and CO_2 for a solution containing 0.1 M NaOH and 0.1 M CH_2O are shown in Figure 1a through 1c.

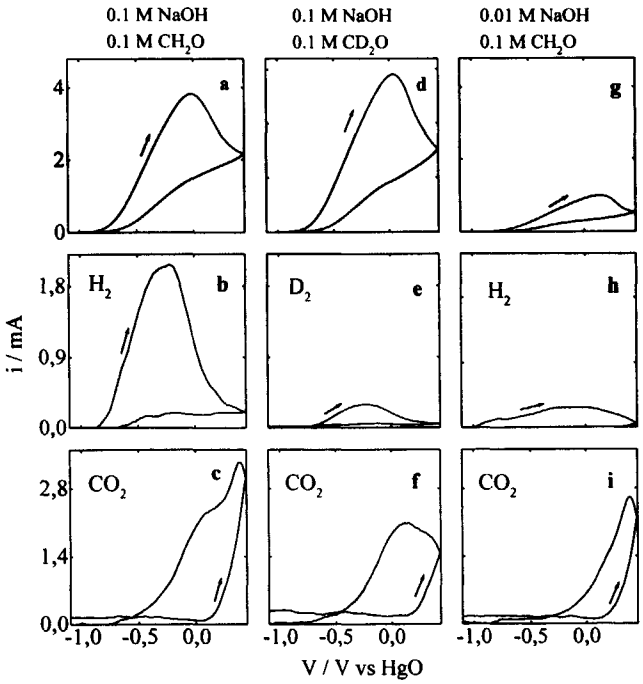

Figure 1. *Cyclic voltammograms and corresponding H_2 ,D_2, and CO_2 mass currents for solutions containing: 0.1 M NaOH and 0.1 M CH_2O (a, b, c), 0.1 M NaOH and 0.1 M CD_2O (d, e, f) and 0.01 M NaOH and 0.1 M CH 2 O (g, h, i). The scan rate was 10 mVs^{-1} in each measurement.*

The faradic current is traced by the hydrogen ion current over a range of potentials reflecting the evolution of hydrogen during the reaction. The hydrogen current drops nevertheless at a lower potential than the faradic current. Besides, a higher hydrogen current and a higher faradic current flow during the positive scan than during the negative scan, an observation that is explained by the diffusion-controlled oxidation at higher potentials.[1,2] The evolution of CO_2 sets in approximately at the potential where the oxidation of the gold surface sets in, *i.e.* at potentials much higher than at which the formaldehyde oxidation current sets in. It confirms the view that formate is the only carbon-containing reaction product at low overpotentials.[2,3] The counterclockwise current-flow of the CO_2 mass current (Figure 1c) suggests that CO_2 evolves on gold-oxides only, as reduction of the oxidized gold surface (Figure 2, Chapter 2) roughly coincides with the drop in the CO_2 mass signal during the negative scan.

Assuming that any adsorbed hydrogen reacts to molecular hydrogen (*i.e.* desorption of adsorbed hydrogen only occurs by step [6] of the mechanism set out in Section 1.3), only one electron flows to the gold surface per enolate anion oxidized and the maximum amount of hydrogen that may evolve can be calculated from the following equation:[4,5]

$$I_{ion} = A\, I_F\, K^* / n \qquad (1)$$

Where: A is the current efficiency for hydrogen evolution, which is one under the current assumption. The ratio between the amount of hydrogen evolved practically, and the maximum amount of hydrogen evolved theoretically, reflects the probability for adsorbed hydrogen to react with itself by step [6] or with hydroxyl ions by step [7]. The calculated ratios are shown in Figure 2. Approximately 55% or less of the adsorbed hydrogen atoms react to molecular hydrogen by Reaction 7 for solutions containing 0.1 M NaOH and 0.1 M CH_2O during the positive scan (Figure 2). This is slightly higher than results published by Baltruschat *et al.* for solutions containing 0.1 M KOH and 0.05 M CH_2O.[5]

0.1 M NaOH and 0.1 M CD_2O - The oxidation current and corresponding D_2 and CO_2 mass signals for a solution containing 0.1 M NaOH and 0.1 M CD_2O are shown in Figure 1d through 1f. Clearly, less D_2 evolves from CD_2O than H_2 from CH_2O: only 10% of the adsorbed deuterium reacts to molecular deuterium during the positive scan versus 55% for the hydrogen equivalent (Figure 2).

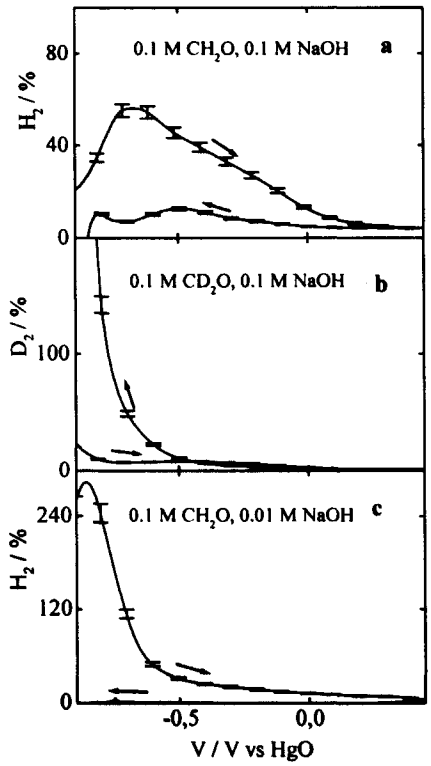

Figure 2. *Probabilities of adsorbed hydrogen and adsorbed deuterium to react to molecular hydrogen for solutions containing: (a) 0.1 M NaOH and 0.1 M CH_2O, (b) 0.1 M NaOH and 0.1 M CD_2O, and (c) 0.01 M NaOH and 0.1 M CH_2O.*

As the calculated ratio in Figure 2 roughly keeps pace with the dependence of the KIE on the potential applied (*see* below in Figure 7e), the lower evolution of hydrogen is explained by a lower adsorption rate of the deuterated enolate anion relative to the undeuterated one. The lower rate may lead to a lower quantity of adsorbed hydrogen at the gold surface with an associated preference of step [7] to proceed over step [6] (section 1.3) for stoichiometric reasons, as illustrated in Figure 3. It can be further seen from Figure 1f that smaller quantities of CO_2 evolve from CD_2O than from CH_2O. This KIE suggest that complete dehydrogenation also proceeds more rapidly for CH_2O than for CD_2O.

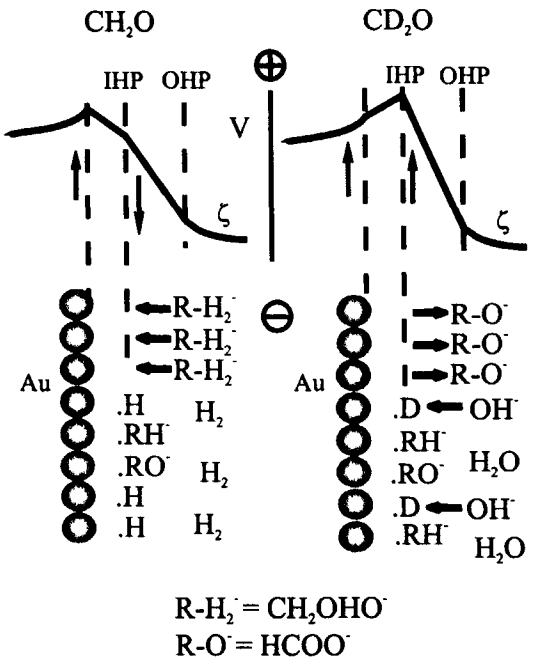

Figure 3. *Model explaining the different gas evolution properties for CH_2O and CD_2O: Positive polarization of the gold surface favours the rate of adsorption of undeuterated enolate anions (CH_2OHO^-) relative to the rate of desorption of formate anions with an associated increase of adsorbed and molecular hydrogen. Positive polarization of the gold surface also favours the rate of desorption of formate anions relative to the rate of adsorption of deuterated enolate anions (CD_2OHO^-) with an associated decrease of adsorbed and molecular hydrogen.*

0.01 M NaOH and 0.1 M CH_2O - The faradic current and the corresponding H_2 and CO_2 mass currents for a solution containing 0.01 M NaOH and 0.1 M CH_2O are shown in Figure 1g through 1i. Comparison with Figure 1a shows that the faradic current sets in at a higher potential and that it reaches lower values. It confirms the importance of hydroxyl ions in the kinetics of the reaction.[1,2] The relatively high evolution of hydrogen (Figure 1h and 2c) is explained by the low concentration of hydroxyl ions, as this may speed up step [6] over step [7] (section 1.3).

Temperature Dependence - The dependence of the evolution of H_2 on temperature is shown in Figure 4.

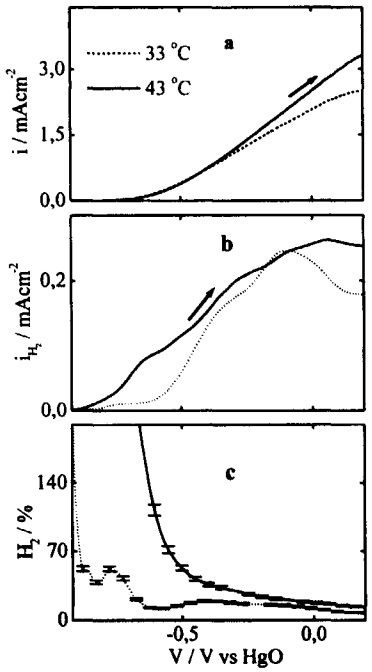

Figure 4. *Linear sweep voltammograms, H_2 mass signals and probabilities of adsorbed hydrogen to react to molecular hydrogen at 33°C and at 43°C (a-c). The scan rate was 10 mVs^{-1} in each measurement*

An increase in temperature speeds up the reaction, as seen from the higher faradic current at 43°C than at 33°C (no comparison should be made with the evolution at room temperature, shown in Figure 1a, as different gold electrodes were used). Besides, the absolute amounts of hydrogen and the amount of hydrogen relative to the faraday current (current efficiency) are higher at 43°C than at 33°C (Figure 4). This observation is explained by a higher relative rate of step [4] at the higher temperature with a consequent preference of step [6] to proceed over step [7] for stoichiometric reasons (more adsorbed hydrogen is formed).

0.1 M NaOH and 0.01 M CH_2O - The evolution of hydrogen from solutions containing 0.1 M NaOH and 0.01 M CH_2O was negligible. Presumably, the lowering of the surface concentration of adsorbed hydrogen goes along with a longer average path of surface migration, favoring the formation of water over the evolution of hydrogen. Furthermore, the HD mass signals were not higher than the background signal, supporting the view that the evolution of hydrogen proceeds by the mechanism outlined in section 1.3.

Rate of hydrogen desorption - The rate of hydrogen evolution does likely not affect the overall rate of the electro-oxidation reaction to great extent. Namely, a comparison of Figures 1a and 1b with Figures 1c and 1d shows that larger amounts of hydrogen evolve

for the solution containing CH_2O than for that containing CD_2O. The oxidation current of the latter is nevertheless higher at potentials where relatively large quantities of hydrogen evolve. Moreover, the rate of the formation of water does not rule the overall rate of the electro-oxidation reaction either since comparison of Figure 4a with 4c shows that higher currents may flow when smaller amounts of water are formed. Hence, steps 6 and 7 do likely play a minor role in the overall rate of the electro-oxidation reaction.

4.2.2 Non-Electrochemical Side Reaction

As mentioned, the data presented in Figure 4 are theoretical results that reflect the practical probabilities of adsorbed hydrogen to react by step [6] only when any hydrogen evolution occurs by step [6] and step [7]. If this is the case, the probability cannot exceed 100%. However, it can be seen in Figure 2 and 4 that the probabilities of adsorbed hydrogen and deuterium to react to H_2 and D_2 do exceed 100%. Besides, hydrogen evolution occurs at the OCP. Both observations confirm the occurrence of a non-electrochemical side reaction.[5,6] The extent to which the side reaction proceeds is nevertheless unclear as it cannot be calculated: two gas evolution steps and two partial faradic steps proceed, whereas only one hydrogen current, one faradic current, and one calibration current is measured. It may be pointed out that the actual occurrence of the side reaction is doubtful, as it could arise from the uncertainty in data due to the low currents, or from slight lowering of the faradic current due to the slight occurrence of the oxygen reduction reaction (nitrogen was bubbled). However, the voltammogram of the gold electrode (Figure 2, Chapter 2) does not give evidence for strong oxygen reduction at potentials around the OCP. Besides, 95% confidence intervals did not give evidence for a high uncertainty in the data either (Figure 2 and 4). Furthermore, as currents are reasonably high at 43°C (Figure 4), and as the occurrence of the side reaction has been reported before, it is concluded that the side-reaction does occur.[5-7]

The origin of the side reaction has been matter of dispute although its increase upon using CD_2O instead of CH_2O suggests that the dehydrogenation step plays an important role in its overall kinetics. Moreover, its presence under open-circuit conditions (OCP) suggests that its kinetics are not ruled by electron-transfer steps. Its strong increase upon lowering the pH suggests that hydroxyl ions are not involved by stochiometry. Furthermore, its strong increase upon raising the temperature suggests that chemical bond ruptures may govern the activation energy. Consequently, the side reaction may be described by the following scheme:

$CH_2OHO^-(aq) \leftrightarrow HCOO^-(aq) + H_2\uparrow$

This scheme is in concordance with Baltruschat *et al.*[5]

4.2.3 Diffusion

A rotating disk electrode was used to study diffusion for solutions containing 0.1 M NaOH and 0.1 M CH_2O (Figure 5). The important role of diffusion in the overall rate of the reaction is evident at higher potentials (Figure 5a). Non-linear Levich plots ($i \sim \sqrt{\omega}$ or $1/i \sim \sqrt{\omega}$) were further obtained, confirming the complicated, non-Fickian character of the diffusion process, as mentioned in Chapter 3 (Figure 5b).[8] The invariance of the current with both the rate of rotation above 49 rps and the scan rate above 10 mVs^{-1} points towards the accumulation of reactants and products at the gold surface (Figure 5c).

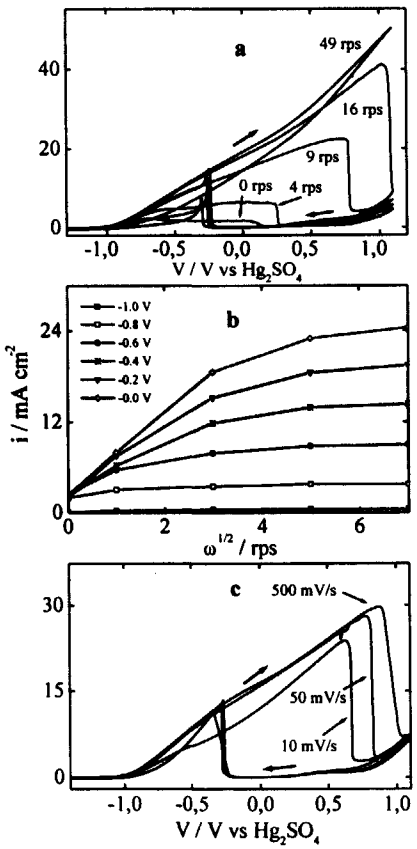

Figure 5. *(a) Cyclic voltammograms recorded at 10 mVs^{-1} and 0, 4, 9, 16, and 49 rps, respectively. (b) Levich plots at different voltages. (c) Cyclic voltammograms recorded at 10, 50, and 500 mVs^{-1}, respectively, and 16 rps.*

4.2.4 pH dependence

The strong influence of the pH on the kinetics of the reaction is evident from the V-i plots (Figure 6a).

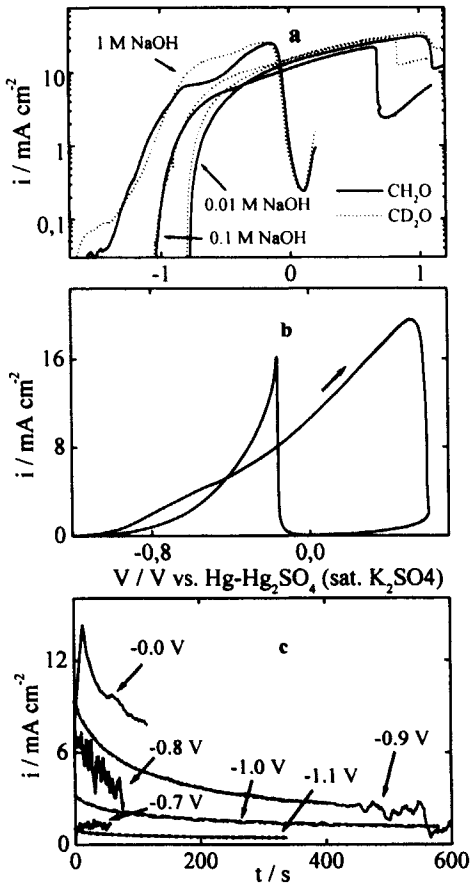

Figure 6. *(a) V-i plots obtained at 1 mVs^{-1} for solutions containing either 0.1 M CH_2O or 0.1 M CD_2O and different concentrations of NaOH. (b) Cyclic voltammogram obtained for a solution containing 0.1 M NaOH and 0.1 M CH_2O at a scan rate of 10 mVs^{-1}. Current transients recorded in the same solution. The arrows indicate the initial potentials relative to the Hg-Hg_2SO_4 reference electrode. (c) The fitted functions are shown for -1.1, -1.0, and -0.9 V and are described in Table I.*

An increase in the hydroxyl concentration by a factor ten speeds up the reaction by multiple orders of magnitude, presumably as a result of the respective stoichiometry of hydroxyl ions in the reaction, the lowering of the local potential at the gold surface by adsorption of hydroxyl ions and the hydroxyl-catalyzed character of C-H bond dissociation.[1,2,9,10] The absence of classical electron-transfer controlled rates with linear slopes of 59 and 118 $mVdec^{-1}$ supports the view that the kinetics of the reaction has a catalytic character rather than electrochemical one, *i.e.* chemical interactions seem more important in the overall reaction kinetics than electron transfers to and from the electrode surface.[8,11] No definite theory exists for the description of catalytic reactions proceeding in charged aqueous, electrical fields, but it was shown in Chapter 3 that adsorption of the enolate anion and desorption of formate is accompanied by large capacitive changes in the inner Helmholtz plane (IHP).[8] The large time constants ($\sim 10^3$ s) of the electrostatic rearrangements may eclipse the exponential dependence of the faradic current on the applied potential at the sweep rates examined in the current study (*see* Chapter 3).

4.2.5 Potential Dependence of Rate-limiting Steps

A cyclic voltammogram together with the corresponding current transients for solutions containing 0.1 M NaOH and 0.1 M CH_2O is shown in Figure 8b and 8c. The transients could be fitted well at voltages up to -0.9 V by the sum of two exponential functions (Table 1).[12] It suggests that the overall reaction kinetics may be conceived by two different kinetic steps.

	Y_0	A_1	A_2	t_1 / s	t_2 / s	t_1 / t_2	KIE	C_3
-1.1	0.45	0.40	0.18	97.6	2.5	39.58	>1	Neg
-1.0	1.05	1.35	0.79	232.6	26.8	8.68	>1	Neg
-0.9	1.75	3.58	3.87	45.5	275	0.17	<1	Pos

Table 1. Parameters fitted on the current transients shown in Figure 6 using $Y = Y_0 + A_1\exp(-x/t_1) + A_2\exp(-x/t_2)$.

The ratio between the first and second decay time of the fitted exponents changes from higher than one at -1.1 V ($t_1 > t_2$) to lower than one at -0.9 V ($t_1 < t_2$), suggesting that different steps may be rate-limiting at different potentials. Interestingly, this trend is traced by the values of the KIE (*see* below in Figure 7) and the appearance of the positive and negative capacitive behaviour in the impedance spectra (Chapter 3).[8] As ionisation, diffusion, physisorption and the desorption of adsorbed hydrogen (Step [1], [2], [3], [6], and [7]) were seen to be of minor significance in the overall reaction kinetics at these potentials (*see* above and Chapter 1 and 5), and as the KIE is higher than one at -1.1 V,

step [4] may be rate-limiting at -1.1 V. Consequently, the remaining step [5] may be rate-limiting at -0.9 V.[8] This view is in accordance with the view developed in Chapter 3.

The decrease in the rate of formate desorption (step [5]) relative to the rate of chemisorption (step [4]) with increasing potentials seems further obvious from the sudden scattering in current after 460 s at -0.9 V, and from the rapid current decline at -0.8 V and -0.7 V (Figure 6). Namely, the rate of desorption may become so slow at these potentials that poisoning of the gold surface sets in. This view is further supported by the irreproducibility and counterclockwise hysteresis of the voltammograms recorded with the upper potential limit in the region of the current decline. At much higher potential (-0.3 V), non-oscillating transients were obtained and poisoned species stripped, as voltammograms with the upper limit in this potential range were entirely reproducible and showed clockwise hysteresis.

4.2.6 Kinetic Isotope Effects and Apparent Activation Energies

0.1 M NaOH and 0.1 M CH_2O or 0.1 M CH_2O - Linear sweep voltammograms recorded at different temperatures in solutions containing 0.1 M NaOH and either 0.1 M CH_2O or 0.1M CD_2O together with the values of the KIE and E_{act} are shown in Figure 7. At lower potentials (~-0.9 V), the rate of oxidation decreases at higher temperature for the solution containing CH_2O but increases for the solution containing CD_2O (Figure 7a and 7b). The activation energies accompany this trend with negative values for CH_2O and positive ones for CD_2O (Figure 7c). It supports the presence of a pre-equilibrium (accumulation) in the reaction due to the rate-limiting character of the formate desorption, as mentioned in Section 3.2.5 and discussed in more detail in Section 4.2.8.

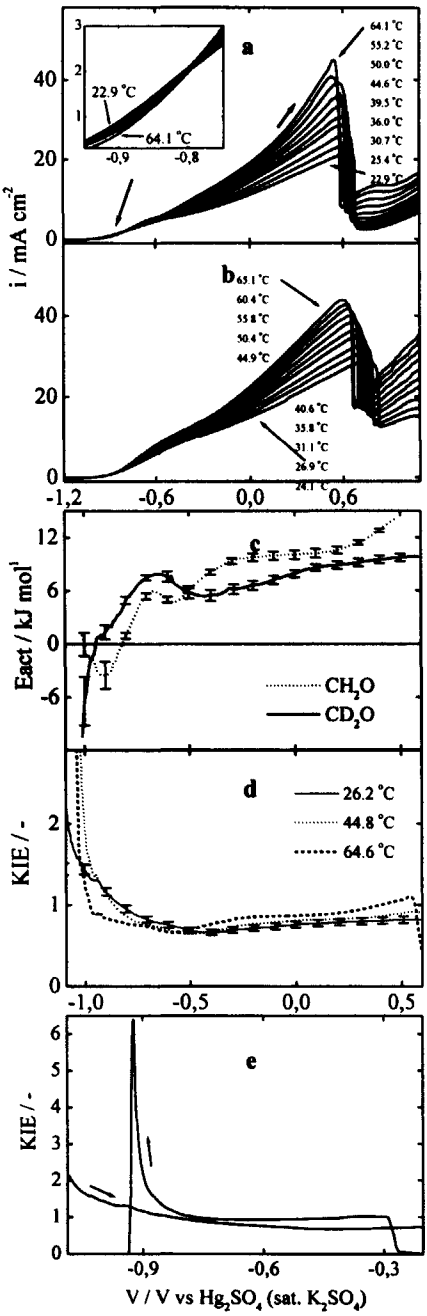

Figure 7. *(a) Linear sweep voltammograms recorded at 10 mVs^{-1} in solutions containing 0.1 M NaOH and 0.1 M CH_2O. The largest current corresponds with the highest temperature, the second largest current with the second highest temperature, etc. (b) Reverse behavior was observed at low overpotentials with lower currents at higher temperatures (inset). Curves obtained for CD_2O. (c) Activation energies calculated at different voltages. (d) KIE calculated at different temperatures. (e) KIE obtained for a positive and a negative scan.*

At higher voltages (-0.8 V), all rates increase at increasing temperatures and the reaction becomes predominantly controlled by diffusion. A significant kinetic role remains nevertheless present in the overall reaction kinetics, as witnessed by the values of the KIE different than 1 (Figure 7d). The values of the KIE are somewhat lower than 1 at higher potentials, which is explained by a higher rate of oxidation of adsorbed deuterium (Step [7]) than of adsorbed hydrogen. The higher stability of adsorbed hydrogen than of adsorbed deuterium is further obvious from the higher amount of hydrogen evolution relative to the amount deuterium gas evolution, as indicated from the DEMS measurements above. The importance of step [6] and [7] in the values of the KIE lower than one seems to become further clear by the strong dependence of the KIE on the pH (*see* below).

The value of the KIE depends strongly on the direction of scanning, as revealed by Figure 7e: the values range between 0.7 and 2 during the positive scan and reach values close to the theoretical maximum of 7 at -0.92 V during the negative scan. Apparently, scanning in negative direction speeds up the rate of desorption of the formate anion (step [5]) relative to the rate of chemisorption (step [4]), making the chemisorption step entirely rate limiting for both CH_2O and CD_2O.

Another interesting concept hidden in the dependence of the KIE on the direction of charging is the direct involvement of steric and electrostatic rearrangements in the transition state. Namely, the simultaneous revelation of high values of the KIE and large capacitive contributions with low associated time constants suggests that both the rupture of the RC bond as well as the electrostatic rearrangements may comprise the transition state between the IHP and the electrode surface.[8]

0.1 M NaOH and 0.01 M CH_2O or 0.01 M CD_2O - Linear sweep voltammograms recorded at different temperatures in solutions containing 0.1 M NaOH and either 0.01 M CH_2O or 0.01 M CD_2O together with their corresponding KIE and E_{act} are shown in Figure 8. The much lower oxidation currents at these lower formaldehyde concentrations roughly confirm the approximate first-order character of the concentration in the overall rate of the reaction (compare Figure 7 with 8), as presented in the next Chapter.[2,12] Comparison of Figure 7c with Figure 8 shows that the concentration plays an important role in the height of the activation energy, as higher values are reached for the lower formaldehyde concentration. The absence of negative activation energies suggests the presence of a pre-equilibrium, an observation that is plausible at these lower concentrations. The values of the KIE strongly decrease at higher temperature pointing toward a decreasing role of the chemisorption step in the overall rate of the reaction.

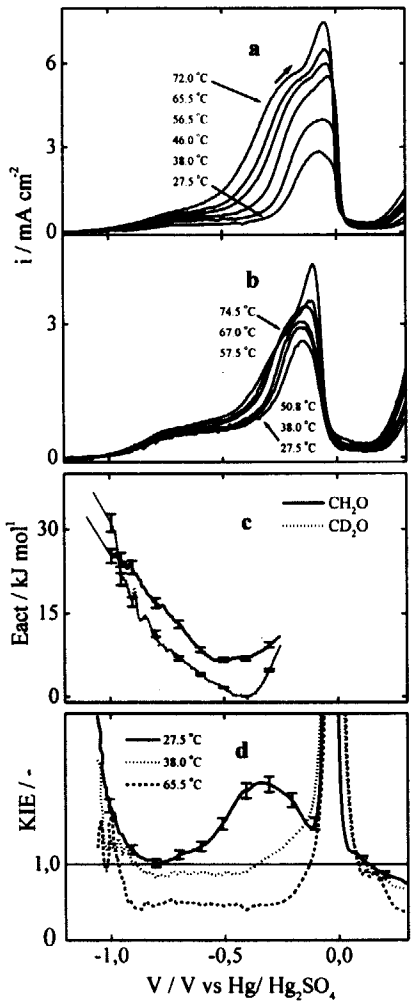

Figure 8. *(a) Linear sweep voltammograms obtained in solutions containing 0.1 M NaOH and 0.01 M CH_2O at 10 mVs^{-1}. The highest current corresponds with the highest temperature, the second highest current with the second highest temperature, etc. (b) Curves obtained for CD_2O. (c) Activation energies calculated at different voltages together with the extrapolated curve. (d) Values of the KIE calculated at different temperatures.*

1 M NaOH and 0.1 M CH_2O or 0.1 M CD_2O - Linear sweep voltammograms recorded at different temperatures in solutions containing 1 M NaOH and either 0.1 M CH_2O or 0.1 M CD_2O together with the corresponding KIE and E_{act} are shown in Figure 9.

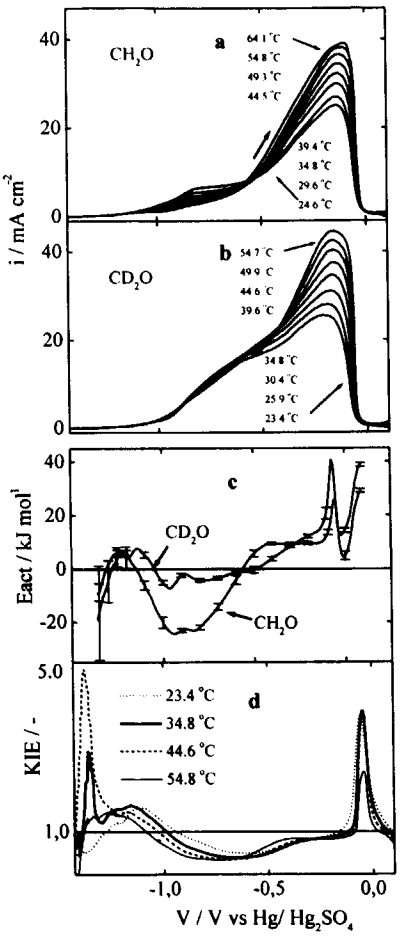

Figure 9. *Linear sweep voltammograms recorded in solutions containing 1 M NaOH and 0.1 M CH_2O at 10 mVs^{-1}. The highest current corresponds with the highest temperature, the second highest current with the second highest temperature, etc. (a) Reverse behaviour was observed at low overpotentials with lower currents at higher temperatures. (b) Curves obtained for CD_2O. (c) Activation energies calculated at different voltages. (d) KIE calculated at different temperatures.*

A strong decrease in the rate of the reaction is seen at higher temperatures for both CH_2O and CD_2O at this pH, reflected by strongly negative activation energies. Low values of the KIE are further observed at low potentials, suggesting that the rate of the reaction is controlled by step [5] under these conditions. At first sight, this seems unexpected, as the higher hydroxyl concentration would primarily speed up step [5], making other steps rate limiting. Apparently, the hydroxyl-catalysed character of the C-H bond rupture step speeds up step [4] more than the change in pH does to step [5]. This view seems supported

by the values of the fitted rate constants of the radiotracer adsorption kinetics as well as by the independence of the reaction rate on the concentration in solutions containing 1 M NaOH (Chapter 5).[1,2,12] It can be further seen from the values of the KIE in Figure 9d that step [5] seems rate-limiting for both CH_2O and CD_2O only at very low potentials and at 45°C. The KIE-values increase with temperature first but decrease at higher temperatures. Presumably, rapid poisoning of the gold surface sets in under these rather vehement conditions.

0.01 M NaOH and either 0.1 M CH_2O or 0.1 M CD_2O - Results obtained for solutions containing 0.01 M NaOH and either 0.1 M CH_2O or 0.1 M CD_2O at different temperatures together with the corresponding KIE and E_{act} are shown in Figure 10.

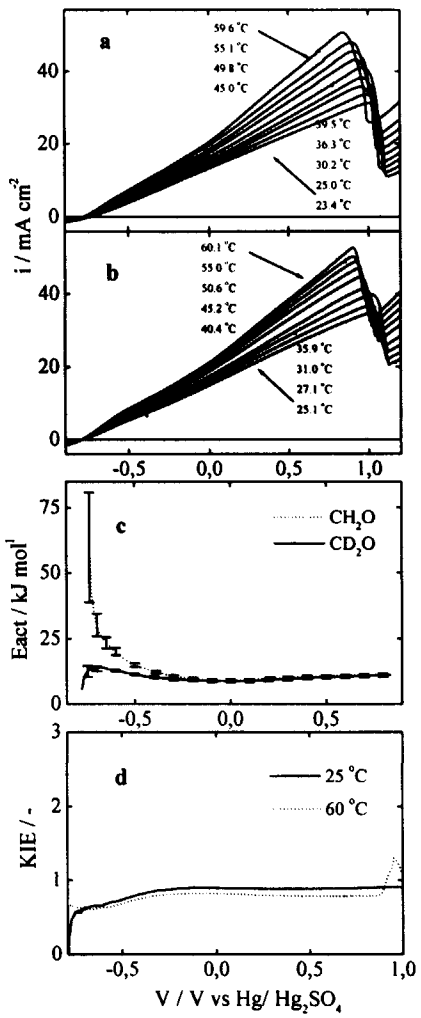

Figure 10. *Linear sweep voltammograms obtained in solutions containing 0.01 M NaOH and 0.1 M CH_2O at 10 mVs^{-1}. (a) The largest current corresponds with the highest temperature, the second largest current with the second highest temperature, etc. (b) Curves obtained for CH_2O. (c) Activation energies calculated at different voltages. (d) KIE calculated at different temperatures.*

The oxidation sets in at a much higher potential in these solutions that in the more alkaline solutions. Besides, the activation energies are much higher than obtained for solutions at higher pH. It confirms the catalytic and stoichiometric role of OH^- in the overall rate of the reaction. The maximum values of the current densities are roughly similar to the more alkaline solutions, implying that OH^- is not primarily involved in the mass-transfer controlled rate at high potentials. Furthermore, the values of the KIE are lower than 1, which is explained by a substantial role of the hydrogen desorption step (Step [6] and [7]) in the overall rate of the reaction.

4.2.7 Negative Apparent Activation Energies

General Remarks - The presence of negative apparent activation energies (Figure 7 and Figure 9) may seem deluding at first sight as it may suggest that reactions occur spontaneously. Negative activation energies are nevertheless an ordinary phenomenon when the reaction is characterized by a pre-equilibrium or by slow rates of desorption.[14] The identified side-reaction does likely not (directly) account for the negative energies, as this was absent under conditions where the negative energy was most apparent (in 1 M NaOH). A look at Figure 7c, 8c, 9c and 10c shows that the apparent energy roughly decreases at the higher pH-values and the higher formaldehyde concentrations. Note, that the values of the apparent activation energies are much lower than the values of the bond dissociation energies (338.1 $kJmol^{-1}$ for C-H and 341.4 $kJmol^{-1}$ for C-D), confirming the highly catalytic activity of gold and the surrounding molecules in the overall rate of the reaction.[13]

Specific Explanations - The negative values of the activation energies obtained for CH_2O and the positive ones obtained for CD_2O at -0.9 V in 0.1 M NaOH (Figure 7c) may be understood by realizing that different steps are rate-limiting step for CH_2O than for CD_2O. Namely, the values of the KIE (Figure 7d) are smaller than 7 and larger than 1 (if they were both rate-limiting in step [3] the KIE would be around 7). These different rate-limiting properties for CH_2O compared to those for CD_2O were revealed by some impedance spectra as well.[8,12] As the C-H bond ruptures more rapid than the C-D bond under the condition examined, step [5] may be referred to as rate limiting for solutions containing CH_2O. On the other hand, step [4] seems rate limiting for solutions containing CD_2O. The difference in rates are nevertheless relatively small, as indicated from the values of the fitted rate constants in the radiotracer adsorption studies and from the (possibly) responsible fitted capacitors in EIS.[8,12]

The values of the activation energies obtained for CH_2O and CD_2O at -0.9 V in 1 M NaOH (Figure 9c) are both negative, suggesting that the pre-equilibrium is present for both species. The KIE-values lower than 1 for both species suggests that the rate of

desorption (step[5]) may be rate-limiting for both species. In 0.01 M NaOH, the high value of E_{act} may be related to the absence of both hydroxyl ions and deprotoneted gem-diols (enolate anions) at the interface (Figure 10 c). The relatively high value of E_{act} for the solution containing 10 mM CH_2O or 10 mM CD_2O suggests that lateral interactions between enolate anions may lower the activation energy, as more enolate anions may be adsorbed at the higher formaldehyde concentrations (Figure 8c).

4.2.8 Semi-Quantitative Reaction Model

Recalling the reaction scheme set out in Chapter 1, a corresponding energy scheme may be constructed at the OCP for solutions containing 0.1 M NaOH and 0.01 M CH_2O by taking into account the following observations and considerations (Figure 11): First, diffusion plays a negligible role at the OCP and diffusion-related steps may therefore be rejected. Second, the kinetics of the physisorption and chemisorption steps have been unraveled at the OCP by the radiotracer technique. Without discussing details, the corresponding activation energies amount to 16.0 and 76.7 $kJmol^{-1}$ (Chapter 5).[12] The overall activation energy was obtained by extrapolation of the apparent activation energy to the OCP using the standard Origin 4.1 program (Figure 10c). It yielded a value of 32.2 $kJmol^{-1}$. The E_{act} of the desorption step was obtained by taking the overall apparent activation energy as the sum of the solution-OHP barrier and the OHP-IHP barrier and by bearing in mind that both the desorption and chemisorption steps proceed between the OHP and the IHP (*see also* Chapter 3 and 5) .[8] Steps related to the desorption of adsorbed hydrogen were not taken into account as these were seen to be of minor significance in the overall reaction kinetics over a broad range of conditions (see above).

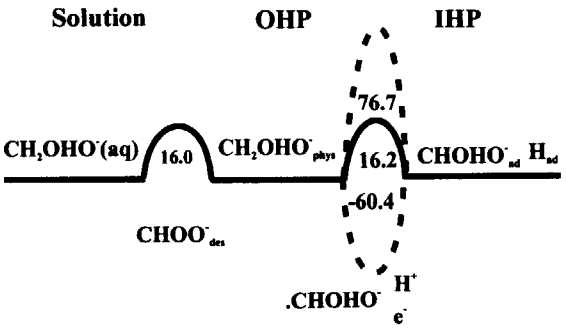

Figure 11. *Quantitative model for the reaction for solutions containing 0.1 M NaOH and 0.01 M CH_2O at the OCP.*

4.3 Conclusions

- The rates of H_2 ,D_2 , and CO_2 gas evolution depend to great extent on experimental conditions but play a minor role in the overall rate of the reaction.
- The evolution of hydrogen at the OCP and the values of the current efficiency higher than 100% confirmed the presence of a non-electrochemical dehydrogenation reaction parallel to the electro-oxidation reaction.
- The overall reaction rate of the reaction in 0.1 M NaOH is likely determined by the chemisorption of the enolate anion at low potentials, by the desorption of the formate anion at higher potentials, and by diffusion at the highest potentials.
- The presence of hydroxyl ions in the solution speeds up the overall rate of the electro-oxidation reaction, as it may favour the respective lowering of the local potential at the gold surface, the chemisorption of the enolate anion, the desorption of both adsorbed hydrogen and adsorbed, dehydrogenated anions, and as it fulfills a stoichiometric role.
- The apparent activation energies for the overall electro-oxidation reaction ranged in value roughly between -25 and 60 $kJmol^{-1}$ confirming the catalytic properties of gold in the overall rate of the reaction.
- The values of the apparent activation energies were generally seen to be lower at high pH-values and at a higher concentration of formaldehyde. Negative values were encountered in 1 M NaOH and in 0.1 M NaOH, most likely due to the presence of a pre-equilibrium (slow rate of formate desorption).

4.4 References

(1) Beltowska-Brzezinska, M.; *Electrochim. Acta*, **1985**, 30, 1193.

(2) Beltowska-Brzezinska, M.; *J. Electroanal. Chem.*, **1985**, 187, 167.

(3) Enyo, M.; *J. Appl. Electrochem.*, **1985**, 15, 907.

(4) Gootzen, J. F. E.; Ph.D. Thesis, University of Technology-Eindhoven, The Netherlands,1997, p. 7.

(5) H. Baltruschat, H.; Anastasijevic, N. A.; Beltowska-Brzezinska, M.; Hambitzer, G.;
Heitbaum, J.; *Ber. Bunsen-Ges. Phys. Chem.*, **1990**, 94, 996.

(6) Jusys, Z.; *J. Electroanal. Chem.*, **1994**, 375, 257.

(7) Jusys, Z.; Vaskelis, A.; *J. Electroanal. Chem.*, **1992**, 335, 93.

(8) Kortenaar, M. V. ten; Tessont, C.; Kolar, Z. I.; Weijde, H. van der.; *J. Electrochem.Soc.* **1999**, 146, 2146.

(9) Bindra, P.; Roldan, J.; *J. Electrochem. Soc.*, **1985**, 132, 2582.

(10) Burke, L. D.; Nugent, P. F.; *Gold. Bull.*, **1998**, 31, 39.

(11) Gileadi, E.; In *Electrode Kinetics*, VCH Publishers Inc., New York, p. 307, 1993.

(12) Kortenaar, M. V. ten.; Kolar, Z. I.; Goeij, J. J. M. de.; Frens, G.; *Langmuir*, Submitted for publication.

(13) Weast, R. C. Editor, In *CRC Handbook of Chemistry and Physics*, 66th ed., p. F-175, CRC Press Inc., Boca Raton, Florida, 1985.

(14) Atkins, P. W.; in *Physical Chemistry*, 3rd ed., p. 706, Oxford University Press, Oxford, U.K., 1986.

Chapter 5

Adsorption, Exchange and Oxidation of Formaldehyde on Gold: A Radiotracer Study*

The adsorption, exchange and oxidation of formaldehyde has been studied on gold by voltammetry, the radiotracer thin-gap method and compartimental analysis. The overall adsorption process at the open circuit potential (OCP) can be well described by a rapid physisorption and a slow chemisorption, both proceeding in a catenary (linear), reversible fashion. Linear adsorption isotherms were obtained under most conditions, implying that of the Gibbs free energy of the reaction depends little on the potential, temperature and pH. At pH 13, the kinetics of the electro-oxidation of formaldehyde is approximately first order in both the concentration of formaldehyde and in the quantity of species adsorbed at the gold surface. The strong dependence of the quantity of species adsorbed on the formaldehyde concentration in the solution, and the invariance of the adsorption isotherms with the potential suggest that potential gradients on the solution side are more important in adsorption rates than the potential of the electrode itself. The rate of the reaction is determined by chemisorption of the enolate anion at low potentials, by desorption of formate at medium potentials, and by diffusion at highest potentials. The values of ΔG_{ad} differ substantially from the solution-variable values of ΔH_{ad} and from the metal-formate formation enthalpy, implying that Gibbs free adsorption enthalpies should be used to validate Sabatier's principle and that solution effects should not be neglected.

* *Langmuir* **2002**, 18, 10279

5.1 Introduction

This chapter aims to further elucidate the oxidation of formaldehyde on gold by using voltammetry, the radiotracer-thin gap technique and compartimental analysis. Special focus is laid on the elucidation of the kinetics and thermodynamics of the adsorption steps of the reaction at different pH-values, concentrations and temperatures. In addition, the influence of solution effects and entropies in the bond strengths are addressed.

5.2 Results and Discussion

5.2.1 Fitted Model

Of all two-compartment and three-compartment models fitted to the data obtained for gold by compartmental analysis (*see* Chapter 2), only the model shown in Figure 1 described all adsorption kinetic data satisfactorily.

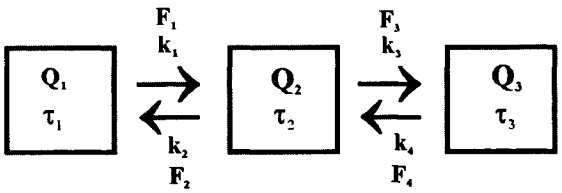

Figure 1. *Fitted model that described the overall adsorption and exchange data most satisfactorily.*

The corresponding equations that bridge the so-called catenary or linear three-compartment model to the data are summed up in the Appendix of this Chapter. The model was unique and plausible in terms of the respective mechanism set in Chapter 1, the fitted equivalent circuit and the electrostatic double-layer structure derived in Chapter 3.[1,2] The fact that data could be fitted by first-order differential equations (with exponential solutions) rather than by root-type equations suggests that the rate of the adsorption processes are ruled by kinetic, electrostatic barriers rather than by mass-controlled, diffusive ones.[2] Hence, the rate of diffusion or convection was larger than the rate of adsorption when the electrode was held in the up position (adsorption data were collected when the electrode was held in the up position). On the other hand, a very slow, diffusive 'random-walk' adsorption seemed to apply to the system when the electrode was held in the down position, as counting rates remained approximately constant under these conditions.[3]

5.2.2 Interpreted Model

The assignments of the fitted mass flows to the actual reaction may be made by bearing in mind the following considerations: First, experiments were carried out in nitrogen saturated solutions at the OCP and consequently, diffusion and electron transfer steps (step [2], [5] and [7] of the mechanism in Section 1.3) may be omitted. Besides, as no hydrogen evolves at the formaldehyde concentrations examined (Section 4.2.1), step [6] may be omitted too.[2] Furthermore, as the pK_a of the weak acidic gem-diol, $CH_2(OH)_2$, amounts to ~13, the gem-diol is largely deprotonated by the alkaline NaOH and the equilibrium of step [1] may be assumed to lie on the right-hand side.[4,5] The occurrence of physisorption (step [3]) in the reaction has been suggested in Section 3.2.1 from studies reported by Beltowska *et al.*[1,6,7] The occurrence of chemisorption (step [4]) has been indicated by the values of the KIE different than 1 (Chapter 4), and by the presence of dissociated enolate anions at the gold surface, as observed by infrared spectroscopy.[2,8] The adsorption process may therefore be described schematically by the model shown in Figure 2a. Physical assignments to the fitted model can be made by comparing Figure 1 with 2a, yielding the picture shown in Figure 2b.[1,2]

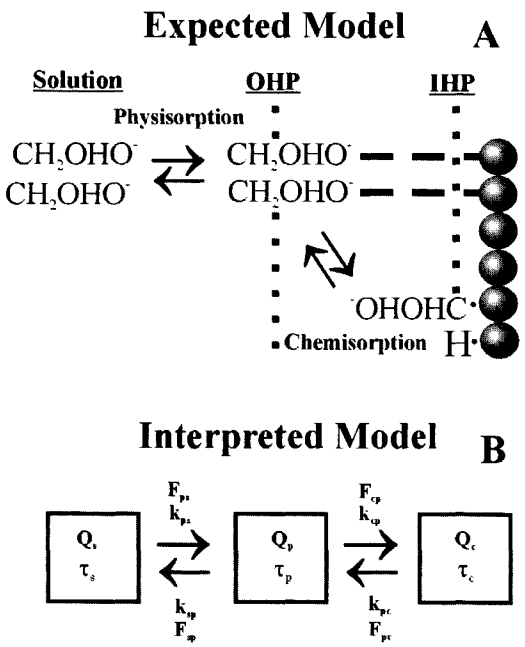

Figure 2. *The expected model (a) and the interpreted model (b) were derived from considerations discussed in the text as well as from data obtained by EIS, voltammetry and DEMS.*[12]

Clearly, physisorption and chemisorption of the enolate anion proceeds in a catenary fashion rather than in a mammillary one (the enolate anion may then adsorb directly on the gold surface by both physisorption and chemisorption). The model shown in Figure 2b will serve as base for the quantitative discussion of the data.

5.2.3 Adsorption and Exchange Kinetics at the OCP

Adsorption Kinetics - The adsorption of formaldehyde on gold at the OCP in a solution containing 0.1 M NaOH and 0.01 M CH_2O (Procedure 1, Table 3, Chapter 2) is shown, together with the fitted curves, in Figure 3a. The steady state in the adsorption process is reached within ~1000 s, attaining a surface coverage of approximately 50% of the available gold sites, as calculated from a roughness factor of 3, an average Au-Au length of 3 Å, and a 'one formaldehyde-to-one gold site' occupation.[9] Analysis of the fitted transition times (Table 1) shows that species spend much more time in the chemisorbed state (τ_c) than in the physisorbed state (τ_p). Besides, the average flow of enolate anions at 'infinite' time between the solution and physisorbed state (F_{sp}) is much higher than the average flow between the physisorbed state and chemisorbed state (F_{pc}). The calculated quantities of species hosting the physisorbed state ($Q_{p,t=\infty}$) and chemisorbed state ($Q_{c,\ t=\infty}$) do not differ to great extent (Procedure 1, Table 3, Chapter 2 and Figure 3a).

Exchange Kinetics - To see if occupation of the gold sites had occurred in a reversible or irreversible manner, the exchange of adsorbed $^{14}CH_2O$-containing formaldehyde with its non-radioactive solute (solution 1, Table 3, Chapter 2) was studied (Figure 3b). Clearly, exchange of adsorbed CH_2O with dissolved CH_2O does occur. The value of 0.13 for the overall fitted residual fraction, as revealed by the sum of $q_p(\infty)/q_e(0)$ and $q_c(\infty)/q_e(0)$ in Table 2 does nevertheless exceed the value expected for a complete reversible system, as then this value should approach zero.

Influence of CD_2O - To see if occupation of the gold sites had occurred by a chemisorption or physisorption, the exchange of formaldehyde (adsorbed from solution 1, Table 3, Chapter 2) with deuterated, non-labelled formaldehyde (solution 2, Table 3, Chapter 2) was studied (Figure 3c). Clearly, a pronounced difference in the rate of exchange is observed between CH_2O and CD_2O, confirming the important role of the C-H bond rupture step in the overall adsorption kinetics of the enolate anion (Figure 3b and 3c).[1,2] Analysis of the fitted curves shows that the difference between CH_2O and CD_2O manifests more pronounced at longer times suggesting that another, more rapid step, practically independent of H/D substitution effects, is involved in the kinetics of the adsorption as well. In accordance with the physical assignments outlined above, the slow step is assigned as the chemisorption step whereas the rapid one is assigned as the

physisorption step. The transition times obtained from the fits for the exchange curves of CH_2O and CD_2O (Procedure 1 and 2 in Table 3, Chapter 2) show similar behaviour as observed for the adsorption kinetics under these conditions (Figure 3a): Species prefer to host the chemisorbed state over the physisorbed state.

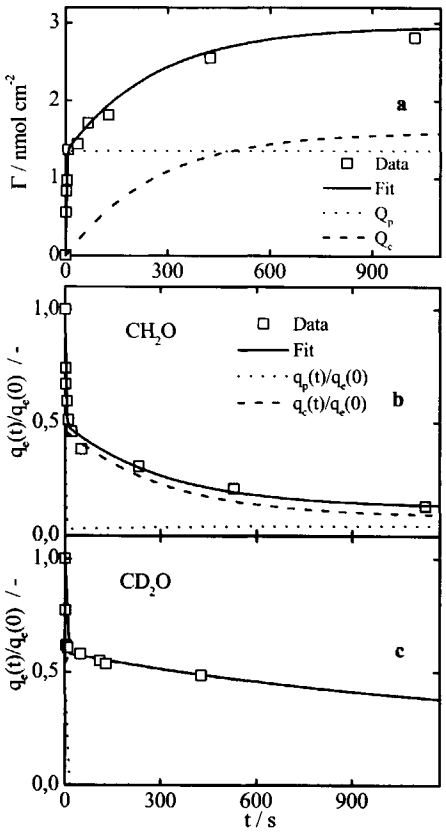

Figure 3. *Adsorption of formaldehyde on gold at the OCP in 0.1 M NaOH and 0.01 M CH_2O. The fitted analogues and the fitted quantities hosting the chemisorbed and physisorbed states are shown as well (a). Exchange of adsorbed, radiolabelled formaldehyde with solute formaldehyde (b) or deuterated formaldehyde (b) together with the fitted analogues.*

Procedure	k_{sp} / s^{-1}	k_{ps} / 10^{-5} s^{-1}	k_{cp} / 10^{-2} s^{-1}	k_{pc} / 10^{-2} s^{-1}	$Q_c(\infty)$/ nmol	$Q_p(\infty)$/ nmol	F_{ps} / nmol s^{-1}	F_{cp} / nmol s^{-1}	τ_p / s	τ_c / s
1	0.47	1.92	0.45	0.38	4.72	4.07	1.92	0.02	2.09	262
3	2.92	6.58	6.47	2.37	6.14	2.25	6.57	0.15	0.34	42.1
4	3.46	28.2	10.6	41.4	2.08	8.16	28.2	0.86	0.28	2.42
5	1.13	4.96	2.84	5.75	2.16	4.38	4.96	0.12	0.86	17.4
6	4.41	24.2	0.11	2.97	0.20	5.49	24.2	0.01	0.23	33.6
7	1.88	3.62	9.40	4.65	0.07	0.03	0.06	0.01	0.51	21.5

Table 1. *Values of the fitted rate constants (k), residual quantities (Q) interstate flows (F) and transition times (τ) for the adsorption kinetic curves.*

Procedure	k_{sp} / s^{-1}	k_{ps} / 10^{-2} s^{-1}	k_{cp} / 10^{-2} s^{-1}	k_{pc} / 10^{-2} s^{-1}	$q_p(\infty)/q_e(0)$ / -	$q_c(\infty)/q_e(0)$ / -	τ_p / s	τ_c / 10^2 s
1	0.39	2.04	0.57	0.29	0.09	0.042	2.56	3.40
2	0.67	0.15	7.19	0.06	0.26	0.002	1.35	16.6
3	1.06	2.37	4.68	2.93	0.033	0.021	0.90	0.34
4	3.10	1.17	56.6	12.2	0.05	0.005	0.27	0.08
5	0.36	0.18	3.55	6.55	0.003	0.005	2.52	0.15
6	0.84	0.10	532	21.3	0.028	0.001	0.16	0.05
7	1.33	7.68	5.40	9.10	0.031	0.053	0.72	0.11

Table 2. *Values of the fitted rate constants, residual fractions ($q(\infty)/q_e(0)$) and residence times for the exchange kinetic curves.*

Residual Fractions – As mentioned, the residual fractions of the exchange curves exceed values expected for a complete reversible system (Figure 3). This observation may be explained by irreversible adsorption, by an increased background signal due to the incomplete removal of the radio-labelled solution upon pumping, by insufficient counting statistics or by the limited measurement time.[10,11] The physical or chemical origin of the non-reversible behaviour could nevertheless not be elucidated in detail, as rinsing with water could cause depletion of adsorbed species, and as measurements with the relatively unstable and volatile formaldehyde could be made only for a limited period of time.[4,5] However, as the values of the fitted residual fractions were too large to be explained by insufficient counting rates or incomplete removal of the radio-labelled solution upon pumping (estimated at 0-5% of the initial value), and as these values exceeded values expected for a complete reversible system by at least a factor of hundred, the relatively high residual fractions are explained by formation of irreversibly adsorbed species (Figure 3c). This view seems further supported by DEMS measurements, which showed gas evolution at the OCP that was explained by the irreversible formation of formate species. In addition, the results obtained by chronoamperometry pointed towards the occurrence of a pre-equilibrium or poisoning (irreversible adsorption) at potentials close to the OCP (Section 4.2.4).[2] The stronger spontaneous, irreversible gas evolution for CD_2O than for CH_2O may be further in line the larger residual fraction for CD_2O than for CH_2O. Consequently, the high residual fraction is explained by formation of irreversibly adsorbed formate ions. Note, that the compartmental analysis did not give unambiguous evidence for the occurrence of the irreversible side-reaction on gold (*see* Figure 2) but it did for copper (Chapter 7).

Temperature Dependence - The dependence of the adsorption and exchange of formaldehyde on temperature in solutions containing 0.1 M NaOH and 0.01 M CH_2O (Procedure 1, 3 and 4, Table 3, Chapter 2) are shown, together with the calculated fits, in Figure 4. A substantial increase in the rate of adsorption and exchange can be observed at higher temperatures. The fitted transition times show too that species spend less time in the physisorbed and chemisorbed states at higher temperatures than at lower temperature (Table 1 and 2). Examination of the mass flows and rate constants shows that this is a consequence of the increased rate of chemisorption, as the rate of physisorption increases to a lesser extent at higher temperatures.

Activation Energies - An attempt was made to evaluate the activation energies of the physisorption and chemisorption steps at the OCP by plotting the values of the calculated rate constants at different temperatures (Table 3, Figure 5).

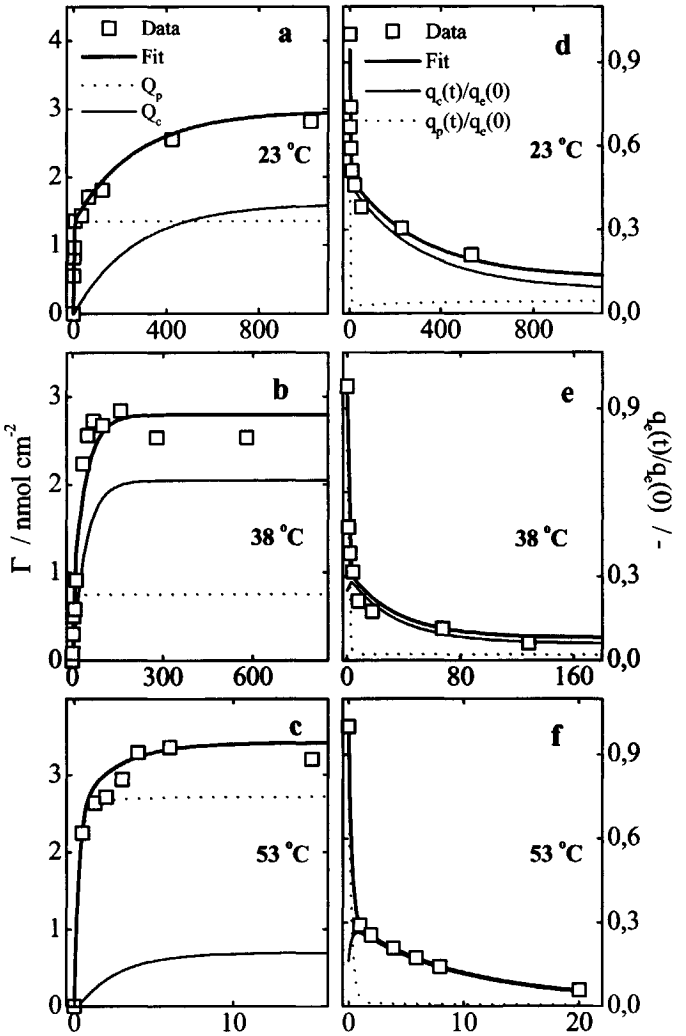

Figure 4. *Adsorption kinetics (a-c) and exchange kinetics (d-f) of formaldehyde on gold at different temperatures in solutions containing 0.1 M NaOH and 0.01 M CH_2O, together with the fitted analogues and the fitted quantities of species hosting the chemisorbed and physisorbed states (a-f).*

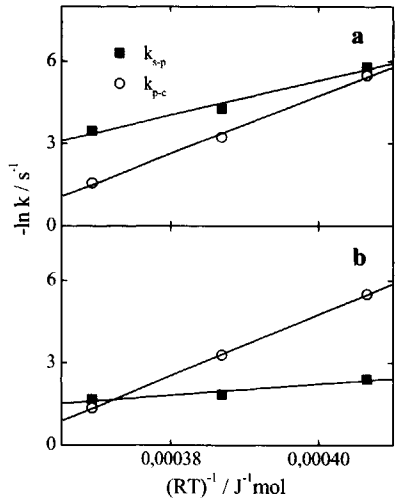

Figure 5. *Arrhenius plots of the physisorption and chemisorption steps for the adsorption kinetics (a) and the exchange kinetics (b).*

Although the results have low reliability as only three points could be taken into account, the values suggest that higher activation energies apply to the chemisorption step than to the physisorption step. Besides, the high absolute values of the activation energies at the OCP may be in line with the relatively high overpotentials required to oxidize formaldehyde at significant rates around the OCP.[2]

Procedure	E_{act}^{sp} / $kJmol^{-1}$	E_{act}^{pc} / $kJmol^{-1}$
Adsorption	62.7	105
Exchange	20.4	111

Table 3. *Activation energies for the physisorption and chemisorption steps. Values were calculated from results shown in Figure 5.*

pH-Dependence - The adsorption and exchange of formaldehyde on gold in solutions containing 0.01 M CH_2O and different concentrations of NaOH (procedure 1, 5 and 6, Table 3, Chapter 2) are shown, together with the calculated fits, in Figure 6. Clearly, the lowest rates of adsorption and exchange are seen in solutions containing 0.1 M NaOH. Examination of the fits shows that more species occupy the chemisorption than the physisorption state under these conditions (Table 2).

The higher occupation of the chemisorption state in solutions containing 0.1 M NaOH than in those containing 0.005 M is explained by the hydroxyl-catalyzed character of the chemisorption step (Section 4.2.4).[6,7] The lower occupation of the chemisorption state in solutions containing 1.0 M than in those containing 0.1 M NaOH is explained by the increased adsorption of hydroxyl ions at the gold surface (Figure 6c). It supports the hydroxyl-mediated adsorption model postulated by Burke *et al.*[12] The fitting results of the exchange curve at the higher pH do nevertheless contradict this view, as it suggests that species prefer to host the chemisorption state.

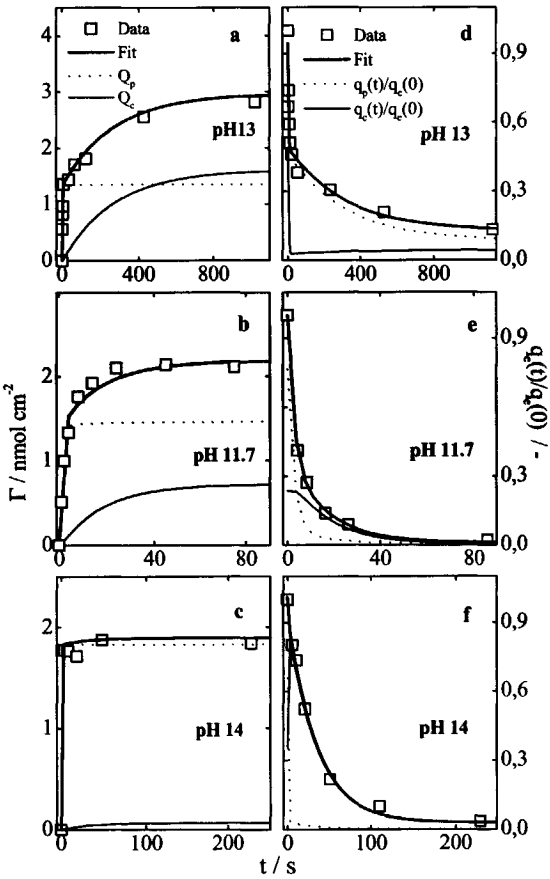

Figure 6. *Adsorption and exchange of 0.01 M formaldehyde at different pH together with the fitted curves and the fitted quantities hosting the chemisorbed and physisorbed states (a-f).*

Concentration Dependence - The adsorption and exchange of formaldehyde on gold in solutions containing 0.1 M NaOH and 0.17 mM CH_2O (Procedure 7, Table 3, Chapter 2) are shown, together with the calculated fits, in Figure 7.

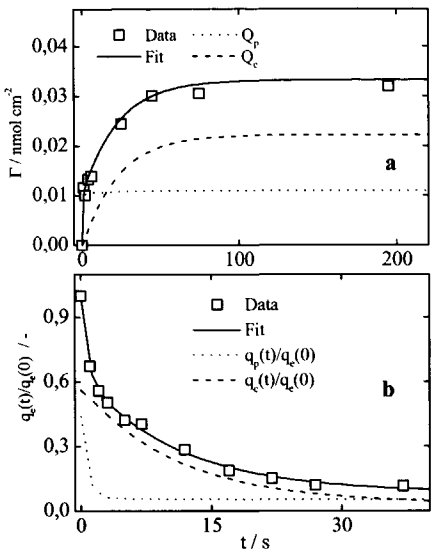

Figure 7. *Adsorption and exchange of formaldehyde in 0.17 mM CH_2O solutions together with the fitted curves and the fitted quantities hosting the chemisorbed and physisorbed states (a and b).*

Comparison of Figure 7 with Figure 4 shows that the adsorption is completed much more rapidly at this low formaldehyde concentration than at 0.01 M. Besides, the enolate anions tend to chemisorb to greater extent, as revealed by the higher relative quantity of species occupying the chemisorption state.

Reliability of the Model – As mentioned, no quantitative evaluation of errors was made for the fitted data, as it was difficult to trace the origin of the errors (Section 2.5.5). However, an indication of the quality of the fits may be obtained by analysing the outcome of the fits in Figure 3, 4, 6 and 7. Clearly, all data could be fitted relatively well by the model outlined in Figure 1. Moreover, a comparison of the values of τ_p and τ_c in Table 1 with those in Table 2 shows that in most cases the ratios do not differ much from one (Table 4). An overall average of all data with (the exclusion of one exceptional point) yielded a value of 0.92, which seems acceptable upon considering the presence of the statistical, systematic and fitting errors (Section 2.5.5). The results for both tables were obtained in an autonomous fashion and further support the view that the adsorption kinetics of the reaction can be described satisfactorily well by the model outlined above.

Procedure	1	3	4	5	6	7
$\tau_{p(ads)} / \tau_{p(ex)}$	0.83	0.38	1.04	0.34	1.44	0.71
$\tau_{c(ads)} / \tau_{c(ex)}$	0.76	1.24	0.30	1.14	(7.18)	1.96

Table 4. *Comparison of residence times for the adsorption and exchange kinetics.*

5.2.4 Adsorption Isotherms at OCP

Adsorption isotherms obtained at OCP in solutions containing different concentrations of NaOH are shown in Figure 8.

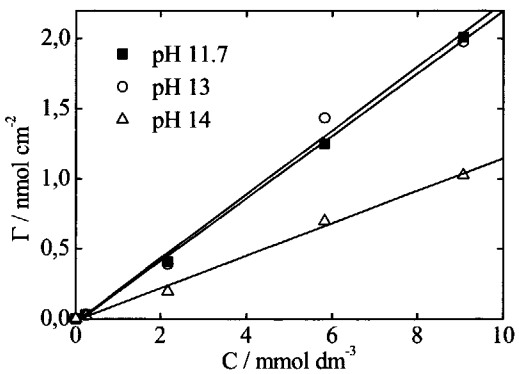

Figure 8. *Adsorption isotherms of formaldehyde at the OCP at different pH.*

The isotherms are linear, implying that adsorbed enolate anions do not inhibit additional adsorption of enolate anions. The lower adsorption on gold at the higher pH is in

concordance with the adsorption data presented in Figure 6 and is explained accordingly by increased adsorption of hydroxyl ions at the gold surface.

The standard free Gibbs adsorption energies, ΔG_{ad}, were calculated from the initial slope of the adsorption isotherms using $\Delta G^* = RTlnK$ (Table 5).[12] Clearly, the lowest Gibbs free adsorption energy is observed at pH 14 although only small differences apply to the adsorption energies (Table 5). Instead, it was shown in Section 4.2.7 that the differences in pH manifest much more pronounced in the E_{act} of the reaction.[2] The influence of the solution effects on the Gibbs free energy of the adsorption process is thus small relative to its influence on the activation energies.

5.2.5 Reaction Kinetics

To study adsorption and oxidation of formaldehyde under dynamic conditions, a few cyclic voltammograms were recorded (Figure 9).

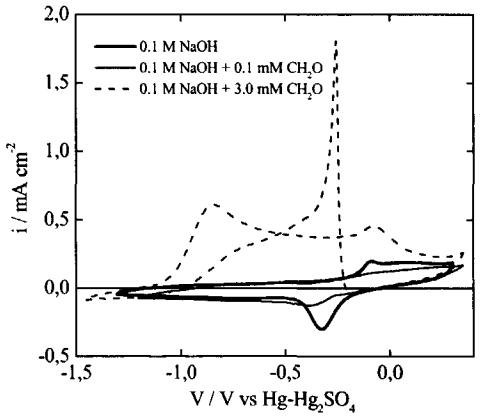

Figure 9. *Cyclic voltammograms recorded at a scan rate of 50 mV s^{-1} in different solutions.*

A negligible electro-oxidation current is observed for the voltammogram recorded in the solution containing 0.1 M NaOH and 0.1 mM CH_2O. Adsorption does nevertheless occur, as revealed by the decline of the current density associated with the oxidation and reduction of the gold surface.[2] At higher concentration, the oxidation of formaldehyde sets in at –1.2 V *vs.* Hg/Hg_2SO_4.

[NaOH]/ M	Procedure T/ °C	V/V *vs.* OCP	ΔG_{ad}^{*} / kJ mol^{-1}	$\Delta G_{ad}^{\#}$ / kJ mol^{-1}	$\Delta H_{ad}^{\#}$ / kJ mol^{-1}	$\Delta S_{ad}^{\#}$ / kJmol^{-1} K^{-1}	$T\Delta S_{ad}^{\#}$ / kJmol^{-1}
0.1	22	0	-27.8	-26.8	-9.1	0.06	17.7
0.005	22	0	-27.7	-	-	-	-
1.0	22	0	-25.3	-	-		
0.1	27	0	-	-26.4	-20.4	0.02	6.0
0.1	32	0	-	-26.4	-32.5	-0.02	-6.1
0.1	38	0	-	-26.8	-48.5	-0.07	-21.8
0.1	43	0	-	-27.3	-62.1	-0.11	-34.8
0.1	48	0	-	-27.9	-79.3	-0.16	-51.4
0.1	53	0	-	-28.7	-93.9	-0.20	-65.2
0.1	22	-1.0	-27.6	-	-	-	-
0.1	22	0.55	-27.7	-	-	-	-
0.1	22	0.3	-	-28.0	-36.9	-0.03	-8.9
0.1	27	0.3	-	-28.3	-37.3	-0.03	-9.0
0.1	32	0.3	-	-28.5	-37.7	-0.03	-9.2
0.1	38	0.3	-	-28.7	-38.0	-0.03	-9.3
0.1	43	0.3	-	-28.8	-38.3	-0.03	-9.5
0.1	48	0.3	-	-29.0	-38.6	-0.03	-9.6
0.1	53	0.3	-	-29.1	-38.9	-0.03	-9.8

Table 5. *Values of ΔG_{ad}, ΔH_{ad}, and ΔS_{ad}. All solutions contained 0.01 M CH_2O. ΔG_{ad}^{*} and $\Delta G_{ad}^{\#}$ were obtained from the initial slopes of the adsorption isotherms (Figure 8 and Figure 16). $\Delta S_{ad}^{\#}$ was obtained from the first derivative of the fitted curves in Figure 16. $\Delta H_{ad}^{\#}$ was calculated at each temperature from $\Delta G_{ad}^{\#} = \Delta H_{ad}^{\#} - T\Delta S_{ad}^{\#}$.*

The dependence of rate of the reaction on the scan rate in a solution containing 0.1 M NaOH and 10 mM CH_2O is shown in Figure 10a.

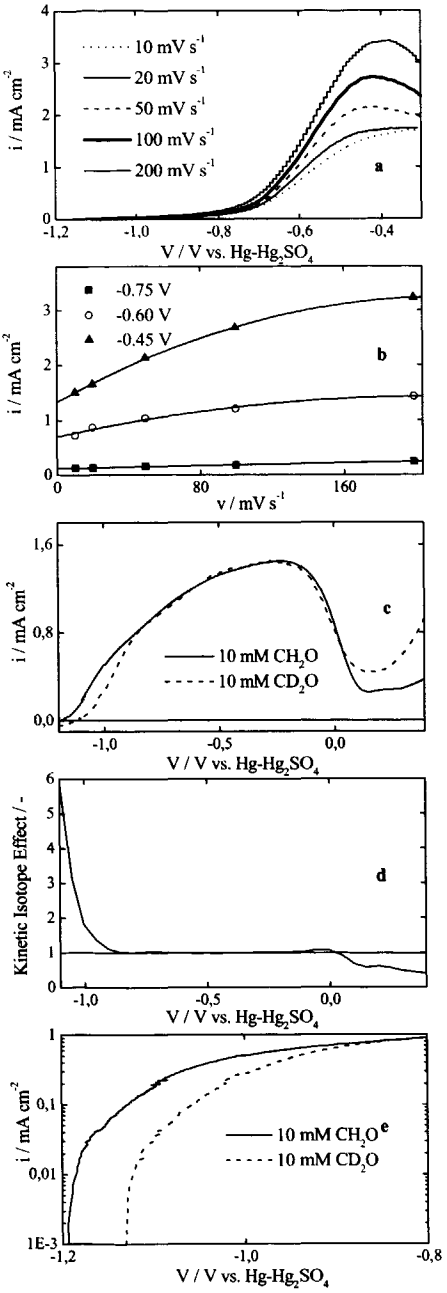

Figure 10. *Linear sweep voltammograms recorded at different scan rates in solutions containing 0.01 M CH_2O and 0.1 M NaOH (a). Dependence of the current density on the scan rate at three different potentials (b). The linear sweep voltammograms recorded in a solution containing 0.1 M NaOH and 0.01 M CH_2O and in one containing 0.1 M NaOH and 0.1 M CD_2O show a significant KIE at low and high potentials (c, d). The voltammograms were not characterized by a linear Tafel slope (e).*

The rate of the reaction is affected to great extent by the scan rate, with a linear dependence at voltages below ~ –0.75 V vs. Hg/Hg_2SO_4 (Figure 10a and 10b). It confirms the kinetic origin of the overall rate of the reaction at these low potentials (Figure 10b).[2] Interestingly, the value of the KIE (Figure 10c and d) amounts to one at potentials where the electro-oxidation current depends on the scan rate in a linear fashion (~ -0.75 V vs. Hg/Hg_2SO_4). It confirms the view that another step than diffusion (step [2]) or chemisorption (step [4]) is rate limiting under these conditions.[2] As physisorption (step [3]) and desorption of atomic hydrogen are rapid too (step [6] and [7]), the rate-limiting step at these potentials is assigned as the desorption of the formate anion.[2] At higher potentials (-0.6 V), the influence of diffusion becomes more apparent although no Fick behavior applies to the system, as indicated from the absence of linear $\sqrt{v}$-i relationships.[2,6,7]

Moreover, the shape of the voltammogram in Figure 10a at 10 mV s^{-1} differs from that of Figure 10c which is explained by the strong dependence of the inset of oxidation to small fluctuations in nitrogen bubbling rates and by poisoning effects (Chapter 4).[2] No linear Tafel plots apply to the system, confirming the view that the rate-limiting step of the reaction is catalytic (chemical) rather than electrochemical (faradic) in nature, *i.e.* the kinetics cannot be described by an exponential Butler-Volmer type equation (Figure 10e).[1]

5.2.6 Potential Dependence of Adsorption in 0.1 M NaOH

The adsorption and oxidation of formaldehyde in solutions containing 0.1 M NaOH and different concentrations of formaldehyde are shown in Figure 11. The almost constant adsorption with increasing potentials points towards a constant ratio between the rate of adsorption of reactants and the rate of desorption of products. The absence of depletion of carbon species at the gold surface under conditions where diffusion rules the overall rate of the reaction suggests that adsorbed species leave the surface upon the approach of reactants rather than upon changes in the electrode potential. Besides, the strong dependence of the surface coverage on the formaldehyde concentration and the invariance of the adsorption isotherms with the potential (*see* below) support the view that potential gradients on the solution side are more important in the adsorption of species than the potential of the electrode. These observations are in concordance with the electrostatic picture derived by EIS, which implied that higher potential gradients apply between the IHP and the solution than between the gold surface and the IHP (Section 3.2.4).[1]

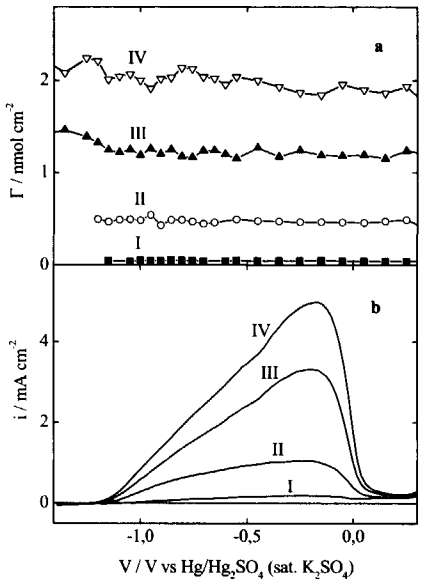

Figure 11. *Adsorption of formaldehyde in 1 M NaOH and: 0.2 mM CH_2O (I), 2.4 mM CH_2O (II), 5.8 mM CH_2O (III) and 9.1 mM CH_2O (III) (a). Current densities were obtained at a scan rate of 10 mVs^{-1} (b).*

5.2.7 Reaction Orders

Quantitative insight into the dependence of the quantity of species adsorbed on the formaldehyde concentration was obtained by plotting the adsorption isotherms at different potentials (Figure 12a). The values of ΔG_{ad} are potential invariable, implying that the electrode potential affects the E_{act} between the various states rather than the (relative) value of the Gibbs energies (Table 5).[2] Moreover, the dependence of the reaction rate on the formaldehyde concentration and the quantity of species adsorbed (Γ) yielded linear 'i-log C' and 'i-logΓ' plots (Figure 12b and c) from which the reaction orders in C and Γ were derived (Table 6). Up to –0.15 V, the values of the orders approach one which is in concordance with results published by Beltowska *et al.*[6,7] (Table 6). At higher voltages, the oxidation of the gold surface sets in and lower reaction orders are obtained.

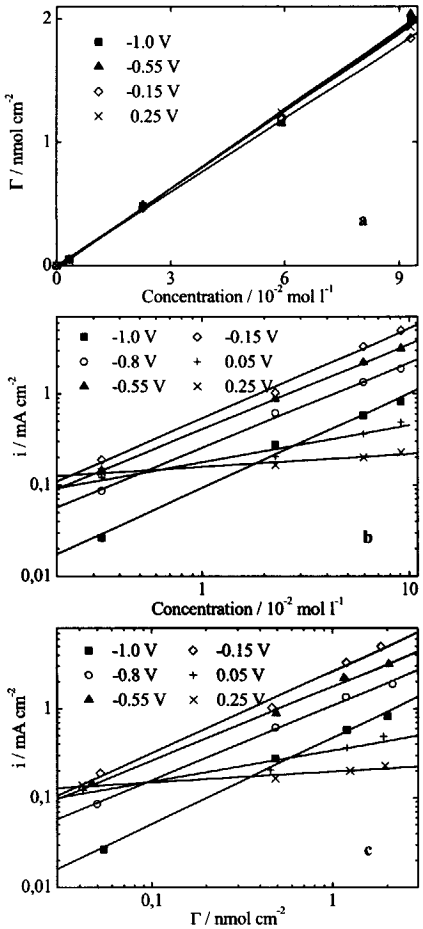

Figure 12. *Adsorption isotherms at different voltages in solutions containing 0.01 M CH_2O (a). Dependencies of the current densities on the concentration and on the quantity of species adsorbed at the electrode (b and c).*

V / V *vs.* Hg/Hg_2SO_4	n_C / -	n_Γ / -
-1.0	1.04	0.97
-0.55	0.94	0.83
-0.15	0.99	0.92
0.25	0.41	0.12

Table 6. *Reaction orders in the concentration (n_c) and surface concentration (n_Γ) for solution containing 0.1 M NaOH and 0.01 M CH_2O.*

5.2.8 Potential Dependence of Adsorption in 0.005 M and 1 M NaOH

0.005 M NaOH - The adsorption and oxidation of formaldehyde on gold in solutions containing 0.005 M NaOH and different concentrations of formaldehyde are shown in Figure 13. Some irregular features are observed at higher concentrations of which the origin is not clear. The electro-oxidation current, recorded at a sweep rate of 10 mVs^{-1}, does not trace the adsorption which is explained in the same fashion as above for solutions containing 0.1 M NaOH. Furthermore, the quantity of species adsorbed is slightly lower in 0.005 M NaOH than in 0.1 M NaOH whereas the current density is much lower. It suggests that the role of hydroxyl ions in the rate of adsorption is less pronounced than the (stoichiometric) role of the hydroxyl ions in the rate of the overall reaction.

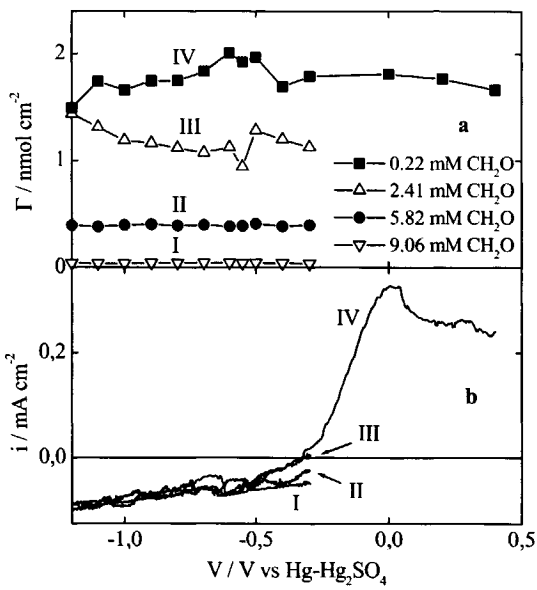

Figure 13. *Adsorption of formaldehyde at different potentials in solutions which contained 5 mM NaOH and: 0.2 mM CH_2O (I), 2.4 mM CH_2O (II), 5.8 mM CH_2O (III) and 9.1 mM CH_2O (IV) respectively (a). The corresponding current densities were recorded at a scan rate of 10 mVs^{-1} (b).*

1.0 M NaOH - The adsorption and oxidation of formaldehyde on gold in solutions containing 1.0 M NaOH and different concentrations of formaldehyde are shown in Figure 14. A local minimum around the OCP and a maximum at -0.7 V can be observed for the highest formaldehyde concentration. The maximum at -0.7 V coincides with the

crossing of the various voltammograms. Below this voltage, poisoning (irreversible accumulation of species) of the gold surface may occur, as witnessed by an increasing coverage. Above this voltage, the irreversibly adsorbed species may be oxidized.[2]

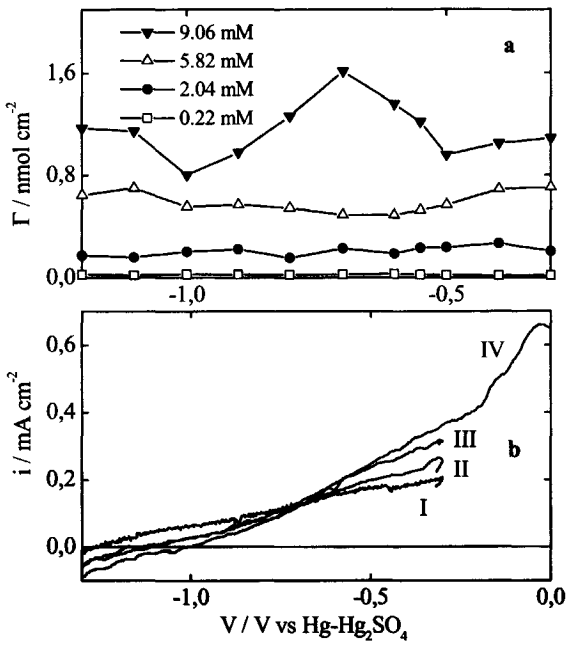

Figure 15. *Adsorption of formaldehyde at different potentials in solutions which contained 5 mM M NaOH and: 0.2 mM CH_2O (I), 2.4 mM CH_2O (II), 5.8 mM CH_2O (III) and 9.1mM CH_2O (IV) respectively (a). The corresponding current densities were recorded at a scan rate of 10 mVs^{-1} (b).*

5.2.9 Temperature Dependence

The adsorption of formaldehyde at different temperatures in solutions containing 0.1 M NaOH and either 10 mM CH_2O or 0.17 mM CH_2O is shown in Figure 16a and 16b. An increase in the adsorption is observed at higher temperatures at the OCP for both solutions although a smaller increase applies to the adsorption at 300 mV *vs.* CP than to that at the OCP. This higher increase in adsorption at the OCP than at 300 mV is in line with the higher relative contribution of the chemisorption to the overall rate at the OCP than at 300 mV, as witnessed by the values of the KIE in Figure 10.[2] At 300 mV *vs* OCP, the E_{act}-

suppressing desorption of the formate ion becomes more important in the kinetics of the reaction favouring the lower increase.[2]

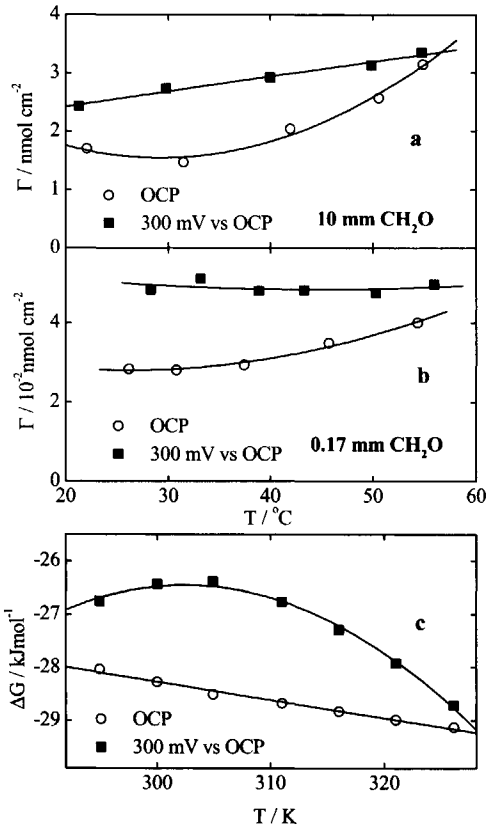

Figure 16. *Adsorption at different temperatures and potentials in solutions which contained 0.1 M NaOH and: 10 mM CH_2O (a) and 0.17 mM CH_2O respectively (b). The Gibbs free adsorption energies were derived at different temperatures from the adsorption isotherms which were constructed from the data presented in (a) and (b).*

Adsorption isotherms were constructed from the three concentrations considered, *i.e.* 10 mM, 0.17 mM and 0.0 mM CH_2O, through which linear isotherms were fitted with correlation factors higher than 0.99. The free energies of adsorption ($\Delta G_{ad}^{\#}$) were derived from the slopes of these isotherms at different temperatures (Table 5 and Figure 16c). A value of –26.8 kJ mol^{-1} was obtained at the OCP at room temperature, which was in reasonable agreement with the value found above from the adsorption isotherms at the OCP (–27.8 kJ mol^{-1}).

The dependence of the values of ΔG_{ad} on temperature obeyed a linear relationship at 300 mV while a second order relationship ($\Delta G_{ad}^{\#} = a + bT + cT^2$) was found at the OCP (Figure 16c). Free heats of adsorption (ΔH_{ad}) and free entropies of adsorption (ΔS_{ad}) were derived at different temperatures from the first derivatives of the fitted polynomials and by using $\Delta G_{ad}^{\#} = \Delta H_{ad} - T\Delta S_{ad}$ (Figure 16c and Table 5). Clearly, the values of ΔH_{ad} and ΔS_{ad} do not depend to a great extent on the temperature for data obtained at 300 mV. On the other hand, a significant increase is seen in ΔH_{ad} and ΔS_{ad} at the OCP. The values of $T\Delta S_{ad}$ give an indication for the contribution of the entropy to the Gibbs free energy of adsorption at a specific temperature (Table 5). In most cases, the enthalpy tends to make the overall reaction exothermic whereas the entropy tends to make it endothermic

5.3 Kinetic and Thermodynamic Model

A semi-quantitative kinetic model was proposed in Chapter 4 which described the reaction at potentials around the OCP in a semi-quantitative manner.[1,2] The model can be specified by taking into account the results and considerations discussed above. Different diagrams can be constructed for different cases (Figure 17):

The energy diagram obtained for the adsorption under steady-state conditions at 25 °C is shown in Figure 17a. The activation energies associated with the transitions between the various states were taken from Table 3 while the Gibbs free energies, the heats of adsorption and the entropies of adsorption were taken from Table 5. The value of the energy representing the OHP and IHP was calculated from the Gibbs free adsorption energies by assuming that the ratio of the energy of the IHP and the OHP is equal to the ratio of the transition times of species in the IHP and OHP (Table 2). It is clear from Figure 17a that the apparent activation energy related to the transition between the IHP and OHP is higher than that between the OHP and the solution. Besides, the Gibbs free energy of the overall reaction consists mainly of a positive entropy term.

The situation is different under dynamic conditions at the OCP, as witnessed by a larger hump associated with the transition of the enolate anion to the OHP and a slightly larger one with the transition of the enolate anion to the IHP. Besides, the level of the OHP is lifted relative to the steady-state equivalent (Figure 17a and 17b).

At 53°C, both the enthalpy of adsorption and the entropy of adsorption decrease drastically (Figure 17c). In this case, the Gibbs free energy of the overall reaction is dominated by the enthalpy. Besides, the state corresponding with the IHP is raised relative to the one corresponding with the OHP.

At potentials close to the OCP, the oxidation of the adsorbed, dissociated enolate anions at the gold surface sets in and the situation changes drastically (Figure 17d). Namely, the

net activation energy is lowered most likely as a result of the suppressing effect associated with the desorption of the formate anion (Chapter 6).[2] The negative contribution dominates at potentials slightly larger than the OCP and may account for negative capacitive or inductive loops in the impedance spectra (Chapter 3).[1] As mentioned, the Gibbs free energy of the overall reaction does not alter under these conditions.

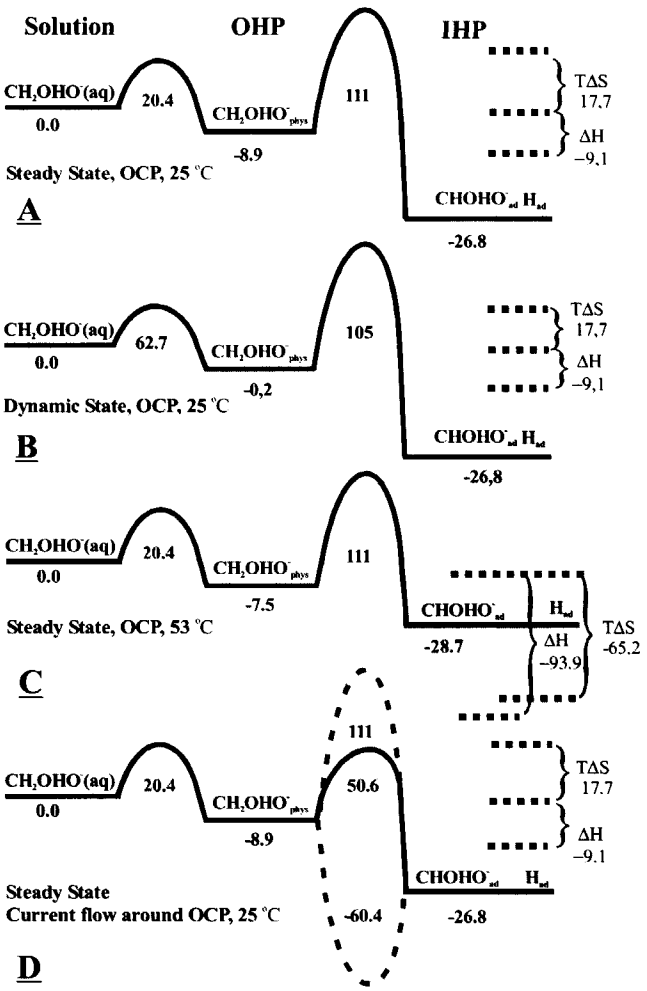

Figure 17. *Thermodynamics and kinetics of the reaction under different conditions. The numbers reflect the values of the energies in kJ mol^{-1} (a-d).*

5.4 Solution Effects and Adsorption Entropies

Solution Effects - The order of magnitude of values of the Gibbs adsorption enthalpies at the OCP and at potentials (-0.55 V) where formate is formed in the rate-limiting step as adsorbed product (Table 6) is substantially larger than the value of the thermodynamic gold-formate formation enthalpy in the literature (-28 kJ mol^{-1} versus ~ -61 kJ mol^{-1}).[9] In addition, the value of the adsorption enthalpies were seen to depend on the compositions of the solution (Table 6). Hence, solution effects and adsorption energies (rather than formation enthalpies) should be taken into account when validating Sabatier's principle from empirical volcano-plots. Adsorption energies obtained in the gas phase may be used only when the relative differences of the adsorption enthalpies between metals resemble the relative differences of the (metal-dependent) adsorption enthalpies in the solution.

Adsorption Entropies - The values of the adsorption enthalpies presented in Table 6 do differ substantially from the values of the corresponding Gibbs adsorption energies. Hence, volcano-plots that are used to validate Sabatier's principle should use values of the Gibbs adsorption energies rather than values of the adsorption enthalpies. Bond strengths at the liquid-gold interface are thus reflected by values of ΔG_{ad} rather than by ΔH_{ad}. Adsorption energies may be used only when the relative differences of the adsorption enthalpies between metals resemble the relative differences of the Gibbs adsorption energies.

5.5 Conclusions

- The adsorption of formaldehyde at the OCP proceeds in a serial fashion with two reversible rates of adsorption: a rapid physisorption and a slow chemisorption. The adsorption isotherms are approximately linear at concentrations below 10 mM formaldehyde.
- In 0.1 M NaOH, the electro-oxidation of formaldehyde is approximately first order in the concentration of formaldehyde and in the quantity of species adsorbed.
- In 0.1 M NaOH, the rate of the overall electro-oxidation reaction is likely ruled by chemisorption of the enolate anion at low potentials (-1.1 V *vs.* Hg/Hg_2SO_4), by desorption of formate at medium potentials (-0.9 to -0.7 V *vs.* Hg/Hg_2SO_4) and by the diffusion of reactants and products at highest potentials (> -0.5 V *vs.* Hg/Hg_2SO_4).
- The value of ΔG_{ad} depends little on the potential, temperature and pH. The value of E_{act} is affected more strongly by these parameters.
- The enthalpy of the reaction mostly tends to make the reaction exothermic whereas the entropy tends to make it endothermic. At 22 °C and at the OCP, the ΔG_{ad} consists mainly of positive entropy. At 53 °C, ΔG is dominated by the negative enthalpy.

- The E_{act} of the chemisorption step in the reaction is dominated by the enthalpy. The E_{act} of the desorption of species seems ruled by the entropy but arises due to a pre-equilibrium at the interface.[2]
- The strong dependence of the quantity of species adsorbed on the formaldehyde concentration and the invariance of the adsorption isotherms with increasing potentials are in line with the view that potential gradients on the solution side are more important in the adsorption of species than the potential of the electrode itself.[11]
- The kinetics and thermodynamics of the formaldehyde electro-oxidation reaction on gold can be described under different conditions by one physical model. In this model, the enolate anion diffuses to the reaction centre, followed by reversible physisorption, reversible chemisorption, irreversible oxidation and desorption of reaction products (hydrogen, water and formate). The model conceives the reaction by three stable states, *i.e.* the solution, the OHP and the IHP, which are interconnected by two energy humps. A kinetic description of simple electroless processes may be accomplished by implementing metal ions in the model.
- As the values of ΔG_{ad} cannot be approximated by values of ΔH_{ad}, the values of ΔS_{ad} should not be neglected in the validation of Sabatier's principle from empirical volcano-plots in electrocatalyis.
- As the value of ΔG_{ads} of the overall electro-oxidation reaction depends on the composition of the solution, solution affects should be taken into account when validating Sabatier's principle.

5.6 References

(1) Kortenaar, M. V.; Tessont C.; Kolar, Z. I.; Weijde, H. van der.; *J. Electrochem. Soc.*, **1999**, 14, 2146.

(2) Gileadi, G.; *Electrode Kinetics*, VCH Publishers, New York, **1993**, p 351.

(3) Laidler, K. J.; Meiser, J. H.; in *Physical Chemistry*, Houghton Mifflin Company, Boston, 1995, p 881.

(4) Walker, J. F.; *Formaldehyde*, Reinhold Publ. Corp., New York, 3rd edition, 1964, p 214.

(5) Meerakker, J. E. M van den, Scholten, E.; *Ber. Bunsenges. Phys. Chem.*, **1989**, 93, 786.

(6) Beltowska-Brzezinska, M.; *Electrochim. Acta*, **1985**, 30, 1193.

(7) Beltowska-Brzezinska, M.; *J. Electroanal. Chem.*, **1985**, 187, 167.

(8) Avramov-Ivic, M. L.; Adzic, R. R.; Bewick, A.; Razaq, M.; *J. Electroanal. Chem.*, **1988**, 240, 161.

(9) Bindra, P.; Roldan, J.; *J. Electrochem. Soc.*, **1985**, 132, 2582.

(10) Kortenaar, M. V.;Kolar, Z. I.; Goeij, J. J. M. de.; Frens, G.; *Langmuir*, **2002**, 18, 10279-10291.

(11) Godfrey, K.; in *Compartmental Models and Their Application*, Academic Press, New York, **1983**, p 58.

(12) Gileadi, G.; *Electrode Kinetics*, VCH Publishers, New York, **1993**, p 403.

5.7 Appendix

Adsorption experiments:

A closed, catenary three-compartment model (Figure 1) has been used for fitting the adsorption data. It can be described by a system of three differential equations:

$$\frac{\partial Q_S(t)}{\partial t} = k_{sp} \times Q_p(t) - k_{ps} \times Q_S(t) \quad (1)$$

$$\frac{\partial Q_p(t)}{\partial t} = k_{ps} \times Q_S(t) + k_{pc} \times Q_c(t) - k_{sp} \times Q_p(t) - k_{cp} \times Q_p(t) \quad (2)$$

$$\frac{\partial Q_c(t)}{\partial t} = k_{cp} \times Q_p(t) - k_{pc} \times Q_c(t) - k_{ic} \times Q_c(t) \quad (3)$$

Where the quantity of unlabeled material (tracee) in a compartment is denoted as Q and the rate constants as k [s^{-1}].[23] As an example, k_{sp} refers to the rate constant related to the transport of species to the solution from the physisorbed state. Q_s, Q_p and Q_c represent the quantities [nmol] in the solution, in the physisorbed and in the chemisorbed state respectively with initial compartment quantities:

$Q_s(0)$=100,000 nmol (Procedure 1-6) or 1710 nmol (Procedure 7), $Q_p(0)$= 0 and $Q_c(0)$ = 0.

The quantity at the electrode is measured and comprises species in the physisorbed and chemisorbed state respectively:

$$Q_e(t) = Q_p(t) + Q_c(t) \quad (4)$$

The $Q_e(t)$ values were obtained from $\Gamma(t)_e$ by using:

$$Q_e(t) = \Gamma_e(t) \times R \times A \quad (5)$$

Where: $\Gamma(t)_e$ is the surface concentration [nmol per real cm^2], R the roughness factor [-] and A the geometrical area of the electrode [cm^2].

The rate of transfer (flow) of tracee is denoted as F [nmol s^{-1}]; F_{ps} represents the flow to the physisorbed state from the solution. Likewise F_{sp}, F_{pc} and F_{cp} represent the flows to the solution from the physisorbed state, to the physisorbed state from the chemisorbed state and to the chemisorbed state from the physisorbed state respectively. The flows in steady state ($t=\infty$, $Q(\infty)$ = constant) between the compartments can be obtained from:

$$F_{ps}(\infty)=F_{sp}(\infty)=k_{ps}\times Q_s(\infty)=k_{sp}\times Q_p(\infty) \quad (6)$$

$$F_{pc}(\infty)=F_{cp}(\infty)=k_{pc}\times Q_c(\infty)=k_{cp}\times Q_p(\infty) \quad (7)$$

The transition times in the compartments can be obtained from:

$$\tau_s=\frac{1}{k_{ps}} \quad (8)$$

$$\tau_p=\frac{1}{(k_{sp}+k_{cp})} \quad (9)$$

$$\tau_c=\frac{1}{k_{pc}} \quad (10)$$

Exchange experiments:

The exchange experiments are, in contrast with the adsorption experiments, initially in steady state: dQ(t)/dt = 0. In this case, the radiotracer quantity (q) on the electrode was measured and fitted. The fractional loss of tracer from the physisorbed and chemisorbed state can be described by:

$$\frac{\partial[q_p(t)/q_e(0)]}{\partial t}=k_{ps}\times\frac{q_s(t)}{q_e(0)}+k_{pc}\times\frac{q_c(t)}{q_e(0)}-k_{sp}\times\frac{q_p(t)}{q_e(0)}-k_{cp}\times\frac{q_p(t)}{q_e(0)} \quad (11)$$

$$\frac{\partial[q_c(t)/q_e(0)]}{\partial t}=k_{cp}\times\frac{q_p(t)}{q_e(0)}-k_{pc}\times\frac{q_c(t)}{q_e(0)} \quad (12)$$

$$\frac{\partial[q_s(t)/q_e(0)]}{\partial t}=k_{sp}\times\frac{q_p(t)}{q_e(0)}-k_{ps}\times\frac{q_s(t)}{q_e(0)} \quad (13)$$

And:

$$\frac{q_e(t)}{q_e(0)}=\frac{q_p(t)}{q_e(0)}+\frac{q_c(t)}{q_e(0)} \quad (14)$$

The initial values for the physisorbed and chemisorbed quantities were obtained from the adsorption experiments at infinite time using the following equations:

$$\frac{q_p(0)}{q_e(0)}=\frac{Q_p(\infty)}{Q_e(\infty)} \quad (15)$$

$$\frac{q_c(0)}{q_e(0)}=\frac{Q_c(\infty)}{Q_e(\infty)} \quad (16)$$

$$\frac{q_p(0)}{q_e(0)}+\frac{q_c(0)}{q_e(0)}=1 \quad (17)$$

$$\frac{q_S(0)}{q_e(0)} = 0 \qquad (18)$$

The system of differential equations was simultaneously solved for the four rate constants k_{sp}, k_{ps}, k_{cp} and k_{pc}.

Chapter 6

Electrocatalytic Oxidation of Formaldehyde on Transition Metals studied by Voltammetry*

The oxidation of CH_2O and CD_2O was studied by voltammetry in 0.1 M NaOH on transition metals (Au, Ag, Cu, Ni, Pd, Pt, Ir) at different temperatures. Au, Pt and Ir promote the reaction to highest rates, while Cu and Ag catalyse the reaction at lowest potentials. Ni and Pd do not catalyse the reaction well. At low overpotentials and temperatures, the rate of the reaction is likely ruled by the rate of chemisorption of the enolate anion on Ag, Cu, Au and Ni, and by the rate of desorption of adsorbed hydrogen on Pt, Pd and Ir. At higher potentials, the reaction may become increasingly controlled by the rate of desorption of the formate anion on all metals studied. A linear relationship was obtained for the dependence of the metal-dependent reaction rate on the kinetic isotope effects (KIE), confirming the view from previous chapters that the rate-limiting step of the reaction comprises the rupture of hydrogen bonds. The rate of these hydrogen bond ruptures seem to be structurally affected by the electronic properties of the metals, as a linear relationship was obtained for the dependence of the reaction rate of the catalytically active metals on the work function. The importance of the chemical rearrangements and the electronic properties of the metals in the rate of the reaction were further indicated from the similar dependencies of the apparent activation energies (E_{act}) on both the metal-formate formation enthalpies and the oxidation potentials of the metals. Moreover, a curved relationship between E_{act} and the inter-atomic bond lengths was found, suggesting that neighbour effects of surface atoms play a role in the lowering of the transition state of the reaction. The values of E_{act} ranged roughly between -20 kJ mol^{-1} and 50 kJ mol^{-1}, confirming the catalytic properties of the metals and the possible presence of a (pseudo) pre-equilibrium in the reaction.

Submitted to J. Electroanalytical Chemistry

6.1 Introduction

The rates (i), the apparent activation energies (E_{act}) and kinetic isotope effects (KIE) of the formaldehyde electro-oxidation reaction on different transition metals are determined by voltammetry under different conditions. The results are compared, followed by a search for correlations between physical properties of the metals and the kinetic parameters of the reaction (steps). This research was conducted in order to see if other parameters than reactant-metal adsorption energies, as suggested by Sabatier and discussed further in Chapter 7, would play an important role in the catalytic properties of the metals as well.

6.2 Results and Discussion

6.2.1 Discussion of the voltammograms

Influence of the scan rate and rotation speed - Cyclic voltammograms recorded on all metals studied at different scan rates (rotation speed 16 rps), and at different rotation speeds (scan rate 50 mV s^{-1}) in solutions containing 0.1 M NaOH and 0.1 M CH_2O are shown in Figure 1. Clearly, the oxidation of formaldehyde sets in at lowest potentials for copper and at highest for nickel, an observation that is in concordance with results published by Ohno *et al.*[1] The oxidation of formaldehyde on gold, silver, palladium, platinum and iridium set in between these two extremes.[2]

Nickel, Copper, Iridium - The scan rate affects the rate of the electro-oxidation reaction to a considerable extent for nickel, copper and iridium, *i.e.* metals which are oxidized at relatively low potentials, as revealed by the sudden decrease of the electro-oxidation current density after the gradual increase upon scanning in positive direction (Figure 1b, 1d and 1e). Presumably, hydroxyl ions are involved in the rate-limiting step of the reaction for these metals.[2] The square root dependencies of the current densities on the scan rates suggest that the rate-limiting step of the reaction may arise from mass transfer processes.[3,4] These mass transfer processes cannot be associated with diffusion at these high concentrations and low current densities, a view which is supported by the independence of the current densities on the rotation speed (Figure 1h, 1j, and 1k).[2-4] Instead, the dependencies of the current densities on the square root of the scan rate may arise from slow mass transfer rearrangements in the double layer (Section 3.2.4).[2,3]

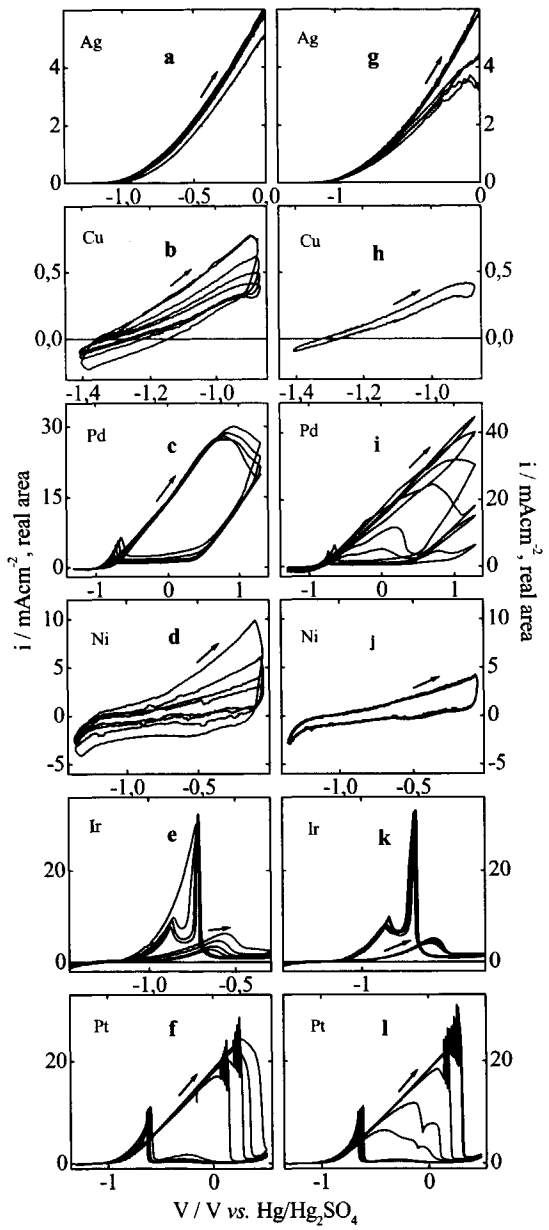

Figure 1. *Voltammograms recorded in 0.1 M NaOH and 0.1 M CH_2O at a rotation speed of 16 rps and a scan rate of: 50 mV s^{-1}, 100 mV s^{-1}, 200 mV s^{-1} and 500 mV s^{-1}. (a-f). Voltammograms recorded at a scan rate of 50 mV s^{-1} and a rotation speed of: 0 rps, 4 rps, 9 rps, 25 rps, 49 rps and 81 rps.*

Silver, Palladium, Gold and Platinum - The rates of oxidation of formaldehyde on the more inert silver, palladium and platinum surfaces do not depend substantially on the scan rate at the (relatively high) scan rates examined (Figure 1a, 1c, 1f, Sections 3.2.4 and 4.2.3). Instead, a strong dependence of the current density (i) on the rotation speed (ω) is seen, in particular at high potentials (Figure 2g, 2i, 2l). The dependencies of i on $\sqrt{\omega}$ and of 1/i on $1/\sqrt{\omega}$ did not yield straight lines, as indicative for a diffusive or semi-diffusive process respectively.[4,5] This behaviour is not completely understood but was seen to apply to the oxidation of formaldehyde on gold as well (Section 3.2.6 and 4.2.3).[2]

A comparison of the electro-oxidation of formaldehyde shows that much lower current densities are attained for nickel, copper and iridium than for the other metals, as the oxidation of the metal surface sets in at lower potentials on nickel, copper and iridium than for the other metals (Figure 1g, 1i, 1l and ref. 15).

6.2.2 Influence of Temperature

Linear sweep voltammograms recorded for the metals studied at various temperatures in solutions containing 0.1 M NaOH and either 0.1 M CH_2O or 0.1 M CD_2O are shown, together with the corresponding values of KIE and E_{act}, in Figures 2-7. The voltammograms are discussed below.

Silver - The oxidation of formaldehyde on silver proceeds at higher rates for CH_2O than for CD_2O over a wide range of conditions (Figure 2a and 2b). The rates do nevertheless increase more for CD_2O than for CH_2O with increasing temperatures. The values of E_{act} support this view quantitatively with values being twice as large for CD_2O than for CH_2O at low potentials and equal at higher potentials. The values of the KIE are higher than 1 at voltages up to –0.6 V *vs.* Hg/Hg_2SO_4, implying that the rate of chemisorption (Step [4]) plays an important role in the overall rate of the reaction under these conditions (Figure 2d). The values of the KIE decrease to 1 at voltages around –0.5 V *vs.* Hg/Hg_2SO_4, suggesting that the rate of the reaction becomes increasingly controlled by desorption of the formate anion (Step [5]). Namely, diffusion (Step [2]) does not play a major role in the reaction kinetics under these conditions (*see* above), and the similar values of E_{act} for CH_2O and CD_2O suggest that the rates of hydrogen desorption (Step [6] and Step [7]) do not play a major role either.[2] At potentials above –0.5 V *vs.* Hg/Hg_2SO_4, the values of the KIE drop below 1 and the rate of desorption of adsorbed hydrogen may become rate-limiting.[2]

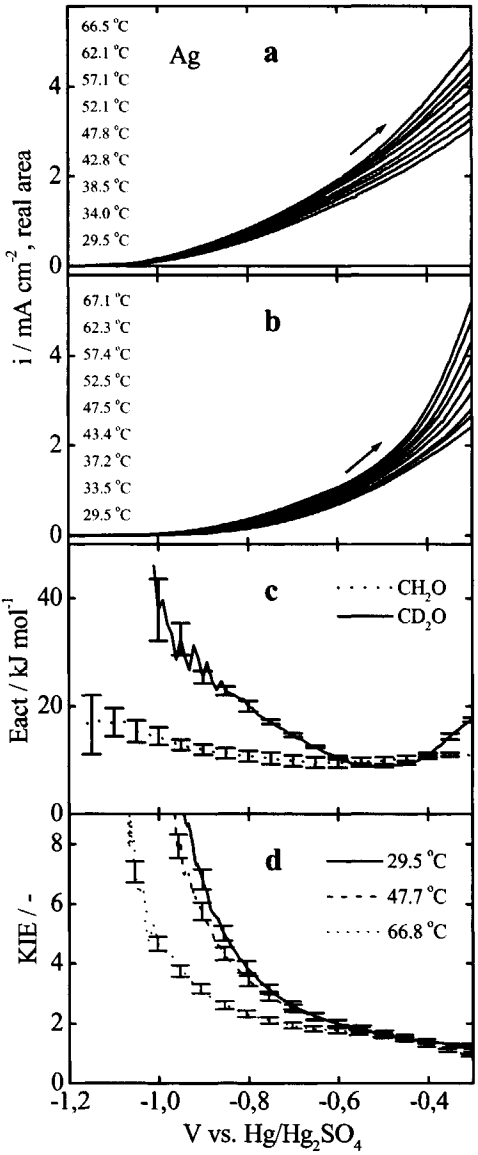

Figure 2. *Linear sweep voltammograms recorded at 10 mV s^{-1} for silver in 0.1 M NaOH and 0.1 M CH_2O (a), and 0.1 M NaOH and 0.1 M CD_2O (b). Calculated values of E_{act} (c). Calculated values of the KIE (d).*

-Copper- The oxidation of CH_2O sets in at much lower potentials on copper than on other metals although the absolute rate of oxidation remains relatively low at higher potentials due to the oxidation of the copper surface (Figure 3a).

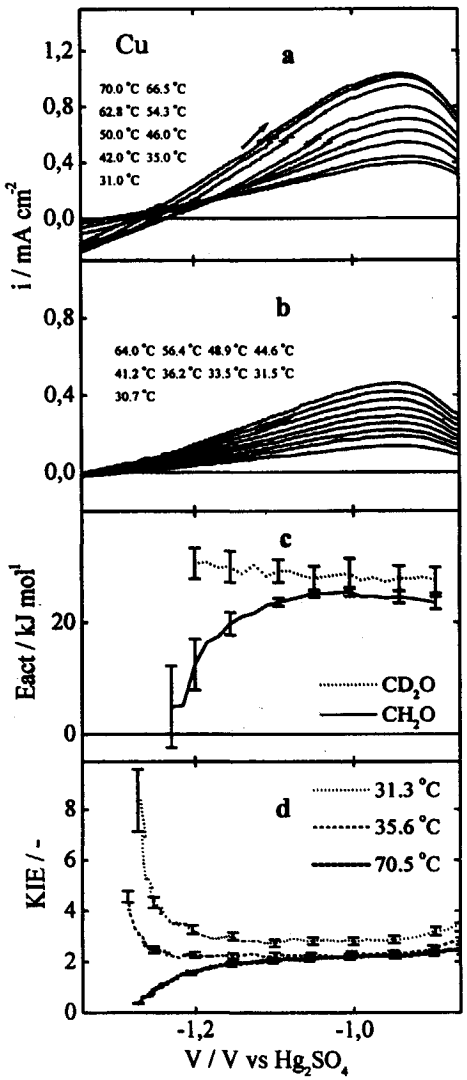

Figure 3. *Linear sweep voltammograms recorded at 10 mV s^{-1} for copper in 0.1 M NaOH and 0.1 M CH_2O (a), and 0.1 M NaOH and 0.1 M CD_2O (b). Calculated values of E_{act} (c). Calculated values of the KIE (d).*

The rate of oxidation of CH_2O increases with increasing temperatures for the higher range of temperatures and potentials, but decreases for the lower range of temperatures and potentials (Figure 3a). The decrease for the lower range of temperatures and potentials points towards a rate-limiting role of a desorption step in the overall rate of the reaction, as rate-limiting desorption steps are often characterized by negative values of the E_{act} (Section 4.2.8).[2] The values for the E_{act} were nevertheless positive in Figure 3c, as they were presented for the higher range of temperatures (these data points showed more convincing Arrhenius behaviour). Moreover, as adsorbed hydrogen is relatively stable on copper, the recombination of adsorbed hydrogen to molecular hydrogen (Step [6]) is referred to be the rate-limiting step for the oxidation of CH_2O at low temperatures.

The oxidation of CD_2O increases at all temperatures and potentials with positive values of E_{act} for all data, suggesting that different steps may be rate-limiting at the lower range of temperatures for the oxidation of CD_2O than for that of CH_2O (Figure 3b and 3c). The values of the KIE between 1 and 7 support this view and suggest that the chemisorption step plays a major role in the reaction kinetics for CD_2O (Figure 3b and 3d).[2,6-9] At high temperatures and low potentials, the values of the KIE drop to 0.14, suggesting that the recombination adsorbed hydrogen (Step [6]) may rule the rate of the reaction for both CD_2O and CH_2O (Section 4.2.6). Note, that when the rate limiting steps for CH_2O and CD_2O are different that the KIE should be conceived as an apparent KIE.

-Palladium- The oxidation of formaldehyde on palladium sets in at the same potential for CD_2O as for CH_2O, but proceeds more rapidly at the lower range of potentials for CD_2O than for CH_2O (Figure 4a and 4b). The lower values of the E_{act} for CD_2O than for CH_2O, and the values of the KIE lower than 1 suggest that the rate of oxidation of adsorbed hydrogen (Step [7]) plays a major role in the overall rate of the reaction (Figure 4c and 4d). The negative values of E_{act} at very low potentials suggest the presence of a (pseudo) pre-equilibrium prior to this hydrogen desorption step. At higher potentials, the values of the KIE approach 1 and either diffusion (Step [2]) or the desorption of formate (Step [5]) may become rate-limiting (Figure 1i and Figure 4d). The E_{act} attains constant values of ~10 kJ mol^{-1} at these potentials (Figure 4c).

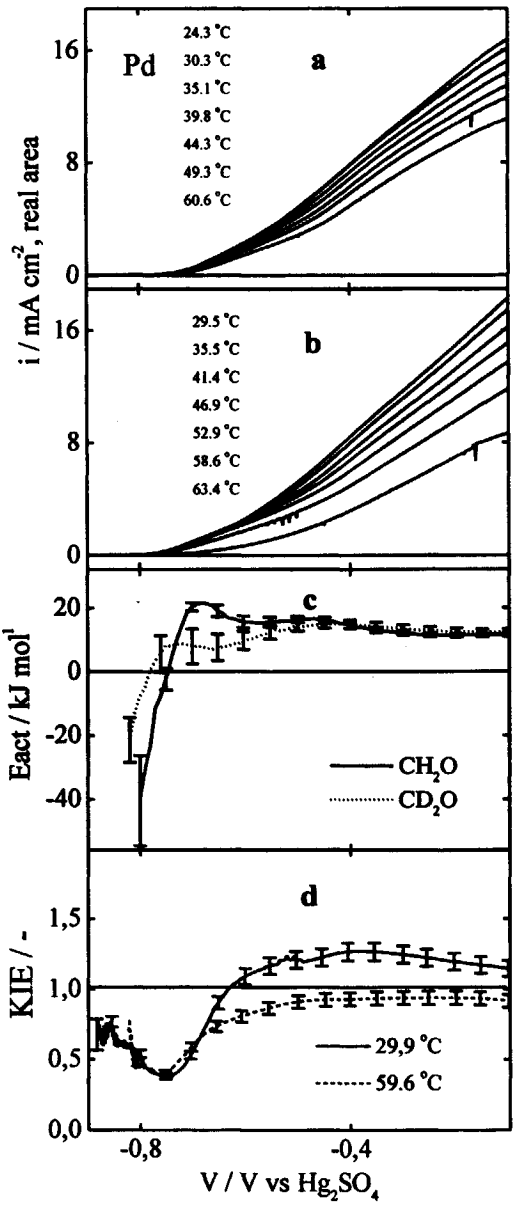

Figure 4. *Linear sweep voltammograms recorded at 10 mV s^{-1} for palladium in 0.1 M NaOH and 0.1 M CH_2O (a), and 0.1 M NaOH and 0.1 M CD_2O (b). Calculated values of E_{act} (c). Calculated values of the KIE (d).*

-Iridium- The oxidation of formaldehyde on iridium sets in at slightly lower potentials for CD_2O than for CH_2O although the current density reaches higher values for CH_2O than for CD_2O (Figure 5a and 5b). The values of E_{act} are much lower for CH_2O than for CD_2O at potentials where the KIE reaches values between 0.14 and 1 (Figure 5c and 5d). This is explained by a rate-limiting role of the desorption of adsorbed hydrogen for CH_2O (Step [7]) and chemisorption for CD_2O (Step [4]).[3] At higher potentials, the values of the KIE converge to 1, suggesting that the desorption of formate (Step [5]) may rule the rate of the reaction. Moreover, the rate of chemisorption plays an important role in the rate of the reaction when the iridium surface is oxidized, as revealed by the high values of the KIE at these potentials (Figure 5d).[4]

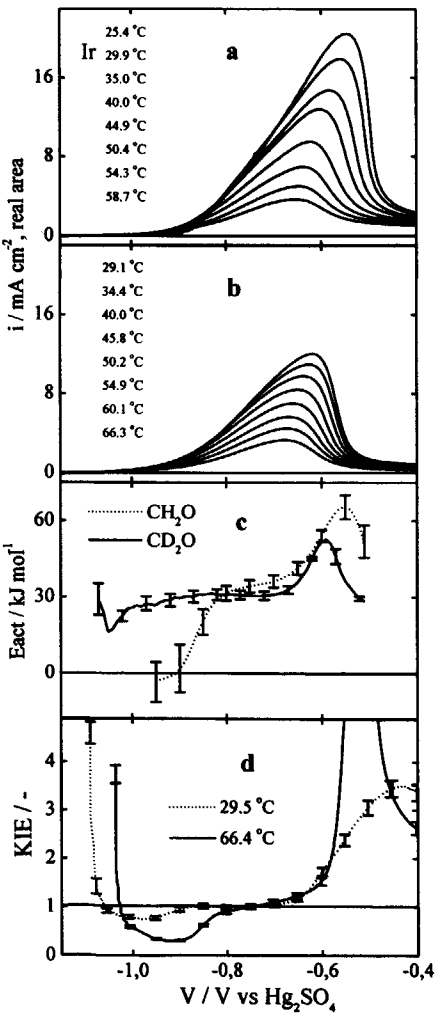

Figure 5. *Linear sweep voltammograms recorded at 10 mV s^{-1} for iridium in 0.1 M NaOH and 0.1 M CH_2O (a), and 0.1 M NaOH and 0.1 M CD_2O (b). Calculated values of E_{act} (c). Calculated values of the KIE (d).*

-Platinum- The oxidation of formaldehyde on platinum sets in approximately at the same potentials for CD_2O than for CH_2O although the current densities increase more at increasing temperatures for CD_2O than for CH_2O (Figure 6a and 6b).

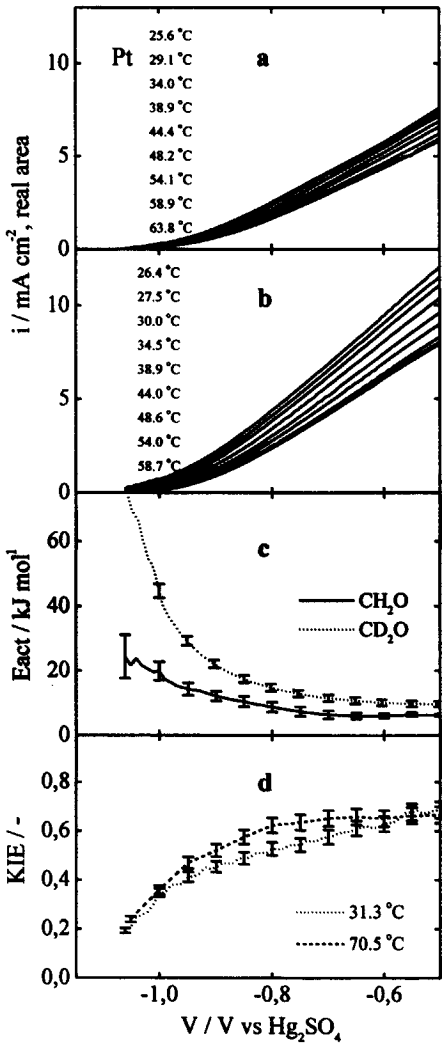

Figure 6. *Linear sweep voltammograms recorded at 10 mV s^{-1} for platinum in 0.1 M NaOH and 0.1 M CH_2O (a), and 0.1 M NaOH and 0.1 M CD_2O (b). Calculated values of E_{act} (c). Calculated values of the KIE (d).*

The values of the E_{act} show that the stronger increase in oxidation rate for CD_2O than for CH_2O at increasing temperatures roughly proceeds by a factor 2 (Figure 6c). The low values for the KIE of ~0.2 at the lower potentials imply that the rate of hydrogen desorption (Step [7]) may play a major role in the overall reaction kinetics for both CD_2O and CH_2O. The high bond strength of hydrogen on platinum may account for these low

desorption rates.[10] The positive values of the E_{act} at low potentials suggest that the contribution of the enthalpy to the rate-limiting step of the reaction is higher than the lowering effect of the pre-equilibrium (the 'entropy' of the apparent activation energy).[2] At higher potentials, the value of the KIE increases to values around 0.7 and the influence of diffusion (Step [2]) becomes more apparent in the overall rate of oxidation.

-Nickel- The oxidation of formaldehyde on nickel proceeds very slowly, as revealed by the low current densities (Figure 7a).

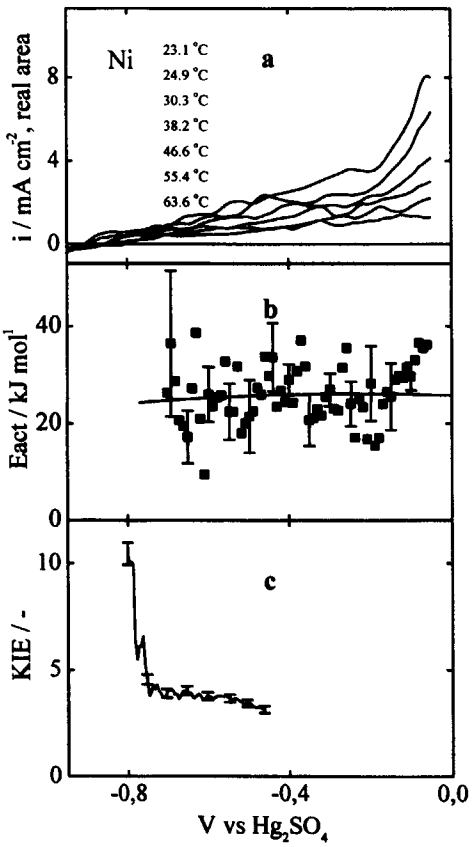

Figure 7. *Voltammograms recorded on nickel in 0.1 M NaOH and 0.1 M CH_2O at 10 mV s^{-1} (a). Calculated values of the E_{act} (c). Calculated values of the KIE (d).*

The relatively high values of the E_{act} for CH_2O (~27 kJ mol^{-1}) are in line with the low electrocatalytic activity (Figure 7b). No data were obtained for CD_2O at higher temperatures, as current densities fluctuated around zero. The values of the KIE were therefore obtained by the method described in Section 2.3.2 (Figure 7c). Clearly, the values of the KIE are relatively high and the rate of chemisorption seems to play a major role in the overall rate of the reaction over a wide range of potentials.

Summary - Summing up these observations, the metals may be divided in three groups:

- Metals with positive values of E_{act} and values of the KIE higher than 1. This group (Ag, Ni and Cu) seems characterized by a major role of the chemisorption step (Step [4]) in the overall reaction kinetics.
- Metals with positive and negative values of the E_{act}, and values of the KIE both lower and higher than 1. This group (Au, Pd, Ir) is characterized by an important role of both the chemisorption (Step [4] and the desorption of formate and adsorbed hydrogen (Step [5]-[7]) in the overall reaction kinetics.
- One metal (only Pt) with positive values of E_{act} and values of the KIE lower than 1. This metal is characterized by a major role of the desorption of adsorbed hydrogen (Step [7]) in the overall reaction kinetics.

Moreover, diffusion (Step [2]) plays an important role at higher current densities for silver, palladium, gold and platinum while strong capacitive current densities are seen for nickel, copper and iridium.

6.3 Electrocatalytic Activities

A comparison of the electro-oxidation rates on the various metals is shown in Figure 8a. Clearly, some metals catalyse the oxidation of formaldehyde well at lower potentials, though poorly at higher potentials, while others catalyse the reaction poorly at lower potentials, though well at higher potentials. In addition, no clear Tafel behaviour applies to any of the metals under the pseudo-steady state conditions examined. The classification of the electrocatalytic activities of the metals has therefore been made according to current densities at potentials relative to the OCP and relative to the Hg/Hg_2SO_4-reference electrode (Table 1). Information on the relative and absolute catalytic properties of the metals may be further obtained by examining the respective values of the E_{act}, the slopes of the voltammograms, the values of the KIE and the potentials at a certain rate of oxidation. The values of these variables have been given at a current density of 0.3 $mAcm^{-2}$ (Table 1). This latter value was chosen, as it was considered to enable kinetic comparisons of all metals with a minimum 'disturbance' from diffusion effects. In addition, some electro-kinetic values have been given at 0.9 V *vs.* Hg/Hg_2SO_4, as this potential enabled the comparison of six metals at sufficient high current densities (Figure 8).

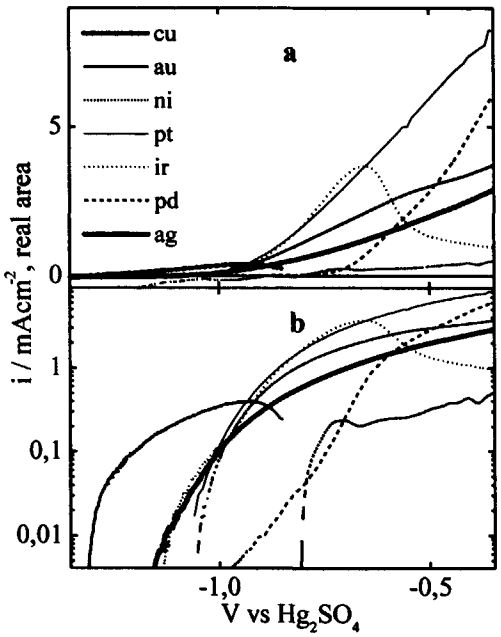

Figure 8. *Linear sweep voltammograms (a) and Tafel plots (b) recorded in 0.1 M NaOH and 0.1 M CH_2O at 1 mV s^{-1} for all metals studied.*

Metal	OCP / V *vs.* Hg/Hg_2SO_4	i (0.3 V *vs.* OCP) / mA cm^{-2}	i (-0.9 V *vs.* Hg/Hg_2SO_4) / mA cm^{-2}	V (0.3 mA cm^{-2}) / V *vs.* Hg/Hg_2SO_4	Slope at 0.3 mA cm^{-2} / $m\Omega^{-1}$	E_{act} at 0.3 mA cm^{-2} / kJ mol^{-1}	KIE at 0.3 mA cm^{-2} /-	KIE 0.3 V *vs.* OCP / -
Ag	-1.16	0.41	0.31	-0.90	2.75	11.9	3.73	2.72
Cu	-1.31	0.34	0.39	-1.04	0.86	25.1	2.80	2.77
Pd	-1.04	0.11	0.01	-0.69	7.21	20.8	0.61	0.39
Ni	-0.81	0.31	0.00	-0.43	0.99	25.7	3.61	3.78
Au	-1.07	1.31	0.48	-0.94	4.36	-3.17	1.27	0.90
Ir	-1.14	1.12	0.50	-0.93	5.30	-2.51	0.86	0.98
Pt	-1.07	2.12	0.56	-0.93	5.98	14.0	0.40	0.54

Table 1. *Electrocatalytic activities and KIE-values obtained.*

It is clear from Table 1 and Figure 8 that gold, platinum and iridium promote the reactions to the highest rates while copper and silver catalyse the oxidation at lowest potentials. Nickel and palladium do not catalyse the reaction in 0.1 M NaOH well. The relatively large differences in the values of the OCP suggest that the metals affect the equilibria of the responsible partial reaction steps substantially. The responsible partial reactions result most likely from the oxidation and reduction of formaldehyde to formate and methanol respectively, as water reduction was suppressed by the adsorption of formaldehyde, and as oxygen reduction was suppressed as well (the solution was purged with nitrogen).[10]

The log(i)-V plots of the various voltammograms are shown in Figure 8b. The absence of straight lines, characteristic for electrochemical systems with a rate-limiting electron transfer step, supports the view that the rate of the reaction may be ruled by chemical bond ruptures or bond formations rather than by electron-transfers under these pseudo-steady state conditions, as discussed in Chapter 3-5.[2,3,11,12] This view seems further supported by the non-linear dependence of the E_{act} on the potentials applied and the values of the KIE lower or higher than 1.[11]

6.4 Physical and Chemical Trends

An attempt was made to correlate the electro-kinetic properties (i, V, KIE and E_a) with some physical and chemical properties of the metals in order to see if other parameters than reactant-metal adsorption energies played an important role in the catalytic properties of the metals. The electro-kinetic data were taken from Table 1. Inter-atomic bond lengths (L) were evaluated, as neighbouring atoms are known to affect electrocatalytic activities.[13,14] The possible role of metal-product enthalpies ($\Delta H_{M(HCOO)n}$) in the electrocatalytic activities was already discussed in Section 1.5, while work functions (W) are known to be related to hydrogen adsorption heats.[15,16] In addition, the relation between the electro-kinetic properties of the catalyst and the values of the KIE were addressed in order to see if the rates of the C-H and M-H rupture steps depended on the catalyst in a structural fashion. Moreover, a comparison of the metal-dependent rates with the oxidation potentials of the preferred valence states (Ag-Ag^+, Cu-Cu^{2+}, Ni-Ni^+, Pd-Pd^{2+} Pt-Pt^{2+}, Au-Au^{3+}, Ir-Ir^{3+}) was made, as the less noble metals were considered to be characterised by a lower electrocatalytic activity during the measurements, and as oxidised surface atoms have been proposed to affect the electrocatalytic characteristics of metals.[17]

6.4.1 Metal-Hydrogen and Metal-Formate Bonds

A curved relationship was found for the dependence of the current density on the values of the KIE (Figure 9a). The curved relationship supports the view from Sections 3.2.7,

4.2.6, 5.2.4 and 5.2.6 that rupture of the C-H and M-H bonds are primarily involved in the rate-limiting steps of the reaction. Note, that the relationship applies to the dependence of the current density at a potential relative to the OCP and not to that relative to the Hg/Hg_2SO_4-reference electrode. The exceptional role of palladium is not completely understood, as it is not in line with the categorization based on values of the KIE and the E_{act} mentioned above. The palladium-characteristic hydrogen absorption properties might manifest predominantly in the pre-exponential factor of the responsible rate-equation (rather than in E_{act}) although more work needs to be done to verify this view.[1]

A curved relationship was found for the dependence of the apparent activation energy on the metal-formate formation enthalpies (Figure 9b), suggesting that the metal-formate bond strength affects the height of the overall apparent activation energy in a straightforward fashion. The presence of a curved relationship rather than a volcano-type relationship suggests nevertheless that Sabatier's principle does not apply to this system. This observation seems plausible, as it was shown in Section 5.4 that formation enthalpies do not necessary reflect real bond strengths (contrary to Gibbs free adsorption energies in the solution). In addition, Sabatier's principle is generally assumed to apply to volcano-type relationships that use reaction rates rather than activation energies. The next chapter will therefore focus on values of the overall rates and on Gibbs-free energies of the adsorbed enolate anions obtained in the solution under *in-situ* conditions.

Another interesting relationship, similar to that in Figure 9b, was found to apply to the dependence of the apparent activation energy on the potentials at which metals are (thermodynamically) oxidized to the preferred valence states (Figure 9c). Assuming that the oxidation potentials apply to the surface atoms as well, the relationship would support the view that formation and rupture of specific bonds goes along with the formation of ionic bonds.

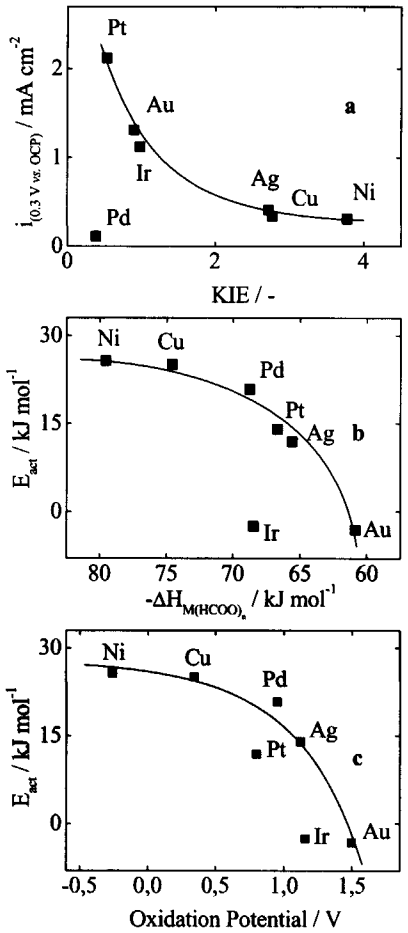

Figure 9. *Relationship obtained for the dependence of the metal-dependent current density on the KIE (a). Relationship for the dependence of the metal-dependent E_{act} (at i = 0.3 mA cm^{-2}) on the metal-formate formation enthalpy (b) and oxidation potential of the preferred valence states (c).*

6.4.2 Electronic Structure of the Metals

Two other roughly linear trends were obtained for the dependencies of the electro-oxidation rates and the values of the KIE on the work function (Figure 10a and 10b). The catalytically inactive metals Ni and Pd (see above) do nevertheless not obey this behaviour. The relationships suggest that the electronic properties of the metals affect the

overall rate of the reaction and that this influence is particularly expressed in the rate of chemisorption (Step [4]) and the rate of desorption of adsorbed hydrogen (Step [6] and [7]). Moreover, the results in Figure 10b suggest that the nobler metals (Pt, Au, Pd, Ir) have lower values of the KIE than the less nobler ones (Cu, Ag, Ni). It suggests that the less nobler metals affect the rate of chemisorption (Step [4]) to greater extent while the nobler ones affect the rate of desorption of adsorbed hydrogen (Step [6] and Step [7]) to greater extent. This observation seems in rough concordance with the categorization of metals discussed (Section 6.2.2). The relatively low electrocatalytic activity for the 'chemisorption' metals (Ag, Cu and Ni) and the relatively high electrocatalytic activity for three 'desorption' metals (Pt, Ir and Au) may point towards Sabatier-behaviour (Figure 10). This issue will nevertheless be addressed in more detail in Chapter 7.

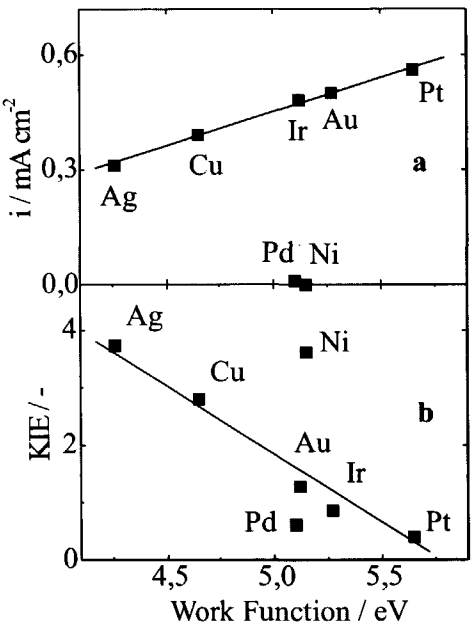

Figure 10. *Relationships obtained for the dependencies of the current density (a) and the KIE at 0.3 mA cm^{-2} on the work functions (b).*

6.4.3 Geometry of the Metals

Finally, a structural relationship was obtained for the dependence of the apparent activation energy on the inter-atomic bond lengths (with the exception of Ir), as shown in Figure 11. It suggests that nearest neighbours of the catalytic sites play an important role in the electrocatalytic activity and that longer inter-atomic bond lengths favour the lowering of the apparent activation energy. The lower apparent activation energies at longer M-M

bond lengths may result from slower lateral recombination of adsorbed hydrogen and adsorbed carbon species after chemisorption, enhancing the time for adsorbed species to react to products.

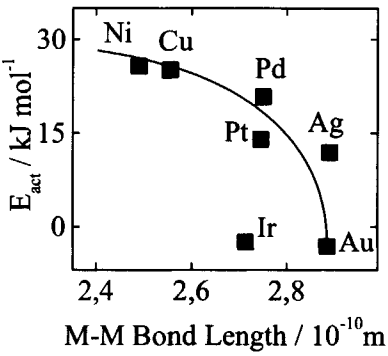

Figure 11. *Relationships obtained for the dependencies of E_{act} on the average interatomic M-M bond lengths.*

6.5 Conclusions

- Au, Pt and Ir catalyse the reactions to highest rates, while Cu and Ag catalyse the reaction at lowest potentials. Ni and Pd do not catalyse the reaction well.
- At low overpotentials and temperatures, the rate of the reaction is likely ruled by chemisorption of the enolate anion on Ag, Cu, Au and Ni, and by desorption of adsorbed hydrogen on Pt, Pd and Ir. At higher potentials, the reaction becomes increasingly controlled by desorption of the formate anion on all metals studied. Diffusion (Step [2]) plays an important role at higher current densities for the reaction on Ag, Pd, Au and Pt while high capacitive current densities are seen for the reaction on Ni, Cu and Ir.
- The rate of the reaction is greatly affected by the rate at which hydrogen bonds are ruptured, as revealed by the presence of KIE-values different than one and a curved relationship between the metal-dependent oxidation rates and the values of the KIE.
- The similar dependencies of the E_{act} on both the metal-formate formation enthalpies and the thermodynamic oxidation potentials of the metals supports the important role of chemical bond strengths between reacting species and the metal surface in the overall rate of the reaction.

- The relationships between the current density and the work function of the metals suggest that the electronic properties of the metals affect the rate of the reaction in a straightforward fashion.
- The dependence of the E_{act} on the inter-atomic bond lengths suggests that nearest-neighbour effects in the metals affect the transition state of the reaction.
- Values of the KIE different than one and the absence of linear Tafel slopes under the pseudo steady-state conditions examined support the view from previous chapters that the kinetics of the reaction has a chemical character rather than an electrochemical one.
- The values of the E_{act} can be both positive and negative, confirming the catalytic role of the metals in the rate of the reaction and the possible presence of a pre-equilibrium.

6.6 References

(1) Ohno, I.; Wakabayashi, O.; Haruyama, S.; *J. Electrochem. Soc.*, **1985**, 132, 2323.
(2) Kortenaar, M. V.;Kolar, Z. I.; Goeij, J. J. M. de.; Frens, G.; *J. Electrochem. Soc.*, **2001**, 148, 1.
(3) Kortenaar, M. V.; Tessont C.; Kolar, Z. I.; Weijde, H. van der.; *J. Electrochem. Soc.*, **1999**, 14, 2146.
(4) Kortenaar, M. V.;Kolar, Z. I.; Goeij, J. J. M. de.; Frens, G.; Langmuir, **2002**, 18, 10279.
(5) Gileadi, E.; in *Electrode Kinetics*, VCH Publishers, Inc., New York, 1993, p. 85.
(6) Beltowska-Brzezinska, M.; *Electrochim. Acta*, **1985**, 30, 1193.
(7) Avramov-Ivic, M. L.; Anastasijevic, N. A.; Adzic, R. R.; *Electrochim. Acta*, **1990**, 35, 725.
(8) Meerakker, J. E. A. M. van den; *J. Appl. Electrochem.*, **1981**, 11, 395.
(9) Meerakker, J. E. A. M. van den; *J. Appl. Electrochem.*, **1981**, 11, 387.
(10) Jusys, Z.; *J. Electroanal. Chem.*, **1994**, 375, 257.
(11) Shriver, D. F.; Atkins P. W.; Langford, C. H.; in *Inorganic Chemistry*, Oxford University Press, 1st edition, Oxford, UK, 1990, p. 569.
(12) Gileadi, E.; in *Electrode Kinetics*, VCH Publishers, Inc., New York, 1993, p. 108-119.
(13) Frelink, T.; PhD Thesis, University of Technology Eindhoven, The Netherlands, 1995, p 119.
(14) Veen, J. A. R. In *Studies in Surface Science and Catalysis*, 1999, Vol 123, 270-283.
(15) Bockris, J. O. M.; Khan, S. U. M.; in *Surface Electrochemistry, A Molecular Level Approach*, Plenum Press, New York, 1993, p. 291.
(16) Bindra, P.; Roldan, J.; *J. Electrochem. Soc.*, **1985**, 132, 2582.
(17) Burke, L. D.; O'Dwyer, K. J.; *Electrochim. Acta*, **1990**, 11, 1829.

Chapter 7

Adsorption and Oxidation of Formaldehyde on Transition Metals studied by the Radiotracer Thin-Gap Technique*

Adsorption, exchange and oxidation of formaldehyde on transition metals (Ag, Cu, Ni, Pd) were studied in 0.1 M NaOH by voltammetry and the radiotracer thin-gap technique. One linear four-compartment model was found to fit to all adsorption and exchange kinetic data at the OCP satisfactorily, suggesting the presence of three adsorption steps in the overall adsorption process: a rapid, reversible physisorption, a slow, reversible chemisorption and an irreversible side-reaction. The rate-limiting chemisorption step was seen to proceed at highest rates on gold under dynamic conditions and at highest rates on copper under equilibrium conditions. The latter observation was in agreement with the lowest Gibbs free adsorption energy (ΔG_{ad}) for copper derived. The values of the OCP and the residence times of species in the chemisorption state (τ_c) were further seen to depend on ΔG_{ad} in a linear way, an observation that may explain the value of the OCP and the occurrence of electroless metal deposition on an atomic scale. Moreover, approximate volcano-type relationships were obtained for the dependencies of the oxidation rates on the values of ΔG_{ad}, τ_c and the surface quantities (Q). It supports the validity of Sabatier's principle for the formaldehyde-transition metal system, a view that seems further supported by the relationships between ΔG_{ad} and τ, ΔG_{ad} and Q, as well as τ_c and Q. Volcano plots used to derive Sabatier's principle should nevertheless use values of ΔG_{ad} in the liquid phase rather than values of ΔG_{ad} derived the gas-phase or values of ΔH_{ad}, as outlined in Chapter 5.

Submitted to Langmuir

7.1. Introduction

The radiotracer thin-gap technique and compartmental analysis is used to address the adsorption and exchange kinetics of formaldehyde on transition metals (Pd, Ag, Cu, Au and Ni). First, adsorption and exchange of formaldehyde on transition metals are studied at the OCP in 0.1 M NaOH. This concentration was chosen, as it was a standard condition in the previous studies, and as the side reaction did not or little proceed at this pH (Section 4.2.1). The adsorption isotherms at the OCP are further determined to derive values of ΔG_{ad} from the initial slopes of the isotherms. The adsorption isotherm presented for gold (Section 5.2.4) has been included for comparison. Next, the adsorption characteristics and current densities (i) are examined at different temperatures and potentials in order to gain qualitative insight into the thermodynamics and kinetics of the adsorption process. Finally, dependencies of the metal-dependent formaldehyde electro-oxidation reaction rates on the Gibbs free adsorption energies, on the residence times (τ) and on the adsorbed quantities (Q) are derived. The relationships may validate the derivation of Sabatier's principle from empirical volcano-type relationships in electrocatalysis, as mentioned in Section 1.6.[1-5]

7.2. Fitted Circuit

Of all possible two-compartment, three-compartment and four-compartment models fitted for all metals studied, only the model shown in Figure 1 described all adsorption kinetic data satisfactorily.

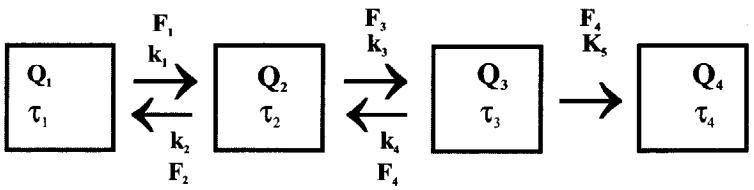

Figure 1. *Fitted model that described the overall adsorption and exchange data most satisfactorily.*

The data were fitted best by first-order differential equations with exponential solutions rather than root-type equations, which was in concordance with fits presented for gold in Chapter 5. The fitted rate equations have been described in the Appendix. It suggests that the rates of the adsorption processes are ruled by kinetic, electrostatic barriers rather than by mass-controlled, diffusive ones.[1] A comparison of the model shown in Figure 1 with that derived in Section 5.2.2 for gold shows that one irreversible flow has been added to

the three-state model. This flow connects a sink (Q_4) with the third compartment. The possible presence of this sink was already discussed in Chapter 5, as some exchange kinetic data then showed a relatively high residual fraction but was rejected then, as the overall fitting results for all gold data showed a lower reliability than for the three-state model, and as a minimum of compartments was pursued. However, it has been included in the fits for the other metals, as data for copper could not be fitted properly without invoking the presence of the sink. Fitting results obtained for gold using the four-state model are presented below as well to compare the results for all metals studied.

7.3 Interpreted Model.

The fitted model seems plausible when considering the following results and views presented in the previous chapters:

- The mechanism derived from literature, as this mechanism supported the presence of a physisorption and chemisorption step (Section 1.6).
- The fitted equivalent circuit and the corresponding electrostatic double-layer structure with the twofold layer structure, comprising physisorbed species in the IHP and chemisorbed species in the OHP (Section 3.2.4).[7]
- The irreversible non-electrochemical side reaction, as observed by DEMS (Section 4.2.2) and mentioned due to the relatively high residual fractions in the exchange kinetic curves for gold (Section 5.2.3).
- The model derived for gold, suggesting the presence of two linearly connected reversible physisorption and chemisorption processes (Chapter 5).
- The view that diffusion and electron transfers do not rule the adsorption and exchange rates around the OCP (Section 3.2.4, 3.2.5, 3.2.7, 4.2.4, 4.2.5, 4.2.6 and 5.2.6).[8,9]
- The observation that reaction rates for other metals than gold were characterized by values of the KIE different from 1 around the OCP, implying a major role of the chemisorption in the overall adsorption, exchange and oxidation kinetics (Section 3.2.4, 3.2.5, 3.2.7, 4.2.6, 5.2.7).

Taking into account these results, and considering the schematic view of the adsorption process, the assignments of the fitted mass flows to the actual reaction can be made according to Figure 2a and 2b. The model suggests that physisorption and chemisorption of the enolate anion proceed in a catenary fashion rather than in a mammillary one. The chemisorption steps reflect the transitions of all species across the activation energy between the OHP and the IHP rather than the single bond rupture step of the enolate anion. The desorption of formate, molecular hydrogen and water from the surface into the solution belong to this transport as well. Like in Chapter 5, the interpreted model shown in Figure 2c will serve as base for the quantitative discussion of the adsorption data.

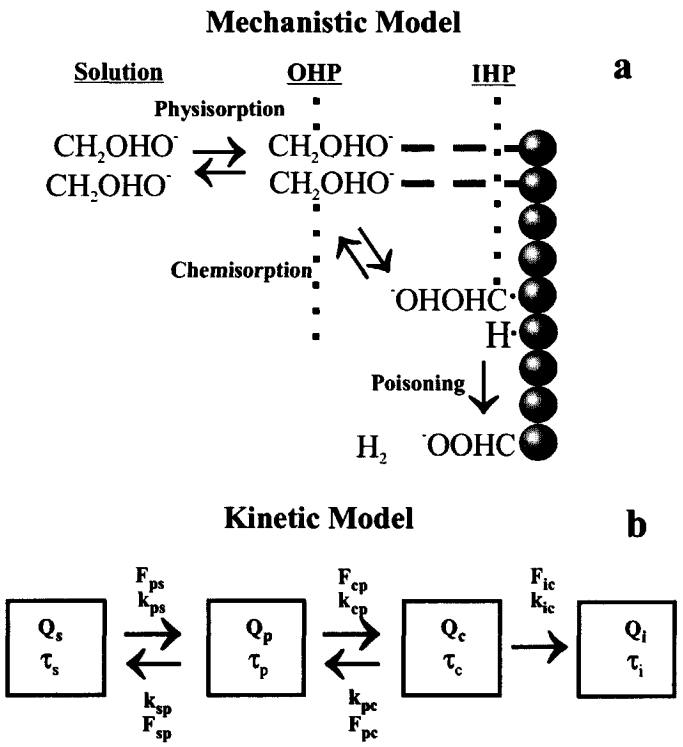

Figure 2. *Expected model (a) and the interpreted model (b) for the adsorption process of formaldehyde on the various metals.*

7.4 Adsorption Kinetics at the OCP

The adsorption of labelled formaldehyde on transition metals at the OCP from solutions containing 0.1 M NaOH and 0.01 M CH_2O is shown, together with the fitted equivalents and the quantities hosting the different states, in Figure 3. The values of the fitted rate constants, the intercompartment flows, residence times and the state quantities are listed in Table 1. Clearly, the steady state in the adsorption process is reached most rapidly on palladium and slowest on nickel, while intermediate adsorption rates are observed on copper, gold and silver (Figure 3). These observations are roughly confirmed by the fitted rate constants and the intercompartment flows as well (Table 1). The exceptional role of palladium and nickel relative to the other metals seems in line with the low catalytic activity for nickel and palladium, as presented in Section 6.3. The surface

coverage at longer times ($Q_e(\infty)$) is different for nickel and palladium too, although it follows a reverse order: it is lowest for palladium and highest for nickel. A more detailed analysis shows that this trend results from the quantity of species hosting the chemisorption state, as $Q_c(\infty)$ is highest for nickel, followed by copper, gold, silver and then palladium (Table 1). Hence, the rate of chemisorption is slow relative to the rate of physisorption, but the adsorption in the chemisorption state seems thermodynamically more favourable than in the physisorption state (Figure 3). This behaviour applies to all metals studied.

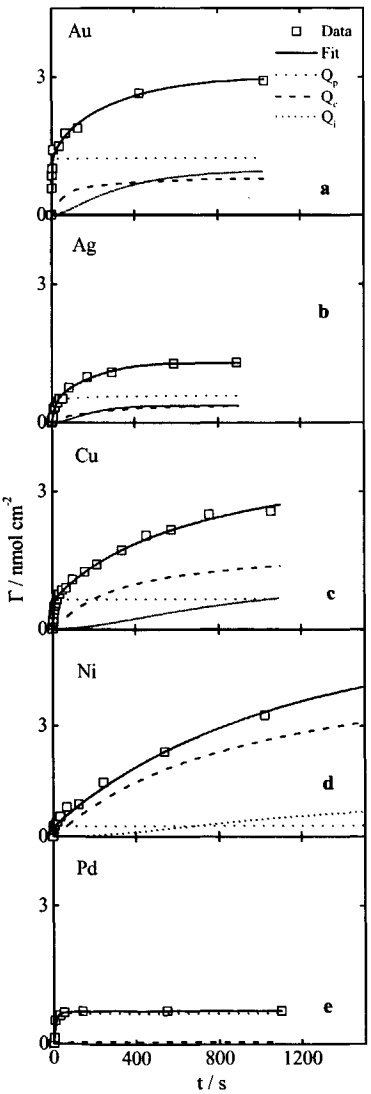

Figure 3. *Adsorption of formaldehyde on different transition metals studied at the OCP from solutions containing 0.1 M NaOH and 0.01 M CH_2O. The fitted data and the fitted quantities hosting the chemisorbed and physisorbed states are shown as well (a-e).*

	k_{sp} / s^{-1}	k_{ps} / 10^{-5} s^{-1}	k_{cp} / 10^{-3} s^{-1}	k_{pc} / 10^{-2} s^{-1}	$Q_c(\infty)$/ nmol	$Q_p(\infty)$/ nmol	$Q_i(\infty)$/ nmol	F_{ps} / 10^{-1} nmol s^{-1}	F_{cp} / 10^{-3} nmol s^{-1}	F_{ic} / 10^{-4} nmol s^{-1}	τ_p / s	τ_c / s
Au	0.56	2.1	9.6	1.5	2.7	3.7	2.9	21	35	40	1.8	61
Ag	0.05	0.15	8.4	1.4	1.7	2.8	1.8	1.5	24	120	16	48
Cu	0.22	0.48	7.7	0.31	5.5	2.2	3.2	4.8	17	19	4.5	290
Ni	0.20	0.15	18	0.14	9.7	0.72	2.1	5.0	13	19	4.5	640
Pd	0.11	0.10	0.98	1.2	0.08	0.97	0.05	24	0.95	0.03	9.3	82

Table 1. *Fitted rate constants (k), residual quantities (Q), interstate flows (F) and transition times (τ) for the adsorption kinetic curves*

Analysis of the fitted transition times (Table 1) shows that species spend much more time in the chemisorbed state (τ_c) than in the physisorbed state (τ_p). Besides, the average flow of enolate anions at 'infinite' time between the solution and physisorbed state (F_{sp}) is much higher than the average flow between the physisorbed state and chemisorbed state (F_{pc}). Hence, the transition between the OHP and IHP in either direction seems rate limiting for all metals studied. Moreover, no multilayer adsorption seems to occur during adsorption, as the surface coverage never exceeded approximately 65% of the available metal sites (calculated from a roughness factor of 3, an average M-M length of 3 Å, and a 'one formaldehyde-to-one metal site' occupation).[2]

7.5 Exchange Kinetics

To see if occupation of the metal sites had occurred in a reversible or irreversible manner, and to derive the values of the times of residence of species adsorbed at the surface, the exchange of adsorbed, radioactive formaldehyde with dissolved formaldehyde was studied (Table 2, Figure 4).

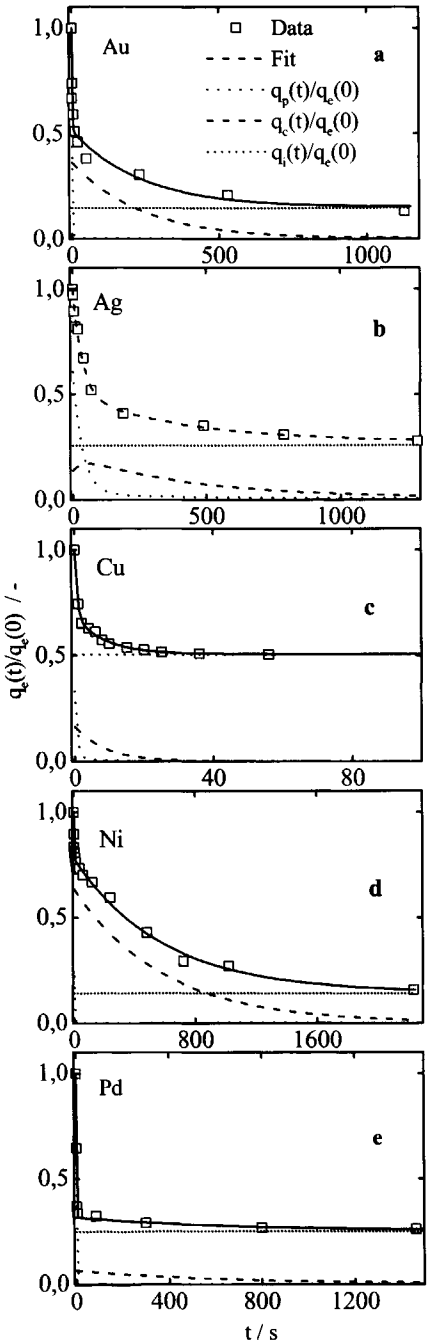

Figure 4. *Exchange of formaldehyde on the transition metals studied at the OCP in solutions containing 0.1 M NaOH and 0.01 M CH_2O. The fitted analogues and the fitted fractions hosting the chemisorbed and physisorbed states are shown as well (a-e).*

	k_{sp} / s^{-1}	k_{ps} / 10^{-4} s^{-1}	k_{cp} / 10^{-3} s^{-1}	k_{pc} / 10^{-2} s^{-1}	$q_p(\infty)/q_e(0)$ / 10^{-3}	$q_c(\infty)/q_e(0)$ / 10^{-3}	$q_i(\infty)/q_e(0)$ / -	F_{ps} / nmol s^{-1}	F_{cp} / nmol s^{-1}	τ_p / s	τ_c / s
Au	0.58	26	4.3	0.39	4.4	4.8	0.15	250	1.9	1.7	250
Ag	0.03	0.35	2.6	0.31	1.3	1.1	0.26	3.5	0.35	35	330
Cu	1.6	65	9.4	12	4.1	0.31	0.50	650	3.8	0.6	8.1
Ni	0.53	21	3.3	18	3.8	7.0	0.14	200	1.3	1.9	550
Pd	0.89	20	3.3	0.23	2.3	3.2	0.25	200	0.75	1.1	430

Table 2. *Fitted rate constants (k), state quantities (q(∞)/q(0)), interstate flows (F) and transition times (τ) for the adsorption kinetic curves*

Clearly, exchange of adsorbed formaldehyde with dissolved formaldehyde does occur for all metals, although the residual fractions remain relatively high, in particular for copper. It may support the occurrence of the irreversible, non-electrochemical side-reaction (although this reaction was seen to proceed to lowest extent in 0.1 M NaOH on gold; Section 4.2.5 and 5.2.3). As copper is the best catalyst for the hydrogen evolution, and as the side-reaction may proceed at the OCP, the residual fraction is explained by the irreversible formation of formate according to side-reaction described in Section 4.2.5 (and shown schematically above in Figure 2):

CH_2OHO^- (aq) $\leftrightarrow$ $HCOO^-_{irr} + H_2\uparrow$

Generally, the intercompartment flows (F) have the lowest value for the chemisorption step (Table 2). The rate at which the activation energy between the IHP and OHP is traversed in either direction seems thus rate limiting for all metals studied. This rate of traverse between the OHP-IHP was seen to be rate limiting in the adsorption kinetic measurements too for all metals studied (Section 7.4). The comparison of metals on this flow shows a highest value for copper and a lowest one for palladium, a trend that is reflected accordingly by the residence times: an enolate anion resides the chemisorbed on copper for 8 s and on palladium for 432 s. Moreover, the rate-limiting flow (F_{cp}) is highest for gold under dynamic conditions and highest for copper under equilibrium conditions (Table 1 and 2). This observation may be in line with the following previous observations:

- The lowest value of the OCP for copper under equilibrium conditions and the associated highest catalytic activity at potentials slightly positive to this OCP.

- The highest catalytic activity for gold under dynamic conditions at a fixed potential relative to the Hg/Hg_2SO_4 electrode (Section 6.3).

7.6 Adsorption Isotherms at the OCP

Adsorption isotherms obtained at the OCP in solutions containing 0.1 M NaOH are shown in Figure 5.

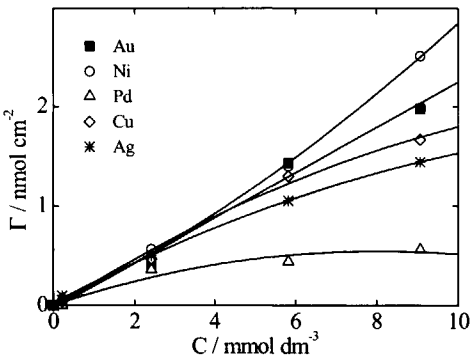

Figure 5. *Adsorption isotherms of formaldehyde in 0.1 M NaOH at the OCP.*

Contrary to the isotherms observed in Chapter 5 for gold, the adsorption isotherms are not linear, implying that adsorbed enolate anions may inhibit (Ag, Cu, Pd) or promote (Ni) additional adsorption of enolate anions. Interestingly, the adsorption of formaldehyde is highest for the poorly catalytic nickel, lowest for the also poorly catalytic palladium, and intermediate for the highly catalytic gold, copper and silver. It roughly supports the volcano-type behaviour needed to validate Sabatier's principle (*see* below). Moreover, the values of the adsorbed, fitted quantities at 10 mM CH_2O are roughly similar with the (estimated) adsorbed quantities at infinite time in Figure 3.

The standard free Gibbs adsorption energies, ΔG_{ad}, were calculated from the initial slopes of the adsorption isotherms by assuming Langmuir behaviour and applying $\Delta G_{ad} = RTlnK$ (Table 3).

Metaal	Au	Ag	Cu	Ni	Pd
ΔG_{ad} / kJ mol^{-1}	-27.8	-27.6	-28.6	-27.1	-25.5
OCP / V *vs.* Hg_2SO_4	-1.04	-0.90	-1.18	-0.81	-0.82

Table 3. *Gibbs adsorption energies of formaldehyde in 0.1 M NaOH.*

Clearly, the differences between the Gibbs free adsorption energies are small. The small differences were also observed for the values of the Gibbs adsorption energies for gold in different solutions (Section 5.2.4). Larger differences were nevertheless seen to apply to the solution-dependent and metal-dependent values of the E_{act} (Section 4.2.6 and Section 6.2.2). Moreover, the Langmuir-assumption seemed reasonable at low concentrations for all metals studied, as fitted adsorption isotherms were approximately linear at low concentrations, and as no multi-layer adsorption seemed to occur even at the higher concentrations (*see* above and Section 5.2.3).

A comparison of the values of the Gibbs free adsorption energies with the values of the OCP in the solution containing 0.1 M NaOH and 0.01 M CH_2O showed that four out of five points obeyed a linear dependence (Figure 6). Assuming the complete removal of oxygen from the bubbling of nitrogen, the OCP-responsible reactions may be the oxidation and reduction of formaldehyde (Chapter 6). Consequently, the adsorption strengths seem related to the equilibrium of these two partial reactions. The side-reaction has nevertheless not been included in this picture, as it was considered to refer to a catalytic dissociation reaction rather than to an electrochemical (potential-determining) reaction.

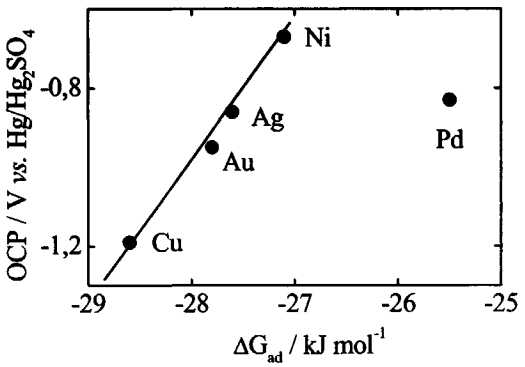

Figure 6. *Values of the OCP versus the Gibbs free adsorption energies.*

7.7 Potential Dependence

The adsorption and oxidation of formaldehyde on various metals at different potentials is shown in Figure 7. The adsorption remains roughly constant at higher potentials on copper, nickel and gold, but decreases slightly for silver and strongly for palladium. As copper, gold and nickel showed a strong degree of chemisorption, and as silver and palladium showed an intermediate and low degree of chemisorption (see Figure 3), the

extent to which the adsorption decreases at higher potentials may be related to the extent to which chemisorption occurs. However, more study is needed to verify this view in detail.

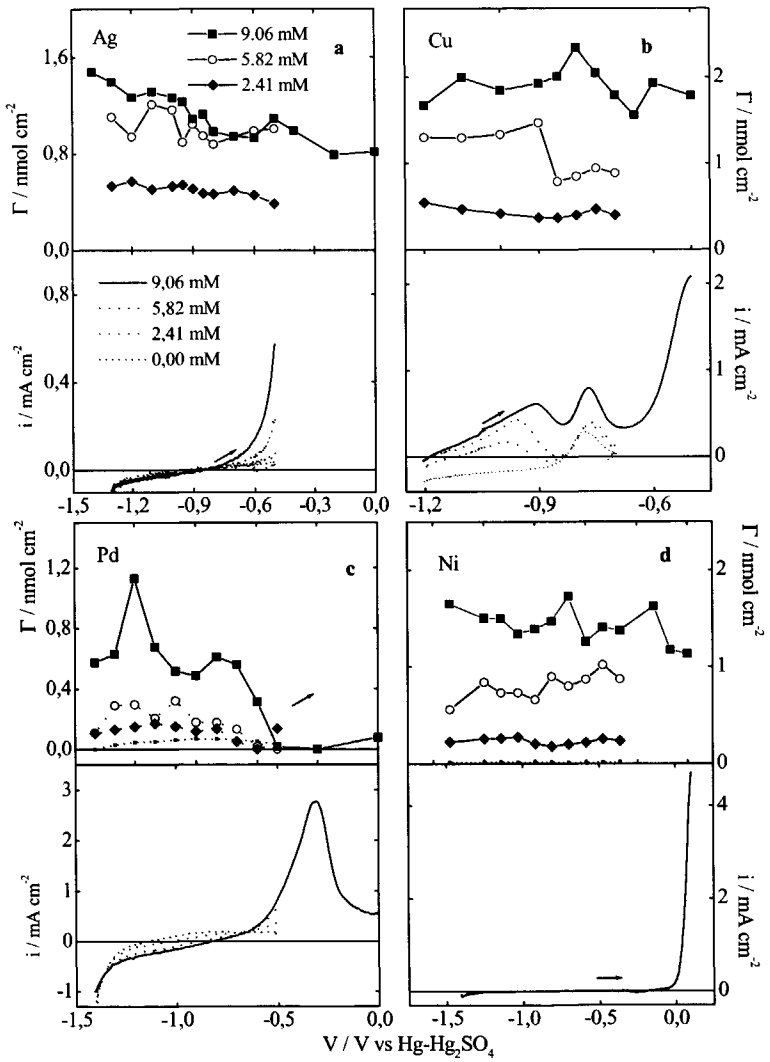

Figure 7. *Adsorption and oxidation of formaldehyde in 0.1 M NaOH at different potentials for different metals (a-d). The corresponding current densities were obtained at a scan rate of 10 mVs^{-1}*

7.8 Temperature Dependence

The influence of temperature on the adsorption of formaldehyde (10 mM) in 0.1 M NaOH under equilibrium conditions at the OCP and at 300 mV *vs.* OCP is shown in Figure 8.

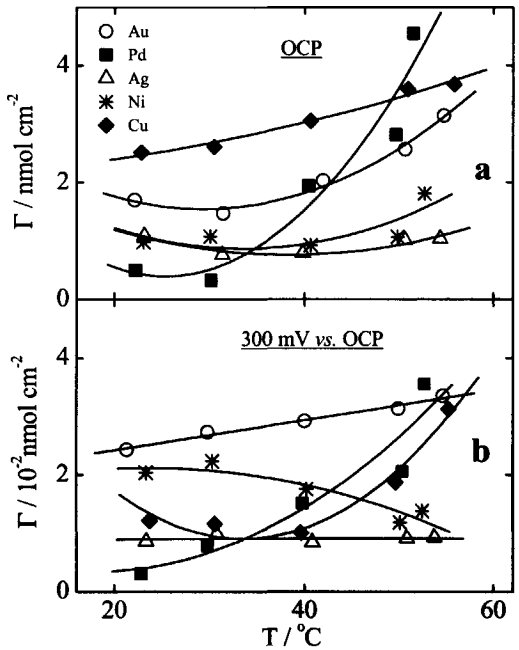

Figure 8. *Adsorption of formaldehyde at different temperatures at the OCP (a) and at 300 mV vs. OCP (b).*

In most cases, the adsorption increases at higher temperatures, suggesting that the Gibbs free adsorption energy of formaldehyde-metal systems is ruled by the enthalpy (Section 5.2.4). Exceptions on this behaviour are seen over the whole range of temperatures for nickel, and at low temperatures for gold, silver, palladium and copper. Moreover, the adsorption of formaldehyde increases much more at higher temperatures both at the OCP and at 300 mV *vs.* OCP for palladium than for the other metals. This stronger increase relative to the other metals is explained by the rate-limiting evolution of the entropy-rich hydrogen gas for this metal (KIE<1 and E_{act}< 0, *see* Section 6.2).

7.9 Volcano-type Relationships

7.9.1 General Considerations

As outlined in Chapter 1, some empirical conditions were proposed that would validate the derivation of Sabatier's principle from empirical volcano-type relationships in electrocatalysis. Briefly, recalling these conditions:

- The value of ΔH_{ad} should approach that of ΔG_{ad}.
- The values of ΔG_{ad} in the gas-phase should approach that in the liquid phase.
- The metal-dependent oxidation rate (i) should depend on ΔG_{ad} in a volcano-type fashion.
- ΔG_{ad} should correlate with the surface quantities (Q) and residence times (τ).

The results presented in Chapter 5 suggested that the first two conditions did not apply to the formaldehyde-gold system. Volcano's used to set Sabatier's prinicple for a particular system should thus better use values of ΔG_{ad} in the liquid phase than values of ΔG_{ad} in the gas-phase or values of ΔH_{ad}. The two remaining empirical conditions are discussed below.

7.9.2 Rates versus Gibbs free Adsorption Energies

To examine the presence of a 'classical' volcano-type relationship for the aqueous formaldehyde-transition metal system, the rate of the reaction at 300 mV *vs.* OCP was plotted against the values of ΔG_{ad} (Figure 9).

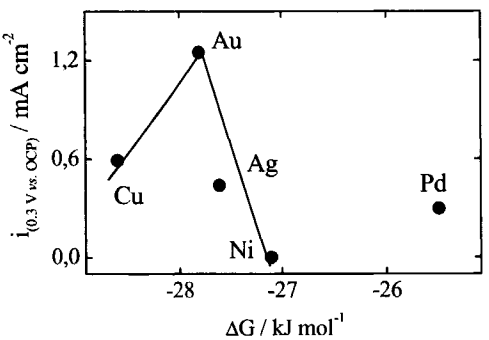

Figure 9. *Dependence of the current density on the Gibbs free adsorption energy for metal-formaldehyde systems.*

This potential was chosen, as it was sufficiently positive to register a current density sufficiently larger than zero, and as the current density likely reflected the reaction rate in the kinetic region. In addition, no single potential relative to the Hg/Hg_2SO_4 (sat. K_2SO_4) electrode existed where the oxidation of formaldehyde was seen to proceed on bare metal sites in the kinetic region for all metals studied (Figure 7). A rough volcano-type

relationship may be recognised when palladium is excluded but unfortunately, the four data points to set this view as fact is too low. The possible validity of than one volcano-type relationship would may nevertheless reduce this uncertainty (*see* below). Moreover, the statistical uncertainty of the data (relative to each other) may be expected to be relatively low, as values of ΔG_{ad} resulted from reasonable fits of four data points, and as most systematic errors do roughly have similar weight for different metals (Section 2.5.5)

7.9.3 Rates, OCP and ΔG_{ad} versus Residence Times

Rates versus Residence Times - Assuming the validity of Eyring's generally accepted picture of fixed and time-invariant potential fields with transition states being in equilibrium with thermodynamic minima, the fourth condition indirectly suggests that a plot of the metal-dependent reaction rate should depend on the average residence times of species at the surface under equilibrium conditions in a volcano-type fashion as well. A look at Figure 10a shows that this indeed seems to be the case.

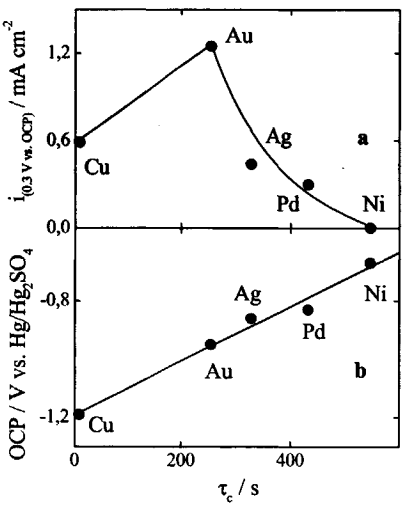

Figure 10. *Dependence of the current density on the residence time for formaldehyde-metal systems (a). Dependence of the OCP on the residence time (b).*

The volcano-type relationship thus suggests that species should remain at the surface neither too long nor too short to attain the highest catalytic activity. Remarkably, palladium is not excluded like it was in the volcano's presented in Figure 9. Different

explanations may be given for this difference: First, an error may have occurred in the determination of the surface area, which may have had consequences for the rates but not for the values of τ_c, as these were determined from the decay in the exchange kinetic curves. Second, the Langmuir assumption used to derive the values of ΔG_{ad} from the initial slopes of the adsorption isotherms may have been wrong for palladium. Third, as atomic hydrogen may not only adsorb at the surface but absorb in the bulk metal as well, the model used to determine values of τ_c may have been incomplete leading to different relative values of ΔG_{ad} and τ_c.[3,4]

OCP and ΔG_{ad} versus Residence Times - The correlation between τ_c and ΔG_{ad}, expected according to the fourth condition in Section 1.6 is further supported by the structural dependence of the OCP on τ_c (Figure 10b). As the values of τ_c depend on the metals under equilibrium conditions (they were taken from the fitted exchange transients after the settling of the equilibrium), and as they correlate linearly with the OCP for all metals studied, the value of the OCP seems determined by the time that species reside in chemisorbed state at the surface. Moreover, as the value of the OCP determines the practical occurrence of plating in electroless metal deposition, this occurrence seems related straightforwardly to the time that chemisorbed species reside at the surface (Chapter 1). Another correlation between τ_c and ΔG_{ad}, expected from the fourth condition given above refers to the dependence of τ_c on ΔG_{ad} (Figure 11).

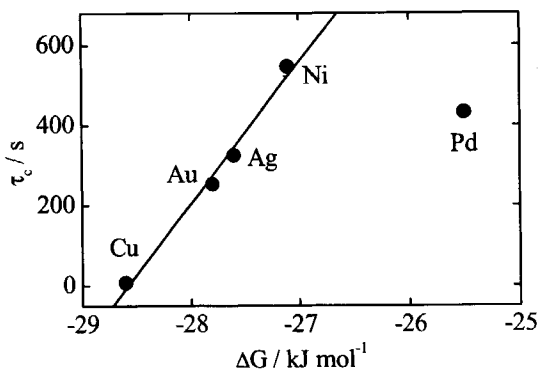

Figure 11. *Dependence of the residence times on* ΔG_{ad} for formaldehyde-metal systems.

This dependence is trivially linear since both τ_c and ΔG_{ad} were seen to depend on the OCP in an approximate linear fashion (compare Figure 6 with 10b). The relationship suggests that more strongly bound species tend to reside shorter at the surface.

7.9.4 Rates, OCP and ΔG_{ad} versus Adsorbed Quantity (Q)

Rates versus Adsorbed Quantity - As the optimum rate, expressed by i, at median adsorption energy should be related to the quantity of surface species according to Sabatier's principle, a plot of the metal-dependent oxidation rate versus the quantity adsorbed should yield a volcano-type dependence.[5,6] This behaviour indeed seems to apply, as shown in Figure 12a. It supports the validity of the fourth condition described above. The comparison of this volcano plot with those presented in Figure 9 and 10 shows nevertheless that nickel has changed from the right wing to the left one. This incidental absence of correlation between ΔG_{ad} (or τ) and Q is explained by the non-Langmuir character of the adsorption isotherm for nickel at the relatively high concentration examined (Figure 5). Chemically, the nickel surface is the only metal studied that may be oxidized in formaldehyde solutions, as its oxidation potential under these conditions is even lower than that of copper (Chapter 6, Figure 9c). Moreover, three (rough) volcano plots are reflected by Figure 9 (i *vs.* ΔG_{ad}), Figure 10a (i *vs.* τ_c) and Figure 12a (i *vs.* Q), making the volcano-type behaviour more likely for the metal-formaldehyde system in general.

OCP and ΔG_{ad} versus Adsorbed Quantity - The values of Q increase (with the exception of nickel) when the values of ΔG_{ad} decrease (Figure 12b). This observation is in line with the view that the surface coverage increases when the bond strength increases.[5,6] The relation further supports the validity of the fourth condition (stating that ΔG_{ad} should correlate structurally with Q). Moreover, the dependence of τ_c on Q shows a systematic decrease and seems to validate this condition as well (Figure 12c).

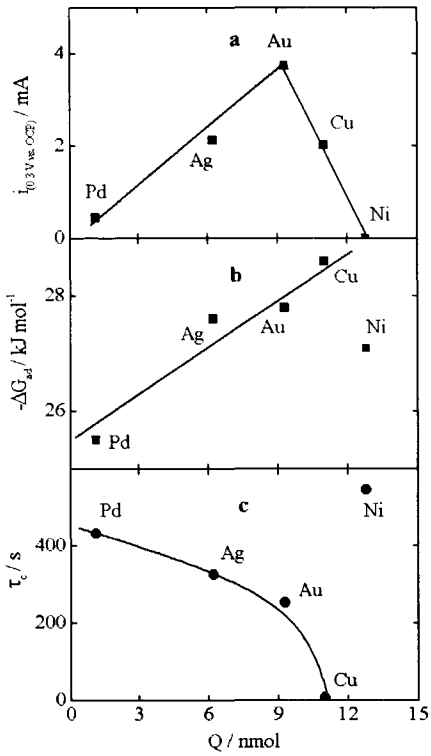

Figure 12. *Dependence of the oxidation rate on the quantity of species adsorbed at $t=\infty$ for formaldehyde-metal systems (a). Dependence of τ_c and ΔG_{ad} on the surface quantities (b and c).*

7.10 Conclusions

- The adsorption and exchange kinetics of formaldehyde on transition metals at the OCP from 0.1 M NaOH can be described by one linear four-compartment model. The model describes the adsorption and exchange process by three partial steps: a relatively slow and reversible physisorption, a relatively rapid and reversible chemisorption and an irreversible side reaction.
- The rate-limiting chemisorption step proceeds most rapidly on gold under dynamic conditions and most slowly on copper under equilibrium conditions. The value of ΔG_{ad} is lowest for copper and highest for palladium.
- Both values of ΔG_{ad} and τ_c depend on the OCP in a linear fashion under equilibrium conditions, implying that the value of the OCP is determined by the bond strength and residence time of chemisorbed species at the surface. As the OCP indirectly

determines the plate potential in electroless metal deposition processes, these values may explain the occurrence of plating on an atomic scale.

- Approximate volcano-type relationships were obtained for the dependence of the oxidation rates (expressed by i) on ΔG_{ad}, τ, and Q, supporting the validity of Sabatier's principle for the formaldehyde-metal system. The systematic dependencies of ΔG_{ad} on τ, ΔG_{ad} on Q, and τ on Q further supported this view.

7.11 References

(1) Gileadi, E.; *Electrode Kinetics*, Chapter. 2.2, VCH Publishers, New York (1993), p.10.

(2) Weast, R. C.; *CRC Handbook of Chemistry and Physics*, CRC Press Inc., 66th edition, Boca Raton, **1985**, p F-87.

(3) Enyo, M.; *J. Appl. Electrochem.*, **1985**, 15, 907.

(4) Burke, L. D.; O'Dwyer, K. J.; *Electrochim. Acta*, **1990**, 11, 1829.

(5) Moulijn, J. A.; Leeuwen, P. W. N. M.; Santen, R. A.; in *Catalysis, An Integrated Approach to Homogeneous, Heterogeneous and Industrial Catalysis*, Elsevier Science Publishers B. V., Amsterdam The Netherlands, 1993, p 83.

(6) Shriver, D. F.; Atkins P. W.; Langford, C. H.; in *Inorganic Chemistry*, Oxford University Press, 1st edition, Oxford, UK, 1990, p 542.

(7) Kortenaar, M. V.; Tessont C.; Kolar, Z. I.; Weijde, H. van der.; *J. Electrochem. Soc.*, **1999**, 14, 2146.

(8) Kortenaar, M. V.; Kolar, Z. I.; Goeij, J. J. M. de.; Frens, G.; *J. Electrochem. Soc.*, **2001**, 148, 1.

(9) Kortenaar, M. V. ten; Kolar, Z. I.; Goeij, J. J. M. de.; Frens, G.; *Langmuir*, **2002**, 18, 10279.

7.12 Appendix

The linear three-compartment model shown in Chapter 5 extended with one linear irreversible flow to a sink compartment (Figure 1) has been used for fitting the adsorption data. The following system of differential equations was used to describe the adsorption and exchange kinetic experiments:

Adsorption experiments:

The quantity at the electrode ($Q_e(t)$) is measured and comprises species in the physisorbed compartment ($Q_p(t)$), in the chemisorbed compartment ($Q_c(t)$), and in the sink compartment ($Q_i(t)$):

$$Q_e(t) = Q_p(t) + Q_C(t) + Q_i(t) \qquad (1)$$

The species adsorbed at the electrode exchange with species in the solution ($Q_s(t)$) and the mass equations for these transport processes are given by the following equations:

$$\frac{\partial Q_S(t)}{\partial t} = k_{sp} \times Q_p(t) - k_{ps} \times Q_S(t) \tag{2}$$

$$\frac{\partial Q_p(t)}{\partial t} = k_{ps} \times Q_S(t) + k_{pc} \times Q_c(t) - k_{sp} \times Q_p(t) - k_{cp} \times Q_p(t) \tag{3}$$

$$\frac{\partial Q_c(t)}{\partial t} = k_{cp} \times Q_p(t) - k_{pc} \times Q_c(t) - k_{ic} \times Q_c(t) \times \frac{Q_i(\infty) - Q_i(t)}{Q_i(\infty)} \tag{4}$$

$$\frac{\partial Q_i(t)}{\partial t} = k_{ic} \times Q_c(t) \times \frac{Q_i(\infty) - Q_i(t)}{Q_i(\infty)} \tag{5}$$

Initial values for the compartment quantities where taken as: $Q_s(0)$=100,000 nmol, $Q_p(0) = Q_i(0) = Q_c(0) = 0$.

The $Q_e(t)$ values were obtained from $\Gamma(t)_e$ by using:

$$Q_e(t) = \Gamma_e(t) \times R \times A \tag{6}$$

Where: $\Gamma_e(t)$ is the surface concentration (nmol per real cm^2), R the roughness factor (-) and A the geometrical area of the electrode (cm^2).

The rate of transfer (flow) of tracee is denoted as F [nmol s^{-1}]; F_{ps} represents the flow to the physisorbed state from the solution. Likewise F_{sp}, F_{pc}, F_{cp}, F_{ic} represent the flows to the solution from the physisorbed state, to the physisorbed state from the chemisorbed state, to the chemisorbed state from the physisorbed state, and to the irreversible sink-compartment from the chemisorbed state respectively. The rate constants are represented by k [s^{-1}]. The flows in the steady state (t=∞, Q(∞) = constant) between the compartments may be obtained from:

$$F_{ps}(\infty) = F_{sp}(\infty) = k_{ps} \times Q_S(\infty) = k_{sp} \times Q_p(\infty) \tag{7}$$

$$F_{pc}(\infty) = F_{cp}(\infty) = k_{pc} \times Q_c(\infty) = k_{cp} \times Q_p(\infty) \tag{8}$$

The flow to the sink-compartment reaches values of 0 when the value of $Q_{i,\infty}$ is attained. Equation (4) then decreases to zero.

The transition times in the compartments can be obtained from:

$$\tau_S = \frac{1}{k_{ps}} \tag{9}$$

$$\tau_p = \frac{1}{(k_{sp} + k_{cp})} \tag{10}$$

$$\tau_C = \frac{1}{k_{pc}} \tag{11}$$

Exchange experiments:

The exchange experiments are, in contrast with the adsorption experiments, initially already in steady state: $dQ_e(t)/dt = 0$. In this case, the radiotracer quantity on the electrode (q_e) was measured. The exchangeable radiotracer quantity was normalized to 1 and fitted using the following first order equations for the fractional loss of tracer from the physisorbed and chemisorbed state:

$$\frac{\partial[q_p(t)/q_e(0)]}{\partial t} = k_{ps} \times \frac{q_s(t)}{q_e(0)} + k_{pc} \times \frac{q_c(t)}{q_e(0)} - k_{sp} \times \frac{q_p(t)}{q_e(0)} - k_{cp} \times \frac{q_p(t)}{q_e(0)} \tag{10}$$

$$\frac{\partial[q_c(t)/q_e(0)]}{\partial t} = k_{cp} \times \frac{q_p(t)}{q_e(0)} - k_{pc} \times \frac{q_c(t)}{q_e(0)} \tag{11}$$

$$\frac{\partial[q_s(t)/q_e(0)]}{\partial t} = k_{sp} \times \frac{q_p(t)}{q_e(0)} - k_{ps} \times \frac{q_s(t)}{q_e(0)} \tag{12}$$

In addition, the exchangeable quantity of radio-labeled species

$$\frac{q_e(t)}{q_e(0)} = \frac{q_p(t)}{q_e(0)} + \frac{q_c(t)}{q_e(0)} \tag{13}$$

The initial values for the physisorbed and chemisorbed quantities were obtained from the adsorption experiments at infinite time using the following equations:

$$\frac{q_p(0)}{q_e(0)} = \frac{Q_p(\infty)}{Q_e(\infty)} \tag{14}$$

$$\frac{q_c(0)}{q_e(0)} = \frac{Q_c(\infty)}{Q_e(\infty)} \tag{15}$$

$$\frac{q_p(0)}{q_e(0)} + \frac{q_c(0)}{q_e(0)} = 1 \tag{16}$$

$$\frac{q_s(0)}{q_e(0)} = 0 \tag{17}$$

The system of differential equations was simultaneously solved for the four rate constants k_{sp}, k_{ps}, k_{cp} and k_{pc}.

Chapter 8

Survey of Work related to the Scope of this Thesis[*#†⊗]

The results that were considered beyond the scope of this thesis are briefly summed up. Anodic dispersion of silver wires in slightly alkaline aqueous solutions was found to yield sub-nanometre-sized silver clusters, nanometre-sized colloid and oxides. The larger colloidal particles and oxides can be removed by centrifugation, leaving small colloids and clusters in the solution. The formation of the (sub)nanometre-sized particles is explained by dissipated Joule-heat in the surface oxide layer. The formation and stability of the sub-nanometre-sized clusters (Ag_4^{2+}) were seen to depend to great extent on the pH values around pH~11. Moreover, conditions were found were silver clusters and monodisperse colloids formed spontaneously from slightly supersaturated silver salt solutions. The colloids are formed by virtue of the reducing properties of hydroxyl ions at this pH. Conditions were found where the spontaneous ion-to-metal transition occurred at surfaces and not in the solution (electroless plating). In this way, silicon structures could be selectively plated in the lowest dimensions ever reported (100 nm at an aspect ratio of 4.25). No smaller silicon structures were available but it is likely that much smaller structures can be plated in this fashion as well.

---

[*] *Journal of Physical Chemistry B.* **1999**, *103 2055.*
[#] *Galvanotechnik* **1999**, *10, 90.*
[†] *Journal of the Electrochemical Society* **2001**, *C28, 148.*
[⊗] *To be submitted to Langmuir*

8.1 Introduction

The most important results that were considered to be beyond the scope of this thesis are summed up. First, some results on the preparation of (sub)nanometre-sized silver clusters and colloids by anodic dispersion are presented together with some comments on the formation of the particles. Then, some results and underlying mechanisms are presented for the 'spontaneous' formation of silver clusters and monodisperse, nanometre-sized silver colloids from slightly supersaturated silver-salt solutions. Finally, some results are discussed on the practical use of the 'spontaneous' ion-to-metal transition in the selective nanometre-sized silver deposition on silicon chips.

8.2 Formation of long-lived Silver Clusters by Anodic Dispersion

Preparation and Characterization of Particles - As mentioned in Chapter 1, it was originally proposed to study the adsorption and exchange behaviour of radiolabelled reducing agents employed in electroless plating on transition metal colloids rather than on electrodes. As the adsorption of reducing agents on colloids prepared by chemical reduction could interfere with the adsorption of chemical agents needed to prepare the colloidal solutions, attempts were made to prepare silver colloids by the electric dispersion of silver wires. This method, practiced for the first time in 1808 by Ritter and often wrongfully referred as Bredig's method, had not been employed for decades but a slightly modified method surprisingly yielded colourless sols that turned yellow after a few days (Figure 1).[1,2] A more detailed analysis by UV-Vis spectroscopy revealed the presence of two peaks: one broad, low peak at ~415 nm, characteristic of polydisperse, nanometre-sized silver colloids, and one peak at 265 nm that remained stable for days (Figure 1).[3] The latter peak was considered to be characteristic for sub-nanometre sized Ag_4^{2+} clusters, a species that had been prepared by pulse radiolysis before but was considered unstable then, as it coalesced within microseconds.[3,4] The Ag_4^{2+} species could not be detected using microscopic techniques (AFM, TEM) although the presence of one-nanometre sized silver particles in the sols was further demonstrated by photon correlations spectroscopy and TEM (Figure 2).

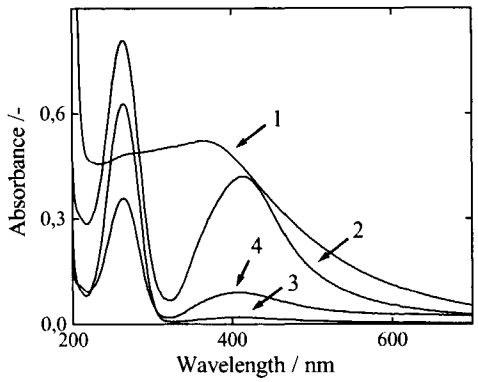

Figure 1. *Absorption spectra of a silver sol prepared in 0.5 × 10^{-3} M NaOH by polarizing 2 silver wires (diameter 2mm) at 65 V for 900 s and centrifuging in 10 ml tubes at 1100 g for 6 minutes. A peak at 265 nm appeared from the initial spectrum (spectrum 1) after 7 days (spectrum 2). The larger particles of the sol were then removed by ultracentrifugation (spectrum 3) but gradually reappeared after 21 days (spectrum 4).*

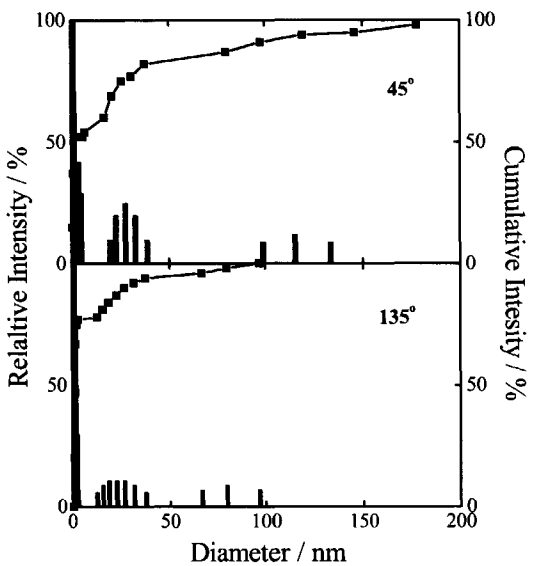

Figure 2. *Particle-size distribution obtained by photon correlation spectroscopy for light transmitted using different geometries.*

Mechanism of Sol Formation - The mechanism of formation and properties of the stable sols was further studied by measuring the heat, current and voltage transients of the dispersion process for silver and gold. The gold transients were recorded for comparison with silver, as no expulsion of particles was seen to occur on gold. The view was finally developed that Joule-heat effects play a crucial role in the expulsion kinetics and that the pH was of paramount significance in the stability of the clusters (Figure 3).[5]

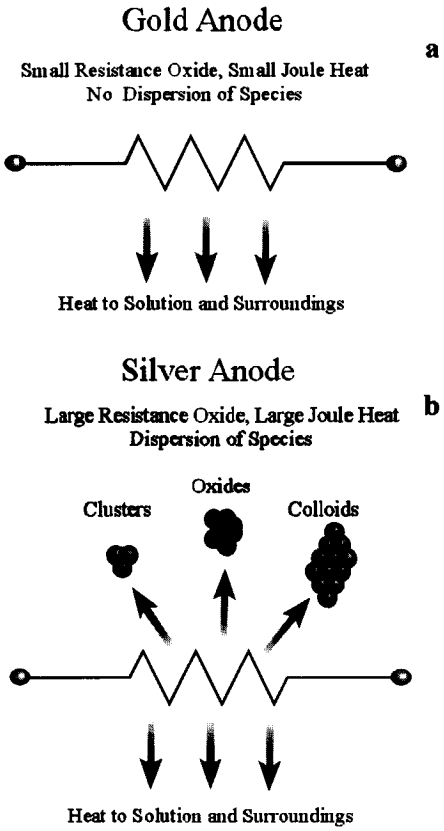

Figure 3. *Explanation for the dispersion of clusters. Contrary to silver, no highly resistant oxide forms at the gold anode and no large Joule heat is dissipated preventing particle dispersion on gold.*

8.3 Formation of Silver Clusters and Colloids from Supersaturated Aqueous Silver Salt Solutions

Formation of Particles - As the stability of the silver clusters was seen to have an optimum around pH~11 in the electric dispersion studies, a range of silver sols was prepared around this pH by other methods (chemical reduction, pulse radiolysis and photochemical reduction). Surprisingly, conditions were found where silver clusters and silver colloids formed spontaneously from slightly supersaturated and slightly heated aqueous silver salt solutions, as indicated by UV-Vis spectroscopy (Figure 4). As the solutions contained either 10^{-4} M $AgNO_3$ or 10^{-4} M $AgClO_4$ or 0.5×10^{-4} M Ag_2SO_4 (and 10^{-3} M NaOH), the identity of the salt anion was seen to be of minor significance.[6] The nuclei were seen to grow further into monodisperse ~1 nm sized colloids, as observed by TEM at higher temperature (Figure 5).

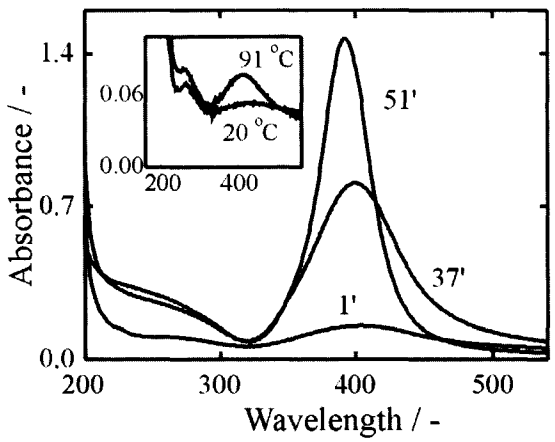

Figure 4. *UV-Vis spectrum of a solution containing 10^{-4} M $AgClO_4$ that had been alkalised in a drop-wise fashion using 0.1 M NaOH to a pH~11. The presence of a small peak at 265 nm (shown in the inset) was ascribed to the presence of $[Ag_4(OH)_2]^{2+}$ clusters. The colloidal peak at ~400 nm formed at ~90 °C (inset) and grew upon boiling the solution for different times.*

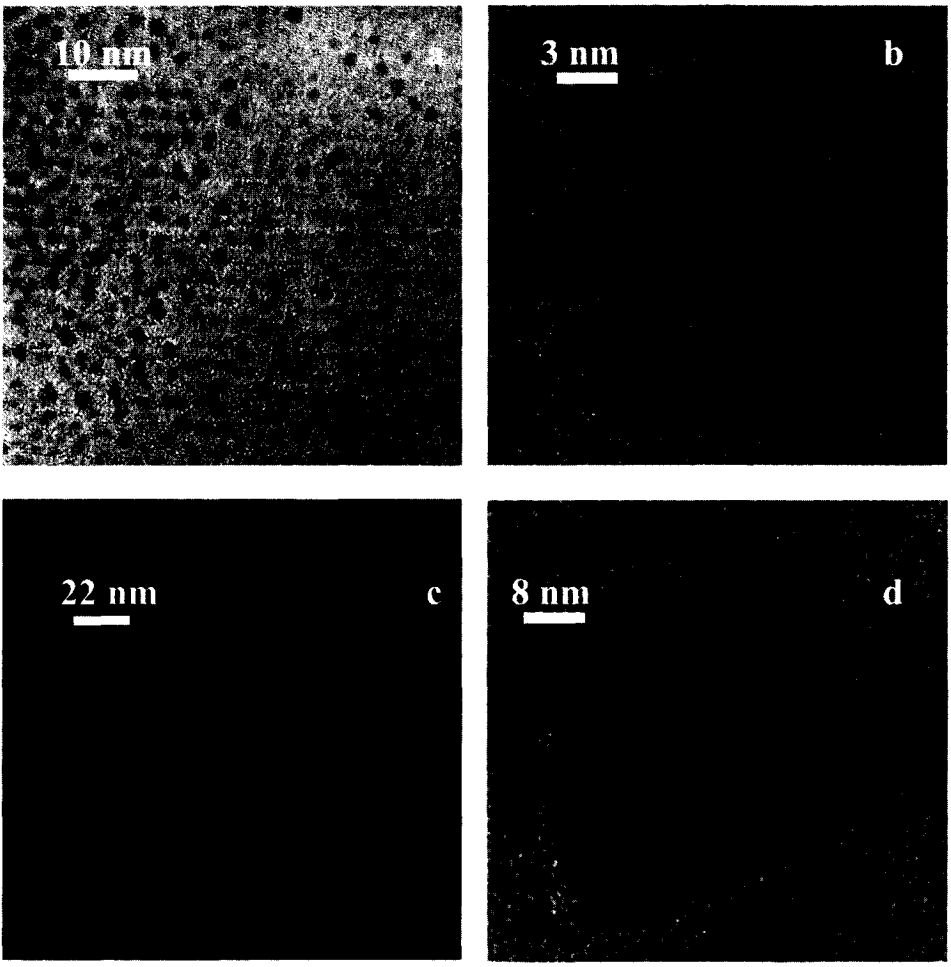

Figure 5. *TEM-micrographs showing the presence of pure, monodisperse silver colloids after boiling the supersaturated silver salt solution for 1 minute (a). A larger particle after 18 minutes of boiling showed metallic crystalline arrays of atoms (b). The sols became slightly more polydisperse at after 37 minutes (c) and some crystalline particles were observed (d).*

Mechanism of Particle Formation - The rate of formation of the colloids was seen to depend on the presence of oxygen in the solution, as bubbling with nitrogen promoted the formation of colloids. Moreover, the pH of the solution was seen to be of great significance in the formation rate and stability of the clusters and colloids. As only water

or hydroxyl ions could have served as the reducing agent in the reduction of ions, and as the Pourbaix-diagram allowed the oxygen evolution reaction to proceed in the Ag_2O area (Figure 6), the formation of metallic silver was explained by the following equations:[7]

$2\ Ag^+ + 2\ OH^- \leftrightarrow Ag_2O + 1\ H_2O$ [1]

$2\ Ag_2O + 2\ H_2O \leftrightarrow [Ag_4(OH)_2]^{2+} + 2\ OH^-$ [2]

$4\ [Ag_4(OH)_2]^{2+} + 4\ OH^- \leftrightarrow 2\ Ag_8 + 3\ O_2 + 6\ H_2O$ [3]

The further growth to metallic colloids most likely occurred by a nuclei-catalysed metal growth mechanism (electroless mechanism) with OH^- acting as reducing agent.[8] Namely, when $NaClO_4$ was added to a solution that contained clusters and a few metallic particles, no formation of (polydisperse) colloids occurred, as indicative for a coalescence-induced growth mechanism.[9] The monodisperse character of the colloids and the formation of silver crystals during the deposition of silver on silicon chips also supported this view (*see* below).

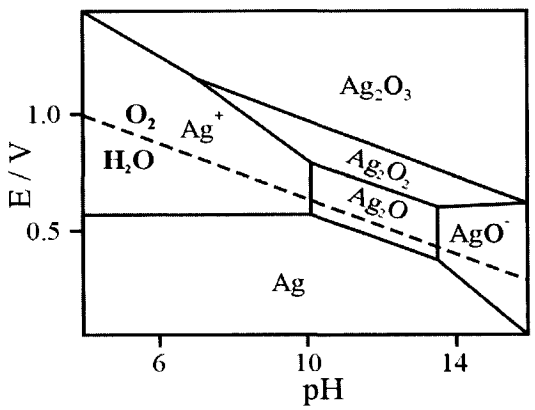

Figure 6. *Pourbaix diagram for 10^{-4} M Ag^+ in water. As the oxygen evolution reaction crosses the Ag_2O phase, the reduction of silver ions to metallic is possible thermodynamically.*

8.4 Selective Silver Deposition on Silicon in 100 nm Dimensions

Incentive - The 'spontaneous' formation of small-dimensional metallic silver in aqueous solution at about 60 °C induced a search for conditions where the reaction would proceed at a surface without occurring in solution. The use of silver in the contact plating of silicon chips offers several advantages over copper, as silver diffuses into silicon to a lesser extent than copper, as silver has the highest electric conductivity of all metals (and lowest dissipation of Joule heat), as it crystallises more easily minimizing voids in the deposited layers, and as it forms a covalent bond with silicon improving the adhesion

characteristics. A range of silicon wafers with different contact hole and line geometries down to 100 nm with an aspect ratio of 4.25 were therefore constructed. Conditions where sought where plating occurred selectively on the silicon surfaces without occurring on the SiO_2 'walls'. This would open up the possibility for a new cheap, clean, low-temperature and small-dimensional plating process.[8]

Development of the Plating Process - First, an appropriate activation procedure was developed that enabled the selective low-rate etching of oxide from the bottom of the silicon holes and lines as well as the adhesion and formation of small silver particles (Figure 7).

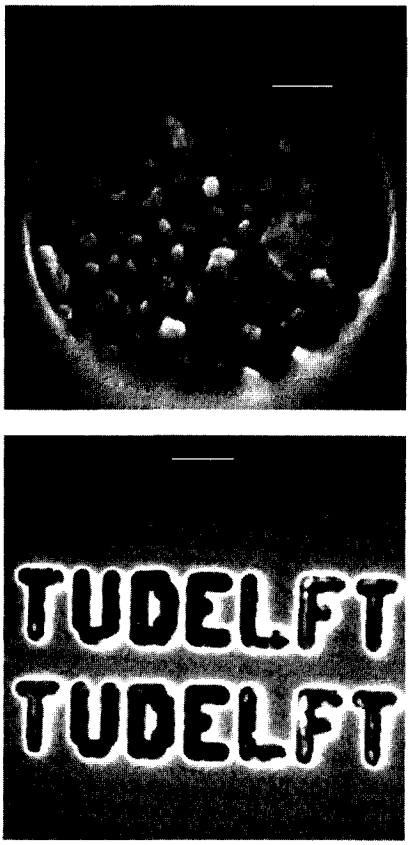

Figure 7. *SEM-micrograph of a wafer activated in a solution containing 0.25 % HF and 5.9 mM $AgNO_3$ (a). Example of a similar activation procedure for silver lines (b).*

The development of the activation step was followed by the development of the propagated metal deposition procedure. Summing up these efforts, the best results were obtained for solutions containing 0.1 M $AgClO_4$ that was brought drop wise to pH 11 by

using 0.1 M NaOH. The silver crystallites were seen to grow above the silicon surface with the smaller structures being filled more rapidly than the large ones (Figure 8).
Wet polishing using 0.25 μm diamond paste nevertheless helped to remove the overgrown crystals leading to beautiful selective silver-plated lines and holes (Figure8). The pictures (also shown on the cover of this thesis) show the selective silver deposition of 100 nm wide lines (written as characters 'TUDelft') at an aspect ratio of 4.25. These plating dimensions were the lowest ever reported for electroless metal deposition processes.[6]

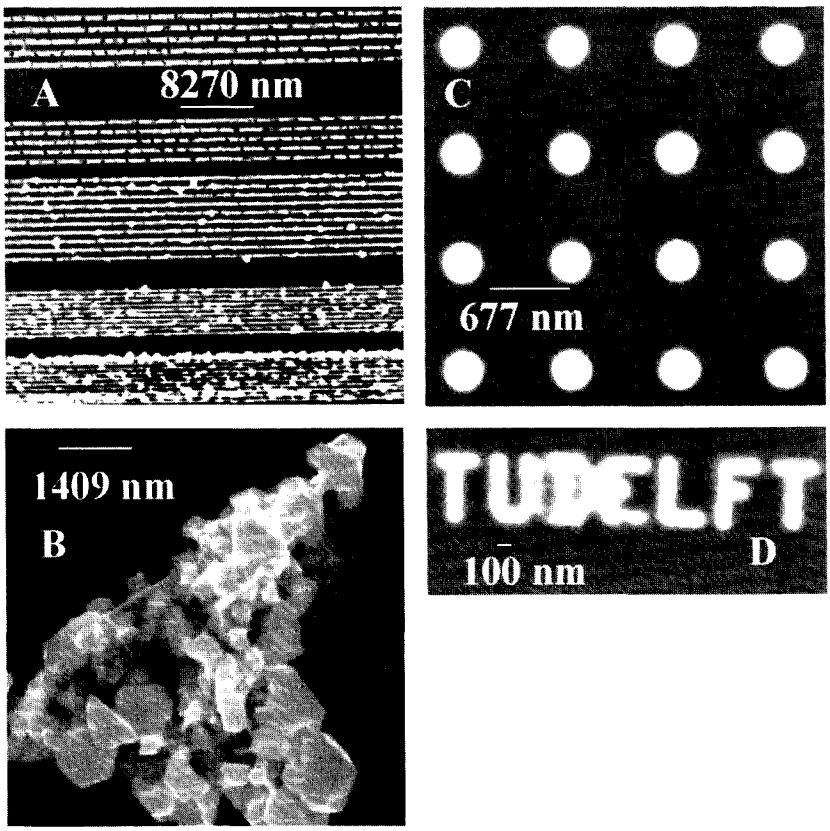

Figure 8. *(a) SEM micrograph of trenches obtained by the procedure described in Figure 7. Smaller trenches were plated more rapidly and uniformly than the broader ones. (b) The holes and trenches were sometimes overfilled with crystalline silver. (c and d) Soft polishing nevertheless yielded well filled holes and lines.*

8.5 References

(1) Ritter, J. W.; *J. Chem. Phys.*, **1808**, 5, 439.

(2) Nouhuys, H. L. in *'Het zilversol'*, PhD thesis, Utrecht University, 1938, p.15.

(3) Henglein, A.; *J. Phys. Chem.*, **1993**, 97, 5457.

(4) Mulvaney, P.; *Langmuir*, **1997**, 12, 788.

(5) Kortenaar, M. V.; Kolar, Z. I.; Tichelaar, F. D.; *J. Phys. Chem. B*, **1999**, 103, 2054.

(6) Kortenaar, M. V.; Kolar, Z. I.; Frens, G.; Lusse, P. J.; Drift, E. W. J. M. van der.; *Galvanotechnik*, **2000**, 12, 3385.

(7) Pourbaix, M.; in *Atlas of Electrochemical Equilibria in Aqueous Solution*, 2nd Ed., National Association of Corrosion Engineers, Houston, 1974, p.394.

(8) Kortenaar, M. V.; Goeij, J. J. M.; Kolar, Z. I.; Frens, G.; Lusse, P. J.; Zuiddam, M. R.; Drift, E. W. J. M. van der.; *J. Electrochem. Soc.*, **2001**, 148, C28.

(9) Hunter Hunter, R. J.; in *Introduction to Modern Colloid Science*, 1st Edition, Oxford University Press, Oxford 1993, p. 7.

Chapter 9

Final Discussions and Practical Interest

The results presented in this thesis are briefly overviewed with emphasis on the added value in relation to the existing literature, the original goals and the possible interest for practical applications. The results have shown that EIS and equivalent-circuit fitting procedures, together with DEMS and the radiotracer thin-gap technique approach are well suited to study electrocatalytic reactions under in-situ conditions. The correlation between the different methods and fitting procedures was shown to be good but complex. The EIS results have further yielded a model for the double layer structure of the system. The results have also given information on various kinetic and thermodynamic aspects of the electrocatalytic oxidation of formaldehyde on various transition metals. Conditions based on practical measurements and fitting results, were further postulated for the derivation of Sabatier's principle from volcano-type relationships in electrocatalysis. Moreover, a practical correlation between the OCP and the values of ΔG_{ad} and the residence times of adsorbed species were found, explaining electroless metal deposition on an atomic scale. Criteria for good metallic catalysts were further derived for the metal-formaldehyde system, implying that good catalytic properties arise for metals characterized by a high metal-formate formation enthalpy, a high oxidation potential, a low work function and a long average metal-metal bond length. Practically, the results may help to choose the right conditions in electroless metal deposition or help to set a springboard for the possible simulation of real plating processes. The results obtained for sub-nanometre sized silver particles and silver plating have further demonstrated a possible application in selective electroless metal deposition in nanometre dimensions. Relevant research for possible applications of these particles lay in the field of conductive coatings, catalysis, microelectronics and optics.

9.1. Introduction

The most important results presented in this thesis are briefly discussed together with an evaluation of achievements in relation to the original goals outlined in Chapter 1. The practical interest of the results is further addressed with emphasis on the added value relative to the literature and to the interest in the practical field of electrochemical methodology, electroless metal deposition, electrocatalysis, conductive coatings, microelectronics and optics. The discussion is accompanied by recommendations for future work and possible applications. The results obtained for colloidal and plated silver, as briefly summed up in Chapter 8 and described in three papers, have been included in the discussions as well.

9.2 Overview of Results

9.2.1. Derivation of the Model

The oxidation of formaldehyde on gold in alkaline, aqueous solutions was studied for the first time by EIS and equivalent circuit fitting procedures, as this method was considered to yield insight into the double-layer structure as well as of the kinetically different steps of the overall reaction. Over 50 plausible circuits were fitted but only one equivalent circuit was found that mimicked all impedance spectra measured for formaldehyde (CH_2O) and deuterated formaldehyde (CD_2O) at different pH-values and voltages. The circuit could be interpreted in terms of the mechanism presented in Section 1.6, which had been taken from the literature. Its resistors and capacitors depended on the voltage applied in a logarithmic fashion under conditions where the hydrogen evolution did not depend on the potential substantially. The logarithmic dependencies suggested that the correlated reaction steps depended on the potential and explained the absence of Tafel behaviour under steady-state conditions. The reliability of the model was relatively high, as data were Kramers Kronig transformable, and as a χ^2-value of $\sim 10^{-4}$ or less was attained in all fits.

A negative capacitance (inductive loop) was observed at low frequencies in the impedance spectra, implying a rate-limiting C-H bond rupture step in the overall kinetics of the reaction, as it was more apparent for solutions containing CD_2O than for those containing CH_2O. Moreover, four time constants were revealed by the impedance spectra at low frequencies (reflecting pseudo steady-state conditions) as a result of positive capacitive, negative capacitive, resistive and diffusive effects.

An electrostatic double-layer structure was constructed from the fitted capacitors that described the electrostatics of the system by an inner Helmhotz plane (IHP) and an outer Helmholtz plane (OHP) mediating the solution and the gold surface. The IHP was

interpreted according to the conventional picture as a layer of adsorbed, non-solvated (chemisorbed) species, the OHP as a layer of adsorbed, solvated (physisorbed) species. The capacitors C_2 and C_3 depended on the potential and therefore represented pseudo-capacitances rather than ordinary ones. They were interpreted to reflect charging processes at the OHP and IHP respectively. Moreover, R_3 was interpreted to correlate with a rate-limiting C-H bond rupture step, while R_4 was interpreted to reflect the inhibition of the reaction due to a slow desorption rate. Depending on the ratio of adsorption and desorption rates, either negative or positive capacitive behaviour was observed being reflected by positive or negative values of the corresponding resistors and capacitors. The high values of the C_{IHP} suggested the possible presence of free radicals between the IHP and the electrode surface, which may reflect chemisorption.

9.2.2. Semi-quantitative Interpretation of the Kinetic Model

The view derived by EIS was further supplemented by voltammetry and DEMS with the derivation of the respective KIE-values, the gas evolution rates, and the apparent activation energies (E_{act}) of the reaction. It was found that the H_2, D_2, and CO_2 gas evolution kinetics depended to a great extent on the pH, potential, and temperature. The rates do nevertheless play a minor role in the overall rate of the electro-oxidation reaction on gold. In addition, the evolution of hydrogen at the open-circuit potential (OCP) and the current efficiencies higher than 100% pointed towards the presence of a non-electrochemical dehydrogenation reaction parallel to the electro-oxidation reaction. This reaction was assigned as a 'spontaneous' gold-catalysed decomposition of formaldehyde into hydrogen and formate.

The values of the KIE and the E_{act} supported the view derived by EIS that the overall rate of the electro-oxidation reaction is determined by the chemisorption of the enolate anion at low potentials, by the desorption of the formate anion at higher potentials, and by diffusion at the highest potentials. The value of E_{act} ranged between -25 and 60 $kJmol^{-1}$, confirming the large influence of the solution on the value of E_{act} and the possible presence of a pre-equilibrium. Moreover, hydroxyl ions were seen to play an important role in the overall reaction rate as result of the stoichiometry and the hydroxyl-catalysed character of C-H bond rupture step.

9.2.3 Quantitative Interpretation of the Kinetic Model

The view derived by DEMS, voltammetry, chronocoulometry and EIS was further specified for the reaction on gold using the radiotracer-thin gap technique, as this method was considered to enable the straightforward monitoring of adsorbed species under *in-situ* conditions. It was found that the adsorption of formaldehyde at the OCP can be described in a serial fashion with two reversible rates of adsorption: a rapid physisorption and a

slow chemisorption. These findings were in concordance with the results obtained by EIS. The adsorption isotherms were approximately linear at concentrations below 10 mM formaldehyde. In 0.1 M NaOH, the electro-oxidation of formaldehyde is approximately first order in the concentration of formaldehyde and in the quantity of species adsorbed. The radiotracer studies further confirmed the view outlined above that the rate of the overall electro-oxidation reaction is ruled by chemisorption of the enolate anion at low potentials, by desorption of formate at medium potentials and by diffusion of reactants and products at highest potentials.

In 0.1 M NaOH, the value of ΔG_{ad} of the overall electro-oxidation reaction at the OCP and at different potentials was found to depend on the composition of the solution, implying that the solution affects the thermodynamics of the reaction substantially. Volcano-plots used to address Sabatier's principle in electrocatalysis should therefore preferably employ adsorption energies derived in the liquid phase rather than those in the gas phase. The values of ΔG_{ad} do not depend to a great extent on the potential, temperature and pH, but the value of E_{act} is strongly affected by these parameters. Moreover, as the values of ΔG_{ad} cannot be approximated by values of ΔH_{ad}, the values of ΔS_{ad} cannot be neglected. Consequently, the derivation of Sabatier's principle from volcano plots that use adsorption enthalpies rather than Gibbs free adsorption energies should be doubted.

Both the dependence of the quantity of adsorbed species on the formaldehyde concentration and the invariance of the adsorption isotherms with increasing potentials are in line with the view obtained by EIS that potential gradients on the solution side are more important in the adsorption rates of species than the potential of the electrode itself.

The various results obtained by EIS, DEMS, voltammetry and the radiotracer thin-gap technique eventually led to a quantitative kinetic and thermodynamic description for the formaldehyde electro-oxidation reaction on gold under different conditions. In this model, the enolate anion diffuses to the reaction centre, followed by reversible physisorption, the reversible chemisorption, the irreversible oxidation and desorption of reaction products (hydrogen, water and formate).

9.2.4 Influence of the Metal on the Reaction Rates

The influence of the metal on the reaction rates in 0.1 M NaOH was studied by voltammetry for CH_2O and CD_2O at different temperatures. The values of the E_{act} and those of the KIE were determined at different potentials. Au, Pt and Ir were found to catalyse the reaction to the highest rate, while Cu and Ag catalyse the reaction and at the lowest potentials. Ni and Pd did not catalyse the reaction well. At low overpotentials and

temperatures, the rate of the reaction was ruled by chemisorption of the enolate anion on Ag, Cu, Au and Ni, and by desorption of adsorbed hydrogen on Pt, Pd and Ir. At higher potentials, the reaction may become increasingly controlled by desorption of the formate anion on all metals studied. Diffusion plays an important role at higher current densities on Ag, Pd, Au and Pt, while strong capacitive current densities are seen for the reaction on Ni, Cu and Ir.

A linear relationship was obtained for the dependence of the metal-dependent reaction rate on the kinetic isotope effects (KIE), confirming the view from previous chapters that the rate-limiting step of the reaction comprises the rupture of hydrogen bonds. The rate of the hydrogen bond ruptures seem to be structurally affected by the electronic properties of the metals, as a linear relationship was obtained for the dependence of the reaction rate of the catalytically active metals on the work function. The importance of the chemical rearrangements and the electronic properties of the metals in the rate of the reaction were further indicated from the similar dependencies of the apparent activation energies (E_{act}) on both the metal-formate formation enthalpies and the oxidation potentials of the metals. Moreover, a curved relationship between E_{act} and the inter-atomic bond lengths was found, suggesting that neighbour effects of surface atoms play a role in the lowering of the transition state of the reaction. The values of E_{act} ranged roughly between –20 kJ mol^{-1} and 50 kJ mol^{-1}, and the possible presence of a (pseudo) pre-equilibrium in the reaction. The values of E_{act} were both positive and negative, confirming the catalytic properties of the metals and the view obtained for gold that a pre-equilibrium of adsorbed intermediates may form at the electrode surface.

9.2.5 Influence of the Metal on the Adsorption Characteristics

The adsorption, exchange and oxidation of formaldehyde on transition metals (Au, Ag, Cu, Ni, Pd) were examined in 0.1 M NaOH by voltammetry and the radiotracer thin-gap technique. One linear four-compartment model was found to fit to all adsorption and exchange kinetic data at the OCP, supporting the presence of three adsorption steps in the overall adsorption process: a relatively rapid and reversible physisorption, a relatively slow and reversible chemisorption and an irreversible poisoning side-reaction. The rate-limiting chemisorption was seen to proceed fastest on gold under dynamic conditions, and slowest on copper under equilibrium conditions. The Gibbs free adsorption energy, (ΔG_{ad}) derived from the initial slopes of the adsorption isotherms, was lowest for copper and highest for palladium. Moreover, the (equilibrium) values of both ΔG_{ad} and the residence times of species at the surface (τ_c) were seen to depend on the OCP in a linear fashion, suggesting that the value of the OCP is determined by the average bond strength and time species reside at the surface. Assuming the validity of the mixed-potential theory, the observation may also explain the occurrence of electroless metal deposition on an atomic

scale. Approximate volcano-type relationships were further obtained for the dependencies of the oxidation rates on the values of ΔG_{ad}, τ_c and the surface quantities (Q), supporting the validity of Sabatier's principle for the formaldehyde-metal system. This view was further supported by the systematic dependencies of ΔG_{ad} on τ_c, ΔG_{ad} on Q, and τ_c on Q. The volcano plots used to derive the principle in electrocatalysis should nevertheless use values of ΔG_{ad} rather than those of ΔH_{ad}. This view is new relative in respect to the existing literature.

9.3 Practical Interest of Results

9.3.1 Electrochemical Methodology

A considerable number of papers has been devoted in the past decades to the advantages of the transfer-function analysis of impedance spectra over equivalent-circuit approaches.[1-6] Remarkably, no study has been reported so far on the use of both methods in practice. Meanwhile, the only partially verified opinions have been frequently misconceived as facts. The two postulated principal disadvantages of the equivalent circuit approach relative to the transfer-function approach may be summed up as follows:[3]

- The equivalent-circuit does not contain information on the identity of reacting species.
- Contrary to a transfer-function analysis, the equivalent circuit approach does not enable the extraction of different kinetic steps of classical reaction mechanisms.

Despite these disadvantages, some studies have attempted to bridge both methods theoretically while others have successfully extracted practical chemical information from equivalent-circuit approaches.[5-9] A comparison of the practical data obtained using equivalent-circuit fitting with those obtained using transfer-function analysis for electrocatalytic systems has nevertheless not been reported yet. The data in this thesis enable this comparison to some extent, as both procedures were followed (compartmental analysis is a transfer-function fitting procedure). Some valuable remarks may therefore be made.

First, the EIS-results presented in this thesis have shown that the equivalent-circuit method is well suited for the derivation of the electrostatic-field picture in the electrochemical double layers under *in-situ* steady-state conditions (Chapter 3, Figure 13). The electrostatic double-layer picture describes the reaction by three pseudo-stable layers (*i.e.* solution, IHP and OHP) and turned out to be qualitatively in line with the fitted three-compartimental system for gold (Chapter 5), the mechanism proposed in literature (Section 1.3) and the explanations for the results obtained by DEMS and voltammetry (Chapter 4). Moreover, the fitted data using equivalent-circuit procedures were different for CH_2O than for CD_2O, implying the extraction of different kinetic steps of a classical

reaction mechanism and the straightforward correlation of capacitors with kinetic steps. The validity of the first disadvantage above seems therefore highly doubtful.

Second, an illustrative practical semi-quantitative comparison of the charging (adsorption) times of the IHP under steady-state conditions from $\tau_c = R_3C_4$ (R_3 was interpreted to correlate with the C-H bond rupture step, while C_4 was interpreted to reflect changes in the IHP in section 3.2.4 and 3.2.5) at the OCP with the time for radioactive species in the chemisorption state to exchange with dissolved species (OHP-IHP transition) under steady-state conditions lay in the same time order: The former amounts to ~1000 s whereas the latter amounts to ~2580 s. Presumably, the difference would have been even smaller when nitrogen had been bubbled in the electrochemical cell as well. Hence, the time constants of the fitted pseudo-capacitors lay in the same order as those of the practical adsorption measurements. The results therefore support the view that equivalent-circuit procedures may help to extract information on different kinetic steps of a classical reaction mechanism. This view contradicts the second disadvantage above.

Third, an attempt was made to derive the partial impedances belonging to the slow reaction steps of the mechanism outlined in Chapter 1 (Section 9.6). The formulae were seen to have a highly complex character but straightforward physical equations could be derived for each transition, *i.e.* for the transport of species from the solution to the OHP, between the OHP and IHP as well as for the transport of charge to the electrode across the double layer. The reliability of this approach, characterised by many unknown fitting variables, highly complex formulae and the necessary choices for mechanisms prior to the fitting procedures is certainly lower than the iterative equivalent-circuit approach followed in Chapter 3. It is therefore recommended to commence a detailed EIS study by the iterative, relatively easy and rapid, equivalent-circuit procedure. The view derived from these studies may set simplifying assumptions for a transfer-function analysis. The derived formulae further show that the physical impedances (elements) can be coupled to the partial reaction steps of the reaction mechanism. The postulated disadvantages seem therefore doubtful.

9.3.2 Electroless Metal Deposition

The possible practical interests of results presented in this thesis in the practical field of electroless metal deposition refer to the following issues:

- Electroless silver deposition.
- Choice of metals upon the use of formaldehyde as reducing agent.
- Practical control of plate processes using simulations.

The electroless plating of silver is characterized by limitations related to bath stability and the related necessary use of the hazardous cyanide as complexing agent (Section 1.2). The findings summed up in Chapter 8 and presented in more detail in ref. 10 have set a

completely different base of silver plating. Namely, conditions were found were silver ions were seen to transfer 'spontaneously' into metallic silver. No reducing agent and no complexing agent have to be used, as hydroxyl-oxygen reaction supplies the electrons to reduce the silver ions. A disadvantage for bulk plating is still that plating rates were low, although the usefulness of this process for microelectronic applications was already demonstrated in Chapter 8. Moreover, it is to be noted that the monodisperse, nanometre-sized silver particles may be used as initiating seeds for the plating of other metals on (non)conductive, non-catalytic substrates (*e.g.* plastic). The use of these seeds in plating of chips was already demonstrated (Chapter 8). The electro-spraying of ionic silver solutions (*e.g.* 10^{-4} M $AgNO_3$, pH 11) on hot substrates might, for instance, lead to the formation of monodisperse, adherent, nanometre-sized particles that induce plate processes with smooth morphologies.

Electroless metal deposition is a key, but highly empiric, technology in metal plating with highest business credits for copper and nickel (Section 1.6). Other metals are also continuously under study for new applications facing choices with respect to the reducing agent and its associated concentration, temperature and pH of operation. From Chapter 1, 4 and 6, it may be certainly understood that electroless processes aiming to deposit a metal on a surface from alkaline solutions using formaldehyde should focus on gold, iridium, platinum, silver and copper rather than on palladium and nickel. In addition, many ideas concerning the right empirical conditions may be obtained from the presented oxidation rates and dependencies of these rates on pH, concentration, and temperature.

As mentioned, the practical control of metal deposition processes using simulations has remained beyond reach for plating companies. The results presented in this thesis have shown that the kinetics of the anodic reaction can be described in terms of the slow kinetic steps of the mechanism outlined in Section 1.6, *i.e.* diffusion, chemisorption and desorption. Incorporation of the reduction and deposition of metal ions in this picture may set a springboard for relevant kinetic descriptions, predictions and simulations. The approach will be facilitated using the mixed-potential theory (Chapter 1).

9.3.3 Electrocatalysis

Sabatier's principle - Conditions were derived for the applicability of Sabatier's principle from volcano-type relationship in electrocatalysis, as mainly discussed in Chapter 1 and 7 The original view related to Sabatier's principle in electrocatalysis was briefly outlined in Chapter 1, suggesting that little is known about the validity to derive the principle from volcano-type relationships that use ΔH_{ad}. The conditions to allow this derivation were fourfold with the first two conditions being related to the disputable approximation of

ΔG_{ad} by ΔH_{ad} and the neglecting of solution effects. It was found in Chapter 5 that these two conditions did not apply to the formaldehyde-metal system, *i.e.* ΔG_{ad} obtained in the solution should be used rather than any other value of the adsorption or formation energy. The two latter conditions to validate Sabatier's principle for the metal-formaldehyde system referred to the necessary presence of an empirical volcano-type relationship between i and ΔG_{ad} and a necessary correlation between Q, τ_c and ΔG_{ad}. Both conditions were fulfilled for the metal-formaldehyde system.

Physical properties of metals - It was shown in Chapter 6 that the metal affects the electro-oxidation rate to great extent. Criteria for good metallic catalysts were related to the work functions, to the inter-atomic bond lengths, to the metal-formate formation enthalpies as well as to the oxidation potential.

Explanation of the OCP – It was found in Chapter 7 that the value of the OCP correlates with τ_c and ΔG_{ad} in a straightforward fashion. Reasonably assuming the minor importance of the spontaneous side-reaction in 0.1 M NaOH, the absence of oxygen evolution and reduction at the interface, this observation suggested that the value of the OCP is related to the average bond strength and to the time that species reside at the surface. Assuming the validity of the mixed-potential theory, this observation may also explain the occurrence of electroless metal deposition on an atomic scale.

Reaction Kinetics - The rate of the reaction can be ruled under kinetic conditions by any reaction step that proceeds at the IHP. Practically, these steps concern the chemisorption reactants and the desorption of products (Chapter 3-7). Kinetically, the oxidation rate should therefore be conceived as a chemical process rather than as an electrochemical one (the transfer of electrons do nevertheless occur). Moreover, an inhibiting effect was identified in the reaction that may cause the accumulation of charge in the IHP upon changing the potential. The inhibiting effect was related to relatively slow desorption rates and correlated with the observed negative apparent activation energies.

General - The elucidation of the kinetic and thermodynamic aspects of the formaldehyde oxidation reaction may help to elucidate problems in the (electro)catalytic oxidation of other organic molecules. The oxidation of methanol closely related in structure to formaldehyde is relevant in the development of fuel cells with practical problems referring to poisoning effects. The irreversible adsorption or pre-equilibrium effects have been discussed extensively throughout this thesis. The view that solution effects seem more important in the adsorption of species or that capacitive effects are important in the kinetics of the reaction seems relevant as well. The results further suggest that, contrary to heterogeneous catalysis, entropy effects play a non-negligible role in the adsorption equilibriums in electrocatalysis.

9.3.4 Microelectronics

The possible practical interests of results presented in this thesis in the practical field of microelectronics refer to a new, cheap, environmental-friendly and facile process to plate contact holes and contact lines in silicon chips selectively in dimensions as low as 100 nm at an aspect ratio of 4.25. Much lower dimensions and higher aspect ratios using this method seem possible too, as plating was seen to proceed more easily in the smaller dimensions, and as monodisperse metallic one-nanometre-sized particles were obtained by the heating method. At this stage, plating in microelectronics is usually attained by physical vapour deposition or by electrolytic methods using aluminium alloys or copper. The use of silver may offer some significant improvements, as silver is the best conducting metal, as it suffers less from diffusion into silicon than copper, and as its bond strength with silicon is superior to that of copper (Chapter 8).

9.3.5 Conductive Coatings, Catalysis and Optics

The production of conductive coatings finds widely use in a number of chemical companies. Generally, polymers are mixed in a process-specific fashion with high quantities of metal particles to attain the right conductive properties. The use of ionic, supersaturated, aqueous silver solutions at pH 11 in these mixtures might yield conductive coatings upon heating or irradiation. The small size of the particles and the absence of harmful chemical reducing agents in the solution may warrant homogenized, environmental-friendly coatings.

Silver particles have been investigated as catalysts for the oxidation of formaldehyde in the gas-phase. The relatively pure and monodisperse nanometre-sized colloids may be spray-dried to yield extremely small monodisperse particles with interesting catalytic properties. The properties of the sub-nanosized particles were seen to be different than the nanometre-sized equivalents, most likely due to confined surface plasmon excitations.[12] The isolation of the clusters may also lead to interesting catalytic properties. The confined surface plasmon excitations result in light absorption characteristics different than from the larger particles with a shift of the peak from the visible region to the invisible region. Irradiation or small changes of the local potential might lead to shifts in colour, a phenomenon that might induce the search for new applications in the field of opto-electronics.[13]

9.4 Summary

- The approach to meet the goals and for the original research was shown to be inadequate, but improved approaches and goals were set and the redefined scope presented in Chapter 1 was met reasonably well.
- The results presented in this thesis have shown the added value of EIS using equivalent-circuit procedures together with DEMS and the radiotracer thin-gap technique in the study of electrocatalytic reactions under *in-situ* conditions. The correlation between the different methods and fitting procedures has been demonstrated to be good but complex.
- The results have further elucidated various kinetic and thermodynamic aspects of the electrocatalytic oxidation of formaldehyde on seven transition metals.
- Conditions, based on results for the metal-formaldehyde 'electrocatalytic model system' obtained by a range of experimental methods and theoretical fitting procedures, were postulated for the validation of Sabatier's principle from volcano-type relationships in the electrocatalysis.
- Criteria for good metallic catalysts were derived for the metal-formaldehyde system, implying that good catalytic properties arise for metals characterized by a high metal-formate formation enthalpy, a high oxidation potential, a low work function and a long average metal-metal bond length.
- A completely new silver-plating process was developed that enabled the selective, cheap, environmental-friendly and facile plating of silicon structures in the lowest dimensions ever reported (100 nm at an aspect ratio of 4.25). The metal is formed by virtue of the reducing properties of hydroxyl ions around pH 11.
- A completely new method was found to prepare long-lived, pure subnanometre-sized silver clusters and pure, monodispere nanometre-sized colloids.
- Practically, the results may have relevance in the field of electroless metal deposition, electrocatalysis, conductive coatings, electrochemical methodology, microelectronics, catalysis and optics.

9.5 References

(1) MacDonald, in *Impedance Spectroscopy*, Chapter 4, John Wiley & Sons, New York (1987)

(2) Gabrielli, C.; In *Identification of Electrochemical Processes by Frequency Response Analysis*, Monograph by the Solartron Instrumentation Group, Chapter 1, MorrisBros Ltd., England (1980).

(3) Gabrielli, C.; Keddam, M.; *Electrochimica Acta*, **1996**, 41, 957.

(4) Gimenez, I.; Diard, J. P.; Le Gorrec, B.; Maximovitch, S.; *Electrochim. Acta*, **1988**, 33, 137.
(5) Bai, L.; Conway, B. E.; *Electrochim. Acta*, **1993**, 38, 1803.
(6) Bai, L.; Conway, B. E.; *J. Electrochem. Soc.* **1991**, 138, 2897.
(7) Taylor, S. R.;Gileadi, E.,; *Corrosion Science,* **1995**, 51, 664
(8) Kroloikowski, A.; Butkiewicz, P.; , *Electrochim. Acta*, **1993**, 38, 1979
(9) Kouwe, E. T.; *Electrochim. Acta*, **1993**, 38, 2093.
(10) Kortenaar, M. V. ten; Kolar, Z. I.; Frens, G.; Lusse, P. J.; Drift, E. W. J. M.; *Galvanotechnik* **1999**, 10, 90.
(11) Gileadi, E.; *Electrode Kinetics*, Chapter. 2.2, VCH Publishers, New York (1993).
(12) Henglein, A.; *J. Phys. Chem.*, **1993**, 97, 5457.
(13) Mulvaney, P.; *Langmuir*, **1997**, 12, 788.

9.6 Appendix: Derivation of Transfer Functions

9.6.1 General Considerations

As mentioned, the results presented in this thesis could be well interpreted using the mechanism outlined in Section 1.6. An equation for the overall impedance of the oxidation of formaldehyde on gold may be obtained taking into account that three steps were seen to be of major importance in the overall reaction kinetics:[4]

$CH_2OHO^- \leftrightarrow CH_2OHO^-_{OHP}$ *(Diffusion)*

$CH_2OHO^-_{OHP} \leftrightarrow {}^{\bullet}CHOHO^-_{IHP} + {}^{\bullet}H_{IHP}$ *(Chemisorption)*

${}^{\bullet}CHOHO^-_{IHP} + OH^- \rightarrow HCOO^- + H_2O + e^-$ *(Oxidation, Desorption)*

The overall impedance is given by:

$$Z_{tot}(\omega)=\frac{V}{I_f} \tag{1}$$

Where, ω represents the frequency [s^{-1}] and I_f the faraday current [A]. The overall impedance comprises three partial impedances that arise from species traversing the OHP and the IHP as well as from charge being transferred across the double layer:

$$Z_{OHP}(\omega)=\frac{C_s}{I_f} \tag{2}$$

$$Z_{IHP}(\omega)=\frac{\theta}{I_f} \tag{3}$$

$$Z_{DL}(\omega)=\frac{\eta}{I_f} \tag{4}$$

$$Z_{tot}(\omega)=Z_{IHP}(\omega)+Z_{OHP}(\omega)+Z_{DL}(\omega) \quad (5)$$

Where: C_s reflects the concentration at the surface [mol m^{-3}], η_{ss} the overpotential [V] and θ the normalized surface coverage, ranging between 0 and 1 [-]. The derivation of the faraday current and the partial impedances in terms of rate constants may be obtained by considering the rate equations for each step, and by realizing that electrons are released in the oxidation step.

9.6.2 Derivation of the Faraday Current

Assuming first order reaction kinetics, a constant hydroxyl concentration at the interface, and linear concentration gradients, the rate equations for each partial reaction step may be written as:

$$r_{dif}=\frac{D(C_b-C_s)}{\delta} \quad (6)$$

$$r_{chem}=\Gamma C_s k_c(1-\theta) \quad (7)$$

$$r_{des}=\Gamma k_d\theta \quad (8)$$

Where: D, C_b, C_s Γ, δ, k_c and k_d, reflect the diffusion constant [m^2 s^{-1}], the bulk concentration [mol m^{-3}], the concentration at the surface [mol m^{-3}], a geometric conversion factor [m], the diffusion layer thickness [m], the adsorption rate constant [s-1] and the desorption rate constant [s^{-1}] respectively.

As electrons are released in the oxidation step, the faraday current may be written as:

$$I_f=Fr_d=\Gamma k_d\theta=\Gamma k_d^0\theta\exp\left(-\frac{\alpha F\eta}{RT}\right) \quad (9)$$

Where α, η, R, F and T reflect the symmetry coefficient amounting to ~0.5 [-], the overpotential relative to the OCP [V], the natural gas constant [J mol^{-1} K^{-1}], F the Faraday constant [C mol^{-1}] and the temperature [K].

The mass balances for the quantities of species adsorbed are given by:

$$\frac{\partial C_s}{\partial t}=r_{dif}-r_{chem}=\frac{D(C_b-C_s)}{\delta}-\Gamma C_s k_c(1-\theta) \quad (10)$$

$$\frac{\partial\theta}{\partial t}=r_{chem}-r_{des}=\Gamma C_s k_c(1-\theta)-\Gamma k_d\theta \quad (11)$$

When the reaction proceeds in the steady state, the quantities in the IHP and OHP may be assumed constant:

$$\frac{\partial C_{OHP}}{\partial t}=0 \quad (12)$$

$$\frac{\partial\theta}{\partial t}=0 \tag{13}$$

The mass balance in Equation (11) may then be rewritten as:

$$\theta=\frac{\Gamma C_s k_c}{\Gamma C_s k_c + k_d} \tag{14}$$

Equation (10) and (11) can be combined with Equation (14) when the steady-state condition applies:

$$\frac{D(C_b - C_s)}{\delta}=\frac{\Gamma C_s k_c k_d}{\Gamma C_s k_c + k_d} \tag{15}$$

The extraction of C_s from this equation goes along with the solving of a square equation using the ABC-formula. The positive solution is:

$$C_s=\frac{C_b Dk_c - Dk_d + \delta k_c k_d - \sqrt{[4C_b D^2 k_c k_d + (-(C_b Dk_c) + Dk_d - \delta k_c k_d)^2]}}{2Dk_c} \tag{16}$$

An expression for the faraday current may obtained by combining Equation (9) and (14):

$$I_f=\frac{\Gamma k_d C_s k_c}{\Gamma C_s k_c + k_d}=\frac{\Gamma k_d^0 C_s k_c}{\Gamma C_s k_c + k_d}\exp\left(-\frac{\alpha F\eta}{RT}\right) \tag{17}$$

The surface concentration in this equation may be rewritten in terms of rate constants using the solution in Equation (16):

$$I_f=\frac{\Gamma k_d k_c\left\{\dfrac{C_b Dk_c - Dk_d + \delta k_c k_d - \sqrt{[4C_b D^2 k_c k_d + (-(C_b Dk_c) + Dk_d - \delta k_c k_d)^2]}}{2Dk_c}\right\}}{\Gamma\left\{\dfrac{C_b Dk_c - Dk_d + \delta k_c k_d - \sqrt{[4C_b D^2 k_c k_d + (-(C_b Dk_c) + Dk_d - \delta k_c k_d)^2]}}{2Dk_c}\right\}k_c + k_d} \tag{18}$$

The right-wing exponential term in Equation (15) reflects the classical equation for a rate-limiting electron transfer step, as described by Butler-Volmer. The pre-exponential term contains the rate constants associated with the chemisorption and desorption steps. Each constant (except k^0_d) contains an exponential term as well according to:

$$k=k^0\exp\left(-\frac{\alpha F\eta}{RT}\right) \tag{19}$$

These exponential dependencies may be in line with the unravelling of the overall impedance into different exponential dependencies using the electrical equivalent circuit,

as discussed in Chapter 3. Unfortunately, there was no time left to verify this observation in detail. Some unpublished attempts to fit the faradic current using Equation (18) nevertheless yielded satisfactory results.

9.6.3 Derivation of the Overall Impedance of the Reaction

The analysis of Equation (15) shows that the Faraday current is a direct function of the potential (incorporated in k as η), the surface coverage (θ) and the surface concentration (C_s). The general expression for the overall impedance and that of the Faraday response using a linearly approximated perturbation in a Taylor series, cut after the first term is given by:

$$Z_{tot}(\omega)=\frac{V}{I_f} \tag{20}$$

$$\Delta I_f=\frac{\partial I}{\partial V}\Delta V+\frac{\partial I}{\partial \theta}\Delta\theta+\frac{\partial I}{\partial C_S}\Delta C_S \tag{21}$$

A combination of these two equations yields:

$$Z_{tot}(\omega)=\frac{1}{\frac{\partial I}{\partial V}}-\frac{\left(\frac{\partial I}{\partial \theta}\right)\Delta\theta}{\left(\frac{\partial I}{\partial V}\right)\Delta I_f}-\frac{\left(\frac{\partial I}{\partial C_S}\right)\Delta C_S}{\left(\frac{\partial I}{\partial V}\right)\Delta I_f} \tag{22}$$

The differentials ($\partial I/\partial V$ etc.) can be determined by differentiating Equation (17) with respect to the voltage, the surface coverage and the surface concentration respectively. The derivation of the (linear) partial impedances expressed in Equation (2)-(4) was attained with the aid of a computer program, 'Mathematica'. First, the three differentiated equations were transformed into the Laplace plane using Kramer's rule.

$$E(p)C_S=fV-bC_S+g\theta \tag{23}$$

$$p\theta=aV+bC_S+c\theta+d\theta \tag{24}$$

$$I_f=eFV+dF\theta \tag{25}$$

With the characters referring to the abbreviations listed below:

$$a=\frac{\alpha F}{RT}k_cC_s\theta+\frac{\alpha F}{RT}k_d\theta \tag{26}$$

$$b=k_c\theta \tag{27}$$

$$c=k_cC_s \tag{28}$$

$$d=k_d \tag{29}$$

$$e=\frac{\alpha F k_d \theta}{RT} \tag{30}$$

$$f=\frac{\alpha F k_c \theta}{RT} \tag{31}$$

$$g=k_c \tag{32}$$

The three solutions were re-transformed and reorganized to yield the three searched partial impedances:

$$Z_{DL}(\omega)=\frac{\Delta C_s}{\Delta I_f}=\frac{1}{eh}+dk \tag{33}$$

$$Z_{IHP}(\omega)=\frac{\Delta \theta}{\Delta I_f}=k \tag{34}$$

$$Z_{OHP}(\omega)=\frac{\Delta \eta}{\Delta I_f}=\left(\frac{a}{beh}\right)-\left(\frac{ck}{b}\right)+\left(\frac{k}{beh}\right) \tag{35}$$

Where:

$$h=\left(\frac{D}{\delta}\right)\left(\frac{j\omega\delta^2}{D}\right)^{0.5}\coth\left(\frac{j\omega\delta^2}{D}\right)^{0.5} \tag{36}$$

$$k=\frac{(befh-aeh(-b-i))}{\left[b\left[-(bdefh^2)+be^2gh^2+ce^2h^2(-b-i)-eh(-b-i)(-(adh)+eh(d-p))\right]\right]} \tag{37}$$

9.6.4 Coupling of Physical Elements with Calculated Impedances

The general impedance in the complex vector representation is given by: [11]

$$Z(\omega)=\mathrm{Re}\,Z-j\,\mathrm{Im}\,Z \tag{38}$$

Where j represents the complex number ($j^2 = -1$) A real part of the overall impedance is independent of the applied frequency while the imaginary is frequency variable. A coupling may therfore be attained by aiming the seperation of frequency-variable and frequency-invariable contributions to the overall impedance, both in the transfer functions for the partial impedances as well as in the physical sub-circuits of the reaction. The latter may be derived by considering the impedances of a pure resistor and a pure capacitor.

$$Z_R=R \tag{39}$$

$$Z_C=\frac{1}{j\omega C} \tag{40}$$

The equivalent sub-circuit for processes proceeding in the IHP was considered to be reflected by ($R_3(C_3R_4)$), and the sub-circuit for processes proceeding in the OHP by (R_2C_2) as discussed in Chapter 3. The separated equations for these sub-circuits are given by:

$$Z_{OHP}(\omega)=\left(\frac{1}{R_2}\right)+(j\omega C_2) \tag{41}$$

$$Z_{IHP}(\omega)=\left(R_3+\frac{1}{R_4}\right)+(j\omega C_3) \tag{42}$$

If the overall transfer of charge across the double layer is reasonably represented by (Chapter 3): ($C_1((R_2C_2)R_3(R_4C_3)$. The partial impedance of $Z_{DL}(\omega)$ may be derived:

$$Z_{DL}(\omega)=\frac{1}{Z_1}+\left[\frac{1}{(Z_{OHP}(\omega)+Z_{IHP}(\omega)}\right] \tag{43}$$

This equation may be written as:

$$Z_{DL}(\omega)=j\omega C_1+\left[\frac{1}{R_3+R_2^{-1}+R_4^{-1}+j\omega(C_2+C_3)}\right] \tag{44}$$

The Equation (33)-(35) may be compared with Equation (41), (42) and (45) to yield equations for the elements in terms of rate constants. It should thereby be taken into account that only θ and C_s may be assumed to reflect frequency-variable quantities (and should therefore be incorporated in the capacitive terms). Unfortunately, there was no time left to come to this coupling in detail.

Samenvatting

Achtergrond - De oxidatie van formaldehyde aan overgangsmetalen is een reactie die een belangrijke rol speelt in de snelheid en selectiviteit waarmee metalen chemisch kunnen worden gedeponeerd vanuit een vloeistof op een oppervlak. De elektronen die benodigd zijn om de metaalionen te reduceren worden niet geleverd door een uitwendige spanningsbron, maar door een reductor zoals formaldehyde. Voorwaarde voor het opstarten van de reactie is dat het oppervlak de reactie katalyseert ten opzichte van de reactie in de oplossing. De depositie verloopt na het deponeren van een eerste atomaire laag metaalatomen autokatalytisch wanneer het gedeponeerde metaal de reactie eveneens katalyseert. Het proces wordt o.a. toegepast bij het vernikkelen van uitlaatpijpen of het verkoperen van printplaten in de micro-elektronica. De foto op de voorkant van dit proefschrift laat een voorbeeld zien van het kleinste, selectieve, chemische depositieproces op microchips dat tot nu toe werd ontwikkeld tijdens het promotieonderzoek dat voorafging aan dit proefschrift.

Praktische motivatie - Het belangrijkste probleem in de ontwikkeling van chemische metaaldepositie voor een bepaalde toepassing schuilt in het gegeven dat vaak veel praktisch werk nodig is om een optimale depositiesnelheid en selectiviteit te bereiken. Het onderzoek beschreven in dit proefschrift werd o.a. opgestart om tot een snellere inschatting van de optimale reactiecondities voor dergelijke depositieprocessen te komen.

Wetenschappelijke motivatie - De snelheid waarmee een molecuul aan een katalysator reageert wordt vaak gekenmerkt door een optimum (een zogenaamde vulkaan-relatie) bij een bepaalde bindingsenthalpie van de reactant aan de katalysator. Vaak wordt uit dit gedrag geconcludeerd dat er dan ook een optimale bindingssterkte, een optimale bedekkingsgraad en een optimale verblijfstijd van de reactant aan het katalytische oppervlak bestaan. Deze interpretatie staat bekend als het principe van Sabatier en is sinds 1912 veelvuldig getoetst in de heterogene gas-vaste-stof katalyse. In de vloeistof-vaste-stof katalyse, waarbij eveneens een spanning wordt aangelegd op de katalysator (elektrokatalyse), is de geldigheid om het principe af te leiden uit de relaties van snelheid en adsorptie-enthalpie echter nooit getoetst. Zo is het bijvoorbeeld de vraag of de adsorptie-enthalpie wel geschikt is voor het afleiden van het principe omdat er mogelijk voorbij wordt gegaan aan de invloed van de entropie. Daarnaast worden in het afleiden van het principe de adsorptie-enthalpieën doorgaans benaderd door adsorptie-enthalpieën uit gasfase studies of door vormingsenthalpieën. Hierbij wordt mogelijk voorbij gegaan aan de invloed van de oplossing op de adsorptie-enthalpie. Een andere discutabele aanname ligt verscholen in het gegeven dat een optimale adsorptie-enthalpie praktisch helemaal geen optimale hoeveelheid, optimale verblijfstijd of optimale bindingssterkte van de reactanten aan het oppervlak behoeft te vertegenwoordigen. Het onderzoek

beschreven in dit proefschrift werd opgestart om deze aannamen praktisch te verifiëren.

Technieken - De belangrijkste reden voor de afwezige wetenschappelijke rechtvaardiging om het principe van Sabatier af te leiden uit 'adsorptie-enthalpie- reactiesnelheid-vulkaan' grafieken in de elektrokatalyse vloeit voort uit het feit dat bindingsenergieën, verblijfstijden en bedekkingsgraden moeilijk met conventionele spectroscopische en elektrochemische technieken gedurende de reactie kunnen worden gemeten. Om deze redenen zijn voor het onderzoek enkele minder conventionele methoden gebruikt, te weten impedantiespectroscopie en de zogenaamde radiochemische dunne-laag techniek. De laatste techniek werd na een periode van testen in de VS gebouwd in Delft. De technieken werden aangevuld met massaspectrometrie en voltammetrie om de kinetiek en gasontwikkeling van de formaldehyde-oxidatie reactie beter in kaart te krijgen. De oxidatie van formaldehyde aan overgangsmetalen werd om drie redenen als modelreactie gekozen: Het mechanisme is relatief veelvuldig beschreven en opgehelderd waardoor het mogelijk leek om sneller aandacht te kunnen leggen op de kinetiek en thermodynamica van de reactie. Verder kent de reactie praktische relevantie binnen de chemische metaaldepositie. Daarnaast bleek het isotopisch gemerkte formaldehyde ($[^{14}C]CH_2O$ and CD_2O) commercieel verkrijgbaar bij diverse bedrijven.

Methoden - De afleiding van bindingsenergieën, verblijfstijden en bedekkingsgraden werd bereikt door het meten en fitten van de adsorptie-isothermen, en de adsorptiekinetiek en de uitwisselingskinetiek van radioactief (^{14}C-gemerkt) formaldehyde onder verschillende condities. Het fitten van de data werd gedaan door middel van een wiskundige fitmethode, genaamd compartimentele analyse. Daarbij was het belangrijk dat het meest realistische model niet alleen alle kinetische data kon beschrijven, maar dat het tevens in het verlengde zou liggen van respectievelijk een grondig getoetst reactiemechanismen uit de literatuur, de verkregen impedantiespectra, de voltammogrammen en de massaspectrometrische data. Bij impedantiespectroscopie werd informatie uit de data geëxtraheerd door zogenaamde equivalent-circuit fit procedures. Bij de andere twee technieken werd die informatie direct afgeleid door de invloed van pH, formaldehydeconcentratie en temperatuur op de reactiesnelheid te bestuderen. Tevens werd formaldehyde vervangen door het gedeutereerd formaldehyde om iets te zeggen over de snelheid waarmee chemische bindingen worden verbroken. De verhouding in de reactiesnelheden tussen beiden species (kinetisch isotoopeffect) geeft namelijk direct informatie over de relatieve snelheid waarmee waterstofbindingen worden verbroken.

Hoofdstuk 3 – Dit hoofdstuk beschrijft de oxidatie van formaldehyde bestudeerd d.m.v. impedantiespectroscopie. Een elektrisch equivalent-circuit werd gevonden dat de oxidatiekinetiek bij verschillende potentialen, pH-waarden, concentraties formaldehyde en CD_2O goed kon beschrijven. Interessant aan het circuit was niet alleen dat het in lijn

lag met het meest geciteerde reactiemechanisme uit de literatuur, maar vooral dat de elementen logaritmisch van de potentiaal afhingen (onder condities waarbij geen potentiaalafhankelijke gasontwikkeling werd waargenomen). De logaritmische afhankelijkheden suggereerden dat de kinetisch-verschillende elektrokatalytische stappen mogelijk ook logaritmisch van de potentiaal af hangen. Ook bleek er enige samenhang te bestaan tussen de stappen van het mechanisme (diffusie, adsorptie, oxidatie, desorptie, etc.) en de identiteit en waarden van de gefitte elementen. Een kwalitatieve dubbellaag structuur voor de vloeistof-elektrode dubbellaag kon worden afgeleid uit de waarden van de gefitte condensatoren, die bestond uit twee potentiaalsprongen, toegeschreven aan toestanden van chemisorptie en fysisorptie. De structuur kon in latere hoofdstukken worden gebruikt om andere elektrokinetische data te verklaren alsmede om het optimale model voor de compartimentele analyse af te leiden. Verder werd bij lage potentialen en frequenties een negatieve weerstand en een negatieve capaciteit gemeten en gefit, die de snelheidsbepalende stap onder "steady-state" condities vertegenwoordigde. Deze waarden vertoonden een KIE dat in overeenstemming lag met waarden die later door voltammetrie werden gemeten. Daarnaast bleken ze sterk afhankelijk van de pH. De negatieve capaciteit werd daarom mechanistisch verklaard door een gecombineerd effect van de (bijna even snelle) desorptie van formaat en de chemisorptie van het enolaat anion. Electro-kinetisch gezien werd het verklaard door een sneller ontladen door specifiek geadsorbeerde formaat ionen dan het opladen door adsorberende enolaat anionen bij het langzaam veranderen van de spanning. De 'snelheidsbepalende' negatieve impedantie verklaarde verder de afwezigheid van een karakteristieke elektrochemische Tafel-helling (een dergelijke helling werd echter wel gevonden voor een kleinere gefitte weerstand).

Hoofdstuk 4 – De reactiekinetiek van de oxidatie van formaldehyde werd in alkalische oplossingen bij verschillende pH, concentraties, potentialen en temperaturen via voltammetrie onderzocht. Tevens werd massaspectrometrie gebruikt om de kinetiek van waterstofgasontwikkeling te bestuderen. Deze kinetiek bleek sterk van de reactiecondities af te hangen, maar bleek niet snelheidsbepalend in de reactiekinetiek van formaldehyde op goud. Verder bleek dat in enkele oplossingen waterstofgas zonder aanleg van een electrisch spanningsverschil vrijkwam. Dit werd verklaard door een niet-elektrochemische nevenreactie waarbij formaat en waterstof spontaan uit formaldehyde en hydroxyl-ionen gevormd worden. De waarden van de gemeten kinetische isotoopeffecten en van de gefitte activeringsenergieën (E_{act}) suggereerden verder dat de snelheidsbepalende stap van de reactie bestond uit de (hydroxyl-gekatalyseerde) chemisorptie van het enolaat ion bij lage potentialen, uit desorptie van het formaat ion bij hogere potentialen en uit diffusie bij de hoogste potentialen. Deze verklaring was conform de interpretaties van de impedantiespectra. De waarden van E_{act} tussen -25 en 60 $kJ.mol^{-1}$ bevestigden niet alleen de katalytische rol van goud in de snelheid van de reactie, maar

tevens de mogelijkheid van een zogenaamd 'pre-evenwicht'. Dit pre-evenwicht leek in het extreemste geval door irreversibele adsorptie tot de vergiftiging van de goud atomen te kunnen leiden. De waarden van E_{act} bleken verder sterk af te hangen van de pH en de formaldehyde concentraties hetgeen het belang van de oplossing in de katalytische reactiekinetiek onderstreepte.

Hoofdstuk 5 – Dit hoofdstuk beschrijft een studie naar het gedrag van adsorptie, uitwisseling en oxidatie van formaldehyde aan goud bestudeerd door middel van de radiotracer dunne-laagtechniek, voltammetrie en compartimentele analyse. De adsorptie-kinetiek bij de evenwichtspotentiaal bleek goed te kunnen worden beschreven door een lineair model met een relatief snelle, reversibele fysisorptie en een relatief langzame, reversibele chemisorptie. Lineaire adsorptieisothermen werden verkregen waarvan de Gibbs vrije adsorptieenergie afhing van de potentiaal, de temperatuur en de pH. Ofschoon verschillen tussen de gevonden Gibbs adsorptie-energieën klein waren bleken ze groot genoeg om oplossingseffecten in de bindingsenergieën als onverwaarloosbaar te bestempelen. De elektro-oxidatie kinetiek bleek praktisch van de eerste orde te zijn in formaldehydeconcentratie alsmede in bedekkingsgraad. De invariantie van de adsorptie-isothermen met de potentiaal, alsmede de sterke variantie van de bedekkingsgraad met de concentratie in de oplossing suggereerden verder dat het potentiaalverloop in de oplossing belangrijker was voor de adsorptiekinetiek dan de absolute potentiaal van de elektrode zelf. In overeenstemming met voorgaande hoofdstukken werd de snelheid van de reactie verder bepaald door chemisorptie van het enolaat anion bij lage potentialen, door desorptie van formaat bij hogere potentialen en door diffusie bij de hoogste potentialen. De gevonden waarden van ΔG_{ad} bleken verder aanzienlijk te verschillen van ΔH_{ad} en van de metaal-formaat enthalpie, hetgeen impliceerde dat waarden van de entropie niet verwaarloosd kunnen worden wanneer het gaat om het toekennen van bindingssterkten voor de afleiding van het principe van Sabatier.

Hoofdstuk 6 – The oxidatie van CH_2O en CD_2O werd in 0,1 M NaOH bestudeerd aan verschillende overgangsmetalen (Au, Ag, Cu, Ni, Pd, Pt, Ir) als functie van de temperatuur. Au, Pt en Ir katalyseerden de reactie naar de hoogste snelheid, terwijl Cu en Ag de reactie bij de laagste potentialen katalyseerden. Ni en Pd werden als slechtste katalysator getypeerd. Bij lage overpotentialen is de reactie waarschijnlijk snelheidsbepalend in de chemisorptie van het enolaat anion voor Ag, Cu, Ni en Au, en in de desorptie van geadsorbeerd waterstof voor Pt, Pd en Ir. Desorptie van formaat leek bij hogere overpotentialen snelheidsbepalend. Diffusie bleek bij hoge stroomdichtheden belangrijk voor de snelheid van Ag, Pd, Au en Pt, terwijl sterk capacitatieve stromen werden waargenomen voor de oxidatie aan Ni, Cu en Ir. Verder werd een lineaire relatie verkregen tussen de reactiesnelheid van de katalytisch-actieve metalen en de uittree-

arbeid. De invloed van de elektronische eigenschappen van het metaal op de snelheid waarmee chemische bindingen worden verbroken werd verder onderstreept door overeenkomstige relaties tussen activeringsenergie enerzijds en de formatie-enthalpie van metaal-formaat als de oxidatiepotentiaal anderzijds. Het belang van 'buureffecten' van de katalytisch-actieve plekken in de snelheid van de reactie bleek verder uit de gevonden lineaire relatie tussen de bindingslengte en snelheid van de reactie. De waarden van E_{act} hingen af van het metaal en varieerden tussen –20 kJ.mol^{-1} and 50 kJ.mol^{-1}, hetgeen de katalytische werking van het metaal en de mogelijke aanwezigheid van een pre-evenwicht bevestigde.

Hoofdstuk 7 – De adsorptie, uitwisseling en oxidatiekinetiek werd aan verschillende metalen bestudeerd in 0,1 M NaOH door middel van voltammetry en de radiotracer dunne-laag techniek. Een lineair vier-compartimenten model werd gevonden dat alle adsorptie en uitwisselingsdata bij de OCP goed kon beschrijven. Het model impliceerde de aanwezigheid van drie kinetisch-verschillende adsorptiestappen, toegekend aan een snelle, reversibele fysisorptie, een langzame, reversibele chemisorptie en een irreversible nevenreactie. De chemisorptie bleek snelheidsbepalend en verliep het snelste op goud onder dynamische condities en op koper onder evenwichtscondities. De laatste waarneming bleek in overeenstemming met de laagste gefitte waarden van ΔG_{ad} uit de adsorptieisothermen voor koper. De waarden van zowel ΔG_{ad} als ook van de gemiddelde verblijfstijd in de chemisorptietoestand bleken lineair af te hangen van de metaalafhankelijke evenwichtspotentiaal. Deze relatie leverde een atomaire verklaring voor de waarde van een evenwichtspotentiaal en daarmee voor het al dan niet optreden van chemische metaaldepositie. Verder werden drie (grove) vulkaancurven verkregen voor de relaties tussen de katalytische activiteit enerzijds, en de waarden van respectievelijk ΔG_{ad}, de hoeveelheid species aan het oppervlak (Q) en de verblijfstijd in chemisorptie toestand (τ_c) anderzijds. De relaties gaven sterke aanwijzing voor de geldigheid van het Sabatier-principe voor het systeem formaldehyde-overgangsmetaal, een visie die verder bekrachtigd leek door de structurele relaties tussen ΔG_{ad} en τ_c, ΔG_{ad} en Q, en tussen τ_c en Q.

Hoofdstuk 8 – Dit hoofdstuk geeft een beknopte samenvatting van de resultaten die buiten de directe strekking van dit proefschrift werden geacht. Anodisch verstuiven van zilverdraden in licht alkalische waterige oplossingen leidde onverwachts tot de vorming van zilverclusters, zilvercolloïden en oxides. De grotere oxiden en colloïden konden worden verwijderd door centrifugeren waarbij kleinere colloïden en clusters in de oplossing achterbleven. De vorming van de deeltjes werd verklaard door gedissipeerde Joule warmte in de slecht-geleidende Ag_2O oppervlaktelaag. De vorming en stabiliteit van de subnanometer grote clusters (Ag_4^{2+}) bleek sterk van de pH af te hangen met een

optimum rond pH 11. Verder werden verrassenderwijs condities gevonden waarbij de subnanometer grote zilverclusters (Ag_4^{2+}) spontaan werden gevormd vanuit licht oververzadigde zilverzout oplossingen. Deze 'spontane' overgang van ion naar metaal werd verklaard door de thermodynamisch toegestane zuurstofontwikkeling bij pH 11. Tevens werden condities gevonden waarbij het metaal wel werd gevormd op een substraat, maar net niet in de oplossing. Op deze manier konden siliciumstructuren in de kleinste dimensies ooit selectief chemisch worden gemetalliseerd (100 nm en een aspect ratio van 4,25).

Hoofdstuk 9 – Dit hoofdstuk evalueert de relevantie van de resultaten ten opzichte van de bestaande literatuur, de initiële doelstellingen van het onderzoek en de (eventuele) toepassingsgebieden. De resultaten hebben laten zien dat impedantiespectroscopie, gekoppeld aan de equivalent-circuit benadering en de radiotracer dunne-laag techniek uitermate geschikt lijkt om elektrokatalytische reacties te bestuderen. Een dergelijk inzicht kan verder worden gebruikt bij het opstarten van nieuwe onderzoeken. Tal van kinetische en thermodynamische kwesties werden verder opgehelderd voor de oxidatie van formaldehyde aan verschillende overgangsmetalen. De inzichten hieruit kunnen worden gebruikt om sneller en beter optimale condities te kiezen voor de ontwikkeling van chemische depositieprocessen. Verder werden een serie condities afgeleid voor de correcte afleiding van het Sabatier-principe uit elektrokatalytische vulkaancurven. Daarnaast werden fysische richtlijnen afgeleid voor de elektrokatalytische activiteit van overgangsmetalen voor het metaal-formaldehyde systeem. Dergelijke condities en richtlijnen brengen de wetenschap van de elektrokatalyse wellicht een stapje verder. De nieuwe bereiding van stabiele, vieratomige zilverclusters alsmede de overgang hiervan naar deeltjes of bulkmetaal op een oppervlak kan mogelijk toepassing vinden in selectieve chemische zilverdepositie, in geleidende coatings alsmede in de technologie van de katalyse en optica.

Summary

Background - Electroless metal deposition (or plating) is an autocatalytic process by which metals can be deposited from a solution without the use of an external electrical current. The metal ions and the reducing agent are both supplied from the same solution, making the process applicable to conductive and non-conductive substrates. Well-known examples of industrial electroless plating processes refer to the nickel plating of car parts or the copper plating of printed circuit boards in microelectronics. Initiation of the metal deposition process can be achieved by using a metallic substrate that induces the adsorption of the reducing agent and subsequent deposition of at least one monolayer of metal atoms. Propagation may then occur in an autocatalytic fashion, provided that the deposited metal layer catalyses the adsorption and oxidation of the reducing agent as well. The rate of adsorption, exchange and oxidation of formaldehyde on transition metals in aqueous solutions is supposed to play a key role in the selectivity and rate of electroless metal deposition. The picture on the cover of this thesis shows an example of the smallest chemical deposition process ever reported, which was developed during the research that preceded this thesis.

Practical motivation - One of the major problems in the development of chemical metal deposition processes for many microelectronic applications is related to the large amount of practical work that is needed to attain optimum deposition rates and selectivity. Practically, the research described in this thesis was commenced in order to set a more structural base for process and product innovations.

Scientific motivation - The dependence of the rate at which a molecule reacts at catalysts often depends on the adsorption enthalpy of the reactants at the catalysts in a volcano-type fashion. It is frequently concluded from this behaviour that optimum catalytic behaviour is related to the optimum bond strength, the optimum coverage and the optimum residence time of reacting species at the surface. This interpretation is known as Sabatier's principle and has been investigated extensively since 1912 within heterogeneous solid-gas catalysis. However, the validity to derive the principle from the empirical rate-adsorption enthalpies has never been verified in electrocatalysis. This validity may be doubted, as the influence of entropies in the bond strengths is implicitly neglected, as adsorption enthalpies in the liquid are frequently approximated by bond energies from the gas-phase or formation enthalpies, and as the optimum adsorption energy may not automatically reflect an optimum coverage, an optimum residence time and an optimum bond strength of reactants at the surface.

Techniques - One of the main reasons for the absence of a profound empirical base for Sabatier's principle in electrocatalysis seems associated with the difficulties to determine *in-situ* the values of adsorption enthalpy, surface coverage and residence time of species

at the catalytic surface. These values cannot be determined by conventional electrochemical techniques. An attempt has been made in this thesis by using the radiotracer thin-gap technique in combination with electrochemical impedance spectroscopy (EIS), voltammetry and differential electrochemical mass spectrometry (DEMS). The radiotracer thin-gap technique was built in Delft after a period of testing in the laboratory of Prof. Dr. Wieckowski (USA). Voltammetry and DEMS were used to elucidate the kinetics and gas evolution characteristics of the reaction. The oxidation of formaldehyde on transition metals was chosen as model reaction for three reasons: First, the mechanism is relatively simple and well understood, enabling a better focus on the kinetic and thermodynamic aspects of the reaction. Second, the reaction has great practical relevance in the area of electroless metal deposition. Third, the required isotopically labelled forms of formaldehyde ($[^{14}C]CH_2O$ and CD_2O) are easily available and suitable for the radiotracer thin-gap technique.

Methods – Bond energies, residence times and surface coverage were obtained by measuring and fitting adsorption isotherms, adsorption kinetics and exchange kinetics of under different conditions. Fitting was performed by compartmental analysis with the consideration that the best fitting model should be plausible in terms of the most cited mechanism in literature and results obtained by impedance spectroscopy, voltammetry and DEMS. Mechanistic and kinetic information was extracted from the impedance spectra by using so-called equivalent-circuit fit procedures, and from the other techniques by studying the influence of pH, kinetic isotope effect (KIE), formaldehyde concentration and temperature on the reaction rate

Chapter 3 - The anodic oxidation of formaldehyde on gold in alkaline aqueous solutions was studied by electrochemical impedance spectroscopy (EIS). One equivalent circuit was found to mimic all impedance spectra measured for formaldehyde (CH_2O) and deuterated formaldehyde (CD_2O) in various solutions at different voltages. The circuit can be interpreted using the reaction mechanism proposed in literature and suggests that large capacitive changes occur at the interface upon the adsorption and desorption of reactants and products. The resistors and capacitors of the circuit depend on the voltage applied in a logarithmic fashion, implying that the overall kinetics of the overall reaction may be unravelled in different Butler-Volmer-type reaction steps. A double layer structure was constructed from the fitted capacitors, which described the electrostatics of the system by an inner Helmholtz plane (IHP) and an outer Helmholtz plane (OHP) mediating the solution and the electrode surface. A negative capacitance (inductive loop) and resistance were further observed at low frequencies, which suggested the depletion of negative charge in the IHP upon positive polarisation. It was explained by a higher desorption rate relative to the adsorption rate upon positive polarisation, as it became more apparent for

solutions containing CD_2O than for those containing CH_2O. Data were Kramers-Kronig transformable and a χ^2-value of $\sim 10^{-4}$ or less was attained in all fits.

Chapter 4 - The electrocatalytic oxidation of formaldehyde (CH_2O) and deuterated formaldehyde (CD_2O) on gold in aqueous, alkaline solution has been studied at different pH-values, concentrations, potentials, and temperatures by voltammetry, chronoamperometry and differential electrochemical mass spectrometry. The H_2, D_2, and CO_2 gas evolution kinetics depend to great extent on the pH, potential, and temperature but likely play a minor role in the overall rate of the electro-oxidation reaction. The evolution of hydrogen at the open-circuit potential (OCP) and the current efficiencies larger than 100% pointed towards the occurrence of a non-electrochemical dehydrogenation reaction parallel to the electro-oxidation reaction. The values of the kinetic isotope effects (KIE) and the apparent activation energies (E_{act}) suggested that the overall rate of the electro-oxidation reaction is determined by the hydroxyl-catalysed chemisorption of the enolate anion at low potentials, by the desorption of the formate anion at higher potentials, and by diffusion at the highest potentials. The apparent activation energies ranged between -25 and 60 $kJ.mol^{-1}$, confirming the highly catalytic properties of gold in the overall rate of the reaction and the possible presence of pre-equilibrium in the overall reaction. The value of the overall E_{act} was further seen to increase at decreasing pH-values and at decreasing formaldehyde concentrations.

Chapter 5 - Adsorption, exchange and oxidation of formaldehyde were studied on gold by voltammetry, the radiotracer thin-gap method and compartmental analysis. The overall adsorption process at the open circuit potential (OCP) can be well described by a rapid physisorption and a slow chemisorption, both proceeding in a catenary (linear), reversible fashion. Linear adsorption isotherms were obtained under most conditions, implying that of the Gibbs free energy of the reaction depends little on the potential, temperature and pH. At pH 13, the kinetics of the electro-oxidation of formaldehyde is approximately first order in both concentration of formaldehyde and in quantity of species adsorbed at the gold surface. The strong dependence of the quantity of species adsorbed on the formaldehyde concentration in the solution, and the invariance of the adsorption isotherms with the potential suggest that potential gradients on the solution side are more important in adsorption rates than the potential of the electrode itself. The rate of the reaction is determined by chemisorption of the enolate anion at low potentials, by desorption of formate at medium potentials, and by diffusion at highest potentials. The values of ΔG_{ad} differ substantially from the solution-variable values of ΔH_{ad} and from the metal-formate formation enthalpy, implying that Gibbs free adsorption enthalpies should be used to validate Sabatier's principle and that solution effects should not be neglected.

Chapter 6 - The oxidation of CH_2O and CD_2O was studied by voltammetry in 0.1 M NaOH on transition metals (Au, Ag, Cu, Ni, Pd, Pt, Ir) at different temperatures. Au, Pt

and Ir promote the reaction to highest rates, while Cu and Ag catalyse the reaction at lowest potentials. Ni and Pd do not catalyse the reaction well. At low overpotentials and temperatures, the rate of the reaction is likely ruled by the rate of chemisorption of the enolate anion on Ag, Cu, Au and Ni, and by the rate of desorption of adsorbed hydrogen on Pt, Pd and Ir. At higher potentials, the reaction may become increasingly controlled by the rate of desorption of the formate anion on all metals studied. A linear relationship was obtained for the dependence of the metal-dependent reaction rate on KIE, confirming the view from previous chapters that the rate-limiting step of the reaction comprises the rupture of hydrogen bonds. The rate of these hydrogen bond ruptures seem to be structurally affected by the electronic properties of the metals, as a linear relationship was obtained for the dependence of the reaction rate of the catalytically active metals on the work function. The importance of the chemical rearrangements and the electronic properties of the metals in the rate of the reaction were further indicated from the similar dependencies of the apparent activation energies (E_{act}) on both metal-formate formation enthalpies and oxidation potentials of the metals. Moreover, a curved relationship between E_{act} and the inter-atomic bond lengths was found, suggesting that neighbour effects of surface atoms play a role in the lowering of the transition state of the reaction. The values of E_{act} ranged between –20 kJ.mol^{-1} and 50 kJ mol^{-1}, confirming the catalytic properties of the metals and the possible presence of a (pseudo) pre-equilibrium in the reaction.

Chapter 7 - Adsorption, exchange and oxidation of formaldehyde on transition metals (Ag, Cu, Ni, Pd) were examined in 0.1 M NaOH by voltammetry and the radiotracer thin-gap technique. One linear four-compartment model was found to fit to all adsorption and exchange kinetic data at the OCP satisfactorily, suggesting the presence of three adsorption steps in the overall adsorption process: a rapid, reversible physisorption, a slow, reversible chemisorption and an irreversible side-reaction. The rate-limiting chemisorption step was seen to proceed at highest rates on gold under dynamic conditions and at highest rates on copper under equilibrium conditions. The latter observation was in agreement with the lowest Gibbs free adsorption energy (ΔG_{ad}) for copper. The values of ΔG_{ad} and of the residence times of species in the chemisorption state (τ_c) were further seen to depend on the OCP in a linear way, an observation that may explain the value of the OCP and the occurrence of electroless metal deposition on an atomic scale. Moreover, approximate volcano-type relationships were obtained for the dependencies of the oxidation rates on the values of ΔG_{ad}, τ_c and the surface quantities (Q). It supports the validity of Sabatier's principle for the formaldehyde-transition metal system, a view that seems further supported by the linear and curved dependencies of ΔG_{ad} on τ_c, ΔG_{ad} on Q,

and τ_c on Q. Volcano plots that are used to derive Sabatier's principle should nevertheless use values of ΔG_{ad} in the liquid phase rather than values of ΔG_{ad} in derived the gas-phase or values of ΔH_{ad}, as outlined in Chapter 5.

Chapter 8 - The results that were related to the scope of this thesis are briefly summed up. Anodic dispersion of silver wires in slightly alkaline aqueous solutions was found to yield subnanometre-sized silver clusters, nanometre-sized colloid and oxides. The large colloids and oxides can be removed by centrifugation leaving small colloids and clusters in the solution. The formation of the (sub)nanometre-sized particles is explained by dissipated Joule heat in the surface oxide layer. As the formation and stability of the subnanometre sized clusters (Ag_4^{2+}) were seen to depend to great extent on the pH-values around 11, a range of silver sols was prepared around this pH. Surprisingly, conditions were found where silver clusters and monodisperse colloids formed spontaneously from slightly supersaturated silver salt solutions. The colloids are formed by virtue of the reducing properties of hydroxyl ions at this pH. Conditions were found where the spontaneous ion-to-metal transition occurred at surfaces and not in the solution (electroless plating). In this way, silicon structures could be selectively plated in the lowest dimensions ever reported (100 nm at an aspect ratio of 4.25). No smaller silicon structures were available, but it is likely that smaller structures can be easily plated in this fashion as well.

Chapter 9 - The results presented in this thesis were briefly overviewed with emphasis on the added value in relation to the existing literature, the original goals and the possible interest for practical applications. The results have shown that EIS and equivalent-circuit fitting procedures, together with DEMS and the radiotracer thin-gap technique approach are well suited to study electrocatalytic reactions under *in situ* conditions. The correlation between the different methods and fitting procedures was shown to be good but complex. The EIS results have further yielded a model for the double-layer structure of the system. The results have also given information on various kinetic and thermodynamic aspects of the electrocatalytic oxidation of formaldehyde on various transition metals. Conditions based on practical measurements and fitting results were further postulated for the derivation of Sabatier's principle from volcano-type relationships in electrocatalysis. Moreover, a practical correlation between the OCP and the values of ΔG_{ad} and the residence times of adsorbed species were found, explaining electroless metal deposition on an atomic scale. Criteria for good metallic catalysts were further derived for the metal-formaldehyde system, implying that good catalytic properties arise for metals characterised by a high metal-formate formation enthalpy, a high oxidation potential, a low work function and a long average metal-metal bond length. Practically, the results may help to choose the right conditions in electroless metal deposition or help to set a springboard for the possible simulation of real plating processes. The results obtained for

subnanometre-sized silver particles and silver plating have further demonstrated a possible application in selective electroless metal deposition in nanometre dimensions. Relevant research for possible applications of these particles lay in the field of conductive coatings, catalysis, microelectronics and optics.

Nawoord

Met enig gevoel van opluchting mag ik dit proefschrift beëindigen. Het bleek niet altijd gemakkelijk om het onderzoekshoofd opgeheven te houden bij een gestolen laptop, bij koerswijzigingen in het onderzoek, bij een parallelle schaatscarrière en bij een samenwerking met mensen die niet vertrouwd waren met serendipitele elektrokatalyse. Toch waren het gelukkig ook dergelijke barrières, die uiteindelijk verwondering, voldoening en kennis brachten. Het loslaten van de mensen die een bijdrage leverden aan dergelijke verrijkingen kan dan ook niet gaan zonder dankbetuiging.

Gert Frens - Ik dank je voor je lessen in colloïdchemie, je lessen om zinnen scherper te formuleren en je lessen om wetenschappenlijk altijd kritisch te blijven. Ook dank ik je voor het schaatsverlof tijdens mijn aanstelling als AIO.

Zvonko Kolar - Een bijzonder dankwoord gaat uit naar jou. Je inspanningen om me rust te doen nemen voor details kwamen me niet altijd gelegen, maar waren uiteindelijk zeker nuttig. Ook onze bakkies thee zullen me altijd bijblijven. Verder was je input aangaande radiochemie en compartimentele analyse van zeer grote waarde.

Jeroen de Goeij - Jou wil ik bedanken voor de constructieve, resultaat-gerichte kritiek. Ook je menselijke manier van werken zal ik niet vergeten, en vooral je onbevooroordeelde en geïnteresseerde houding aangaande nieuwe onderwerpen, zelfs tijdens je ziekte. Ook ben ik je dankbaar voor je steun bij mijn streven om een proefschrift te schrijven dat primair mijn werk en visie reflecteert.

Rob van Veen – Ik ben je dankbaar voor de gastvrijheid om je laboratorium open te stellen voor metingen, voor onze korte maar krachtige samenwerking, en voor je bereidwilligheid om als medepromotor op te treden. Je scherpe inzichten aangaande elektrochemie en je vaardigheid om stevig tegengas te bieden zonder te bijten hebben me veel geholpen.

Diverse studenten hielpen om nieuwe wegen te banen in het onderzoek. Daarom bedankt: Marlon Fraai, Celine Tessont, Martine Bouwmeester, Geneitha Otto, Pieter Lusse en Walter van Leeuwen. Bijzondere dank gaat uit naar de altijd helpende vaste medewerkers: Wim den Hollander, Tona Verburg en Folkert Geurink. Voor de samenwerking of hulp in data-acquisitie ben ik erkentelijk: prof. dr. A Wiekowski (USA), dr. A. Kolics (USA), dr. A. Thomas (USA), dr. F. Tichelaar, dr. P. Kooyman, dr. J.F.E. Gootzen, dr. E.J.W.M. van der Drift, Ing. M.R. Zuiddam, dr. H. van der Weijde en Ing. P. C. van Dijk.

Tenslotte een innige dankbetuiging aan mijn moeder omdat ze me de interesse en volharding bijbracht die nodig waren om dit boekje tot stand te laten komen, alsmede aan mijn lieve vrouw Magriet omdat ze me de steun, rust en warmte gaf om het af te ronden.

Publications

Papers within the scope of this thesis

- M.V. ten Kortenaar, C. Tessont, Z.I. Kolar, H. van der Weijde. Anodic Oxidation of Formaldehyde on Gold studied by Electrochemical Impedance Spectroscopy: An Equivalent Circuit Approach. *Journal of the Electrochemical Society,* **1999,** 146, 2146.

- M.V. ten Kortenaar, Z.I. Kolar, J.J.M. de Goeij, G. Frens. Electrocatalytic Oxidation of Formaldehyde on Gold Studied by Differential Electrochemical Mass Spectrometry and Voltammetry. *Journal of the Electrochemical Society,* **2001,** 14, E327.

- M.V. ten Kortenaar, Z.I. Kolar, J.J.M. de Goeij, G. Frens. Adsorption, Exchange and Oxidation of Formaldehyde on Gold: A Radiotracer Study. *Langmuir*, **2002**, 18, 10279.

- M.V. ten Kortenaar, Z.I. Kolar, J.J.M. de Goeij. Electrocatalytic Oxidation of Formaldehyde on Transition Metals. *Submitted for publication to J. Electroanalytical Chemistry.*

- M.V. ten Kortenaar, Z.I. Kolar, J.J.M. de Goeij. Adsorption, Exchange and Oxidation of Formaldehyde on Transition Metals: A Radiotracer Study. *Submitted for publication to Langmuir.*

Papers related to the scope of this thesis

- M.V. ten Kortenaar, Z.I. Kolar, F.D. Tichelaar. Formation of Long-Lived Silver Clusters in Aqueous Solution by Anodic Dispersion. *Journal of Physical Chemistry B,* **1999,** 103, 2055.

- M.V. ten Kortenaar; Z.I. Kolar; G. Frens; P.J. Lusse; E.W.J.M. van der Drift. Chemische Abscheidung von Silber im Nanometer Bereich: Grenzen und Möglichkeiten. *Galvanotechnik,* **1999,** 10, 90.

- M.V. ten Kortenaar, J.J.M. de Goeij, Z.I. Kolar, G. Frens, P.J. Lusse, M.R. Zuiddam, E.W.J.M. van der Drift. Electroless Silver Deposition in 100 nm Silicon Structures. *Journal of the Electrochemical Society,* **2001**, *C28, 148.*

- M.V. ten Kortenaar, Z.I. Kolar, J.J.M. de Goeij. Formation and Properties of Monodisperse Nanometer-Sized Silver Colloids in Aqueous Alkaline Solution. *To be published.*

Curriculum Vitae

Marnix Victor ten Kortenaar behaalde iets minder dan 18 jaar na zijn geboorte op 19 Augustus 1970 te Voorburg het diploma VWO aan het Oranje-Nassau College te Zoetermeer. Na één jaar studie Farmacie aan de Rijksuniversiteit Utrecht veranderde hij van studie om in 1994 aan de Rijksuniversiteit Leiden het doctoraal diploma Scheikunde te behalen. In de éénjarige afstudeerstage in de vaste-stof chemie en een zesmaandse werkperiode aan het Paul Scherrer Institut in Zwitserland werden verschillende katalysatoren bereid, gekarakteriseerd, verwerkt in elektroden en getest in zink-zuurstof batterijen. Dit werk resulteerde in een publicatie.

Enkele maanden na het afstuderen trad hij als AIO in dienst van de TU Delft. Hij voerde zijn onderzoek uit op de afdeling Radiochemie van het Interfacultair Reactor Instituut (Ir. Z.I. Kolar, prof. dr. ir. J.J.M. de Goeij) en op het laboratorium voor Fysische Chemie van de faculteit TNW (Prof. dr. G. Frens). Een deel van het onderzoek werd verricht in het Laboratorium voor Anorganische Chemie van de faculteit Scheikundige Technologie van de TU Eindhoven (Prof. dr. J.A.R. Van Veen).

Na de AIO-periode werkte hij tussen oktober 1999 en oktober 2002 als ambassadeur (50%) en projectmanager duurzame energietechnologie (50%) voor Essent. Sinds November 2002 is hij Senior Researcher bij Friesland Coberco Dairy Foods - Corporate Research te Deventer. Daar werkt hij aan projecten op het gebied van emulgeren, sproeidrogen, oleochemie en poedertechnologie.

Naast bovengenoemde wetenschappelijke en technische activiteiten behaalde hij gedurende zijn AIO-periode diverse internationale successen als schaatser, getuige o.a. deelname aan de Olympische spelen van 1998 te Nagano. Tevens werkte hij freelance als bedrijfscoach, als ambassadeur voor Univé en als schrijver. Sinds 11 oktober 2002 is hij getrouwd met Margriet.

ISBN 90-407-2445-8

TU Delft

Delft University of Technology

Delft University Press